A STUDY OF INELASTIC DECAY AMPLITUDES IN ^{51}Mn

by

Katherine Meiburg Whatley

Department of Physics
Duke University

Dissertation submitted in partial fulfillment of
the requirements for the degree of Doctor
of Philosophy in the Department of
Physics in the Graduate School
of Duke University

1982

ABSTRACT

(Physics-Nuclear)

A STUDY OF INELASTIC DECAY AMPLITUDES IN ^{51}Mn

by

Katherine Meiburg Whatley

Department of Physics
Duke University

An abstract of a dissertation submitted in partial
fulfillment of the requirements for the degree
of Doctor of Philosophy in the Department of
Physics in the Graduate School
of Duke University

1982

ABSTRACT

Detailed angular distribution measurements on inelastically scattered protons and de-excitation γ-rays in the $^{50}Cr(p,p')$ and $^{50}Cr(p,p'\gamma)$ reactions were performed for 107 resonances in ^{51}Mn in the proton energy range 3.0-4.4 MeV. An overall resolution of 425 eV was obtained with the tandem Van de Graaff accelerator and the high resolution system at the Triangle Universities Nuclear Laboratory.

Spin and parity assignments for the 107 resonances studied were as follows: $1/2^+$ (4); $1/2^-$ (6); $3/2^-$ (30); $3/2^+$ (20); $5/2^+$ (38); $5/2^-$ (7); $7/2^+$ (1); and $9/2^+$ (1). Mixing ratios for the inelastic decay amplitudes were uniquely determined for all resonances except those assigned $J^\pi = 1/2^+$, $1/2^-$, or $3/2^+$. For $1/2^+$ and $1/2^-$ resonances there is only one open decay channel. For $3/2^+$ resonances, insufficient information is obtained from this experiment to determine a unique solution for the mixing ratios.

Statistical studies were performed on the set of $3/2^-$ resonances and on the set of $5/2^+$ resonances. Strong channel-channel correlations were observed in the distributions of the reduced widths and the reduced width amplitudes for $5/2^+$ resonances. The existence of such correlations is a violation of the extreme statistical model. The present results agree with the reduced width amplitude distribution of Krieger and Porter which includes channel-channel correlations.

ACKNOWLEDGEMENTS

I would like to express my appreciation to my advisor, Dr. E. G. Bilpuch, for his support and guidance during all phases of this research project. I would also like to thank Dr. G. E. Mitchell for his guidance throughout the course of these experiments, and for the hours he invested in the editing of this manuscript.

I owe special thanks to C. R. Westerfeldt for assistance and support above and beyond the call of duty. I am indebted to J. F. Shriner, Jr., Dr. W. A. Watson III, Dr. K. B. Sales, Dr. Chou Biing Hui, Dr. F. O. Purser, and J. F. Wilkerson for many helpful discussions and suggestions. The assistance of R. O. Nelson, P. Ramakrishnan, and B. J. Warthen in taking portions of these data is appreciated.

The assistance of Mr. S. Edwards in the maintenance of the electronics equipment and of Mr. R. Rummel and Mr. P. Carter in the maintenance of the accelerator systems is gratefully acknowledged. The fine work and cooperation of the machine shop, headed by Mr. A. W. Lovette, are especially appreciated. Special thanks are due to Mrs. Joseph Bailey for the many hours spent in the careful preparation of the figures for this dissertation.

To my families, both the Meiburgs and the Whatleys, go warm thanks for their constant support and encouragement. Most of all, I want to thank my husband, Jac, for his patience during many long nights in the lab, and for his love and support during the course of these experiments. Without his

encouragement this dissertation would not have been possible.

This work was supported in part by the United States Department of Energy. Portions of the data analysis were performed at the Triangle Universities Computation Center, which is supported in part by the National Science Foundation.

TABLE OF CONTENTS

ABSTRACT iii

ACKNOWLEDGEMENTS iv

LIST OF FIGURES viii

LIST OF TABLES xii

Chapter
I. INTRODUCTION 2

II. ANGULAR CORRELATIONS 5

A. Theoretical Background 5
B. Angular Correlations for Compound Nuclear States 17
1. p-wave Resonances 17
2. d-wave Resonances 20
3. f-wave Resonances 28
4. g-wave Resonances 32

III. EXPERIMENTAL EQUIPMENT AND PROCEDURES 41

A. The High Resolution System 41
1. Accelerator Control 41
2. Magnet Control 44
B. Scattering Chambers and Counting Electronics 45
C. Targets 63
D. Experimental Procedure 64

IV. DATA AND PRELIMINARY ANALYSIS 68

A. Proton Elastic Scattering Experiments 68
B. Preliminary Analysis 68
1. p-wave Resonances 71
2. d-wave Resonances 81
3. f-wave Resonances 124
a. Preliminary Analysis 124
b. Analog States 147
4. g-wave Resonances 153

V. STATISTICAL PROPERTIES 159

A. Introduction 159
B. Level Spacings and Proton Strength Functions 159

C. Reduced Width Amplitudes 161
1. p-wave Resonances 164
2. d-wave Resonances 164
D. Mixing Ratios 171
1. p-wave Resonances 171
2. d-wave Resonances 183
E. Linear Correlation Coefficients 200
1. p-wave Resonances 200
2. d-wave Resonances 203

IV. CONCLUSIONS 206

APPENDIX 208

BIBLIOGRAPHY 228

LIST OF FIGURES

2.1 Energy level scheme and angular momentum coupling schemes for the reaction $^{50}Cr(p,p'\gamma)^{50}Cr$ when the incident proton has $\ell=1$ 19

2.2 Energy level scheme and angular momentum coupling schemes for the reaction $^{50}Cr(p,p'\gamma)^{50}Cr$ when the incident proton has $\ell=2$ 22

2.3 Experimental Legendre coefficients for proton and γ-ray distributions for the 38 resonances in ^{51}Mn assigned $J^{\pi}= 5/2^{+}$ 27

2.4 Energy level scheme and angular momentum coupling schemes for the reaction $^{50}Cr(p,p'\gamma)^{50}Cr$ when the incident proton has $\ell=3$ 30

2.5 Energy level scheme and angular momentum coupling schemes for the reaction $^{50}Cr(p,p'\gamma)^{50}Cr$ when the incident proton has $\ell=4$ 35

3.1 Schematic diagram of the high resolution feedback system 43

3.2 Schematic diagram of the analyzing magnet control system 47

3.3 Top view of the charged particle scattering chamber 50

3.4 Block diagram of the counting electronics for the proton experiment 54

3.5 Top view of the γ-ray detection chamber 56

3.6 Side view of the new 0° leg beam line collimator 59

3.7 Block diagram of the counting electronics for the γ-ray experiment 62

3.8 Typical spectra for the reactions $^{50}Cr(p,p')$ and $^{50}Cr(p,p'\gamma)$ . . . 66

4.1 Sample angular distributions for a $3/2^{-}$ resonance 73

4.2 Plots of reduced widths and the cumulative sums of reduced widths for the elastic and total inelastic decay channels for $3/2^{-}$ resonances in ^{51}Mn 87

4.3 Plots of reduced widths and the cumulative sums of reduced widths for the two inelastic decay channels for $3/2^{-}$ resonances in ^{51}Mn in the total angular momentum representation 89

4.4 Plots of reduced widths and the cumulative sums of reduced widths for the two inelastic decay channels for $3/2^{-}$ resonances in ^{51}Mn in the channel spin representation 91

4.5 Products of inelastic decay amplitudes and cumulative sums of the products versus energy for the two inelastic decay channels for $3/2^-$ resonances in ^{51}Mn in both representations 93

4.6 Sample angular distributions for a $5/2^+$ resonance 95

4.7 Plot of ϕ_{CA} versus ϕ_{BA} for 20 $3/2^+$ resonances in ^{51}Mn in the total angular momentum representation 108

4.8 Plot of ϕ_{CA} versus ϕ_{BA} for 20 $3/2^+$ resonances in ^{51}Mn in the channel spin representation 110

4.9 Plot of ϕ_{CA} versus ϕ_{BA} for 38 $5/2^+$ resonances in ^{51}Mn in the total angular momentum representation 121

4.10 Plot of ϕ_{CA} versus ϕ_{BA} for 38 $5/2^+$ resonances in ^{51}Mn in the channel spin representation 123

4.11 Plots of reduced widths and the cumulative sums of reduced widths for the elastic and total inelastic decay channels for $5/2^+$ resonances in ^{51}Mn 130

4.12 Plots of reduced widths and the cumulative sums of reduced widths for the three inelastic decay channels for $5/2^+$ resonances in ^{51}Mn in the total angular momentum representation 132

4.13 Plots of reduced widths and the cumulative sums of reduced widths for the three inelastic decay channels for $5/2^+$ resonances in ^{51}Mn in the channel spin representation 134

4.14 Products of inelastic decay amplitudes and cumulative sums of the products versus energy for the three inelastic decay channels for $5/2^+$ resonances in ^{51}Mn in the total angular momentum representation 136

4.15 Products of inelastic decay amplitudes and cumulative sums of the products versus energy for the three inelastic decay channels for $5/2^+$ resonances in ^{51}Mn in the channel spin representation . 138

4.16 Sample angular distributions for a $5/2^-$ resonance 141

4.17 Mixing angles versus incident proton energy for $5/2^-$ resonances . . 146

4.18 Plots of reduced widths and the cumulative sums of reduced widths for the elastic and total inelastic decay channels for $5/2^-$ resonances in ^{51}Mn 151

5.1 The distribution of reduced widths for the elastic and total inelastic decay channels for $3/2^-$ resonances in ^{51}Mn 166

5.2 The distribution of reduced widths for the inelastic decay channels for $3/2^-$ resonances in ^{51}Mn in the total angular momentum representation 168

5.3 The distribution of reduced widths for the inelastic decay channels for $3/2^-$ resonances in ^{51}Mn in the channel spin representation . 170

5.4 The distribution of reduced widths for the elastic and total inelastic decay channels for $5/2^+$ resonances in ^{51}Mn 173

5.5 The distribution of reduced widths for the inelastic decay channels for $5/2^+$ resonances in ^{51}Mn in the total angular momentum representation 175

5.6 The distribution of reduced widths for the inelastic decay channels for $5/2^+$ resonances in ^{51}Mn in the channel spin representation . 177

5.7 Histograms of the number of resonances with a given mixing angle for $3/2^-$ resonances in ^{51}Mn in both representations 180

5.8 Histograms of the number of resonances with a given mixing angle, normalized for equal average reduced widths, for $3/2^-$ resonances in ^{51}Mn in both representations 182

5.9 Plots of the mixing angle ϕ versus the energy of the incident proton for $3/2^-$ resonances in ^{51}Mn in both representations 185

5.10 Histograms of the number of resonances with a given mixing angle for $5/2^+$ resonances in ^{51}Mn in the total angular momentum representation 189

5.11 Histograms of the number of resonances with a given mixing angle for $5/2^+$ resonances in ^{51}Mn in the channel spin representation . . . 191

5.12 Histograms of the number of resonances with a given mixing angle, normalized for equal average reduced widths, for $5/2^+$ resonances in ^{51}Mn in the channel spin representation 193

5.13 Histograms of the number of resonances with a given mixing angle, normalized for equal average reduced widths, for $5/2^+$ resonances in ^{51}Mn in the total angular momentum representation 195

5.14 Plots of the mixing angles versus the energy of the incident proton for $5/2^+$ resonances in ^{51}Mn in the total angular momentum representation 197

5.15 Plots of the mixing angles versus the energy of the incident proton for $5/2^+$ resonances in ^{51}Mn in the channel spin representation . 199

A.1 Differential cross section of proton elastic and inelastic scattering on ^{50}Cr from E_p = 3.240 MeV to E_p = 3.440 MeV 210

A.2 Differential cross section of proton elastic and inelastic scattering on ^{50}Cr from E_p = 3.440 MeV to E_p = 3.640 MeV 212

A.3 Differential cross section of proton elastic and inelastic scattering on ^{50}Cr from E_p = 3.620 MeV to E_p = 3.820 MeV 214

A.4 Differential cross section of proton elastic and inelastic scattering on ^{50}Cr from E_p= 3.820 MeV to E_p= 4.040 MeV 216

A.5 Differential cross section of proton elastic and inelastic scattering on ^{50}Cr from E_p= 4.040 MeV to E_p= 4.400 MeV 218

LIST OF TABLES

2.1 Values of the Penetrability Ratio for p-wave Resonances 11

2.2 Values of the Phase Factor and Penetrability Ratio for d-wave Resonances 13

2.3 Values of the Phase Factor and Penetrability Ratio for f-wave Resonances 16

2.4 Values of the Phase Factor and Penetrability Ratio for g-wave Resonances 16

3.1 Charged Particle Detector Properties 51

3.2 γ-ray Detector Properties 60

4.1 Legendre Polynomial Coefficients for ℓ=1 Resonances in ^{51}Mn 74

4.2 Mixing Ratios and Mixing Angles for $3/2^-$ Resonances in ^{51}Mn: Total Angular Momentum Representation 77

4.3 Mixing Ratios and Mixing Angles for $3/2^-$ Resonances in ^{51}Mn: Channel Spin Representation 79

4.4 Inelastic Reduced Widths and Amplitude Products for $3/2^-$ Resonances in ^{51}Mn: Total Angular Momentum Representation 82

4.5 Inelastic Reduced Widths and Amplitude Products for $3/2^-$ Resonances in ^{51}Mn: Channel Spin Representation 84

4.6 Legendre Polynomial Coefficients for ℓ=2 Resonances in ^{51}Mn 97

4.7 Mixing Ratios, Mixing Angles, and ε^2 for $3/2^+$ Resonances in ^{51}Mn: Total Angular Momentum Representation 101

4.8 Mixing Ratios, Mixing Angles, and ε^2 for $3/2^+$ Resonances in ^{51}Mn: Channel Spin Representation 104

4.9 Mixing Ratios, Mixing Angles, and ε^2 for $5/2^+$ Resonances in ^{51}Mn: Total Angular Momentum Representation 112

4.10 Mixing Ratios, Mixing Angles, and ε^2 for $5/2^+$ Resonances in ^{51}Mn: Channel Spin Representation 116

4.11 Inelastic Reduced Widths and Amplitude Products for $5/2^+$ Resonances in ^{51}Mn: Total Angular Momentum Representation 125

4.12 Inelastic Reduced Widths and Amplitude Products for $5/2^+$ Resonances in ^{51}Mn: Channel Spin Representation 127

4.13 Legendre Polynomial Coefficients for ℓ=3 Resonances in ^{51}Mn 142

4.14 Mixing Ratios, Mixing Angles, and ε^2 for $5/2^-$ Resonances in ^{51}Mn: Total Angular Momentum Representation 143

4.15 Mixing Ratios, Mixing Angles, and ε^2 for $5/2^-$ Resonances in ^{51}Mn: Channel Spin Representation 144

4.16 Inelastic Reduced Widths and Amplitude Products for $5/2^-$ Resonances in ^{51}Mn: Total Angular Momentum Representation 148

4.17 Inelastic Reduced Widths and Amplitude Products for $5/2^-$ Resonances in ^{51}Mn: Channel Spin Representation 149

4.18 Spectroscopic Factors for $5/2^-$ Analog States 154

4.19 Legendre Polynomial Coefficients for ℓ=4 Resonances in ^{51}Mn 156

4.20 Mixing Ratios, Mixing Angles, and ε^2 for ℓ=4 Resonances in ^{51}Mn: Total Angular Momentum Representation 157

4.21 Inelastic Reduced Widths And Amplitude Products for ℓ=4 Resonances in ^{51}Mn: Total Angular Momentum Representation 158

5.1 Proton Strength Functions for 30 $3/2^-$ Resonances in ^{51}Mn 162

5.2 Proton Strength Functions for 38 $5/2^+$ Resonances in ^{51}Mn 163

5.3 Linear Correlation Coefficients Between Reduced Widths for $3/2^-$ Resonances in ^{51}Mn: Total Angular Momentum Representation . . . 201

5.4 Linear Correlation Coefficients Between Reduced Widths for $3/2^-$ Resonances in ^{51}Mn: Channel Spin Representation 203

5.5 Linear Correlation Coefficients Between Reduced Widths for $5/2^+$ Resonances in ^{51}Mn: Total Angular Momentum Representation . . . 204

5.6 Linear Correlation Coefficients Between Reduced Widths for $5/2^+$ Resonances in ^{51}Mn: Channel Spin Representation 205

A.1 Resonance Parameters for Resonances in ^{51}Mn 219

Our revels now are ended. These our actors,
As I foretold you, were all spirits and
Are melted into air, into thin air:
And, like the baseless fabric of this vision,
The cloud-capp'd towers, the gorgeous palaces,
The solemn temples, the great globe itself,
Yea, all which it inherit, shall dissolve
And, like this insubstantial pageant faded,
Leave not a rack behind. We are such stuff
As dreams are made on, and our little life
Is rounded with a sleep. --Sir, I am vex'd:
Bear with my weakness; my old brain is troubled.
Be not disturb'd with my infirmity.
If you be pleas'd, retire into my cell
And there repose: a turn or two I'll walk,
To still my beating mind.

<u>The Tempest</u> 4. 1. 148-63

A STUDY OF INELASTIC DECAY AMPLITUDES IN ^{51}Mn

CHAPTER I

INTRODUCTION

Numerous high resolution proton scattering experiments have been performed at the Triangle Universities Nuclear Laboratory with both the tandem Van de Graaff accelerator and the 3 MV Van de Graaff accelerator. With few exceptions, compound nuclei formed by the addition of a proton to even-even nuclei have been studied. Resonance information such as energy, angular momentum, parity, and elastic and inelastic partial widths, obtained in high resolution proton scattering experiments, are used in the study of statistical properties and of special states of the compound nucleus.

The present work is one of a series of experiments designed to measure the magnitudes and relative signs of inelastic decay amplitudes for isolated resonances. Angular distributions of the inelastically scattered protons and the subsequent γ-ray decay are measured and fit with Legendre polynomial expansions. The spin and parity of a resonance can be uniquely determined from the angular distributions. In addition, the distributions are functions of the inelastic decay amplitudes. Ratios of the amplitudes (mixing ratios) can be conveniently determined from the angular distributions. From the mixing ratios and the total inelastic width, which is easily determined, the inelastic channel reduced widths can be found.

The above technique for the determination of the magnitude and relative signs of mixing ratios has been applied successfully to the two, three, and

four channel cases (Dittrich 1976, Wells 1978, Chou 1980, Watson et al. 1980, Shriner et al. 1982). In the present work, two, three, and four channel cases are studied. Since there are no ℓ=1 or ℓ=2 analog states in the energy range considered, this experiment is suitable for the study of the statistical behavior of these resonances. Thirty resonances with $J^\pi = 3/2^-$ and thirty-eight resonances with $J^\pi = 5/2^+$ were studied. In addition, twenty resonances were assigned $J^\pi = 3/2^+$. Insufficient information is obtained in this experiment to determine a unique solution for the mixing ratios for $3/2^+$ resonances. Seven ℓ=3 resonances were found, two of which were determined to be analog states. Due to the limited size of this sample and to the presence of analog states, no statistical studies could be performed on these resonances. Two ℓ=4 resonances were studied.

Knowledge of the relative sign between reduced width amplitudes for different channels permits tests of aspects of statistical theory. According to the extreme statistical model, the distribution of mixing ratios should obey a Cauchy distribution. For the $3/2^-$, $5/2^+$, and $5/2^-$ resonances studied, there are strong non-random effects, in contradiction to the extreme statistical model. The experimental results for $5/2^+$ resonances also disagree with the prediction (Lane 1971) that the reduced width correlation coefficient should be approximately equal to the square of the reduced width amplitude correlation coefficient. The present results are consistent with results obtained from the previous measurements in this laboratory. Chou (1980) obtained expressions for the distribution of mixing ratios based on the probability density function derived by Krieger and Porter (1963) for reduced width amplitudes. The predicted distribution matches the general trends of the experimental results.

A brief sketch of the theory of angular correlations is presented in

Chapter II. Expressions for the angular distributions of the inelastically scattered protons and de-excitation γ-rays from resonances of various spins and parities are presented, and the method by which the mixing ratios are obtained from the measured angular distributions is described. A discussion of the experimental equipment and procedures is found in Chapter III. In Chapter IV, the data and preliminary analysis are presented. Statistical and non-statistical behavior of groups of $3/2^-$ and $5/2^+$ resonances are discussed in Chapter V, and Chapter VI is a summary of results and conclusions. The appendix contains excitation functions for the reactions $^{50}Cr(p,p')$ and $^{50}Cr(p,p'\gamma)$, reproduced from Salzmann (1975) and Salzmann et al. (1977), and a list of resonances and resonance information for all resonances considered.

CHAPTER II

ANGULAR CORRELATIONS

A. Theoretical Background

One of the motivations for performing the experiments discussed in this dissertation was the determination of spin and parity assignments for states in ^{51}Mn. From elastic scattering one can determine the ℓ value of a given resonance, and it is possible in many cases to assign a J value as well. However, angular correlation studies on the inelastic protons and γ-rays emitted in the nuclear reaction provide a much more reliable method for determining the spin of states. Fano (1953) and Coester and Jauch (1953) developed mathematical methods which greatly simplify the derivation of a complete angular correlation formula. A brief summary of the major concepts involved in this derivation are given here. The complete derivation of angular correlations for inelastically scattered protons and the resulting γ-ray decay is given by Dittrich (1976).

In the method of Fano and of Coester and Jauch, the assumption is made that the quantum system is not in a pure state and cannot be represented by a wave function. Rather, the system has probability P_1, P_2, P_3,...,P_m,... of being in the dynamical states $|1\rangle$, $|2\rangle$, $|3\rangle$,...,$|m\rangle$,..., and its behavior is described by a density matrix ρ, defined as $\rho = \sum_{\alpha} |\alpha\rangle P_\alpha \langle\alpha|$, where P_α is the probability that the system is in state $|\alpha\rangle$. The expectation value of an

operator O acting on the mixed state is $\langle O \rangle = Tr(O\rho)$. The advantage of the density matrix description of the system is that it includes by definition the averaging over unobserved random variables of the system.

In order to represent a realistic experimental situation, a matrix ε, called the efficiency matrix, is introduced. The efficiency matrix is a function of the parameters of the detection of the outgoing radiation such as detector size and position. If a measurement W is made on the system described by ρ and ε, then $W = \langle \varepsilon \rangle = Tr(\varepsilon\rho)$. W is the probability that an event will be recorded in a detector, and in a nuclear scattering experiment is a function of Θ, the relative angle between the incident beam and the position of the detector.

The density and efficiency matrices can become difficult to treat mathematically. Tensors, however, have simple angular momentum and rotational transformation properties. It is therefore convenient to define a transformation relation between matrices and tensors. If a density matrix consists of eigenfunctions $|B_1\beta_1\rangle$ and $|B_2\beta_2\rangle$ of angular momenta B_1 and B_2, then the associated statistical tensor is defined in terms of its 2k+1 elements:

$$\rho_{kn}(B_1B_2) = \sum_{\beta_1\beta_2} (-1)^{B_2-\beta_2} (B_1\beta_1 B_2 -\beta_2 | kn) \langle B_1\beta_1 | \rho | B_2\beta_2 \rangle \ , \qquad (2.1)$$

where $n = -k, -k+1, \ldots, k$, and $\vec{k} = \vec{B}_1 - \vec{B}_2$. In the same manner, efficiency tensors $\varepsilon_{kn}(B_1B_2)$ can be defined in terms of the efficiency matrix ε. Written in terms of the density and efficiency tensors, the correlation formula becomes:

$$W = Tr(\varepsilon\rho) = \sum_{B_1B_2kn} \rho_{kn}(B_1B_2)\varepsilon^{*}_{kn}(B_1B_2) \ . \qquad (2.2)$$

In order for eqn. 2.2 to be useful, it must be specialized to nuclear reactions. Nuclear reactions proceed by a series of transitions, each of

which has an initial and final state. The total angular momentum of the system is thus formed by a series of vector sums of two angular momenta. It is convenient to express the vector sums in terms of tensors because of the symmetry properties of tensors. The vector to tensor conversion is accomplished by means of the "tensor of a vector sum" theorem, stated as follows. Consider the following angular momentum sum: $\vec{B} = \vec{C} + \vec{j}'$. In tensor notation, this becomes:

$$\rho_{k_B n_B}(B_1 B_2) = \sum_{k_c n_c k_j' n_j'} (k_c n_c k_j' n_j' | k_B n_B)\, \hat{k}_c \hat{k}_j' \hat{B}_1 \hat{B}_2 \qquad (2.3)$$

$$\cdot \begin{Bmatrix} C_1 & j_1' & B_1 \\ C_2 & j_2' & B_2 \\ k_c & k_j' & k_B \end{Bmatrix} \cdot \rho_{k_c n_c}(c_1 c_2)\, \rho_{k_j' n_j'}(j_1' j_2') \ ,$$

where $\rho_{k_c n_c}(c_1 c_2)$ and $\rho_{k_j' n_j'}(j_1' j_2')$ are the statistical tensors of the respective angular momenta, the circumflex over a quantum number signifies, for example, $\hat{k}_c = (2k_c+1)^{1/2}$, and the quantity in brackets is a Wigner 9-j coefficient.

In a nuclear reaction in which particle absorption (emission) occurs, there are three angular momenta involved: the spin of the target (final state), and the spin and orbital angular momentum of the incident (exit) particle. Conventionally, there are two ways of combining these momenta: the total angular momentum representation and the channel spin representation. For the $(p,p'\gamma)$ reaction the general correlation functions for the inelastically scattered proton and the subsequent γ-ray decay are given in both representations for the following system: an isolated resonance with definite states A (0^+), B, C (2^+), and D (0^+):

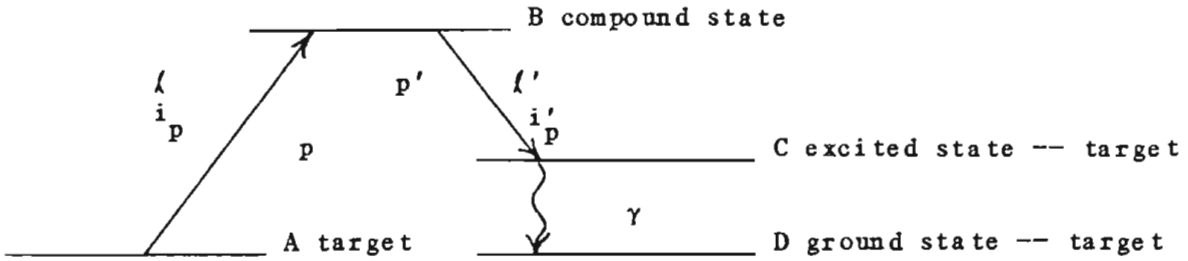

The following results are from Dittrich, simplified for the above system. In the total angular momentum representation,

$$W_p(\theta) \propto \sum_{\ell_1'\ell_2'j_1'j_2'k} (-1)^{-2j_1'} \bar{Z}(\ell j \ell j; \tfrac{1}{2}k)\, W(jBjB;0k) \qquad (2.4)$$

$$\cdot\, \bar{Z}(\ell_1' j_1' \ell_2' j_2'; \tfrac{1}{2}k)\, W(j_2' B j_1' B; 2k)$$

$$\cdot\, P_k(\theta) \langle j_1 \rangle \langle j_2 \rangle^* ,$$

$$W_\gamma(\theta) \propto \sum_{j'k} (-1)^{j'+\frac{1}{2}}\, \bar{Z}(\ell j \ell j; \tfrac{1}{2}k)\, W(jBjB;0k) \qquad (2.5)$$

$$\cdot\, W(B2B2; j'k) W(2222;0k) (212{-}1|k0)$$

$$\cdot\, P_k(\theta) J_k |\langle j' \rangle|^2 ,$$

and in the channel spin representation,

$$W_p(\theta) \propto \sum_{\ell_1'\ell_2's'k} (-1)^{s'+\frac{1}{2}}\, \bar{Z}(\ell B \ell B; \tfrac{1}{2}k)\, \bar{Z}(\ell_1' B \ell_2' B; s'k) \qquad (2.6)$$

$$\cdot\, P_k(\theta) \langle s' \ell_1' \rangle \langle s' \ell_2' \rangle^* ,$$

$$W_\gamma(\theta) \propto \sum_{\ell' s_1' s_2' k} (-1)^{-s_1'-s_2'+\ell'} \hat{s}_1' \hat{s}_2'\, \bar{Z}(\ell B \ell B; \tfrac{1}{2}k) \qquad (2.7)$$

$$\cdot\, W(Bs_2'Bs_1'; \ell' k)\, W(s_2' 2 s_1' 2; \tfrac{1}{2}k)\, W(2222;0k) (212{-}1|k0)$$

$$\cdot\, P_k(\theta) J_k \langle s_1' \ell' \rangle \langle s_2' \ell' \rangle^* .$$

In eqns. 2.4-2.7, the $\bar{Z}$ coefficients are the Z coefficients defined by Blatt and Biedenharn (1952) as corrected by Huby (1954), the W coefficients are Racah coefficients, the P_k coefficients are Legendre polynomials, and the J_k coefficients are the cylindrical attenuation coefficients defined in Ferguson (1965). Note that here and in equations to follow, $\vec{B}_1 = \vec{B}_2 = \vec{B}$, the spin of the compound nuclear state.

Consider the matrix elements in eqns. 2.4-2.7. If the entrance channel is $s_1 \ell_1$, then

$$\langle s_1' \ell_1' \rangle = \langle B s_1' \ell_1' | O_c | B s_1 \ell_1 \rangle \simeq \frac{\exp[i(\xi_{\ell_1} + \xi_{\ell_1'})]\ i g_1 g_1'}{E_o - E - i\Gamma/2}, \tag{2.8}$$

where $g_1 = \pm(\Gamma^{1/2}_{s_1 \ell_1})$ and $g_1' = \pm(\Gamma^{1/2}_{s_1' \ell_1'})$, $\Gamma_{s_1 \ell_1}$ and $\Gamma_{s_1' \ell_1'}$ are the partial laboratory widths, Γ is the total width, and E_o is the resonance energy. The ξ_ℓ's are energy dependent phase shifts which contain the Coulomb phase shift and a hard sphere phase shift:

$$\xi_\ell = -\tan^{-1}(F_\ell / G_\ell) + \sum_{m=1}^{\ell} \tan^{-1}(\eta/m), \tag{2.9}$$

where F_ℓ and G_ℓ are the regular and irregular radial wave functions, and η is the Coulomb parameter: $\eta = 0.1574\ Z_o Z_1 (M/E)^{1/2}$, where Z_o is the charge of the target nucleus, Z_1 is the charge on the incident particle, M is the mass of the incident particle in amu, and E is the incident particle energy in MeV in the laboratory frame. The products of matrix elements in eqns. 2.4-2.7 are therefore:

$$\langle s_1' \ell_1' \rangle \langle s_2' \ell_2' \rangle^* = \langle B s_1' \ell_1' | O_c | B s_1 \ell_1 \rangle \langle B s_2' \ell_2' | O_c | B s_2 \ell_2 \rangle^* \tag{2.10}$$

$$\simeq \frac{\cos(\xi_{\ell_1} + \xi_{\ell_2} - \xi_{\ell_1'} - \xi_{\ell_2'})}{(E_o - E)^2 + \Gamma^2/4}\ g_1 g_2 g_1' g_2' \ .$$

Also, define

$$Y = \frac{\langle Bs_1'\ell_1'|O_c|Bs_1\ell_1\rangle}{\langle Bs_2'\ell_2'|O_c|Bs_2\ell_2\rangle} \qquad (2.11)$$

$$= \cos(\xi_{\ell_1} + \xi_{\ell_1'} - \xi_{\ell_2} - \xi_{\ell_2'}) \cdot \frac{g_1 g_1'}{g_2 g_2'} \ .$$

Now, $\Gamma_{\ell c} = 2P_\ell \gamma_{\ell c}^2$, where P_ℓ is the Coulomb barrier penetrability and $\gamma_{\ell c}^2$ is the channel reduced width. If $\ell_1=\ell_2$, $s_1=s_2$, and $\ell_1'=\ell_2'$, then $Y = \gamma_{s_1'\ell}/\gamma_{s_2'\ell} = \delta$. The mixing ratio δ is defined as the ratio of two channel reduced width amplitudes. In the case where $\ell_1=\ell_2$, $s_1=s_2$, but $\ell_1'\neq\ell_2'$,

$$Y = \cos(\xi_{\ell_1'} - \xi_{\ell_2'}) \left[\frac{P(\ell_1')}{P(\ell_2')}\right]^{1/2} \delta \qquad (2.12)$$

$$= \text{phase} \cdot P^{1/2} \cdot \delta \ ,$$

$$\text{where phase} = \cos(\xi_{\ell_1'} - \xi_{\ell_2'}) \ , \text{ and } P = \frac{P(\ell_1')}{P(\ell_2')} \ .$$

If for two given ℓ' values P and phase are small, then contributions from the higher ℓ' value can be neglected. Values of P are listed in table 2.1 for p-wave resonances for $\ell'=1$ and $\ell'=3$. Contributions from $\ell'=3$ are neglected in the calculations for p-wave resonances. Values of phase and P are listed in table 2.2 for d-wave resonances for $\ell'=0$ and $\ell'=2$, in table 2.3 for f-wave resonances for $\ell'=1$ and $\ell'=3$, and in table 2.4 for g-wave resonances for $\ell'=2$ and $\ell'=4$. Contributions from $\ell'=4$ have been neglected for d-wave resonances, contributions from $\ell'=5$ have been neglected for f-wave resonances, and contributions from $\ell'=6$ have been neglected for g-wave resonances. For consistency of notation, all widths, reduced widths, and reduced width amplitudes will be labeled by representation, ℓ' value, and twice the j or s value: for example, γ(channel spin representation, $\ell'=0, s=3/2) = \gamma_{s03}$.

TABLE 2.1

VALUES OF THE PENETRABILITY RATIO FOR p-WAVE RESONANCES

Resonance Number	E_p (MeV)	P P(3)/P(1)
M1	3.0594	0.021
M3	3.1075	0.022
M4	3.1125	0.022
M5	3.1634	0.023
M6	3.1668	0.023
M7	3.1872	0.023
M8	3.2148	0.024
5	3.2691	0.024
7	3.2923	0.025
9	3.2980	0.025
13	3.3454	0.026
21	3.4095	0.027
32	3.5074	0.028
37	3.5413	0.029
41	3.5538	0.029
47	3.5779	0.030
56	3.6385	0.031
60	3.6503	0.031
63	3.6642	0.031
69	3.6947	0.032
77	3.7399	0.033

TABLE 2.1 (continued)

Resonance Number	E_p (MeV)	P P(3)/P(1)
83	3.7600	0.033
87	3.7763	0.034
88	3.7801	0.034
94	3.8051	0.034
95	3.8111	0.034
116	3.9240	0.037
117	3.9329	0.037
125	3.9812	0.038
135	4.0156	0.039
136	4.0177	0.039
143	4.0722	0.040
147	4.0948	0.041
158	4.1893	0.043
162	4.2158	0.044
175	4.2953	0.046

TABLE 2.2

VALUES OF THE PHASE FACTOR AND PENETRABILITY RATIO FOR d-WAVE RESONANCES

Resonance Number	E_p (MeV)	Phase $\cos(\xi_0 - \xi_2)$	P P(2)/P(0)
2	3.2594	−0.477	0.097
6	3.2867	−0.473	0.098
8	3.2946	−0.472	0.099
16	3.3693	−0.463	0.102
18	3.3745	−0.463	0.103
22	3.4177	−0.457	0.105
26	3.4549	−0.453	0.107
27	3.4697	−0.451	0.108
29	3.4767	−0.451	0.108
33	3.5150	−0.447	0.110
42	3.5554	−0.442	0.112
45	3.5657	−0.441	0.113
48	3.5850	−0.439	0.114
49	3.5958	−0.438	0.115
55	3.6157	−0.436	0.116
59	3.6472	−0.433	0.118
61	3.6532	−0.432	0.118
62	3.6549	−0.432	0.118
65	3.6732	−0.430	0.119
66	3.6750	−0.430	0.119

TABLE 2.2 (continued)

Resonance Number	E_p (MeV)	Phase $\cos(\xi_0 - \xi_2)$	P P(2)/P(0)
68	3.6823	-0.430	0.120
70	3.7074	-0.427	0.121
71	3.7099	-0.427	0.121
73	3.7224	-0.426	0.122
75	3.7321	-0.425	0.123
78	3.7440	-0.424	0.123
80	3.7528	-0.423	0.124
81	3.7540	-0.423	0.124
82	3.7578	-0.423	0.124
84	3.7662	-0.422	0.125
89	3.7876	-0.420	0.126
92	3.7960	-0.420	0.127
96	3.8135	-0.418	0.128
100	3.8314	-0.417	0.129
101	3.8336	-0.417	0.129
103	3.8399	-0.416	0.129
106	3.8606	-0.414	0.131
107	3.8635	-0.414	0.131
110	3.8815	-0.413	0.132
114	3.9067	-0.411	0.134
115	3.9176	-0.410	0.134
118	3.9500	-0.408	0.137

TABLE 2.2 (continued)

Resonance Number	E_p (MeV)	Phase $\cos(\xi_0 - \xi_2)$	P P(2)/P(0)
120	3.9622	-0.407	0.137
121	3.9677	-0.407	0.138
122	3.9703	-0.406	0.138
123	3.9758	-0.406	0.138
130	3.9984	-0.405	0.140
134	4.0133	-0.404	0.141
138	4.0338	-0.402	0.142
141	4.0613	-0.401	0.144
150	4.1302	-0.397	0.149
151	4.1401	-0.396	0.150
152	4.1619	-0.395	0.152
160	4.2036	-0.393	0.155
161	4.2105	-0.393	0.155
164	4.2200	-0.392	0.156
165	4.2355	-0.391	0.157
173	4.2779	-0.390	0.160

TABLE 2.3

VALUES OF THE PHASE FACTOR AND PENETRABILITY RATIO FOR f-WAVE RESONANCES

Resonance Number	E_p (MeV)	Phase $\cos(\xi_1 - \xi_3)$	P P(3)/P(1)
10	3.3149	0.019	0.025
12	3.3323	0.022	0.025
40	3.5518	0.060	0.029
86	3.7740	0.092	0.033
98	3.8233	0.099	0.035
109	3.8764	0.106	0.036
144	4.0788	0.130	0.040

TABLE 2.4

VALUES OF THE PHASE FACTOR AND PENETRABILITY RATIO FOR g-WAVE RESONANCES

Resonance Number	E_p (MeV)	Phase $\cos(\xi_2 - \xi_4)$	P P(4)/P(2)
1A	3.2461	0.339	0.007
1	3.2587	0.341	0.008

B. Angular Correlations for Compound Nuclear States

Three transitions are involved in the $^{50}Cr(p,p'\gamma)^{50}Cr$ reaction. First, the target nucleus ^{50}Cr, in its ground state (0^+), captures the incident proton and forms an excited state in the compound nucleus ^{51}Mn. The compound nucleus decays by emission of a proton, leaving the target nucleus in its first excited state (2^+). The target nucleus then decays back to its ground state by emission of a γ-ray. The compound nuclear states created in this reaction can have a variety of angular momenta, and there is usually more than one inelastic decay channel open for the emitted proton.

1. p-wave Resonances

The angular momentum coupling schemes when the incident proton has $\ell = 1$ are shown in figure 2.1. The angular correlation equations have the form:

$$W_p(\theta) = a_{op}(1 + a_{2p}P_2) \tag{2.13}$$

$$W_\gamma(\theta) = a_{o\gamma}(1 + a_{2\gamma}P_2), \tag{2.14}$$

where the P's are Legendre polynomials. If $\ell = 1$, then resonances may be formed in ^{51}Mn with spin and parity $1/2^-$ or $3/2^-$. For $1/2^-$ resonances, $a_{2p} = a_{2\gamma} = 0$, and there is only one exit channel. For $3/2^-$ resonances, at least one of the a_2 coefficients must be non-zero. There are two open exit channels, as shown in figure 2.1. The mixing ratio is defined as $\delta_j = \gamma_{j13}/\gamma_{j11}$ in the total angular momentum representation, and as $\delta_s = \gamma_{s15}/\gamma_{s13}$ in the channel spin representation. In terms of the mixing ratios, the a_2 coefficients become:

$$a_{2p} = \frac{-\frac{1}{5}(4\delta_j + 3\delta_j^2)}{1 + \delta_j^2}, \qquad a_{2\gamma} = \frac{\frac{1}{2}Q_2}{1 + \delta_j^2} \tag{2.15}$$

in the total angular momentum representation, and

FIGURE 2.1 Energy level scheme and angular momentum coupling schemes for the reaction $^{50}Cr(p,p'\gamma)^{50}Cr$ when the incident proton has $\ell=1$.

ANGULAR MOMENTUM COUPLING FOR $\ell = 1$ RESONANCES

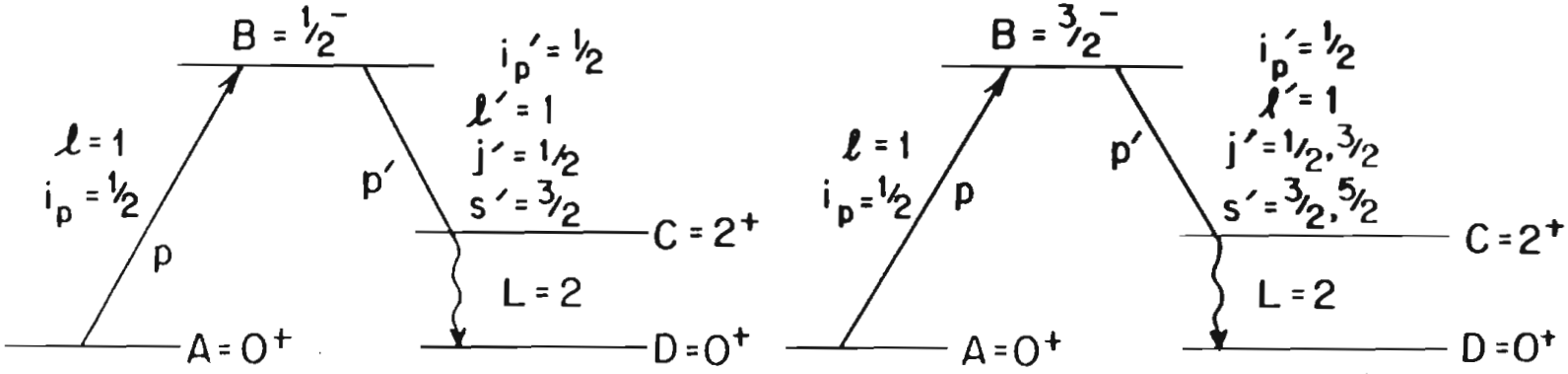

	ENTRANCE CHANNEL	EXIT CHANNEL
CHANNEL SPIN REPRESENTATION	$\vec{s} = \vec{A} + \vec{i}_p$ $\vec{B} = \vec{s} + \vec{\ell}$	$\vec{s}' = \vec{C} + \vec{i}_p'$ $\vec{B} = \vec{s}' + \vec{\ell}'$
TOTAL ANGULAR MOMENTUM REPRESENTATION	$\vec{j} = \vec{\ell} + \vec{i}_p$ $\vec{B} = \vec{A} + \vec{j}$	$\vec{j}' = \vec{\ell}' + \vec{i}_p'$ $\vec{B} = \vec{C} + \vec{j}'$

$$a_{2p} = \frac{\frac{1}{5}(\delta_s^2 - 4)}{1 + \delta_s^2}, \qquad a_{2\gamma} = \frac{\frac{1}{10}(1 - 2\delta_s)^2 Q_2}{1 + \delta_s^2} \tag{2.16}$$

in the channel spin representation. Q_2 is an attenuation coefficient (Ferguson 1965). For the charged particle detectors, the angular spread is so small that the finite geometry effect is neglected. The mixing ratios may be transformed from one representation to the other with the following equations:

$$\delta_j = \frac{2 + \delta_s}{1 - 2\delta_s}, \qquad \delta_s = \frac{-2 + \delta_j}{1 + 2\delta_j}. \tag{2.17}$$

The variable $\phi = \tan^{-1}\delta$ proves convenient: the range of ϕ is $-90^\circ \leq \phi \leq 90^\circ$. The transformation from ϕ_j to ϕ_s is: $\phi_j = \phi_s - \tan^{-1}(-2)$. Transformations from one representation to the other thus correspond to rotations by 63.4°.

2. d-wave Resonances

The angular momentum coupling schemes when the incident proton has $\ell = 2$ are shown in figure 2.2. The angular correlation equations have the form:

$$W_p(\theta) = a_{op}(1 + a_{2p}P_2 + a_{4p}P_4) \tag{2.18}$$

$$W_\gamma(\theta) = a_{o\gamma}(1 + a_{2\gamma}P_2 + a_{4\gamma}P_4). \tag{2.19}$$

If $\ell = 2$, then resonances may be formed in ^{51}Mn with spin and parity $3/2^+$ or $5/2^+$. For $3/2^+$ resonances, $a_{4p} = a_{4\gamma} = 0$. There are three open exit channels for $3/2^+$ resonances, as shown in figure 2.2. The mixing ratios are defined as: $\delta_{jBA} = \gamma_{j23}/\gamma_{j01}$, $\delta_{jCA} = \gamma_{j25}/\gamma_{j01}$, and $\delta_{jCB} = \gamma_{j25}/\gamma_{j23}$ in the total angular momentum representation, and as $\delta_{sBA} = \gamma_{s23}/\gamma_{s03}$, $\delta_{sCA} = \gamma_{s25}/\gamma_{s03}$ and $\delta_{sCB} = \gamma_{s25}/\gamma_{s23}$ in the channel spin representation. Only two of the mixing ratios are independent. In terms of the mixing ratios, the a_2 coefficients

FIGURE 2.2 Energy level scheme and angular momentum coupling schemes for the reaction $^{50}Cr(p,p'\gamma)^{50}Cr$ when the incident proton has $\ell=2$.

ANGULAR MOMENTUM COUPLING FOR $\ell = 2$ RESONANCES

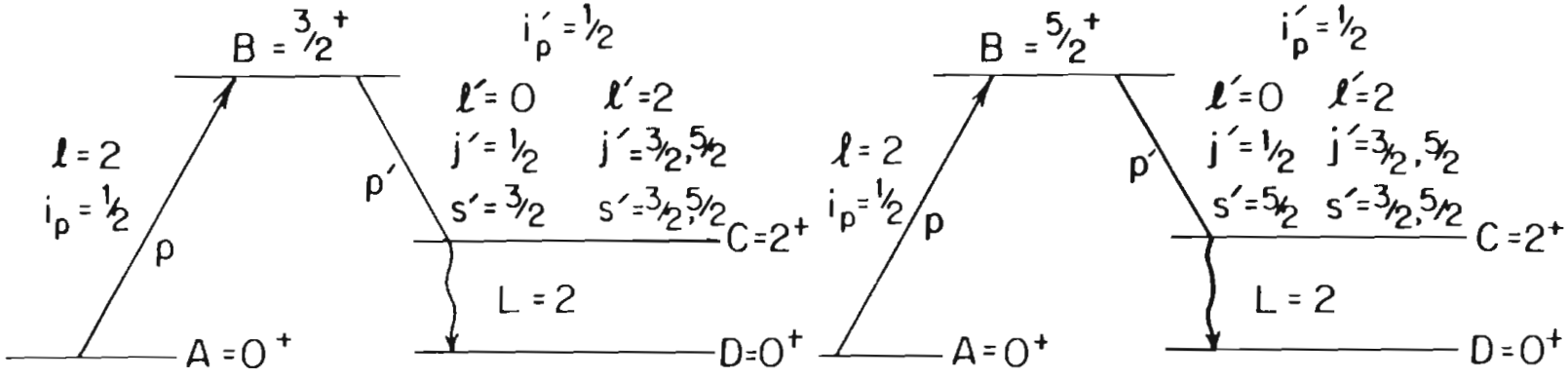

	ENTRANCE CHANNEL	EXIT CHANNEL
CHANNEL SPIN REPRESENTATION	$\vec{s} = \vec{A} + \vec{i}_p$ $\vec{B} = \vec{s} + \vec{\ell}$	$\vec{s}' = \vec{C} + \vec{i}'_p$ $\vec{B} = \vec{s}' + \vec{\ell}'$
TOTAL ANGULAR MOMENTUM REPRESENTATION	$\vec{j} = \vec{\ell} + \vec{i}_p$ $\vec{B} = \vec{A} + \vec{j}$	$\vec{j}' = \vec{\ell}' + \vec{i}'_p$ $\vec{B} = \vec{C} + \vec{j}'$

become:

$$a_{2p} = \frac{[-\frac{3}{5}P\delta^2_{jBA} - \frac{4}{35}P\delta^2_{jCA} + \frac{4}{35}\sqrt{21}\,P\delta_{jBA}\delta_{jCA}]}{1 + P\delta^2_{jBA} + P\delta^2_{jCA}} \tag{2.20}$$

$$- \frac{[\frac{4}{5}\delta_{jBA} + \frac{2}{5}\sqrt{21}\,\delta_{jCA}]P^{1/2}\cos(\xi_0 - \xi_2)}{1 + P\delta^2_{jBA} + P\delta^2_{jCA}} ,$$

$$a_{2\gamma} = \frac{[\frac{1}{2} - \frac{5}{14}P\delta^2_{jCA}]\,Q_2}{1 + P\delta^2_{jBA} + P\delta^2_{jCA}} , \tag{2.21}$$

in the total angular momentum representation, and

$$a_{2p} = \frac{-2P^{1/2}\cos(\xi_0 - \xi_2)\delta_{sBA} - \frac{5}{7}P\delta^2_{sCA}}{1 + P\delta^2_{sBA} + P\delta^2_{sCA}}, \tag{2.22}$$

$$a_{2\gamma} = \frac{[\frac{1}{2} - \frac{3}{10}P\delta^2_{sBA} - \frac{2}{35}P\delta^2_{sCA} - \frac{2}{35}\sqrt{21}\,P\delta_{sBA}\delta_{sCA}]\,Q_2}{1 + P\delta^2_{sBA} + P\delta^2_{sCA}} , \tag{2.23}$$

in the channel spin representation. By convention, δ_{BA} and δ_{CA} are used in these definitions. In all four of these equations, $P = P(2)/P(0)$, the ratio of Coulomb penetrabilities, and $\cos(\xi_0 - \xi_2)$ is the phase factor resulting from the multiplication of matrix elements. These equations and others to follow were derived by Chou (1980) and by J. F. Shriner, Jr.

It is convenient to define mixing angles ϕ, where $\phi_{BA} = \tan^{-1}\delta_{BA}$, $\phi_{CA} = \tan^{-1}\delta_{CA}$, and $\phi_{CB} = \tan^{-1}\delta_{CB}$ in each representation, and the range of ϕ is $-90^\circ \leq \phi \leq 90^\circ$. The transformation between representations is particularly simple in terms of the mixing angles: $\phi_{jCB} = \phi_{sCB} + 66.42^\circ$.

Since the a_4 coefficients are identically zero for the $3/2^+$ resonances, there is only one quadratic equation from each experiment for the two independent variables δ_{BA} and δ_{CA}. Therefore, the experiment provides

insufficient information to determine a unique solution for the mixing ratios for $3/2^+$ resonances.

For $5/2^+$ resonances, there are two quadratic equations for the two independent variables δ_{BA} and δ_{CA} for each experiment. Therefore, unique solutions for the two mixing ratios can be obtained. There are three exit channels for $5/2^+$ resonances, as shown in figure 2.2. The mixing ratios are defined as $\delta_{jBA} = \gamma_{j23}/\gamma_{j01}$, $\delta_{jCA} = \gamma_{j25}/\gamma_{j01}$, and $\delta_{jCB} = \gamma_{j25}/\gamma_{j23}$ in the total angular momentum representation, and as $\delta_{sBA} = \gamma_{s23}/\gamma_{s05}$, $\delta_{sCA} = \gamma_{s25}/\gamma_{s05}$, and $\delta_{sCB} = \gamma_{s25}/\gamma_{s23}$ in the channel spin representation. Only two mixing ratios are independent. In terms of the mixing ratios, the a_2 and a_4 coefficients become, in the total angular momentum representation:

$$a_{2p} = \frac{[-\frac{4}{35}P\delta_{jBA}^2 + \frac{4}{35}P\delta_{jCA}^2 + \frac{192}{245}P\delta_{jBA}\delta_{jCA}]}{1 + P\delta_{jBA}^2 + P\delta_{jCA}^2} + \frac{[\frac{16}{35}\sqrt{14}\,\delta_{jBA} - \frac{12}{35}\sqrt{14}\,\delta_{jCA}]\,P^{1/2}\cos(\xi_0 - \xi_2)}{1 + P\delta_{jBA}^2 + P\delta_{jCA}^2}, \tag{2.24}$$

$$a_{4p} = \frac{-\frac{3}{7}P\delta_{jCA}^2 - \frac{72}{49}P\delta_{jBA}\delta_{jCA}}{1 + P\delta_{jBA}^2 + P\delta_{jCA}^2}, \tag{2.25}$$

$$a_{2\gamma} = \frac{[\frac{4}{7} + \frac{10}{49}P\delta_{jBA}^2 - \frac{10}{49}P\delta_{jCA}^2]\,Q_2}{1 + P\delta_{jBA}^2 + P\delta_{jCA}^2}, \tag{2.26}$$

$$a_{4\gamma} = \frac{[-\frac{4}{7} + \frac{32}{49}P\delta_{jBA}^2 - \frac{18}{49}P\delta_{jCA}^2]\,Q_4}{1 + P\delta_{jBA}^2 + P\delta_{jCA}^2}. \tag{2.27}$$

In the channel spin representation, the a_2 and a_4 coefficients are:

$$a_{2p} = \frac{\frac{20}{49}P(\delta_{sBA}^2 - \delta_{sCA}^2) - \frac{4}{7}\sqrt{14}\,P^{1/2}\cos(\xi_0 - \xi_2)\delta_{sCA}}{1 + P\delta_{sBA}^2 + P\delta_{sCA}^2}, \tag{2.28}$$

$$a_{4p} = \frac{-\frac{48}{49}P\delta^2_{sBA} + \frac{27}{49}P\delta^2_{sCA}}{1 + P\delta^2_{sBA} + P\delta^2_{sCA}}, \tag{2.29}$$

$$a_{2\gamma} = \frac{[\frac{4}{7} - \frac{2}{35}P\delta^2_{sBA} + \frac{2}{35}P\delta^2_{sCA} - \frac{96}{245}P\delta_{sBA}\delta_{sCA}]\ Q_2}{1 + P\delta^2_{sBA} + P\delta^2_{sCA}}, \tag{2.30}$$

$$a_{4\gamma} = \frac{[-\frac{4}{7} + \frac{2}{7}P\delta^2_{sCA} - \frac{48}{49}P\delta_{sBA}\delta_{sCA}]\ Q_4}{1 + P\delta^2_{sBA} + P\delta^2_{sCA}}. \tag{2.31}$$

Again, $P = P(2)/P(0)$, the ratio of Coulomb penetrabilities, $\cos(\xi_0 - \xi_2)$ is the phase factor resulting from the multiplication of matrix elements, and Q_2 and Q_4 are attenuation coefficients. It is convenient to define mixing angles ϕ such that $\phi_{BA} = \tan^{-1}\delta_{BA}$, $\phi_{CA} = \tan^{-1}\delta_{CA}$, and $\phi_{CB} = \tan^{-1}\delta_{CB}$ in each representation, and the range of ϕ is $-90^\circ \leq \phi \leq 90^\circ$. The transformation between representations is: $\phi_{jCB} = \phi_{sCB} + 53.13^\circ$. One can also define a variable ε^2, which is a measure of the $\ell'=2$ admixture in the decay: $\varepsilon^2 = (\gamma^2_{j23} + \gamma^2_{j25})/(\gamma^2_{j01} + \gamma^2_{j23} + \gamma^2_{j25})$. Note that for d-wave resonances ε^2 is not an independent parameter, and that the penetrability factors have been removed from its definition.

Due to the requirement that the mixing ratios be real, there are restrictions on the physical range of the a_2 and a_4 coefficients. Figure 2.3 shows a plot of the experimental a_2 coefficients versus the experimental a_4 coefficients for both the inelastically scattered protons and the γ-rays. The solid lines define the physically allowed region. For inelastically scattered protons, the origin ($a_{2p} = 0, a_{4p} = 0$) corresponds to $\varepsilon^2=0$, that is, no $\ell'=2$ admixture in the decay. For the γ-ray coefficients, the point $a_{2\gamma} = 4/7$, $a_{4\gamma} = -4/7$ (the lower right corner of the triangle) corresponds to $\varepsilon^2=0$. Since the ratio of Coulomb penetrabilities P(2)/P(0) ranges from 0.097 to 0.161 for

FIGURE 2.3 Experimental Legendre coefficients for proton and γ-ray distributions for the 38 resonances in ^{51}Mn assigned $J^{\pi} = 5/2^{+}$. The solid lines show the physically allowed regions.

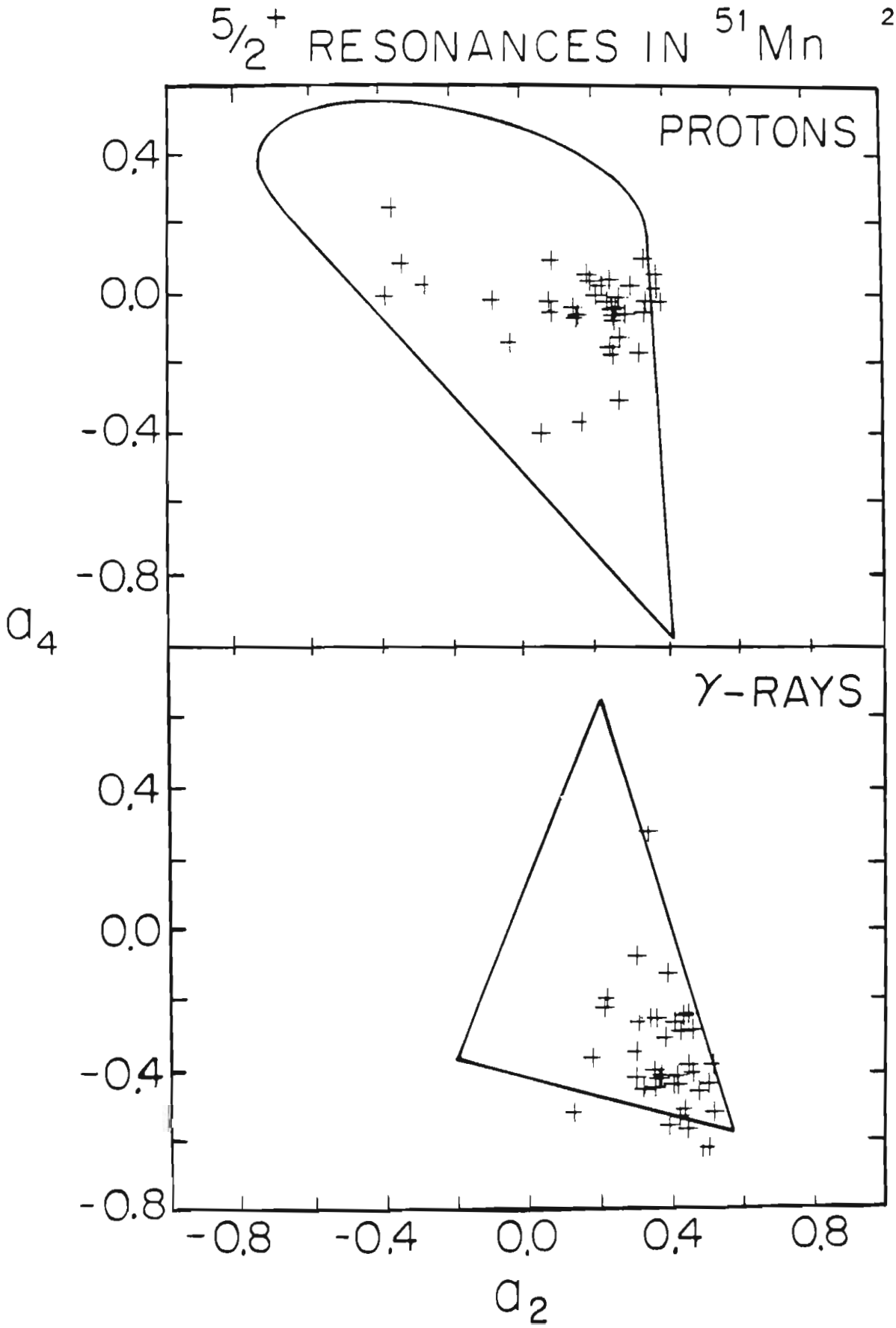
5/2+ RESONANCES IN 51Mn
PROTONS
γ-RAYS
0.4
0.0
-0.4
-0.8
a4
a2
-0.8
-0.4
0.0
0.4
0.8

d-wave resonances in the energy range studied, the $\ell'=2$ admixture is expected to be fairly small.

It is possible for both a_4 coefficients for a $5/2^+$ resonance to be zero. If this occurs, the mixing ratios and hence the a_2 coefficients are restricted to certain fixed values. If $a_{4p}= a_{4\gamma}= 0$, then $a_{2p}= -0.053 \pm 0.853\cos(\xi_0 - \xi_2)$, and $a_{2\gamma}= 0.4$. If $a_{4\gamma}= 0$, then ε^2 is large; that is, there is a large $\ell'=2$ admixture for the resonance. As noted previously, a large $\ell'=2$ admixture is unlikely for resonances in the energy range studied. No resonances were found which satisfied the above conditions. Therefore, all resonances for which $a_{4p}= a_{4\gamma}= 0$ were assigned $J^\pi= 3/2^+$.

3. f-wave Resonances

The angular momentum coupling schemes for incident particles with $\ell= 3$ are shown in figure 2.4. The angular correlation equations have the form

$$W_p(\Theta) = a_{op}(1 + a_{2p}P_2 + a_{4p}P_4 + a_{6p}P_6) , \qquad (2.32)$$

$$W_\gamma(\Theta) = a_{o\gamma}(1 + a_{2\gamma}P_2 + a_{4\gamma}P_4) . \qquad (2.33)$$

If $\ell= 3$, then resonances may be formed in ^{51}Mn with spin and parity $5/2^-$ or $7/2^-$. For $5/2^-$ resonances $a_{6p}= 0$. There are four open exit channels, as shown in figure 2.4. Two independent mixing ratios are defined: $\delta_{jL}= \gamma_{j13}/\gamma_{j11}$ and $\delta_{jU}= \gamma_{j37}/\gamma_{j35}$ in the total angular momentum representation, and $\delta_{sL}= \gamma_{s15}/\gamma_{s13}$ and $\delta_{sU}= \gamma_{s35}/\gamma_{s33}$ in the channel spin representation. One can also define ε^2, an independent parameter which is a measure of the admixture of $\ell'=3$ in the decay: $\varepsilon^2= (\Gamma_{j35}+ \Gamma_{j37})/\Gamma_p$, in the total angular momentum representation. In terms of the mixing ratios and ε^2, the a_2 and a_4 coefficients are:

FIGURE 2.4 Energy level scheme and angular momentum coupling schemes for the reaction $^{50}Cr(p,p'\gamma)^{50}Cr$ when the incident proton has $\ell=3$.

ANGULAR MOMENTUM COUPLING FOR $\ell = 3$ RESONANCES

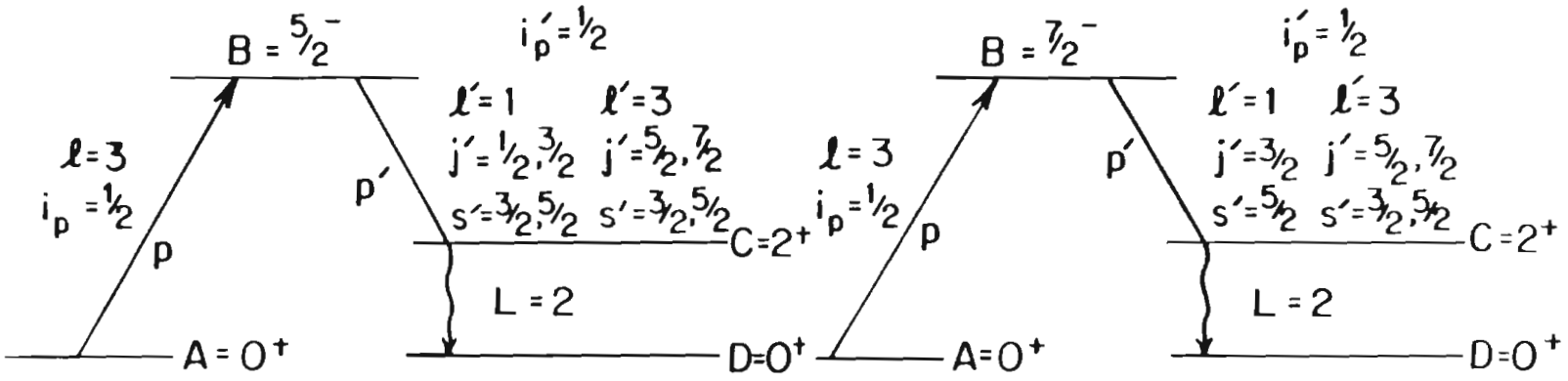

	ENTRANCE CHANNEL	EXIT CHANNEL
CHANNEL SPIN REPRESENTATION	$\vec{s} = \vec{A} + \vec{i}_p$ $\vec{B} = \vec{s} + \vec{\ell}$	$\vec{s}' = \vec{C} + \vec{i}'_p$ $\vec{B} = \vec{s}' + \vec{\ell}'$
TOTAL ANGULAR MOMENTUM REPRESENTATION	$\vec{j} = \vec{\ell} + \vec{i}_p$ $\vec{B} = \vec{A} + \vec{j}$	$\vec{j}' = \vec{\ell}' + \vec{i}'_p$ $\vec{B} = \vec{C} + \vec{j}'$

$$a_{2p} = (1 - \varepsilon^2)\frac{[\frac{16}{5}\sqrt{\frac{2}{7}}\,\delta_{jBA} - \frac{4}{35}\delta^2_{jBA}]}{1 + \delta^2_{jBA}} \tag{2.34}$$

$$+ \varepsilon^2\frac{[\frac{4}{35} + \frac{8}{35}\sqrt{6}\,\delta_{jCA} + \frac{10}{21}\delta^2_{jCA}]}{1 + \delta^2_{jCA}}$$

$$+ [\varepsilon^2(1 - \varepsilon^2)]^{1/2}\frac{[\frac{192}{245}\delta_{jBA} - \frac{108}{245}\sqrt{6}\,\delta_{jBA}\delta_{jCA} - \frac{12}{5}\sqrt{\frac{2}{7}}]\cos(\xi_1 - \xi_3)}{(1 + \delta^2_{jBA})^{1/2}(1 + \delta^2_{jCA})^{1/2}}$$

$$a_{4p} = [\varepsilon^2(1 - \varepsilon^2)]^{1/2} \tag{2.35}$$

$$\cdot \frac{[-\frac{72}{49}\delta_{jBA} - \frac{8}{21}\sqrt{21}\,\delta_{jCA} - \frac{50}{49}\sqrt{\frac{2}{3}}\,\delta_{jBA}\delta_{jCA}]\cos(\xi_1 - \xi_3)}{(1 + \delta^2_{jBA})^{1/2}(1 + \delta^2_{jCA})^{1/2}}$$

$$- \frac{3}{7}\varepsilon^2,$$

$$a_{2\gamma} = (1 - \varepsilon^2)\frac{[\frac{4}{7} + \frac{10}{49}\delta^2_{jBA}]}{1 + \delta^2_{jBA}}\,Q_2 \quad - \quad \varepsilon^2\frac{[\frac{10}{49} - \frac{17}{49}\delta^2_{jCA}]}{1 + \delta^2_{jCA}}\,Q_2\,, \tag{2.36}$$

$$a_{4\gamma} = (1 - \varepsilon^2)\frac{[-\frac{4}{7} + \frac{32}{49}\delta^2_{jBA}]}{1 + \delta^2_{jBA}}\,Q_4 \quad + \quad \varepsilon^2\frac{[-\frac{18}{49} + \frac{16}{147}\delta^2_{jCA}]}{1 + \delta^2_{jCA}}\,Q_4, \tag{2.37}$$

in the total angular momentum representation, and

$$a_{2p} = (1 - \varepsilon^2)\frac{[\frac{4}{5} - \frac{32}{35}\delta^2_{sBA}]}{1 + \delta^2_{sBA}} + \varepsilon^2\frac{[\frac{22}{35} - \frac{4}{105}\delta^2_{sCA}]}{1 + \delta^2_{sCA}} \tag{2.38}$$

$$- [\varepsilon^2(1 - \varepsilon^2)]^{1/2}\frac{[\frac{12}{35}\sqrt{6} + \frac{108}{35}\sqrt{\frac{2}{7}}\,\delta_{sBA}\delta_{sCA}]\cos(\xi_1 - \xi_3)}{(1 + \delta^2_{sBA})^{1/2}(1 + \delta^2_{sCA})^{1/2}},$$

$$a_{4p} = -\frac{3}{7}\varepsilon^2 \tag{2.39}$$

$$+ [\varepsilon^2(1-\varepsilon^2)]^{1/2}\frac{[-\frac{6}{7}\sqrt{6} + \frac{16}{7}\sqrt{\frac{2}{7}}\,\delta_{sBA}\delta_{sCA}]}{(1+\delta_{sBA}^2)^{1/2}(1+\delta_{sCA}^2)^{1/2}}$$

$$\cdot \cos(\xi_1 - \xi_3),$$

$$a_{2\gamma} = (1-\varepsilon^2)\frac{[\frac{2}{5} - \frac{24}{35}\sqrt{\frac{2}{7}}\,\delta_{sBA} + \frac{92}{245}\delta_{sBA}^2]}{1+\delta_{sBA}^2} Q_2 \tag{2.40}$$

$$-\varepsilon^2\frac{[\frac{11}{35} + \frac{12}{245}\sqrt{6}\,\delta_{sCA} + \frac{58}{245}\delta_{sCA}^2]}{1+\delta_{sCA}^2} Q_2,$$

$$a_{4\gamma} = (1-\varepsilon^2)\frac{[\frac{16}{7}\sqrt{\frac{2}{7}}\,\delta_{sBA} + \frac{4}{49}\delta_{sBA}^2]}{1+\delta_{sBA}^2} Q_4 \tag{2.41}$$

$$+\varepsilon^2\frac{[\frac{8}{49}\sqrt{6}\,\delta_{sCA} - \frac{38}{147}\delta_{sCA}^2]}{1+\delta_{sCA}^2} Q_4,$$

in the channel spin representation. These equations were derived by J. F. Shriner, Jr. and W. A. Watson (Watson et al. 1980). For convenience, one may define mixing angles ϕ, where $\phi_L = \tan^{-1}\delta_L$ and $\phi_U = \tan^{-1}\delta_U$ in each representation. The range of ϕ_L is $-90^\circ \leq \phi_L \leq 90^\circ$, and the range of ϕ_U is $-180^\circ \leq \phi_U \leq 180^\circ$. The transformation form one representation to the other is linear in terms of the mixing angles: $\phi_{jL} = \phi_{sL} + 43.1^\circ$, and $\phi_{jU} = \phi_{sU} + 61.4^\circ$. All f-wave resonances studied in these experiments were assigned $J^\pi = 5/2^-$.

4. g-wave Resonances

The angular momentum coupling schemes when the incident proton has $\ell = 4$

are shown in figure 2.5. The angular correlation equations have the form:

$$W_p(\theta) = a_{op}(1 + a_{2p}P_2 + a_{4p}P_4 + a_{6p}P_6 + a_{8p}P_8) \ , \tag{2.42}$$

$$W_\gamma(\theta) = a_{o\gamma}(1 + a_{2\gamma}P_2 + a_{4\gamma}P_4). \tag{2.43}$$

If $\ell = 4$, then resonances may be formed in ^{51}Mn with spin and parity $7/2^+$ or $9/2^+$. For $7/2^+$ resonances, $a_{8p} = 0$, and there are four open exit channels, as shown in figure 2.5. The mixing ratios are defined as: $\delta_{jL} = \gamma_{j25}/\gamma_{j23}$ and $\delta_{jU} = \gamma_{j49}/\gamma_{j47}$ in the total angular momentum representation, and $\delta_{sL} = \gamma_{s25}/\gamma_{s23}$ and $\delta_{sU} = \gamma_{s45}/\gamma_{s43}$ in the channel spin representation. One can also define ε^2, an independent parameter which is a measure of the $\ell'=4$ admixture for each resonance: $\varepsilon^2 = (\Gamma_{j47} + \Gamma_{j49})/\Gamma_p$, in the total angular momentum representation. In terms of the mixing ratios and ε^2, the a_2, a_4, and a_6 coefficients are:

$$a_{2p} = (1 - \varepsilon^2)\frac{[\frac{5}{7} + \frac{40}{49}\delta_{jL} + \frac{10}{21}\delta_{jL}^2]}{1 + \delta_{jL}^2} \tag{2.44}$$

$$+ \varepsilon^2\frac{[\frac{5}{9} + \frac{580}{4851}\sqrt{11}\,\delta_{jU} + \frac{530}{693}\delta_{jU}^2]}{1 + \delta_{jU}^2}$$

$$+ [\varepsilon^2(1 - \varepsilon^2)]^{1/2}\frac{[-\frac{20}{49}\sqrt{3} + \frac{20}{63}\sqrt{3}\,\delta_{jL} - \frac{50}{147}\sqrt{\frac{11}{3}}\,\delta_{jL}\delta_{jU}]}{(1 + \delta_{jL}^2)^{1/2}(1 + \delta_{jU}^2)^{1/2}}$$

$$\cdot \cos(\xi_2 - \xi_4) \ ,$$

FIGURE 2.5 Energy level scheme and angular momentum coupling schemes for the reaction $^{50}Cr(p,p'\gamma)^{50}Cr$ when the incident proton has $\ell=4$.

ANGULAR MOMENTUM COUPLING FOR $\ell = 4$ RESONANCES

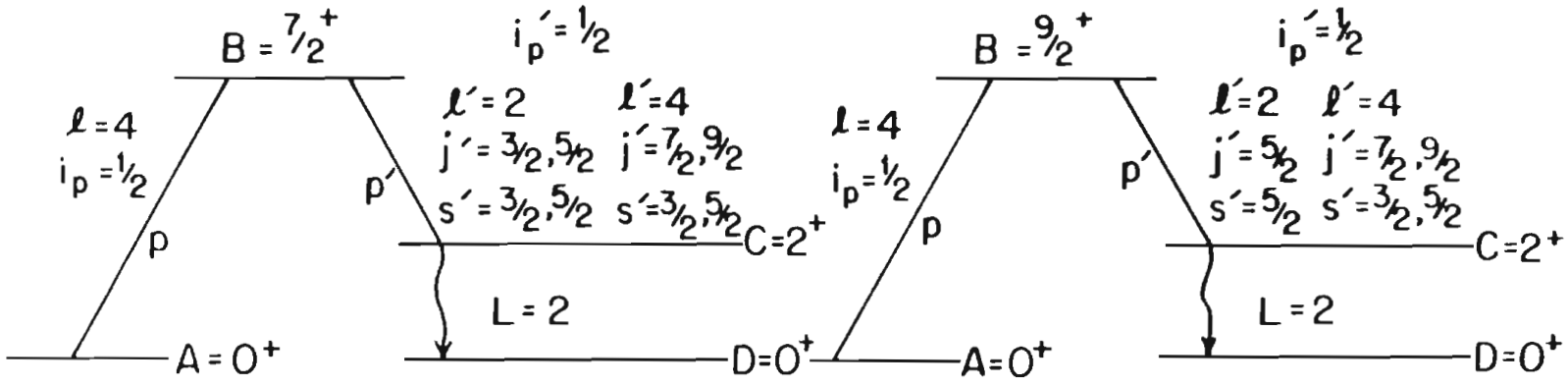

	ENTRANCE CHANNEL	EXIT CHANNEL
CHANNEL SPIN REPRESENTATION	$\vec{s} = \vec{A} + \vec{i}_p$ $\vec{B} = \vec{s} + \vec{\ell}$	$\vec{s}' = \vec{C} + \vec{i}_p'$ $\vec{B} = \vec{s}' + \vec{\ell}'$
TOTAL ANGULAR MOMENTUM REPRESENTATION	$\vec{j} = \vec{\ell} + \vec{i}_p$ $\vec{B} = \vec{A} + \vec{j}$	$\vec{j}' = \vec{\ell}' + \vec{i}_p'$ $\vec{B} = \vec{C} + \vec{j}'$

$$a_{4p} = [1 - \varepsilon^2]\frac{[\frac{72}{49}\delta_{jL} - \frac{3}{7}\delta_{jL}^2]}{1 + \delta_{jL}^2} \tag{2.45}$$

$$+ \varepsilon^2\frac{[-\frac{27}{77} + \frac{1080}{5929}\sqrt{11}\,\delta_{jU} - \frac{27}{847}\delta_{jU}^2]}{1 + \delta_{jU}^2}$$

$$+ [\varepsilon^2(1 - \varepsilon^2)]^{1/2}\cos(\xi_2 - \xi_4)$$

$$\cdot \frac{[-\frac{36}{49}\sqrt{3} + \frac{24}{77}\sqrt{3}\,\delta_{jL} - \frac{72}{77}\sqrt{\frac{3}{11}}\,\delta_{jU} - \frac{1308}{539}\sqrt{\frac{3}{11}}\,\delta_{jL}\delta_{jU}]}{(1 + \delta_{jL}^2)^{1/2}(1 + \delta_{jU}^2)^{1/2}},$$

$$a_{6p} = [\varepsilon^2(1 - \varepsilon^2)]^{1/2}\frac{[-\frac{100}{99}\sqrt{3}\,\delta_{jL} - \frac{40}{11}\sqrt{\frac{3}{11}}\,\delta_{jU} - \frac{70}{1089}\sqrt{33}\,\delta_{jL}\delta_{jU}]}{(1 + \delta_{jL}^2)^{1/2}(1 + \delta_{jU}^2)^{1/2}} \tag{2.46}$$

$$\cdot \cos(\xi_2 - \xi_4)$$

$$+ \varepsilon^2\frac{[-\frac{25}{99} - \frac{140}{1089}\sqrt{11}\,\delta_{jU} - \frac{520}{1089}\delta_{jU}^2]}{1 + \delta_{jU}^2},$$

$$a_{2\gamma} = (1 - \varepsilon^2)\frac{[\frac{25}{49} + \frac{25}{294}\delta_{jL}^2]}{1 + \delta_{jL}^2}\,Q_2 \quad + \quad \varepsilon^2\frac{[-\frac{40}{147} - \frac{95}{294}\delta_{jU}^2]}{1 + \delta_{jU}^2}\,Q_2, \tag{2.47}$$

$$a_{4\gamma} = (1 - \varepsilon^2)\frac{[-\frac{18}{49} + \frac{32}{49}\delta_{jL}^2]}{1 + \delta_{jL}^2}\,Q_4 \quad + \quad \varepsilon^2\frac{[-\frac{24}{49} + \frac{96}{539}\delta_{jU}^2]}{1 + \delta_{jU}^2}\,Q_4. \tag{2.48}$$

in the total angular momentum representation. In the channel spin representation,

$$a_{2p} = (1 - \varepsilon^2)\frac{[\frac{50}{49} + \frac{25}{147}\delta_{sL}^2]}{1 + \delta_{sL}^2} + \varepsilon^2\frac{[\frac{130}{147} + \frac{235}{539}\delta_{sU}^2]}{1 + \delta_{sU}^2} \tag{2.49}$$

$$+ [\varepsilon^2(1 - \varepsilon^2)]^{1/2}\frac{[-\frac{10}{49}\sqrt{5} - \frac{20}{147}\sqrt{55}\,\delta_{sL}\delta_{sU}]}{(1 + \delta_{sL}^2)^{1/2}(1 + \delta_{sU}^2)^{1/2}}$$

$$\cdot \cos(\xi_2 - \xi_4) ,$$

$$a_{4p} = (1 - \varepsilon^2)\frac{[\frac{27}{49} - \frac{48}{49}\delta_{sL}^2]}{1 + \delta_{sL}^2} + \varepsilon^2\frac{[\frac{81}{539} - \frac{3159}{5929}\delta_{sU}^2]}{1 + \delta_{sU}^2} \tag{2.50}$$

$$+ [\varepsilon^2(1 - \varepsilon^2)]^{1/2}\frac{[-\frac{324}{539}\sqrt{5} - \frac{1116}{539}\sqrt{\frac{5}{11}}\,\delta_{sL}\delta_{sU}]}{(1 + \delta_{sL}^2)^{1/2}(1 + \delta_{sU}^2)^{1/2}}$$

$$\cdot \cos(\xi_2 - \xi_4),$$

$$a_{6p} = [\varepsilon^2(1 - \varepsilon^2)]^{1/2}\frac{[-\frac{10}{11}\sqrt{5} + \frac{80}{33}\sqrt{\frac{5}{11}}\,\delta_{sL}\delta_{sU}]\cos(\xi_2 - \xi_4)}{(1 + \delta_{sL}^2)^{1/2}(1 + \delta_{sU}^2)^{1/2}} \tag{2.51}$$

$$+ \varepsilon^2\frac{[-\frac{20}{33} - \frac{15}{121}\delta_{sU}^2]}{1 + \delta_{sU}^2} ,$$

$$a_{2\gamma} = (1 - \varepsilon^2)\frac{[\frac{5}{14} - \frac{20}{49}\delta_{sL} + \frac{5}{21}\delta_{sL}^2]}{1 + \delta_{sL}^2}\,Q_2 \tag{2.52}$$

$$+ \varepsilon^2\frac{[-\frac{13}{42} - \frac{2}{147}\sqrt{11}\,\delta_{sU} - \frac{2}{7}\delta_{sU}^2]}{1 + \delta_{sU}^2}\,Q_2 .$$

$$a_{4\gamma} = (1 - \varepsilon^2)\frac{[\frac{48}{49}\delta_{sL} + \frac{2}{7}\delta_{sL}^2]}{1 + \delta_{sL}^2}\,Q_4 \tag{2.53}$$

$$+ \varepsilon^2\frac{[\frac{96}{539}\sqrt{11}\,\delta_{sU} - \frac{24}{77}\delta_{sU}^2]}{1 + \delta_{sU}^2}\,Q_4 .$$

These equations and the equations for $9/2^+$ resonances to follow were derived by J. F. Shriner, Jr. and P. Ramakrishnan. The mixing angles are $\phi_L = \tan^{-1}\delta_L$ and $\phi_U = \tan^{-1}\delta_U$ in each representation. The ranges of ϕ_L and ϕ_U are the same as for f-wave resonances. The transformation from one representation to the other in terms of the mixing angles is linear: $\phi_{jL} = \phi_{sL} + 36.9^\circ$, and $\phi_{jU} = \phi_{sU} + 58.9^\circ$.

A $9/2^+$ resonance has three open exit channels, as shown in figure 2.5. The system is specified by one mixing ratio, $\delta_{jU} = \gamma_{j49}/\gamma_{j47}$ in the total angular momentum representation and $\delta_{sU} = \gamma_{s45}/\gamma_{s43}$ in the channel spin representation, and by $\varepsilon^2 = (\Gamma_{j47} + \Gamma_{j49})/\Gamma_{p'}$, an independent parameter which is a measure of the $\ell'=4$ admixture for each resonance. The Legendre polynomial coefficients are:

$$a_{2p} = \frac{20}{21}(1 - \varepsilon^2) + [\varepsilon^2(1 - \varepsilon^2)]^{1/2}\frac{[\frac{40}{21}\sqrt{\frac{2}{33}} - \frac{20}{693}\sqrt{231}\,\delta_{jU}]\cos(\xi_2 - \xi_4)}{(1 + \delta_{jU}^2)^{1/2}} + \varepsilon^2\frac{[\frac{530}{693} + \frac{760}{1089}\sqrt{\frac{2}{7}}\,\delta_{jU} + \frac{860}{1089}\delta_{jU}^2]}{1 + \delta_{jU}^2}, \tag{2.54}$$

$$a_{4p} = \frac{3}{7}(1 - \varepsilon^2) + [\varepsilon^2(1 - \varepsilon^2)]^{1/2}\frac{[\frac{120}{77}\sqrt{\frac{6}{11}} - \frac{60}{11}\sqrt{\frac{3}{77}}\,\delta_{jU}]}{(1 + \delta_{jU}^2)^{1/2}} \cdot \cos(\xi_2 - \xi_4) + \varepsilon^2\frac{[-\frac{27}{847} + \frac{2160}{1573}\sqrt{\frac{2}{7}}\,\delta_{jU} + \frac{27}{1573}\delta_{jU}^2]}{1 + \delta_{jU}^2}, \tag{2.55}$$

$$a_{6p} = [\varepsilon^2(1-\varepsilon^2)]^{1/2}\frac{[\frac{160}{33}\sqrt{\frac{2}{33}} - \frac{80}{33}\sqrt{\frac{7}{33}}\,\delta_{jU}]\cos(\xi_2 - \xi_4)}{(1+\delta_{jU}^2)^{1/2}} \tag{2.56}$$

$$+ \varepsilon^2\frac{[-\frac{520}{1089} + \frac{32}{1089}\sqrt{14}\,\delta_{jU} - \frac{512}{1089}\delta_{jU}^2]}{1+\delta_{jU}^2},$$

$$a_{8p} = \varepsilon^2\frac{[-\frac{784}{1573}\sqrt{14}\,\delta_{jU} - \frac{196}{1573}\delta_{jU}^2]}{1+\delta_{jU}^2}, \tag{2.57}$$

$$a_{2\gamma} = \frac{10}{21}(1-\varepsilon^2)Q_2 + \varepsilon^2\frac{[\frac{5}{231} - \frac{10}{33}\delta_{jU}^2]}{1+\delta_{jU}^2}\,Q_2, \tag{2.58}$$

$$a_{4\gamma} = -\frac{2}{7}(1-\varepsilon^2)Q_4 + \varepsilon^2\frac{[\frac{48}{77} - \frac{6}{11}\delta_{jU}^2]}{1+\delta_{jU}^2}\,Q_4, \tag{2.59}$$

in the total angular momentum representation. In the channel spin representation,

$$a_{2p} = \frac{20}{21}(1-\varepsilon^2) + [\varepsilon^2(1-\varepsilon^2)]^{1/2}\frac{[-\frac{20}{21}\sqrt{\frac{5}{11}}\,\delta_{sU}]\cos(\xi_2 - \xi_4)}{(1+\delta_{sU}^2)^{1/2}} \tag{2.60}$$

$$+ \varepsilon^2\frac{[\frac{350}{363} + \frac{500}{847}\delta_{sU}^2]}{1+\delta_{sU}^2},$$

$$a_{4p} = \frac{3}{7}(1-\varepsilon^2) + [\varepsilon^2(1-\varepsilon^2)]^{1/2}\frac{[-\frac{180}{77}\sqrt{\frac{5}{11}}\,\delta_{sU}]\cos(\xi_2 - \xi_4)}{(1+\delta_{sU}^2)^{1/2}} \tag{2.61}$$

$$+ \varepsilon^2\frac{[\frac{567}{1573} - \frac{41311}{11011}\delta_{sU}^2]}{1+\delta_{sU}^2},$$

$$a_{6p} = [\varepsilon^2(1 - \varepsilon^2)]^{1/2}\frac{[-\frac{80}{33}\sqrt{\frac{5}{11}}\,\delta_{sU}]}{(1 + \delta_{sU}^2)^{1/2}}\cos(\xi_2 - \xi_4) \qquad (2.62)$$

$$+ \varepsilon^2\frac{[-\frac{152}{363} - \frac{64}{121}\delta_{sU}^2]}{1 + \delta_{sU}^2},$$

$$a_{8p} = \varepsilon^2\frac{[-\frac{1568}{1573} + \frac{1372}{1573}\delta_{sU}^2]}{1 + \delta_{sU}^2}, \qquad (2.63)$$

$$a_{2\gamma} = \frac{10}{21}(1 - \varepsilon^2)Q_2 + \varepsilon^2\frac{[-\frac{5}{33} - \frac{20}{33}\sqrt{\frac{2}{7}}\,\delta_{sU} - \frac{10}{77}\delta_{sU}^2]}{1 + \delta_{sU}^2}\,Q_2, \qquad (2.64)$$

$$a_{4\gamma} = -\frac{2}{7}(1 - \varepsilon^2)Q_4 + \varepsilon^2\frac{[-\frac{24}{11}\sqrt{\frac{2}{7}}\,\delta_{sU} + \frac{6}{77}\delta_{sU}^2]}{1 + \delta_{sU}^2}\,Q_4. \qquad (2.65)$$

The mixing angle is $\phi_U = \tan^{-1}\delta_U$ in each representation, and has range $-180^\circ \leq \phi_U \leq 180^\circ$. The transformation from one representation to the other is linear in terms of the mixing angle: $\phi_{jU} = \phi_{sU} + 46.91^\circ$.

CHAPTER III

EXPERIMENTAL EQUIPMENT AND PROCEDURES

A. The High Resolution System

1. Accelerator Control

The Triangle Universities Nuclear Laboratory FN tandem Van de Graaff accelerator and its high resolution feedback system were used to perform the experiments discussed in this dissertation. The high resolution feedback system permits operation of the accelerator with extreme energy stability. For these experiments a total energy resolution of 400-450 eV for proton beams in the 3-5 MeV range was routinely obtained. This resolution figure includes the effects of beam energy fluctuations, the incoherent spread in energy of particles as they leave the ion source, the spread in energy due to straggling in the charge exchange canal and in the target, and Doppler broadening due to motion of the target nuclei.

A schematic diagram of the high resolution feedback system, or triple loop system, is shown in figure 3.1. The beam emerges from the high energy end of the accelerator, is bent through two 90° angles by the 90-90 analyzing magnets, and impinges on two control slits downstream from the 90-90 magnets. Current collected by each control slit is sent to a preamplifier, which converts the current to a voltage, and then to a difference amplifier which

FIGURE 3.1 Schematic diagram of the high resolution feedback system.

TRIPLE LOOP STABILIZER SYSTEM

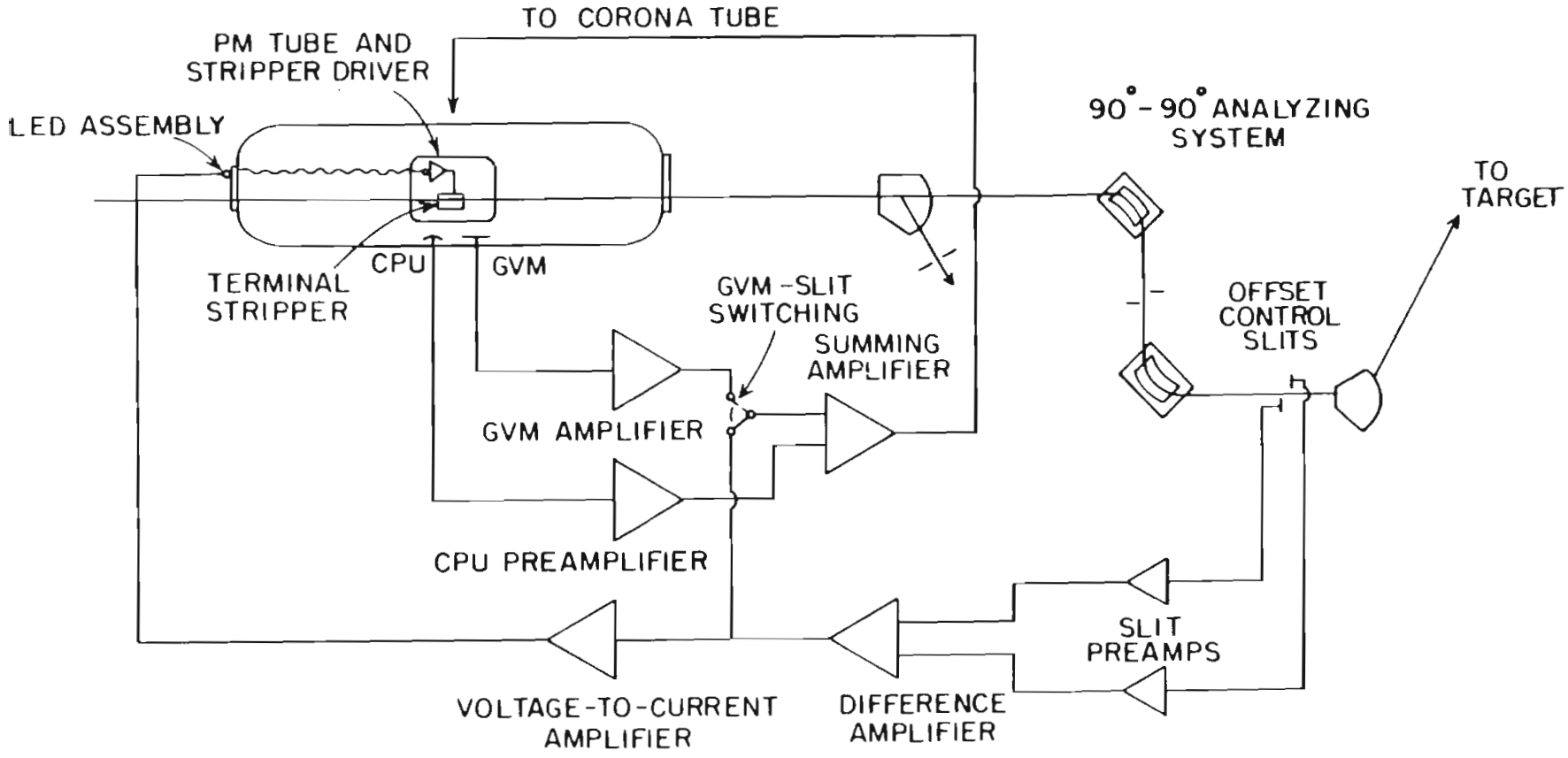

generates a control signal. The control signal is sent to a summing amplifier where it is added to a control signal from the capacitive pickup (CPU) located in the wall of the accelerator tank. The resulting signal drives the grid of the corona tube. If no beam impinges on the control slits, the input to the summing amplifier is automatically switched from the output of the control slit difference amplifier to the output of the generating voltmeter (GVM) amplifier. The GVM is located in the accelerator tank across from the CPU. This part of the high resolution feedback system is essentially a Gere type control system (Gere et al. 1967). In addition, however, the control signal from the difference amplifier is sent through a voltage to current amplifier to a light emitting diode (LED) mounted in front of a window in the low energy end of the accelerator. The intensity of light emitted by the LED is modulated by the input current. Once inside the accelerator the light travels along the accelerator column in a lucite light pipe to the terminal where it is detected by a photomultiplier tube. Here the signal is converted back to a voltage and fed into a high voltage amplifier located in the terminal. The output from the amplifier is capacitively coupled to the terminal stripper. Thus as fluctuations in the beam energy are detected at the control slits, a correction voltage is applied to the terminal stripper. This feedback loop is capable of responding to high frequency fluctuations in beam energy. It is not limited, as is the corona feedback system, by ion drift time through the insulating gas. More detailed discussions of the three loop stabilizer system can be found in Bleck (1978) and Watson (1980).

2. Magnet Control

For the triple loop stabilizer system to function properly, the 90-90 analyzing magnets must be extremely stable. To ensure this stability and for

accuracy and reproducibility of results, the 90-90 analyzing magnets are voltage programmable and are field locked with standard NMR techniques. Figure 3.2 is a schematic diagram of the analyzing magnet programmable power supply and the field control equipment. The master proportionality control determines the current sent to power supplies for the 90-90 magnets, the 70-70 switching magnet, and the quadrupoles and sextupoles located along the beam line. The control voltage for the master control is supplied by a pair of mercury batteries through two voltage dividing potentiometers, one coarse and one fine. The fine pot is turned by a stepping motor which is normally computer controlled.

As described by Watson, the field locking of the magnets is accomplished by sending an RF signal to an NMR probe in the magnet. The frequency of the RF signal must be changed for every energy step. A computer-controlled digitally programmable frequency synthesizer (Fluke model 6039A), which uses a 5 MHz frequency standard, varies the RF frequency. Thus, both the magnet programming voltage and the NMR frequency are incremented under computer control, reducing the possibility of non-uniform energy steps due to operator error or energy drift.

A small fraction of the data at low energy presented in this dissertation was measured with the Triangle Universities Nuclear Laboratory 3 MV Van de Graaff accelerator and its associated high resolution system. A description of the accelerator and data acquisition systems used in this work is given by Chou (1980).

B. Scattering Chambers and Counting Electronics

Two scattering chambers were used for these experiments. The proton

FIGURE 3.2 Schematic diagram of the analyzing magnet control system.

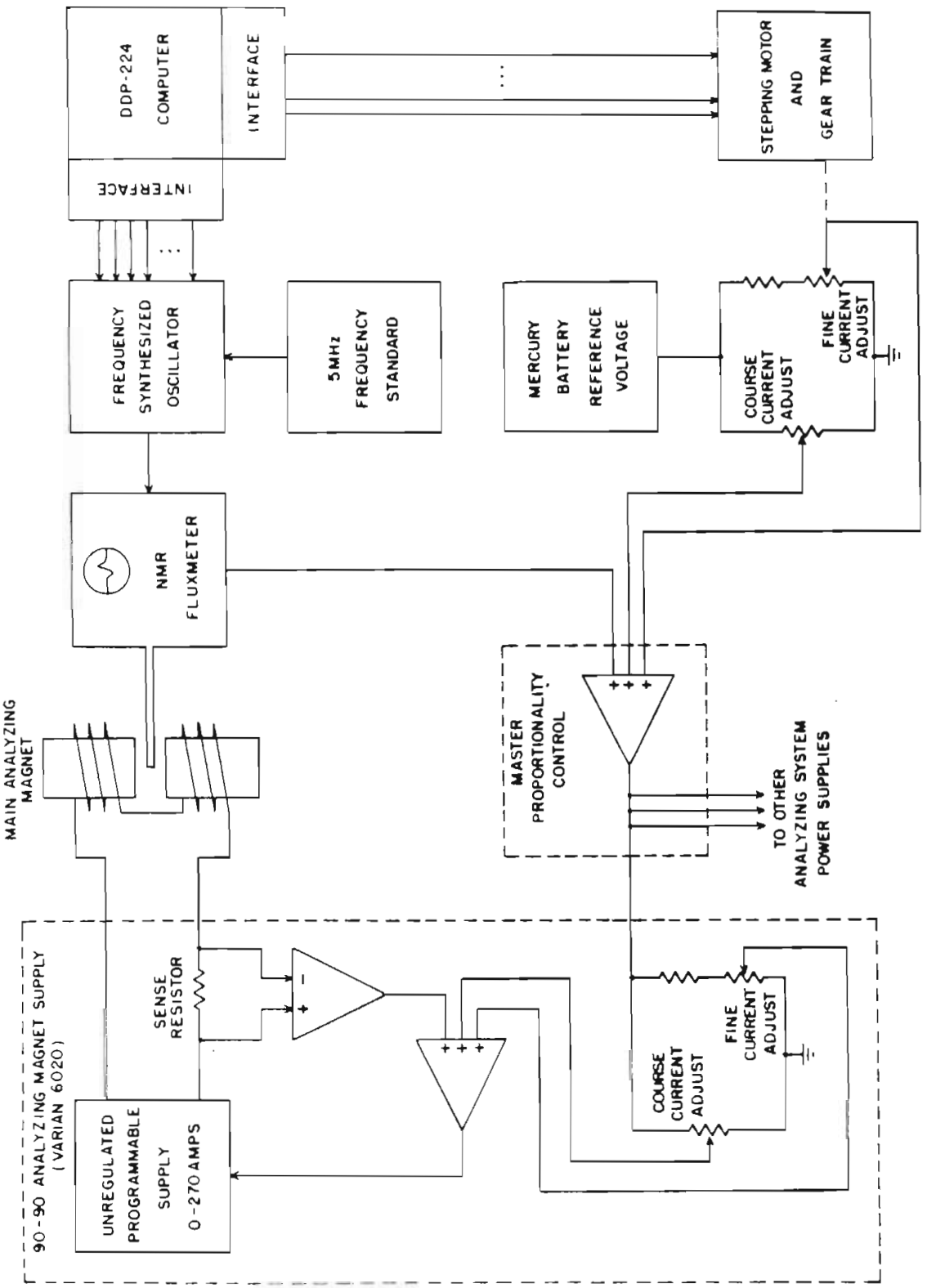

ANALYZING MAGNET POWER SUPPLY

experiment was performed in the large (23.5" i.d.) aluminum scattering chamber on the 60° left port of the 70–70 switching magnet. This chamber is equipped with freon cooling for detectors on both its top and bottom plates, and with a turbo-mechanical pump which maintains a vacuum of 2×10^{-6} torr. Figure 3.3 is a top view of this chamber showing placement of detectors and collimators.

Final beam collimation was accomplished with two sets of collimators. The first was a rotating ring box with three positions: a 0.08" hole, a 0.1" hole, and a blank side. The 0.1" hole was used for this experiment. The second set of collimators was a pair of vertical and horizontal slits placed 4" from the target. Both slits had 0.08" apertures. Signals from all collimators were monitored in the control room to aid in tuning the beam.

After passing through the target, the beam was collected in a split Faraday cup, which was divided into quadrants. The signal from each quadrant was sent to a feedback system which was used to control the beam line steerers in order to improve beam stability. Signals from all four quadrants together were used to monitor total beam current.

Six surface barrier detectors were located at the following laboratory angles: 89°, 112°, 124°, 135°, 150°, and 165°. Each detector had its own collimator holder assembly which held three collimator rings. The collimator ring closest to the detector defined the solid angle of the detector. Solid angles for all the detectors were chosen to be equal. The second and third collimator rings limited the area of the target and its surroundings seen by the detector, thus limiting the low energy background registered by the detector. A list of detector and collimator properties is given in table 3.1.

Signals from the detectors were sent to preamplifiers (Ortec model number 142A) located at the target chamber, and then to spectroscopy amplifiers (Ortec 572) located in the control room. A block diagram of the

FIGURE 3.3 Top view of the charged particle scattering chamber.

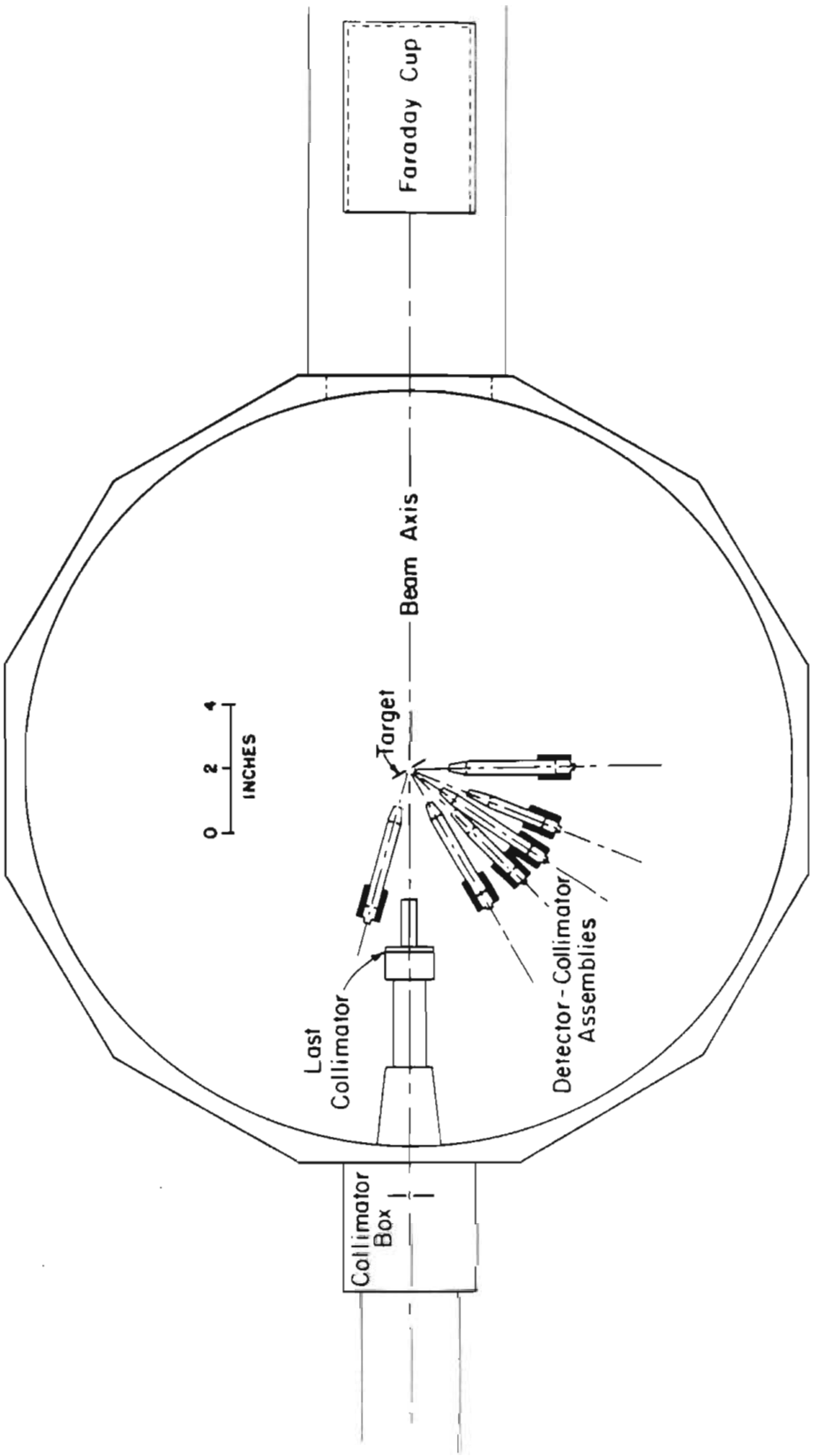
Faraday Cup
Beam Axis
Target
0 2 4
INCHES
Last
Collimator
Detector - Collimator
Assemblies
Collimator
Box

TABLE 3.1

CHARGED PARTICLE DETECTOR PROPERTIES

θ_{lab}	89°	112°	124°	135°	150°	165°
Ortec serial number	19-870D	13-455E	19-870B	20-170C	16-867D	16-868C
Ortec model number	BA-017-50-300	BA-016-50-500	BA-017-50-300	BA-017-50-300	BA-014-50-500	BA-014-50-500
bias voltage (volts)	105.	135.	105.	100.	250.	250.
active area (mm^2)	50.	50.	50.	50.	50.	50.
length of collimator holder (in.)	3.25	3.25	2.50	2.50	3.25	3.25
diameter of ring 1 (in.)	0.28	0.28	0.28	0.28	0.28	0.28
diameter of ring 2 (in.)	0.21	0.21	0.25	0.25	0.21	0.21
diameter of ring 3 (in.)	0.1875	0.1875	0.21	0.21	0.1875	0.1875
distance to target (in.)	4.5	4.5	4.5	4.5	4.5	4.5
solid angle (msr.)	3.04	3.04	3.04	3.04	3.04	3.04

counting electronics for the proton experiment is shown in figure 3.4. The bipolar output of each spectroscopy amplifier was connected to two timing single channel amplifiers (TSCA's). One TSCA functioned as an upper and lower level discriminator. The second TSCA acted as a window for the carbon or aluminum elastic peak (depending on the target backing), and was used in anticoincidence with the signal from the first TSCA to produce a gate signal. The gate signal was sent from the coincidence module to a linear gate and stretcher, whose input was connected to the unipolar output of the spectroscopy amplifier. Signals that corresponded to the carbon or aluminum peak and signals whose voltages were too high or too low were discarded at the linear gate and stretcher. Since fewer signals were sent to the ADC, the dead time in the ADC was reduced. A typical value of the dead time was about 10%. All linear signals for which there were gates were summed and sent to the ADC. Gate signals from the coincidence modules were also sent to the router. The router had an input for each angle. On receiving a gate pulse, the router sent a gate to the ADC. This gate enabled the next linear signal which reached the ADC to be processed. The router also kept track of which angle generated the linear signal, and enabled the computer to sort events into the correct spectrum.

The γ-ray experiment was performed in a thin-walled scattering chamber 6.63" in diameter located on the 0° port of the 70-70 switching magnet. A diffusion pump maintained a vacuum of about 2.5×10^{-6} torr in the chamber. A top view of this chamber showing placement of collimators and detectors is presented in figure 3.5.

In order to improve beam collimation, a new beam line collimator was designed and fabricated based on the beam line collimators in the 3 MV Laboratory (Wimpey 1974). Spaces for collimating rings of either 0.1" or

FIGURE 3.4 Block diagram of the counting electronics for the proton experiment.

PROTON DETECTION ELECTRONICS

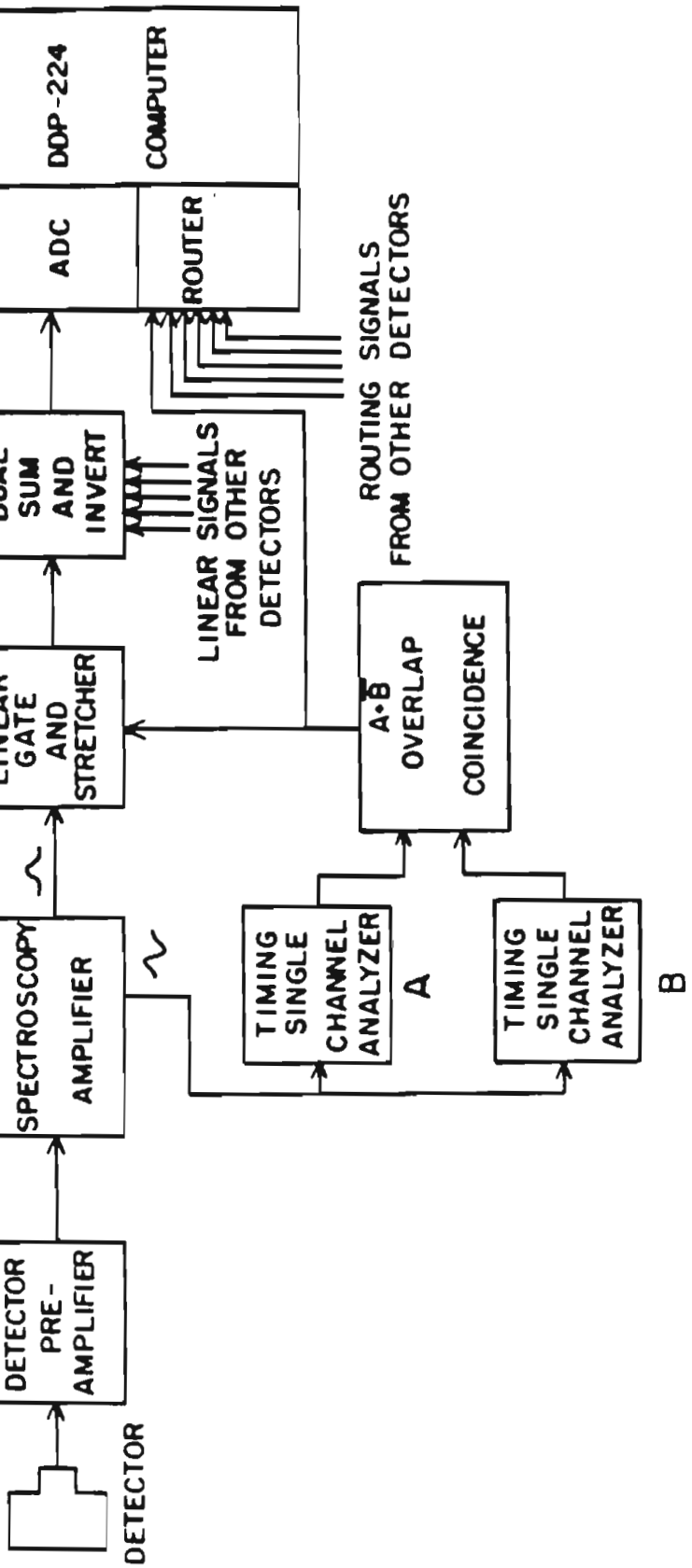

FIGURE 3.5 Top view of the γ-ray detection chamber. For the purposes of the present experiment, 135^{o} is equivalent to 45^{o}, and 120^{o} is equivalent to 30^{o}.

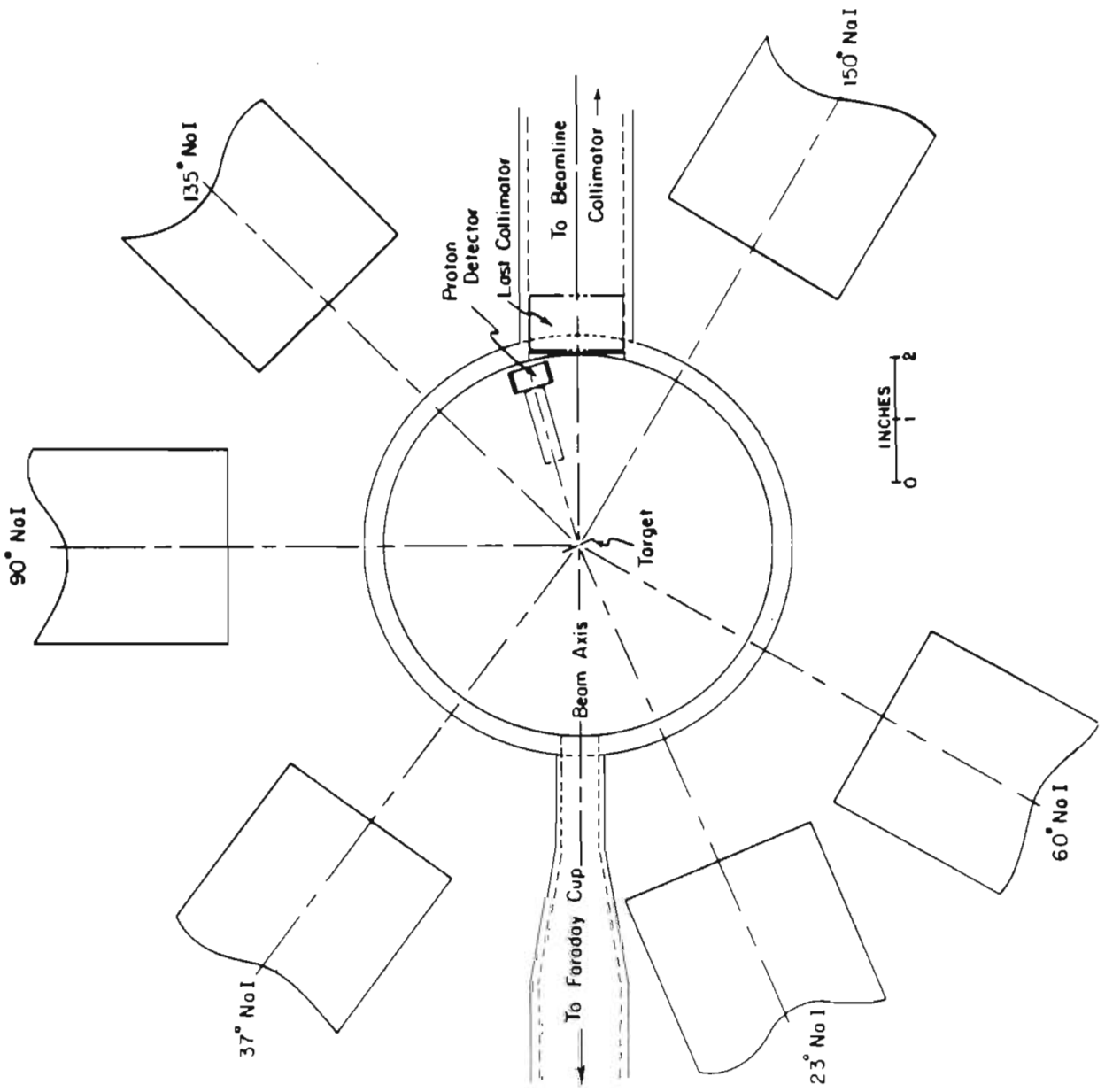
90° NaI
135° NaI
150° NaI
37° NaI
23° NaI
60° NaI
Proton Detector
Lost Collimator
To Beamline
Collimator
Target
Beam Axis
To Faraday Cup
INCHES
0
1
2

0.125" i.d. are provided at distances of approximately 14", 19", and 24" from the target. A diagram of the assembly is shown in figure 3.6. In practice, the beam was collimated using 0.1" rings at 19" and 24" from the target. In addition, a 0.125" collimating ring with an attached tantalum shield was inserted into the beam line about 3" from the target. The shield prevented particles scattered by the collimator assembly from reaching the target area, thereby reducing the background seen by the detectors. After passing through the target, the beam was collected in a Faraday cup located 9 ft. from the chamber.

Six 3"x3" sodium iodide (NaI) crystals were used to detect scattered γ-rays at the following laboratory angles: 90°, 60°, 45°, 37°, 30°, and 23°. The size of the beam line limited the forward angle to 23°. Attached to each crystal was a photomultiplier tube. The front face of each detector was placed 5.5" from the center of the chamber. Over eight hundred pounds of lead was used to shield the detectors from background radiation. In addition to the NaI crystals, one surface barrier detector was placed in the chamber at an angle of 165°. The surface barrier detector was used to monitor the elastic and inelastic proton yield curves to aid in locating resonances. Properties of the detectors are listed in table 3.2.

The output from the NaI crystals was sent to preamplifiers which connected directly into the phototube bases. Signals were then sent to spectroscopy amplifiers in the control room. A block diagram of the γ-ray counting electronics is shown in figure 3.7. The bipolar output of the amplifier was sent to a TSCA which acted simply as an upper and lower level discriminator. The unipolar output of the amplifier was sent to a linear gate and stretcher, where signals were discarded if too high or too low using the gate from the TSCA. Gates from the TSCA were also sent to the router.

FIGURE 3.6 Side view of the new 0^{o} leg beam line collimator.

BEAMLINE COLLIMATOR

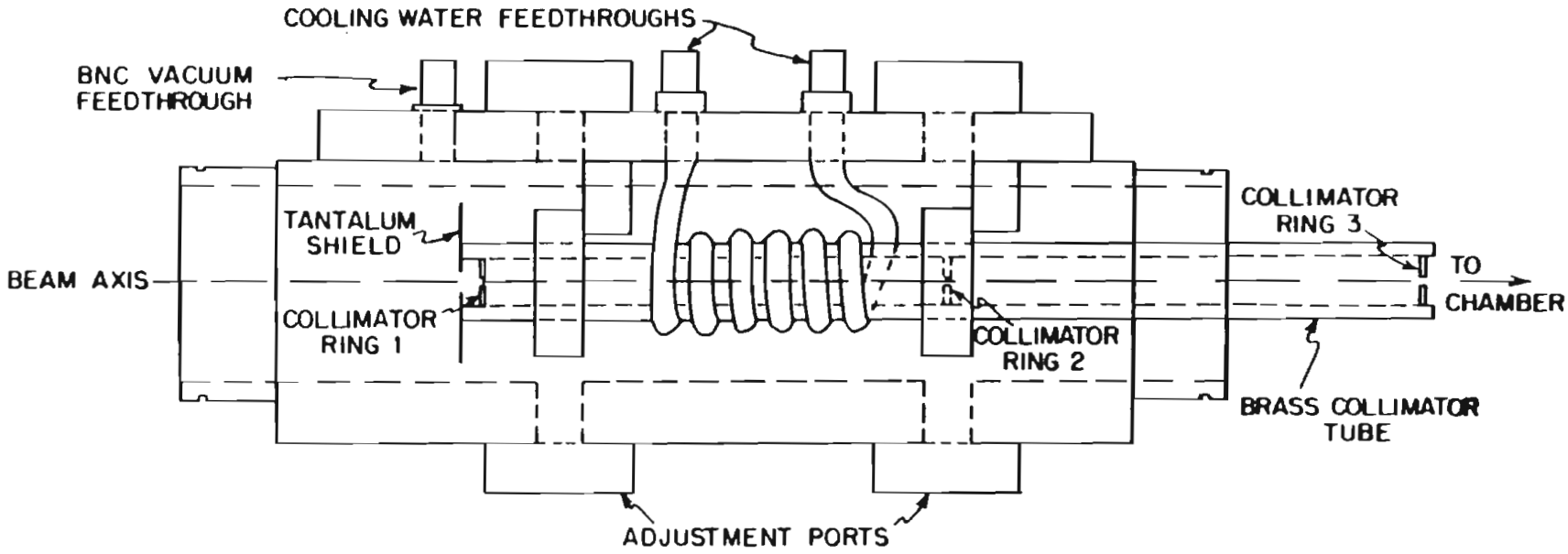

COLLIMATOR RINGS 1, 2 AND 3: 0.10" I.D. TANTALUM

TABLE 3.2

γ-RAY DETECTOR PROPERTIES

θ_{lab}	90^{o}	60^{o}	45^{o}	37^{o}	30^{o}	23^{o}	165^{o}
Serial number	NaI Harshaw EZ-668	NaI Harshaw CX-696R2	NaI Harshaw KP521	NaI Harshaw KP525	NaI Harshaw JE161	NaI Harshaw BS-802	Ortec 19-727D
bias voltage (volts)			1300.				190.
active area			7.07 $in.^2$				50 mm^2
distance to target (in.)			5.5				2.6
solid angle (sr.)			0.234				.00845

The 165^{o} charged particle detector (Ortec model TA-023-50-300) was equipped with a collimator holder 1.2" long which held two collimating rings, the first next to the detector, with an i.d. of 0.28", and the second at the end of the collimator holder, with an i.d. of 0.222".

FIGURE 3.7 Block diagram of the counting electronics for the γ-ray experiment.

γ-RAY DETECTION ELECTRONICS

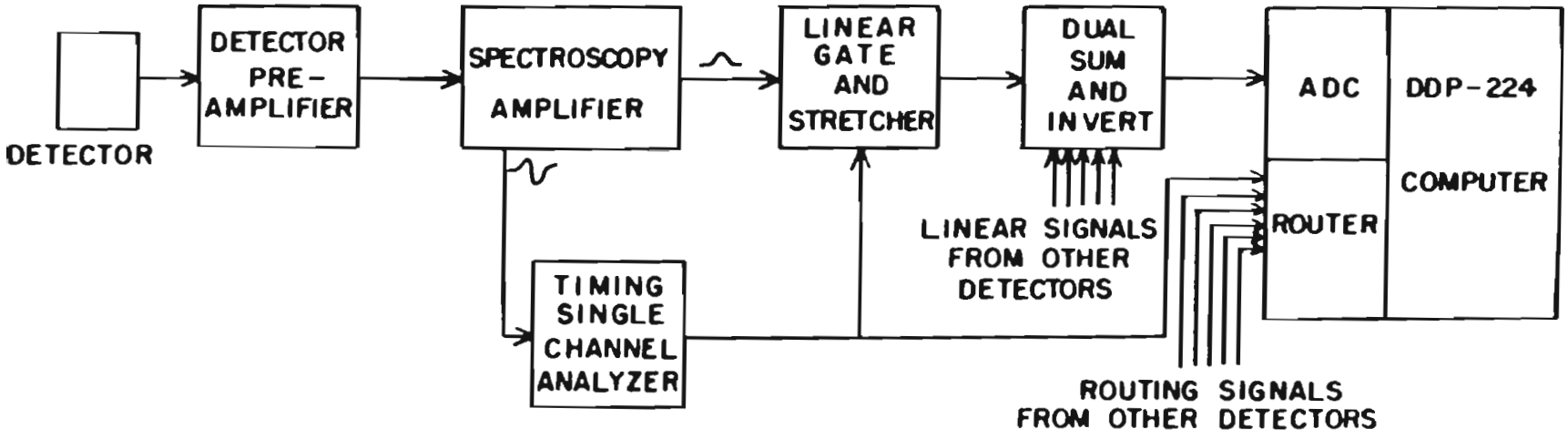

Acceptable signals from the linear gate and stretcher were summed and sent to the ADC. The computer used the router signals to sort events into the proper spectrum.

C. Targets

Two types of targets were used in these experiments. For the γ-ray experiments, a high current evaporator was used to evaporate 2-3.5 $\mu g/cm^2$ of ^{50}Cr onto self-supporting 5 $\mu g/cm^2$ carbon backings (Arizona Carbon Foil Co.). For the proton experiment, ^{50}Cr was evaporated onto self-supporting aluminum foils ranging from 14-22 $\mu g/cm^2$ in thickness. At some point in the energy range studied the ^{50}Cr inelastic peak was overlapped completely by the carbon elastic peak at $\theta_{lab} = 165^\circ$, 150°, 135°, and 124°. It was therefore necessary to use aluminum-backed targets for the proton experiment. A small amount of carbon, deposited by pump oil vapor and alcohol fumes, remained on the aluminum-backed targets. Aluminum-backed targets had less carbon, were much stronger, and lasted longer in the beam than did targets backed with thin (1 $\mu g/cm^2$) carbon foils.

Aluminum backings were produced in the following manner: first, a layer of cesium iodide, a release agent, was evaporated onto clean glass slides. The CsI and aluminum to be used for the backing were both placed in a 0.01" thick tungsten boat clamped between the high voltage electrodes, approximately eight inches from the slides and separated from them by a shutter. The CsI evaporated at a current of 110 A, corresponding to a temperature of about $600^\circ F$, and the aluminum evaporated at 170 A or $1090^\circ F$. The thickness of the deposited layer was monitored using a Sloan deposition meter, and controlled by manipulation of the shutter. When the evaporation was complete, the slides

were removed from the evaporator and the aluminum foils were lifted onto target rings and allowed to dry. Once dry, the prepared aluminum backings were treated in the same manner as carbon backings: rings were placed in the evaporator chamber, approximately eight inches from the high current electrodes. A sample of isotopically enriched (96.80%) ^{50}Cr metallic powder, obtained from Oak Ridge National Laboratory, was placed in a 0.01" thick tungsten boat between the electrodes. The chromium evaporated at approximately 200 A or 1250^{o}F. Targets were stored under vacuum in order to minimize oxidation.

Typical spectra from both carbon and aluminum-backed targets are shown in figure 3.8.

D. Experimental Procedure

Salzmann (1975) performed the $^{50}Cr(p,p)$ and $^{50}Cr(p,p')$ experiments which provided certain parameters (spin, energy, elastic width, and in some cases inelastic width) for the resonances under study. For both of the present experiments each resonance was first located by taking a short yield curve, beginning ~ 2 keV below the resonance energy and continuing to ~ 1 keV above the resonance energy. These yield curves were generally measured in 100–200 eV steps. For each set of spectra in the yield curve, 90–120 μC of charge was collected, depending on the target thickness. Each set of spectra was recorded on tape while the fields of the magnets were stepped automatically and the NMR frequency was incremented. Both the yield curve and the current spectra were available for inspection by the operator. Once the resonance was located, the beam energy was tuned to the resonance energy, and a set of spectra was accumulated with at least 7000–10,000 counts under the

FIGURE 3.8 Typical spectra for the reactions $^{50}Cr(p,p')$ and $^{50}Cr(p,p'\gamma)$.

The top figure is a γ-ray spectrum from a carbon-backed target. The peak of interest is the 0.7833 MeV γ-ray emitted from the first excited state of ^{50}Cr.

The middle figure is a proton spectrum from a carbon-backed target. The peak due to the proton inelastically scattered from ^{50}Cr is beginning to overlap the carbon peak.

The bottom figure is a proton spectrum from an aluminum-backed target. Both the ^{16}O and the aluminum peak have been removed from the spectrum electronically, and the scale has been expanded. The carbon peak is much smaller here than in the spectrum above. Note that the peak due to the proton inelastically scattered from ^{50}Cr is completely resolved from the carbon peak, even though the two peaks are closer together in energy at 3.4696 MeV than at 3.2982 MeV in the figure above.

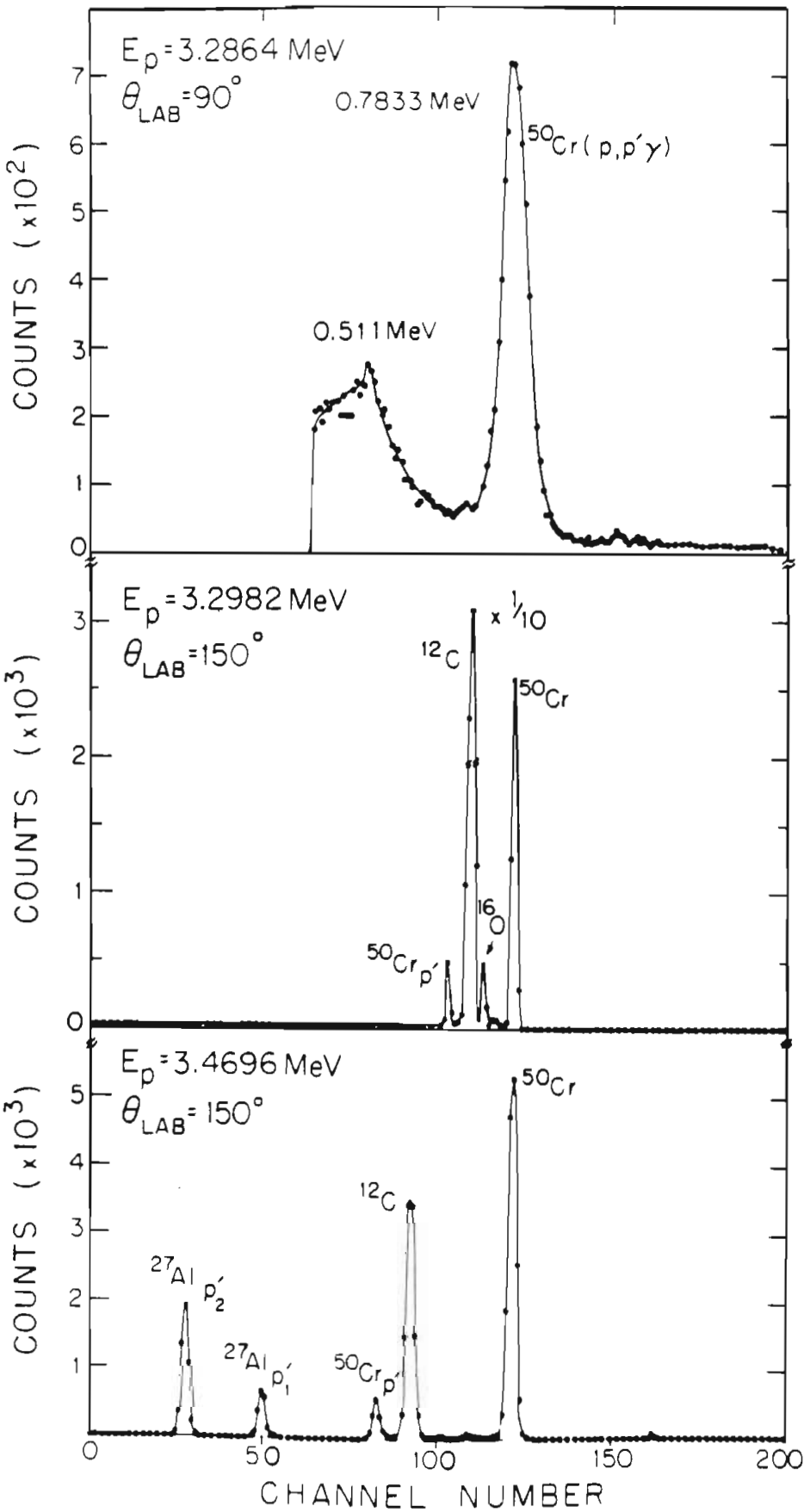
E_p = 3.2864 MeV
θ_{LAB} = 90°
0.7833 MeV
^{50}Cr (p,p'γ)
0.511 MeV
COUNTS (x10^2)
E_p = 3.2982 MeV
θ_{LAB} = 150°
x 1/10
^{12}C
^{50}Cr
^{16}O
^{50}Cr p'
COUNTS (x10^3)
E_p = 3.4696 MeV
θ_{LAB} = 150°
^{50}Cr
^{12}C
^{27}Al p'$_2$
^{27}Al p'$_1$
^{50}Cr p'
COUNTS (x10^3)
CHANNEL NUMBER

peak of interest. Usually this required the collection of 3000–10,000 μC of charge.

For the $^{50}Cr(p,p')$ experiment, a set of gold spectra was taken immediately following the long spectra. Approximately 300 μC of charge was collected, yielding ~ 100,000 counts under the 89^{o} elastic peak. The gold spectra were used for normalization purposes. Rutherford scattering was assumed to obtain relative efficiencies for the detectors. The laboratory angular distribution was converted to the center of mass system, and then fit to a Legendre polynomial expansion.

Normalization factors for the $^{50}Cr(p,p'\gamma)$ experiment were obtained by two methods. In the first method, a ^{22}Na source was placed in the target holder. Normalization factors obtained by this method proved unsatisfactory: systematic and background effects resulting from the presence of beam on target were not taken into account. Excellent normalization factors were obtained from data taken for $1/2^{-}$ resonances, which exhibit isotropic angular distributions. Data for $1/2^{-}$ resonances were obtained in exactly the same manner as data for all other resonances.

For both experiments, the proton beam was tuned through a ring of 0.1" i.d. placed in the target holder. Most data were taken with a beam intensity of about 4 μA on target. Best results were obtained when the current on the tuning ring was less than 30 nA and the current on the last collimator was less than 50 nA.

CHAPTER IV

DATA AND PRELIMINARY ANALYSIS

A. Proton Elastic Scattering Experiments

The $^{50}Cr(p,p)$ and $^{50}Cr(p,p')$ experiments were performed by Salzmann et al. (1977) in the energy range E_p = 3.2-4.4 MeV, and by Moses (1970) in the energy range E_p = 1.8-3.3 MeV. In both sets of experiments excitation functions at various angles were measured, and the energy, spin, parity, and elastic and inelastic widths of many resonances were determined. The excitation function measured by Salzmann from E_p = 3.24-4.42 MeV is presented for both reactions in the appendix. All 182 resonances observed by Salzmann plus eight p-wave resonances measured by Moses were studied in the present work.

B. Preliminary Analysis

Angular distribution measurements on the inelastically scattered proton and the de-excitation γ-ray were performed for most of the 190 resonances. Resonances with insufficient inelastic strength and resonances for which interference from nearby states led to inconsistencies were omitted from further analysis. In all, 107 resonances were analyzed in detail. The spin and parity assignments were as follows: $1/2^+$ (4); $1/2^-$ (6); $3/2^-$ (30); $3/2^+$

(20); $5/2^+$ (38); $5/2^-$ (7); $7/2^+$ (1); and $9/2^+$ (1). Resonance parameters (energy, spin, parity, elastic and total inelastic laboratory width, and reduced widths) for all resonances are presented in the appendix. Changes in spin assignments or widths are denoted by an asterisk. Uncertain spin assignments are indicated by parentheses.

To obtain an angular distribution from the raw data, the following procedure was adopted. First, a set of spectra was measured at various angles at the resonance energy. The peak of interest in both the γ-ray and proton spectra was fit with a Gaussian function, and the area under the peak was determined. The areas were normalized to correct for differences in detector efficiencies. The angular distributions of the inelastically scattered protons and the γ-rays were fit with a Legendre polynomial expansion to determine the a_p and a_γ coefficients. Fractional errors in the proton data ranged from 4-6% and in the γ-ray data from 3-5%.

As demonstrated in Chapter II, the coefficients of the Legendre polynomials in the angular distribution equations are functions of the mixing ratios δ or equivalently the mixing angles ϕ. In practice the fit to the angular distribution is performed with ϕ as the free parameter. The absolute minimum point of χ^2 as a function of ϕ corresponds to the best solution for the mixing ratio. The search for the χ^2 minimum was performed with the gradient search routine "ROCORD". Typical plots of the χ^2 minimum in ϕ-space are given by Chou (1980).

The total inelastic widths for all resonances were determined following the procedure of Gove (1959) with the relation:

$$\frac{(2J+1)}{(2I_o+1)(2J_o+1)} \frac{\Gamma_p \Gamma_{p'}}{\Gamma} = \frac{2Y}{\lambda^2 t} , \qquad (4.1)$$

where J = spin of the compound nuclear state,

J_o = spin of the target,

I_o = spin of the incident particle,

Γ_p = proton elastic width in eV,

$\Gamma_{p'}$ = total inelastic width in eV,

Γ = total width in eV,

t = target thickness in atoms per square centimeter,

λ = center of mass wavelength of the incident protons in centimeters,

Y = area of the resonance yield curve in units of reactions times energy(eV) per incident particle.

If contributions from other channels are neglected, the total width is $\Gamma \simeq \Gamma_p + \Gamma_{p'}$, and $\Gamma_{p'} = (\Gamma_p Y')/(\Gamma_p - Y')$, where

$$Y' = \frac{2Y(2I_o + 1)(2J_o + 1)}{\lambda^2 t\ (2J + 1)} \quad . \tag{4.2}$$

Since $\Gamma_{p'}$ must be positive, Y' must be smaller than the elastic width, Γ_p. The elastic width was taken from the previous elastic scattering measurements, and Y' was determined in the present experiment. When Y' was greater than Γ_p, the resonance was refit with "MULTI", a multilevel, multichannel R-matrix computer program first developed by Sellin (1969). Channel widths were obtained from the total width and the mixing ratios. The channel reduced widths were determined by application of the equation $\gamma^2_{\lambda c} = \Gamma_{\lambda c}/2P_c$, where $\Gamma_{\lambda c}$ is the channel laboratory width, and P_c is the Coulomb penetrability. The penetrabilities were calculated at a channel radius of $1.25(A^{1/3} + 1)F$, where A is the mass number of the target.

1. p-wave Resonances

As shown in Chapter II, if the incident proton has $\ell = 1$ and the target has spin zero, then resonances may be formed with spin and parity $1/2^-$ or $3/2^-$. The angular distribution equations for the inelastically scattered proton and the de-excitation γ-ray have the form:

$$W_p(\theta) = a_{op}(1 + a_{2p}P_2) \tag{4.3}$$

$$W_\gamma(\theta) = a_{o\gamma}(1 + a_{2\gamma}P_2). \tag{4.4}$$

For $1/2^-$ resonances, $a_{2p} = a_{2\gamma} = 0$. For $3/2^-$ resonances, at least one of the a_2 coefficients must be non-zero. Thus if the angular distributions are plotted versus $\cos^2\theta$, horizontal lines result for $1/2^-$ resonances, and straight lines result for $3/2^-$ resonances. Sample angular distributions are shown for a $3/2^-$ resonance in figure 4.1. The solid line is the best fit to the data. In all, six resonances were assigned $J^\pi = 1/2^-$, and thirty were assigned $J^\pi = 3/2^-$. A list of $\ell = 1$ resonances with their spin assignments and the measured Legendre polynomial coefficients is given in table 4.1.

Resonances with $J^\pi = 1/2^-$ have only one open exit channel; further analysis is therefore unnecessary. Most of the $1/2^-$ resonances observed were used for normalization purposes. The $3/2^-$ resonances have two open exit channels: in the total angular momentum representation the exit channels are $\ell'=1$ $j'=1/2$, and $\ell'=1$ $j'=3/2$. In the channel spin representation the exit channels are labeled as $\ell'=1$ $s'=3/2$, and $\ell'=1$ $s'=5/2$. Any $\ell'=3$ contributions are neglected due to penetrability considerations. As discussed in Chapter II, the mixing ratio δ is defined as $\delta_j = \gamma_{j13}/\gamma_{j11}$ in the total angular momentum representation, and as $\delta_s = \gamma_{s15}/\gamma_{s13}$ in the channel spin representation. Also, $\phi_j = \tan^{-1}\delta_j$, and $\phi_s = \tan^{-1}\delta_s$. Tables 4.2 and 4.3 list values of δ and ϕ for $3/2^-$ resonances in the total angular momentum

FIGURE 4.1 Sample angular distributions for a $3/2^-$ resonance. The top figure is the inelastically scattered proton distribution, and the bottom figure is the γ-ray distribution.

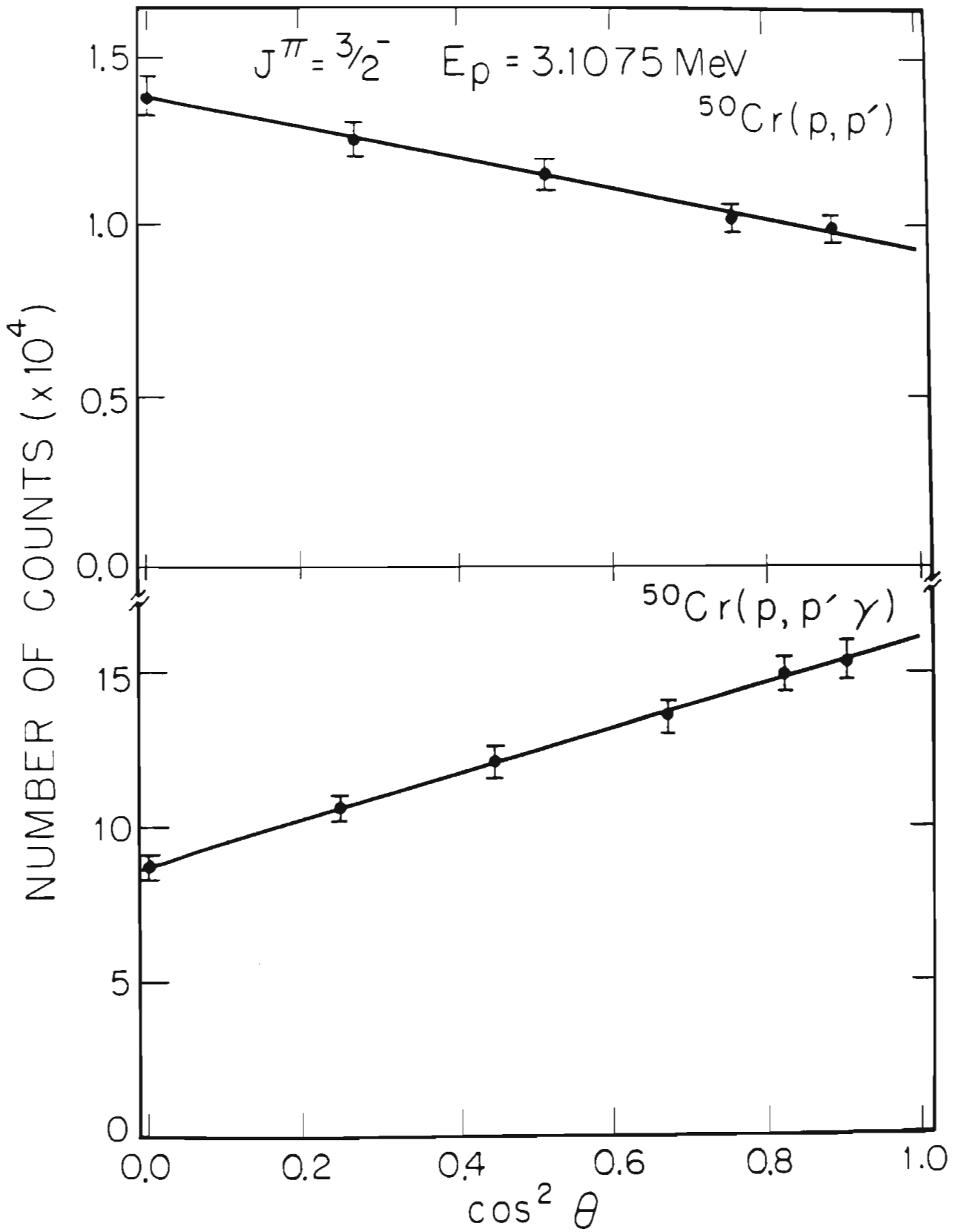
$J^{\pi} = 3/2^-$ $E_p = 3.1075$ MeV
$^{50}Cr(p,p')$
$^{50}Cr(p,p'\gamma)$
NUMBER OF COUNTS ($\times 10^4$)
1.5
1.0
0.5
0.0
15
10
5
0
0.0
0.2
0.4
0.6
0.8
1.0
$\cos^2\theta$

TABLE 4.1

LEGENDRE POLYNOMIAL COEFFICIENTS FOR ℓ=1 RESONANCES IN ^{51}Mn

Resonance Number	J^{π}	Experiment	a_2
M1	$3/2^-$	p	-0.545 ± 0.026
		γ	0.062 ± 0.036
M3	$3/2^-$	p	-0.242 ± 0.033
		γ	0.451 ± 0.038
M4	$1/2^-$	p	-0.062 ± 0.036
		γ	0.000 ± 0.035
M5	$3/2^-$	p	-0.399 ± 0.029
		γ	0.400 ± 0.038
M6	$3/2^-$	p	-0.141 ± 0.036
		γ	0.040 ± 0.035
M7	$3/2^-$	p	-0.149 ± 0.042
		γ	0.036 ± 0.036
M8	$3/2^-$	p	-0.178 ± 0.042
		γ	0.029 ± 0.035
5	$3/2^-$	p	-0.760 ± 0.014
		γ	0.028 ± 0.034
7	$3/2^-$	p	0.239 ± 0.036
		γ	0.351 ± 0.038
9	$1/2^-$	p	0.032 ± 0.042
		γ	0.051 ± 0.037
13	$3/2^-$	p	-0.272 ± 0.036
		γ	0.398 ± 0.039
21	$3/2^-$	p	0.169 ± 0.044
		γ	0.190 ± 0.038
32	$1/2^-$	p	0.016 ± 0.052
		γ	0.000 ± 0.037

TABLE 4.1 (continued)

Resonance Number	J^{π}	Experiment	a_2
37	$3/2^-$	p	0.082 ± 0.043
		γ	0.316 ± 0.038
41	$3/2^-$	p	-0.345 ± 0.050
		γ	0.094 ± 0.039
47	$1/2^-$	p	0.063 ± 0.054
		γ	0.024 ± 0.037
56	$3/2^-$	p	-0.160 ± 0.071
		γ	0.046 ± 0.038
60	$3/2^-$	p	-0.468 ± 0.073
		γ	0.308 ± 0.039
63	$3/2^-$	p	-0.488 ± 0.075
		γ	-0.008 ± 0.038
69	$1/2^-$	p	-0.035 ± 0.087
		γ	0.051 ± 0.038
77	$3/2^-$	p	-0.392 ± 0.091
		γ	-0.017 ± 0.039
83	$3/2^-$	p	-0.185 ± 0.085
		γ	0.161 ± 0.039
87	$3/2^-$	p	-0.350 ± 0.091
		γ	0.075 ± 0.037
88	$3/2^-$	p	-0.728 ± 0.094
		γ	-0.003 ± 0.038
94	$3/2^-$	p	-0.544 ± 0.033
		γ	0.004 ± 0.038
95	$3/2^-$	p	0.131 ± 0.050
		γ	0.224 ± 0.040
116	$3/2^-$	p	-0.423 ± 0.032
		γ	0.381 ± 0.039
117	$3/2^-$	p	0.109 ± 0.043
		γ	0.294 ± 0.039

TABLE 4.1 (continued)

Resonance Number	J^{π}	Experiment	a_2
125	$3/2^-$	p	0.118 ± 0.059
		γ	0.339 ± 0.039
135	$3/2^-$	p	-0.308 ± 0.057
		γ	0.093 ± 0.037
136	$3/2^-$	p	-0.046 ± 0.062
		γ	0.086 ± 0.038
143	$3/2^-$	p	-0.348 ± 0.055
		γ	0.104 ± 0.037
147	$1/2^-$	p	-0.034 ± 0.041
		γ	0.081 ± 0.039
158	$3/2^-$	p	-0.245 ± 0.045
		γ	0.079 ± 0.040
162	$3/2^-$	p	0.013 ± 0.043
		γ	0.195 ± 0.038
175	$3/2^-$	p	-0.136 ± 0.057
		γ	0.388 ± 0.039

TABLE 4.2

MIXING RATIOS AND MIXING ANGLES FOR $3/2^-$ RESONANCES IN ^{51}Mn

Total Angular Momentum Representation

Resonance Number	ϕ_j (degrees)	δ_j
M1	-86.07 ± 1.42	$-14.56\ (+3.88\ -8.26)$
M3	15.22 ± 1.63	$0.27\ (+0.03\ -0.03)$
M5	24.29 ± 1.41	$0.45\ (+0.03\ -0.03)$
M6	-63.91 ± 1.75	$-2.04\ (+0.15\ -0.17)$
M7	-64.91 ± 2.06	$-2.14\ (+0.19\ -0.22)$
M8	-66.45 ± 2.06	$-2.29\ (+0.21\ -0.25)$
5	75.11 ± 1.72	$3.76\ (+0.51\ -0.41)$
7	-29.68 ± 4.10	$-0.57\ (+0.09\ -0.10)$
13	17.38 ± 2.00	$0.31\ (+0.04\ -0.04)$
21	-44.42 ± 2.88	$-0.98\ (+0.09\ -0.10)$
37	-41.16 ± 3.67	$-0.87\ (+0.11\ -0.12)$
41	-72.49 ± 2.77	$-3.17\ (+0.46\ -0.63)$
56	-66.20 ± 3.03	$-2.27\ (+0.29\ -0.37)$
60	32.47 ± 3.40	$0.64\ (+0.09\ -0.08)$
63	-83.15 ± 4.18	$-8.33\ (+3.19\ -13.11)$
77	-78.97 ± 3.89	$-5.13\ (+1.38\ -2.85)$
83	-60.26 ± 3.40	$-1.75\ (+0.22\ -0.27)$
87	-71.92 ± 3.78	$-3.06\ (+0.57\ -0.86)$
88	81.30 ± 6.14	$6.54\ (+15.82\ -2.76)$

TABLE 4.2 (continued)

Resonance Number	ϕ_j (degrees)	δ_j
94	-86.19 ± 2.14	$-15.02\ (+5.42\ -19.28)$
95	-44.76 ± 3.06	$-0.99\ (+0.10\ -0.11)$
116	25.77 ± 1.78	$0.48\ (+0.04\ -0.04)$
117	-41.69 ± 3.26	$-0.89\ (+0.10\ -0.11)$
125	-35.14 ± 4.60	$-0.70\ (+0.11\ -0.13)$
135	-70.22 ± 2.89	$-2.78\ (+0.39\ -0.51)$
136	-59.58 ± 2.71	$-1.70\ (+0.17\ -0.20)$
143	-71.89 ± 2.94	$-3.06\ (+0.46\ -0.63)$
158	-68.09 ± 2.38	$-2.49\ (+0.27\ -0.33)$
162	-51.60 ± 2.57	$-1.26\ (+0.11\ -0.12)$
175	10.94 ± 3.45	$0.19\ (+0.06\ -0.06)$

TABLE 4.3

MIXING RATIOS AND MIXING ANGLES FOR $3/2^-$ RESONANCES IN ^{51}Mn

Channel Spin Representation

Resonance Number	ϕ_s (degrees)	δ_s
M1	30.50 ± 1.42	0.59 (+ 0.03 - 0.03)
M3	-48.22 ± 1.63	-1.12 (+ 0.06 - 0.07)
M5	-39.14 ± 1.41	-0.81 (+ 0.04 - 0.04)
M6	52.66 ± 1.75	1.31 (+ 0.09 - 0.08)
M7	51.65 ± 2.06	1.26 (+ 0.10 - 0.09)
M8	50.12 ± 2.06	1.20 (+ 0.09 - 0.08)
5	11.67 ± 1.72	0.21 (+ 0.03 - 0.03)
7	86.89 ± 4.10	18.39 (+99.99 -10.48)
13	-46.05 ± 2.00	-1.04 (+ 0.07 - 0.08)
21	72.14 ± 2.88	3.10 (+ 0.63 - 0.46)
37	75.41 ± 3.67	3.84 (+ 1.34 - 0.81)
41	44.07 ± 2.77	0.97 (+ 0.10 - 0.09)
56	50.36 ± 3.03	1.21 (+ 0.14 - 0.12)
60	-30.96 ± 3.40	-0.60 (+ 0.08 - 0.08)
63	33.41 ± 4.18	0.66 (+ 0.11 - 0.10)
77	37.60 ± 3.89	0.77 (+ 0.11 - 0.10)
83	56.30 ± 3.40	1.50 (+ 0.21 - 0.18)
87	44.65 ± 3.78	0.99 (+ 0.14 - 0.12)
88	17.86 ± 6.14	0.32 (+ 0.12 - 0.11)

TABLE 4.3 (continued)

Resonance Number	ϕ_s (degrees)	δ_s
94	30.38 ± 2.14	0.59 (+ 0.05 - 0.05)
95	71.81 ± 3.06	3.04 (+ 0.65 - 0.47)
116	-37.67 ± 1.78	-0.77 (+ 0.05 - 0.05)
117	74.87 ± 3.26	3.70 (+ 1.06 - 0.69)
125	81.42 ± 4.60	6.63 (+ 7.77 - 2.36)
135	46.34 ± 2.89	1.05 (+ 0.11 - 0.10)
136	56.99 ± 2.71	1.54 (+ 0.17 - 0.15)
143	44.67 ± 2.94	0.99 (+ 0.11 - 0.10)
158	48.48 ± 2.38	1.13 (+ 0.10 - 0.09)
162	64.97 ± 2.57	2.14 (+ 0.28 - 0.23)
175	-52.49 ± 3.45	-1.30 (+ 0.15 - 0.18)

representation and the channel spin representation, respectively. Values of the two channel reduced widths and the product of the channel reduced width amplitudes are given in table 4.4 for the total angular momentum representation, and in table 4.5 for the channel spin representation. The total inelastic width and the total inelastic reduced width for each resonance are listed in table A.1. Differential and integral plots of the elastic and total inelastic reduced widths versus energy are shown in figure 4.2. No unusual structure is visible in these plots. Differential and integral plots of the channel reduced widths versus energy are presented in figures 4.3 and 4.4 for the total angular momentum and channel spin representations. Figure 4.5 shows the product of channel reduced width amplitudes for both representations. A non-statistical sign distribution is evident in the plot of channel reduced width products in both representations, although the effect is slightly more striking in the plot of $\gamma_{s13}\gamma_{s15}$ versus energy.

2. d-wave Resonances

If the proton incident on the ^{50}Cr target has $\ell = 2$, then $3/2^+$ or $5/2^+$ resonances are formed in ^{51}Mn. The angular distribution equations for decay from $5/2^+$ resonances are:

$$W_p(\theta) = a_{op}(1 + a_{2p}P_2 + a_{4p}P_4) \tag{4.5}$$

$$W_\gamma(\theta) = a_{o\gamma}(1 + a_{2\gamma}P_2 + a_{4\gamma}P_4). \tag{4.6}$$

For $3/2^+$ resonances, $a_{4p} = a_{4\gamma} = 0$. Plotted versus $\cos^2\theta$ the angular distributions for $3/2^+$ resonances are straight lines. For $5/2^+$ resonances, the a_4 terms are not necessarily zero, and the resulting angular distribution plots are not straight lines when plotted versus $\cos^2\theta$. Sample angular distribution plots for a $5/2^+$ resonance are shown in figure 4.6. The solid

TABLE 4.4

INELASTIC REDUCED WIDTHS AND AMPLITUDE PRODUCTS FOR $3/2^-$ RESONANCES IN ^{51}Mn

Total Angular Momentum Representation

Resonance Number	γ^2_{j11} (keV)	γ^2_{j13} (keV)	$\gamma_{j11}\gamma_{j13}$ (keV)
M1	0.002	0.392	-0.027
M3	1.145	0.085	0.312
M5	2.262	0.461	1.021
M6	0.157	0.653	-0.320
M7	0.047	0.215	-0.101
M8	0.070	0.369	-0.161
5	0.080	1.125	0.299
7	0.074	0.024	-0.042
13	0.703	0.069	0.220
21	0.058	0.056	-0.057
37	0.185	0.141	-0.162
41	0.060	0.602	-0.190
56	0.023	0.117	-0.052
60	0.348	0.141	0.221
63	0.012	0.816	-0.098
77	0.030	0.781	-0.152
83	0.386	1.184	-0.676
87	0.148	1.386	-0.452
88	0.036	1.554	0.238

TABLE 4.4 (continued)

Resonance Number	γ_{j11}^2 (keV)	γ_{j13}^2 (keV)	$\gamma_{j11}\gamma_{j13}$ (keV)
94	0.001	0.312	-0.021
95	0.133	0.130	-0.132
116	1.884	0.439	0.909
117	1.579	1.253	-1.406
125	0.857	0.425	-0.604
135	0.056	0.434	-0.156
136	0.024	0.069	-0.041
143	0.015	0.141	-0.046
158	0.052	0.320	-0.129
162	0.141	0.224	-0.177
175	0.568	0.021	0.110

TABLE 4.5

INELASTIC REDUCED WIDTHS AND AMPLITUDE PRODUCTS FOR $3/2^-$ RESONANCES IN ^{51}Mn

Channel Spin Representation

Resonance Number	γ^2_{s13} (keV)	γ^2_{s15} (keV)	$\gamma_{s13}\gamma_{s15}$ (keV)
M1	0.292	0.101	0.172
M3	0.546	0.684	-0.611
M5	1.638	1.085	-1.333
M6	0.298	0.512	0.390
M7	0.101	0.161	0.128
M8	0.180	0.258	0.216
5	1.155	0.049	0.239
7	0.000	0.098	0.005
13	0.372	0.400	-0.386
21	0.011	0.103	0.033
37	0.021	0.305	0.079
41	0.341	0.320	0.331
56	0.057	0.083	0.069
60	0.359	0.129	-0.216
63	0.577	0.251	0.381
77	0.509	0.302	0.392
83	0.483	1.087	0.725
87	0.776	0.757	0.767
88	1.440	0.150	0.464

TABLE 4.5 (continued)

Resonance Number	γ^2_{s13} (keV)	γ^2_{s15} (keV)	$\gamma_{s13}\gamma_{s15}$ (keV)
94	0.233	0.080	0.137
95	0.026	0.237	0.078
116	1.455	0.867	-1.123
117	0.193	2.639	0.713
125	0.029	1.254	0.189
135	0.234	0.257	0.245
136	0.028	0.065	0.042
143	0.079	0.077	0.078
158	0.163	0.208	0.185
162	0.065	0.299	0.140
175	0.218	0.371	-0.285

FIGURE 4.2 Plots of reduced widths and the cumulative sums of reduced widths for the elastic and total inelastic decay channels for $3/2^-$ resonances in ^{51}Mn.

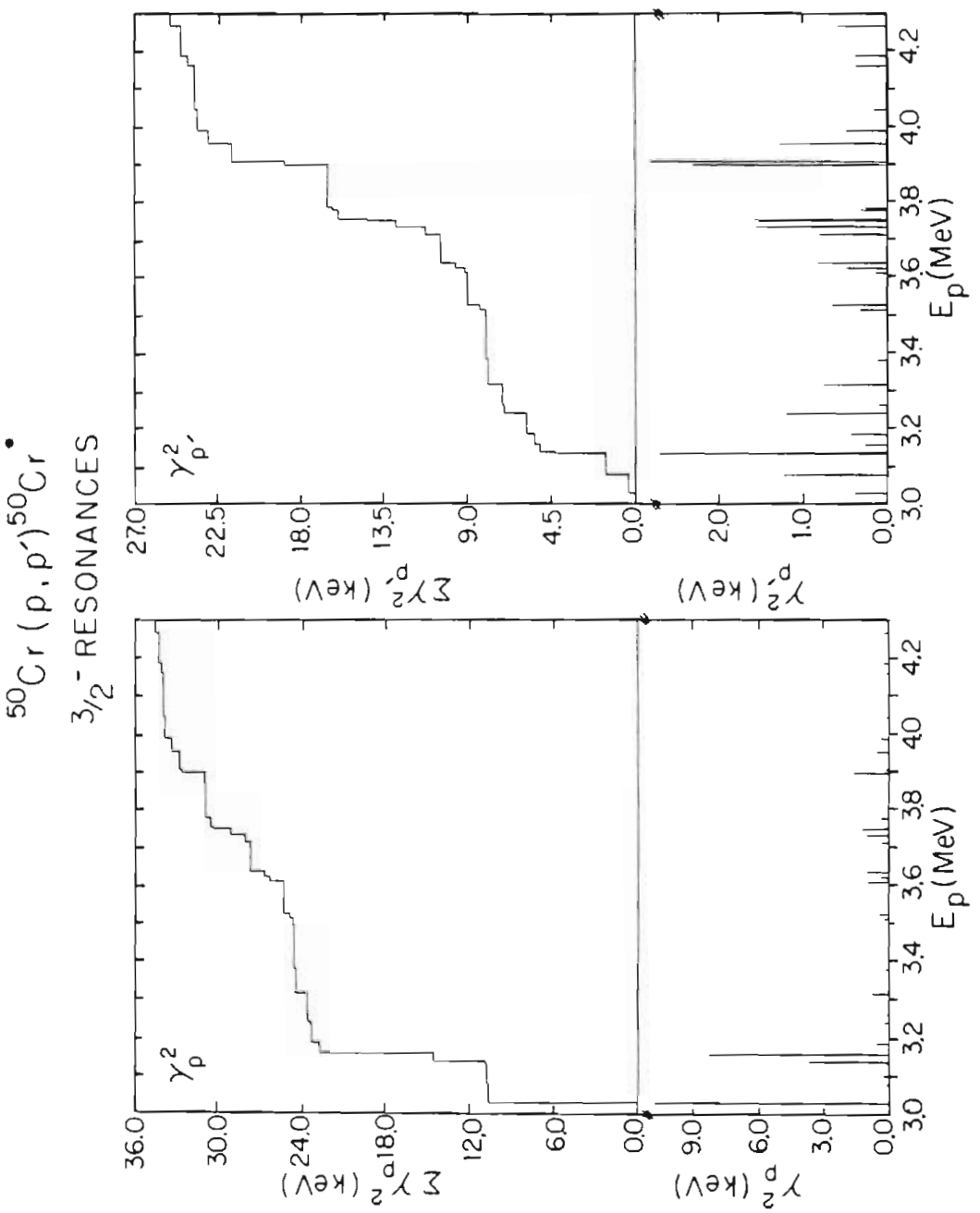
$^{50}Cr(p,p')^{50}Cr^{\bullet}$
$3/2^-$ RESONANCES
γ_p^2
$\gamma_{p'}^2$
$\Sigma\gamma_p^2$ (keV)
$\Sigma\gamma_{p'}^2$ (keV)
γ_p^2 (keV)
$\gamma_{p'}^2$ (keV)
E_p(MeV)
E_p(MeV)

FIGURE 4.3 Plots of reduced widths and the cumulative sums of reduced widths for the two inelastic decay channels for $3/2^-$ resonances in ^{51}Mn in the total angular momentum representation.

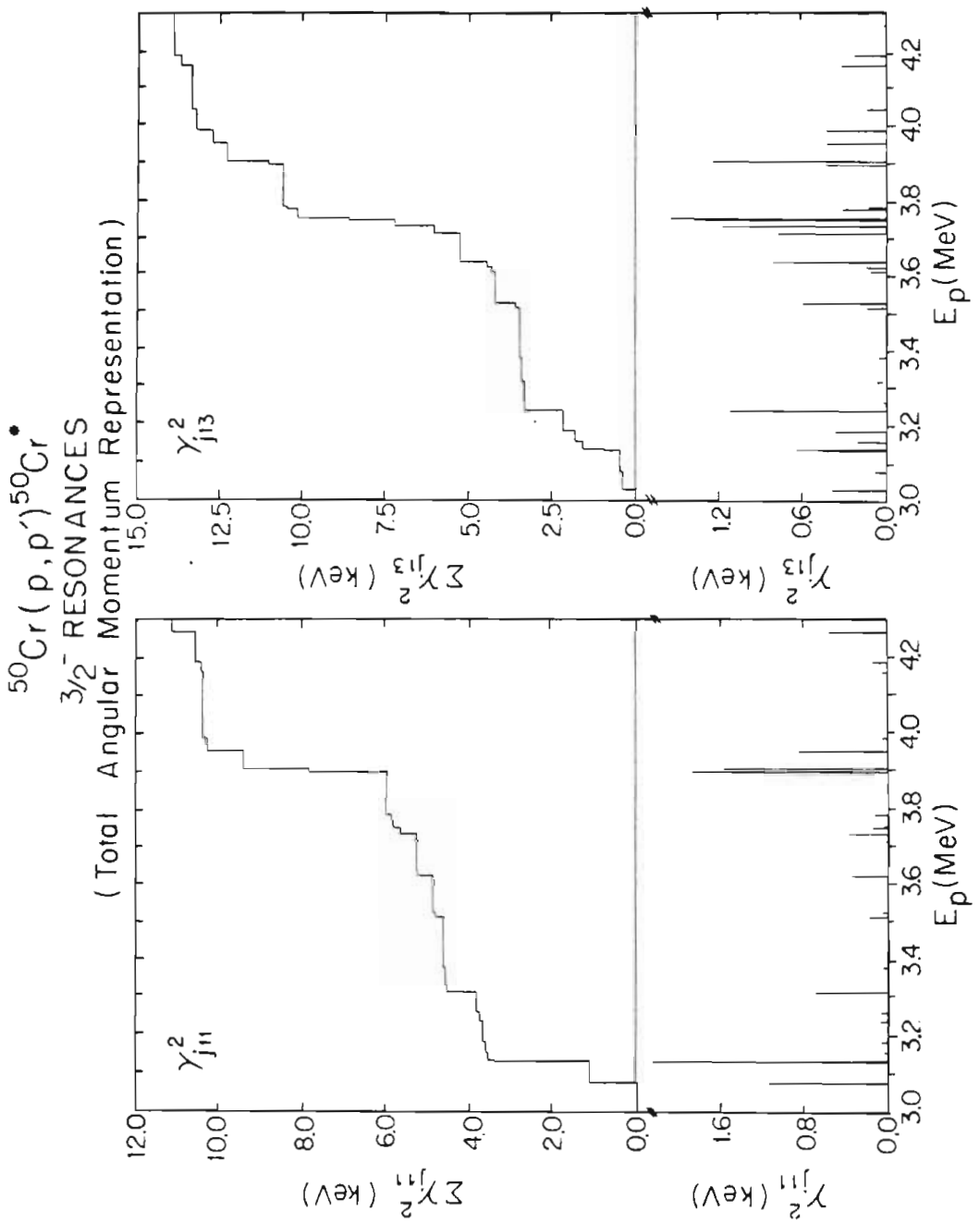
$^{50}Cr(p,p')^{50}Cr^{*}$
$3/2^{-}$ RESONANCES
(Total Angular Momentum Representation)
γ^2_{j11}
γ^2_{j13}
$\Sigma\gamma^2_{j11}$ (keV)
$\Sigma\gamma^2_{j13}$ (keV)
γ^2_{j11} (keV)
γ^2_{j13} (keV)
E_p(MeV)
E_p(MeV)

FIGURE 4.4 Plots of reduced widths and the cumulative sums of reduced widths for the two inelastic decay channels for $3/2^-$ resonances in ^{51}Mn in the channel spin representation.

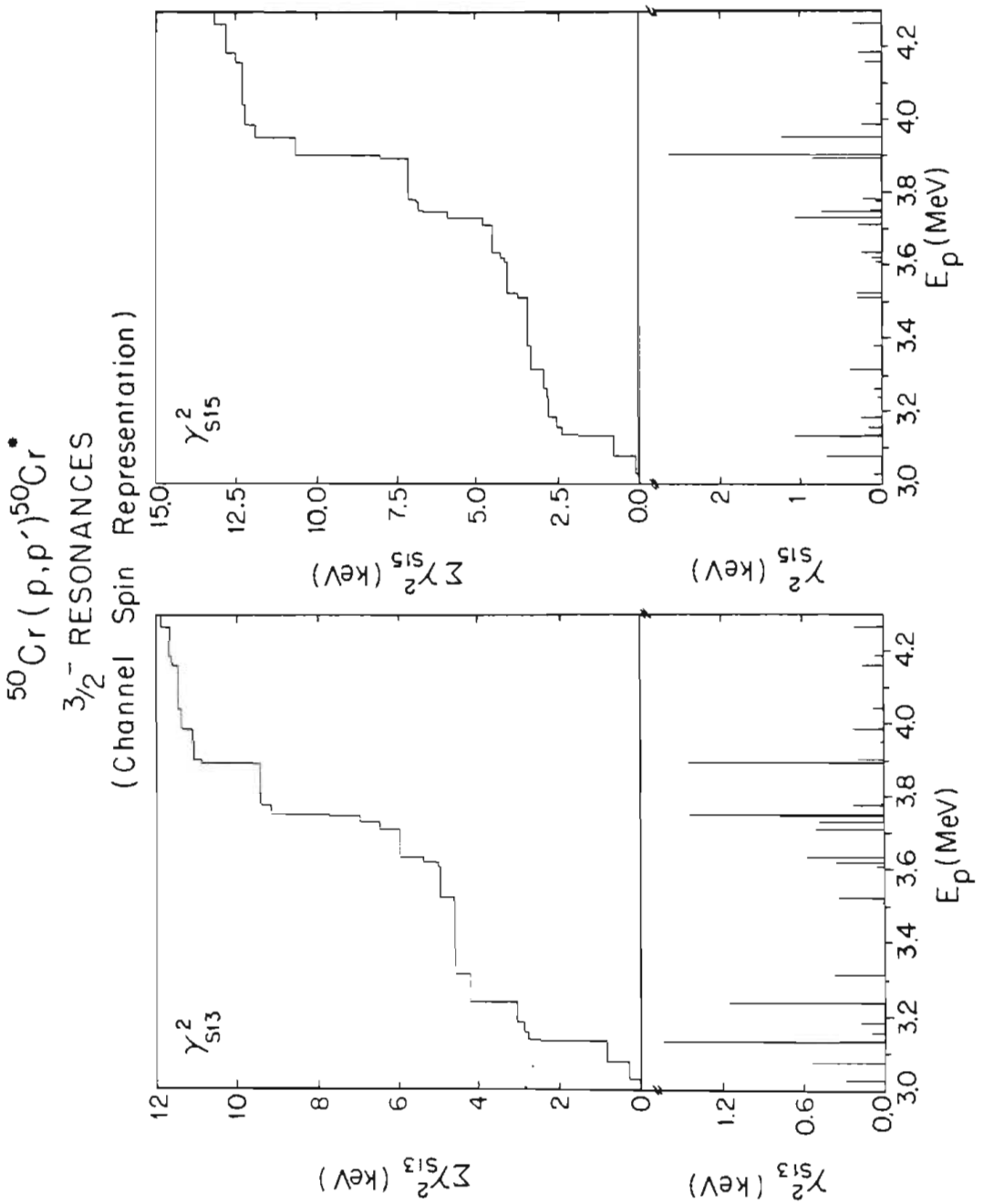
$^{50}Cr(p,p')^{50}Cr^{*}$
$3/2^{-}$ RESONANCES
(Channel Spin Representation)
γ^2_{s13}
γ^2_{s15}
$\Sigma\gamma^2_{s13}$ (keV)
$\Sigma\gamma^2_{s15}$ (keV)
γ^2_{s13} (keV)
γ^2_{s15} (keV)
E_p(MeV)
E_p(MeV)

FIGURE 4.5 Products of inelastic decay amplitudes and cumulative sums of the products versus energy for the two inelastic decay channels for $3/2^-$ resonances in ^{51}Mn in both representations.

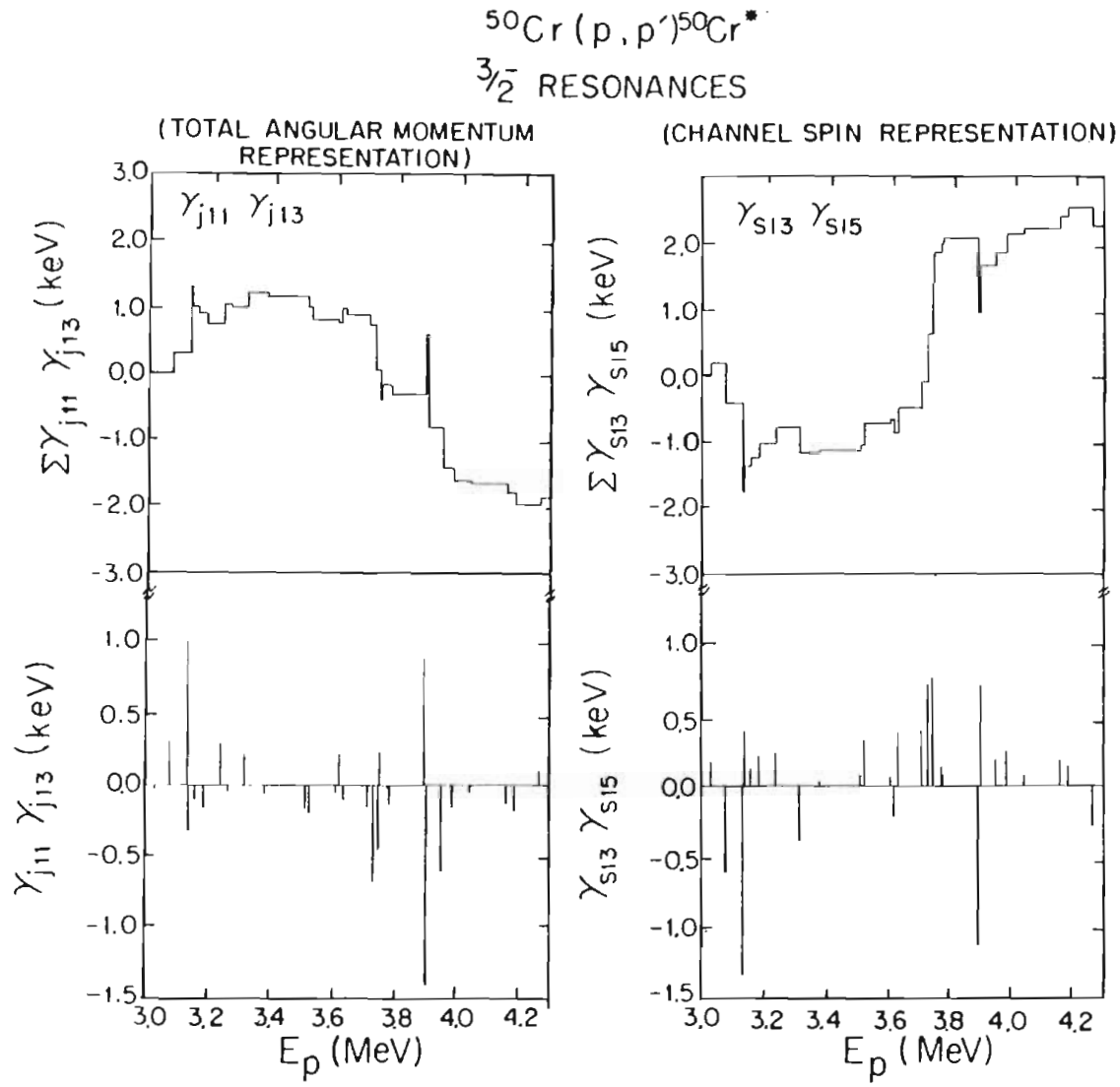
$^{50}Cr(p,p')^{50}Cr^*$
$3/2^-$ RESONANCES
(TOTAL ANGULAR MOMENTUM REPRESENTATION)
(CHANNEL SPIN REPRESENTATION)
$\gamma_{j11}\ \gamma_{j13}$
$\gamma_{S13}\ \gamma_{S15}$
$\Sigma\gamma_{j11}\ \gamma_{j13}$ (keV)
$\Sigma\gamma_{S13}\ \gamma_{S15}$ (keV)
$\gamma_{j11}\ \gamma_{j13}$ (keV)
$\gamma_{S13}\ \gamma_{S15}$ (keV)
E_p (MeV)
E_p (MeV)

FIGURE 4.6 Sample angular distributions for a $5/2^+$ resonance. The top figure is the inelastically scattered proton distribution, and the bottom figure is the γ-ray distribution.

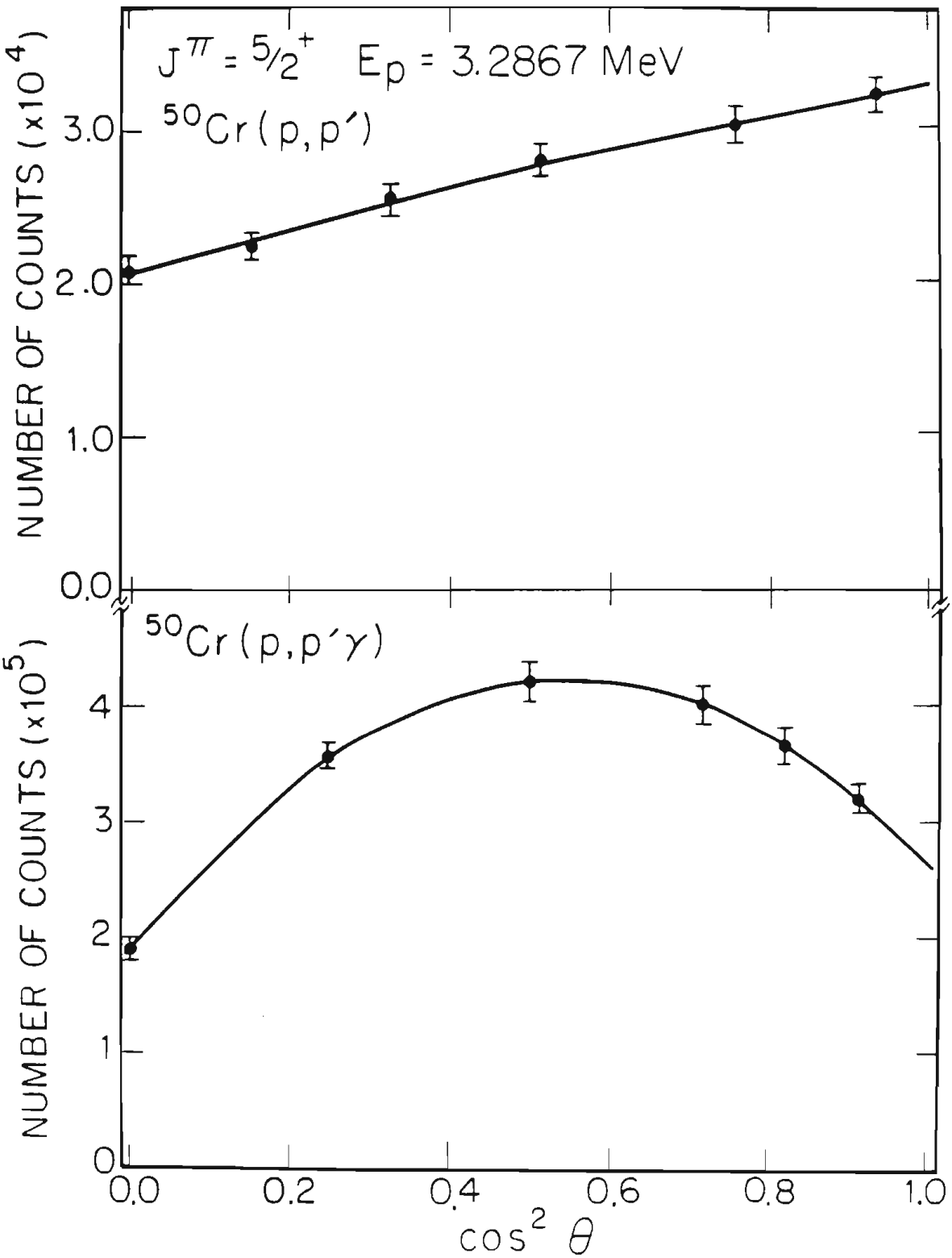
$J^{\pi} = 5/2^{+}$ $E_p = 3.2867$ MeV
$^{50}Cr(p,p')$
NUMBER OF COUNTS ($\times 10^4$)
3.0
2.0
1.0
0.0
$^{50}Cr(p,p'\gamma)$
NUMBER OF COUNTS ($\times 10^5$)
4
3
2
1
0
0.0
0.2
0.4
0.6
0.8
1.0
$\cos^2\theta$

line is the best χ^2 fit to the data. A J^π value of $3/2^+$ was assigned to 20 resonances, while 38 resonances were labeled $5/2^+$. A list of $\ell = 2$ resonances with J^π assignments and measured Legendre polynomial coefficients is presented in table 4.6.

Resonances with $J^\pi = 3/2^+$ have three open exit channels: in the total angular momentum representation, $\ell'=0$ $j'=1/2$, $\ell'=2$ $j'=3/2$, and $\ell'=2$ $j'=5/2$, and in the channel spin representation, $\ell'=0$ $s'=3/2$, $\ell'=2$ $s'=3/2$, and $\ell'=2$ $s'=5/2$. Any $\ell'=4$ contributions are neglected because the Coulomb penetrability is extremely low relative to the $\ell'=0$ and $\ell'=2$ contributions. The two independent mixing ratios are taken to be: $\delta_{jBA} = \gamma_{j23}/\gamma_{j01}$ and $\delta_{jCA} = \gamma_{j25}/\gamma_{j01}$ in the total angular momentum representation, and $\delta_{sBA} = \gamma_{s23}/\gamma_{s03}$ and $\delta_{sCA} = \gamma_{s25}/\gamma_{s03}$ in the channel spin representation. Two independent mixing angles are also defined: in the total angular momentum representation $\phi_{jBA} = \tan^{-1}\delta_{jBA}$ and $\phi_{jCA} = \tan^{-1}\delta_{jCA}$, and in the channel spin representation, $\phi_{sBA} = \tan^{-1}\delta_{sBA}$ and $\phi_{sCA} = \tan^{-1}\delta_{sCA}$. There is a third mixing ratio, δ_{CB}, defined as $\gamma_{j25}/\gamma_{j23}$ in the total angular momentum representation, and as $\gamma_{s25}/\gamma_{s23}$ in the channel spin representation, and a corresponding ϕ_{CB} in both representations. This third mixing ratio is not independent of the other two. There is one additional parameter, ε^2, which is not independent and represents the $\ell'=2$ admixture. Note that for d-wave resonances the penetrability factors have been removed from the definition of ε^2.

As explained in Chapter II, since both a_4 coefficients are zero for $3/2^+$ resonances, a unique solution for the mixing ratios cannot be obtained. No further analysis was performed on these resonances. Both acceptable solutions are listed in table 4.7 for the total angular momentum representation, and in table 4.8 for the channel spin representation. The corresponding plots for the measured mixing angles are shown in figures 4.7 and 4.8. For both

TABLE 4.6

LEGENDRE POLYNOMIAL COEFFICIENTS FOR ℓ=2 RESONANCES IN ^{51}Mn

Resonance Number	J^{π}	Experiment	a_2	a_4
2	$5/2^+$	p	0.212 ± 0.036	0.025 ± 0.045
		γ	0.405 ± 0.031	−0.439 ± 0.045
6	$5/2^+$	p	0.334 ± 0.036	−0.020 ± 0.046
		γ	0.393 ± 0.029	−0.556 ± 0.043
8	$5/2^+$	p	0.251 ± 0.036	−0.039 ± 0.045
		γ	0.445 ± 0.029	−0.566 ± 0.044
16	$3/2^+$	p	0.379 ± 0.036	
		γ	0.266 ± 0.036	
18	$3/2^+$	p	0.342 ± 0.040	
		γ	0.216 ± 0.038	
22	$5/2^+$	p	0.330 ± 0.040	−0.052 ± 0.051
		γ	0.437 ± 0.037	−0.510 ± 0.054
26	$5/2^+$	p	0.259 ± 0.040	−0.009 ± 0.052
		γ	0.353 ± 0.037	−0.447 ± 0.054
27	$5/2^+$	p	0.365 ± 0.041	0.017 ± 0.052
		γ	0.422 ± 0.036	−0.529 ± 0.054
29	$3/2^+$	p	0.219 ± 0.041	
		γ	0.380 ± 0.039	
33	$3/2^+$	p	0.272 ± 0.053	
		γ	0.383 ± 0.039	
42	$3/2^+$	p	−0.259 ± 0.051	
		γ	−0.314 ± 0.034	
45	$3/2^+$	p	0.104 ± 0.053	
		γ	0.309 ± 0.039	
48	$5/2^+$	p	0.145 ± 0.166	−0.059 ± 0.157
		γ	0.389 ± 0.040	−0.124 ± 0.056
49	$5/2^+$	p	0.364 ± 0.072	0.058 ± 0.080
		γ	0.407 ± 0.039	−0.263 ± 0.056

TABLE 4.6 (continued)

Resonance Number	J^{π}	Experiment	a_2	a_4
55	$3/2^+$	p	-0.238 ± 0.073	
		γ	0.374 ± 0.038	
59	$5/2^+$	p	0.246 ± 0.070	-0.076 ± 0.081
		γ	0.476 ± 0.037	-0.458 ± 0.055
61	$3/2^+$	p	-0.264 ± 0.071	
		γ	0.245 ± 0.039	
62	$5/2^+$	p	0.262 ± 0.165	-0.124 ± 0.159
		γ	0.351 ± 0.037	-0.398 ± 0.055
65	$3/2^+$	p	-0.257 ± 0.072	
		γ	0.355 ± 0.038	
66	$5/2^+$	p	0.140 ± 0.069	-0.068 ± 0.080
		γ	0.415 ± 0.037	-0.415 ± 0.054
68	$5/2^+$	p	-0.394 ± 0.180	-0.006 ± 0.164
		γ	0.357 ± 0.038	-0.251 ± 0.055
70	$5/2^+$	p	0.239 ± 0.069	-0.043 ± 0.080
		γ	0.506 ± 0.037	-0.619 ± 0.054
71	$5/2^+$	p	-0.283 ± 0.222	0.027 ± 0.178
		γ	0.432 ± 0.039	-0.243 ± 0.056
73	$5/2^+$	p	0.243 ± 0.216	-0.174 ± 0.188
		γ	0.308 ± 0.038	-0.262 ± 0.055
75	$3/2^+$	p	0.410 ± 0.060	
		γ	-0.112 ± 0.036	
78	$5/2^+$	p	0.377 ± 0.201	-0.021 ± 0.173
		γ	0.321 ± 0.036	-0.453 ± 0.054
80	$5/2^+$	p	-0.045 ± 0.226	-0.139 ± 0.189
		γ	0.301 ± 0.037	-0.345 ± 0.055
81	$5/2^+$	p	0.155 ± 0.233	-0.366 ± 0.207
		γ	0.211 ± 0.037	-0.221 ± 0.055
82	$3/2^+$	p	-0.123 ± 0.043	
		γ	-0.047 ± 0.037	

TABLE 4.6 (continued)

Resonance Number	J^{π}	Experiment	a_2	a_4
84	$3/2^+$	p	0.167 ± 0.076	
		γ	0.359 ± 0.039	
89	$3/2^+$	p	−0.334 ± 0.039	
		γ	0.078 ± 0.038	
92	$3/2^+$	p	−0.014 ± 0.046	
		γ	0.380 ± 0.039	
96	$5/2^+$	p	−0.095 ± 0.225	−0.018 ± 0.181
		γ	0.370 ± 0.037	−0.413 ± 0.055
100	$5/2^+$	p	0.040 ± 0.239	−0.398 ± 0.210
		γ	0.178 ± 0.036	−0.363 ± 0.054
101	$5/2^+$	p	0.227 ± 0.050	−0.021 ± 0.054
		γ	0.300 ± 0.037	−0.419 ± 0.055
103	$3/2^+$	p	0.155 ± 0.050	
		γ	0.149 ± 0.039	
106	$5/2^+$	p	0.071 ± 0.215	−0.052 ± 0.180
		γ	0.446 ± 0.039	−0.238 ± 0.056
107	$5/2^+$	p	0.234 ± 0.050	0.042 ± 0.052
		γ	0.219 ± 0.038	−0.195 ± 0.055
110	$5/2^+$	p	0.170 ± 0.051	0.057 ± 0.054
		γ	0.516 ± 0.039	−0.382 ± 0.056
114	$5/2^+$	p	0.243 ± 0.049	−0.060 ± 0.054
		γ	0.424 ± 0.039	−0.288 ± 0.056
115	$5/2^+$	p	0.179 ± 0.051	0.038 ± 0.054
		γ	0.447 ± 0.038	−0.383 ± 0.056
118	$5/2^+$	p	0.072 ± 0.067	0.098 ± 0.078
		γ	0.364 ± 0.039	−0.423 ± 0.063
120	$3/2^+$	p	0.514 ± 0.053	
		γ	0.169 ± 0.039	
121	$5/2^+$	p	−0.348 ± 0.040	0.087 ± 0.050
		γ	0.382 ± 0.038	−0.307 ± 0.056

TABLE 4.6 (continued)

Resonance Number	J^{π}	Experiment	a_2	a_4
122	$3/2^+$	p	-0.208 ± 0.056	
		γ	0.391 ± 0.038	
123	$5/2^+$	p	0.132 ± 0.043	-0.038 ± 0.053
		γ	0.503 ± 0.038	-0.437 ± 0.056
130	$3/2^+$	p	0.385 ± 0.057	
		γ	0.160 ± 0.039	
134	$5/2^+$	p	0.234 ± 0.072	-0.152 ± 0.083
		γ	0.127 ± 0.034	-0.519 ± 0.052
138	$5/2^+$	p	0.195 ± 0.071	-0.003 ± 0.082
		γ	0.519 ± 0.038	-0.518 ± 0.055
141	$3/2^+$	p	0.332 ± 0.048	
		γ	0.019 ± 0.037	
150	$5/2^+$	p	-0.376 ± 0.059	0.248 ± 0.076
		γ	0.458 ± 0.041	-0.284 ± 0.064
151	$3/2^+$	p	0.220 ± 0.054	
		γ	0.357 ± 0.039	
152	$5/2^+$	p	0.277 ± 0.052	-0.057 ± 0.058
		γ	0.334 ± 0.042	0.276 ± 0.056
160	$5/2^+$	p	0.292 ± 0.055	0.025 ± 0.069
		γ	0.417 ± 0.037	-0.440 ± 0.055
161	$5/2^+$	p	0.315 ± 0.050	-0.168 ± 0.065
		γ	0.302 ± 0.041	-0.075 ± 0.063
164	$5/2^+$	p	0.260 ± 0.072	-0.305 ± 0.094
		γ	0.340 ± 0.038	-0.252 ± 0.056
165	$5/2^+$	p	0.064 ± 0.069	-0.020 ± 0.089
		γ	0.459 ± 0.037	-0.406 ± 0.054
173	$5/2^+$	p	0.329 ± 0.074	0.103 ± 0.089
		γ	0.487 ± 0.038	-0.620 ± 0.061

TABLE 4.7

MIXING RATIOS, MIXING ANGLES, AND ε^2 FOR $3/2^+$ RESONANCES IN ^{51}Mn

Total Angular Momentum Representation

Resonance Number	ϕ_{jBA} (degrees)	ϕ_{jCA} (degrees)	δ_{jBA}	δ_{jCA}	ε^2
16	13.4 ± 16.8	62.0 ± 2.4	0.24 + 0.34 − 0.30	1.88 + 0.21 − 0.18	0.78
	57.2 ± 6.3	57.8 ± 3.0	1.55 + 0.46 − 0.32	1.59 + 0.20 − 0.17	0.83
18	−6.1 ± 13.3	65.1 ± 2.3	−0.11 + 0.23 − 0.24	2.15 + 0.24 − 0.21	0.82
	64.6 ± 3.6	59.7 ± 3.5	2.11 + 0.39 − 0.30	1.71 + 0.27 − 0.22	0.88
29	−11.8 ± 14.7	48.6 ± 5.8	−0.21 + 0.26 − 0.29	1.13 + 0.26 − 0.21	0.57
	52.1 ± 8.3	33.7 ± 6.4	1.28 + 0.48 − 0.33	0.67 + 0.17 − 0.15	0.68
33	7.7 ± 29.4	48.1 ± 6.9	0.13 + 0.62 − 0.53	1.11 + 0.32 − 0.24	0.56
	44.9 ± 16.7	40.5 ± 7.1	1.00 + 0.86 − 0.46	0.85 + 0.24 − 0.19	0.63
42	−39.9 ± 30.0	−85.6 ± 1.3	−0.84 + 0.67 − 1.89	−13.10 + 3.05 − 5.67	0.99
	−84.4 ± 3.7	88.1 ± 1.5	−10.16 + 4.05 − 19.15	30.18 + 9.24 − 13.27	1.00
45	−40.6 ± 6.6	54.8 ± 3.9	−0.86 + 0.18 − 0.22	1.42 + 0.23 − 0.19	0.73
	64.5 ± 3.3	28.1 ± 10.0	2.10 + 0.35 − 0.28	0.53 + 0.25 − 0.21	0.82

TABLE 4.7 (continued)

Resonance Number	ϕ_{jBA} (degrees)	ϕ_{jCA} (degrees)	δ_{jBA}	δ_{jCA}	ε^2
55	36.8 ± 22.0	-45.1 ± 8.5	0.75 + 0.90 − 0.49	-1.00 + 0.26 − 0.35	0.61
	-57.0 ± 4.4	13.6 ± 25.8	-1.54 + 0.23 − 0.30	0.24 + 0.58 − 0.46	0.71
61	-65.5 ± 2.6	50.0 ± 7.7	-2.20 + 0.24 − 0.30	1.19 + 0.39 − 0.28	0.86
	69.3 ± 4.3	-35.4 ± 16.1	2.65 + 0.75 − 0.50	-0.71 + 0.36 − 0.55	0.88
65	41.6 ± 18.0	-46.8 ± 9.6	0.89 + 0.81 − 0.45	-1.07 + 0.31 − 0.44	0.66
	-59.2 ± 3.7	18.3 ± 23.7	-1.68 + 0.22 − 0.28	0.33 + 0.57 − 0.42	0.75
75	58.5 ± 16.5	77.7 ± 1.2	1.64 + 2.12 − 0.73	4.58 + 0.50 − 0.42	0.96
	58.5 ± 16.5	77.7 ± 1.2	1.63 + 2.12 − 0.73	4.58 + 0.50 − 0.42	0.96
82	-66.9 ± 2.2	75.6 ± 1.4	-2.35 + 0.23 − 0.28	3.90 + 0.45 − 0.37	0.95
	84.8 ± 2.0	80.2 ± 5.2	11.01 + 7.24 − 3.14	5.77 + 6.64 − 2.05	0.99
84	-23.1 ± 12.8	49.0 ± 4.8	-0.43 + 0.24 − 0.30	1.15 + 0.22 − 0.18	0.60
	55.7 ± 5.7	29.5 ± 9.4	1.46 + 0.37 − 0.27	0.57 + 0.24 − 0.20	0.71
89	-71.8 ± 1.5	67.6 ± 2.9	-3.04 + 0.24 − 0.29	2.42 + 0.40 − 0.31	0.94
	81.1 ± 2.0	20.2 ± 30.0	6.35 + 1.83 − 1.17	0.37 + 0.83 − 0.54	0.98

TABLE 4.7 (continued)

Resonance Number	ϕ_{jBA} (degrees)	ϕ_{jCA} (degrees)	δ_{jBA}	δ_{jCA}	ε^2
92	−43.1 ± 5.6	39.1 ± 7.9	−0.94 + 0.17 − 0.20	0.81 + 0.26 − 0.21	0.61
	55.5 ± 6.3	−4.6 ± 10.7	1.46 + 0.41 − 0.30	−0.08 + 0.19 − 0.19	0.68
103	−39.1 ± 6.8	66.0 ± 2.0	−0.81 + 0.18 − 0.22	2.24 + 0.22 − 0.19	0.85
	71.5 ± 2.0	57.8 ± 4.8	2.99 + 0.39 − 0.32	1.59 + 0.34 − 0.26	0.92
120	43.8 ± 10.3	64.4 ± 2.0	0.96 + 0.42 − 0.30	2.09 + 0.20 − 0.18	0.84
	43.8 ± 10.3	64.4 ± 2.0	0.96 + 0.42 − 0.30	2.09 + 0.21 − 0.18	0.84
122	30.9 ± 22.0	−40.1 ± 7.6	0.60 + 0.72 − 0.44	−0.84 + 0.20 − 0.26	0.52
	−51.9 ± 5.3	10.5 ± 23.5	−1.28 + 0.22 − 0.28	0.19 + 0.49 − 0.42	0.63
130	28.8 ± 30.3	64.7 ± 2.1	0.55 + 1.12 − 0.58	2.12 + 0.22 − 0.19	0.83
	53.7 ± 14.8	63.4 ± 2.8	1.36 + 1.18 − 0.55	2.00 + 0.27 − 0.22	0.85
141	12.7 ± 20.6	71.4 ± 1.4	0.22 + 0.43 − 0.36	2.97 + 0.26 − 0.22	0.90
	66.8 ± 4.4	71.1 ± 1.9	2.34 + 0.60 − 0.42	2.92 + 0.35 − 0.29	0.93
151	−6.8 ± 15.3	47.5 ± 4.7	−0.12 + 0.27 − 0.29	1.09 + 0.20 − 0.16	0.55
	49.0 ± 7.9	35.8 ± 6.7	1.15 + 0.38 − 0.28	0.72 + 0.19 − 0.16	0.65

TABLE 4.8

MIXING RATIOS, MIXING ANGLES, AND ε^2 FOR $3/2^+$ RESONANCES IN ^{51}Mn

Channel Spin Representation

Resonance Number	ϕ_{sBA} (degrees)	ϕ_{sCA} (degrees)	δ_{sBA}	δ_{sCA}	ε^2
16	61.2 ± 2.2	28.1 ± 14.4	1.82 + 0.18 − 0.16	0.53 + 0.38 − 0.29	0.78
	64.3 ± 2.4	−38.2 ± 12.4	2.07 + 0.24 − 0.20	−0.79 + 0.30 − 0.43	0.83
18	62.6 ± 2.5	43.8 ± 7.5	1.93 + 0.22 − 0.19	0.96 + 0.29 − 0.22	0.82
	67.5 ± 2.5	−51.3 ± 6.4	2.41 + 0.33 − 0.27	−1.25 + 0.25 − 0.34	0.88
29	43.7 ± 5.0	32.8 ± 12.7	0.96 + 0.18 − 0.15	0.65 + 0.37 − 0.28	0.57
	48.3 ± 5.9	−42.3 ± 10.7	1.12 + 0.26 − 0.21	−0.91 + 0.29 − 0.42	0.68
33	47.0 ± 4.9	17.9 ± 28.4	1.07 + 0.20 − 0.17	0.32 + 0.72 − 0.51	0.56
	49.7 ± 5.7	−29.8 ± 24.9	1.18 + 0.27 − 0.21	−0.57 + 0.49 − 0.84	0.63
42	−85.4 ± 1.3	−77.4 ± 8.7	−12.35 + 2.74 − 4.90	−4.48 + 1.91 − 10.27	0.99
	87.6 ± 3.2	87.3 ± 3.2	23.75 + 99.99 − 13.57	21.51 + 99.99 − 11.70	1.00
45	43.8 ± 5.6	53.5 ± 4.3	0.96 + 0.21 − 0.17	1.35 + 0.24 − 0.20	0.73
	53.0 ± 5.7	−59.6 ± 3.8	1.33 + 0.32 − 0.24	−1.71 + 0.23 − 0.29	0.82

TABLE 4.8 (continued)

Resonance Number	ϕ_{sBA} (degrees)	ϕ_{sCA} (degrees)	δ_{sBA}	δ_{sCA}	ε^2
55	-31.8 ± 23.6	-47.4 ± 19.9	-0.62 + 0.48 − 0.83	-1.09 + 0.57 − 1.30	0.61
	-21.5 ± 19.9	56.5 ± 6.2	-0.39 + 0.37 − 0.49	1.51 + 0.42 − 0.31	0.71
61	12.1 ± 17.5	68.1 ± 2.2	0.21 + 0.35 − 0.31	2.49 + 0.30 − 0.25	0.86
	22.3 ± 28.7	-69.8 ± 3.0	0.41 + 0.83 − 0.52	-2.71 + 0.38 − 0.50	0.88
65	-31.9 ± 26.2	-51.1 ± 17.4	-0.62 + 0.52 − 0.98	-1.24 + 0.57 − 1.30	0.66
	-20.1 ± 20.3	59.1 ± 4.9	-0.37 + 0.37 − 0.48	1.67 + 0.38 − 0.28	0.75
75	78.4 ± 1.6	18.5 ± 30.0	4.85 + 0.81 − 0.61	0.33 + 0.80 − 0.53	0.96
	78.4 ± 1.6	18.5 ± 30.0	4.85 + 0.81 − 0.61	0.33 + 0.80 − 0.53	0.96
82	69.2 ± 2.5	74.9 ± 1.3	2.63 + 0.39 − 0.31	3.71 + 0.36 − 0.30	0.95
	84.1 ± 2.0	-82.7 ± 1.9	9.71 + 4.87 − 2.44	-7.79 + 1.61 − 2.70	0.99
84	41.4 ± 6.0	40.4 ± 8.9	0.88 + 0.21 − 0.17	0.85 + 0.31 − 0.24	0.60
	47.9 ± 6.1	-48.1 ± 7.6	1.11 + 0.27 − 0.21	-1.11 + 0.26 − 0.35	0.71
89	45.1 ± 8.2	75.1 ± 1.2	1.00 + 0.34 − 0.25	3.76 + 0.36 − 0.30	0.94
	70.8 ± 7.9	-80.0 ± 2.2	2.88 + 2.16 − 0.92	-5.67 + 1.05 − 1.64	0.98

TABLE 4.8 (continued)

Resonance Number	ϕ_{sBA} (degrees)	ϕ_{sCA} (degrees)	δ_{sBA}	δ_{sCA}	ε^2
92	20.3 ± 9.5	49.8 ± 5.3	0.37 + 0.20 − 0.18	1.18 + 0.25 − 0.20	0.61
	27.0 ± 12.0	−53.8 ± 5.5	0.51 + 0.30 − 0.24	−1.37 + 0.24 − 0.32	0.68
103	60.0 ± 2.9	58.7 ± 3.1	1.73 + 0.22 − 0.19	1.64 + 0.22 − 0.19	0.85
	69.4 ± 2.5	−64.6 ± 3.0	2.66 + 0.40 − 0.32	−2.11 + 0.26 − 0.32	0.92
120	66.5 ± 1.9	−2.4 ± 19.1	2.30 + 0.23 − 0.20	−0.04 + 0.34 − 0.35	0.84
	66.5 ± 1.9	−2.4 ± 19.1	2.30 + 0.23 − 0.20	−0.04 + 0.34 − 0.35	0.84
122	−28.1 ± 20.9	−41.5 ± 21.9	−0.53 + 0.41 − 0.62	−0.89 + 0.53 − 1.11	0.52
	−18.8 ± 17.1	51.2 ± 7.7	−0.34 + 0.31 − 0.38	1.24 + 0.41 − 0.29	0.63
130	65.2 ± 2.8	18.9 ± 20.0	2.16 + 0.32 − 0.25	0.34 + 0.47 − 0.36	0.83
	67.2 ± 2.4	−24.1 ± 20.0	2.38 + 0.31 − 0.26	−0.45 + 0.38 − 0.52	0.85
141	70.4 ± 1.9	44.5 ± 9.9	2.81 + 0.32 − 0.26	0.98 + 0.42 − 0.29	0.90
	74.5 ± 1.5	−44.2 ± 13.4	3.61 + 0.41 − 0.34	−0.97 + 0.38 − 0.61	0.93
151	43.6 ± 4.8	28.6 ± 12.5	0.95 + 0.17 − 0.15	0.55 + 0.33 − 0.26	0.55
	48.3 ± 5.0	−37.5 ± 11.1	1.12 + 0.22 − 0.18	−0.77 + 0.27 − 0.37	0.65

FIGURE 4.7 Plot of ϕ_{CA} versus ϕ_{BA} for 20 $3/2^+$ resonances in ^{51}Mn in the total angular momentum representation. Data points indicated by a large circle correspond to the set of solutions with the smaller $\ell'=2$ admixture, and data points indicated by a small triangle correspond to the set of solutions with the larger $\ell'=2$ admixture. Note that for two resonances the solutions are degenerate.

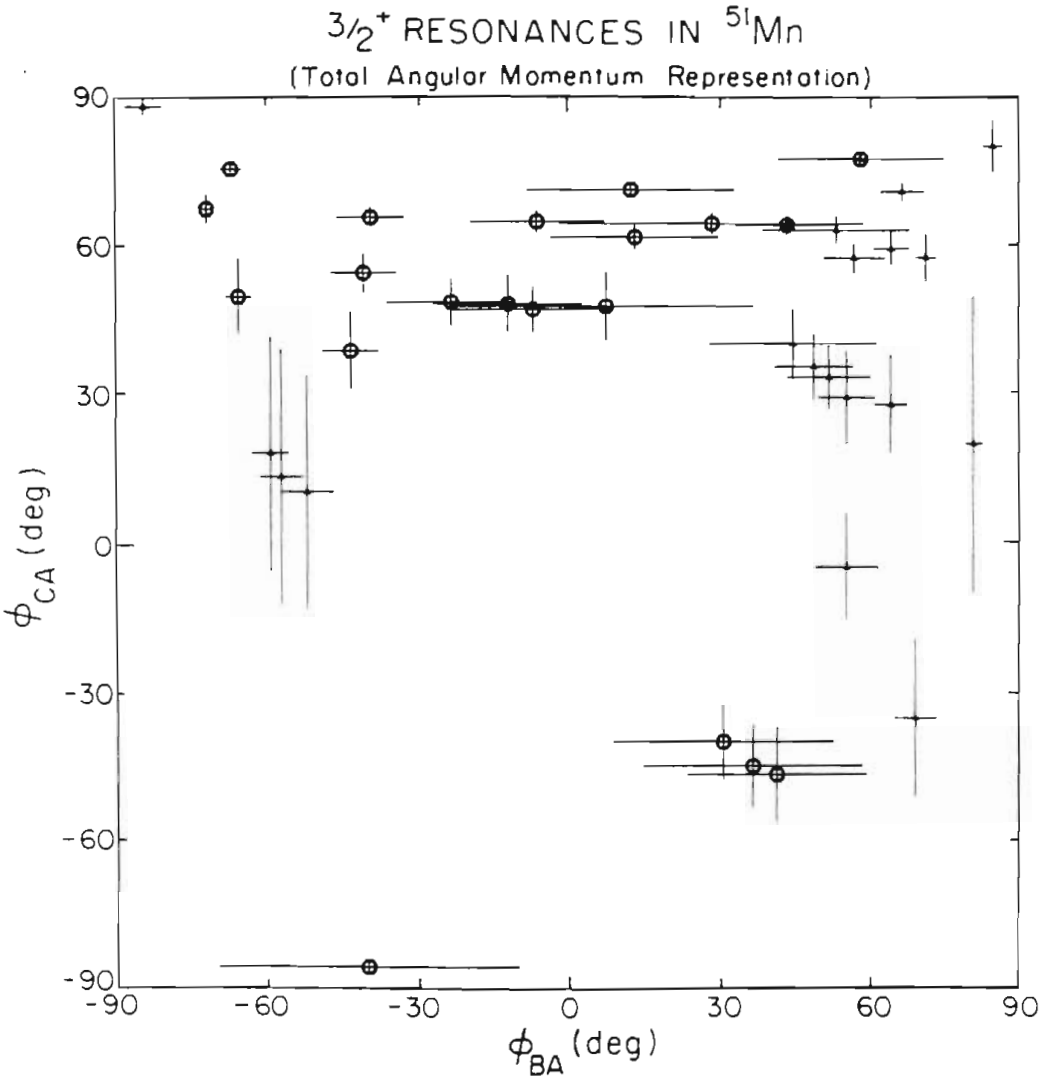
3/2+ RESONANCES IN 51Mn
(Total Angular Momentum Representation)
90
60
30
0
-30
-60
-90
-90
-60
-30
0
30
60
90
φCA (deg)
φBA (deg)

FIGURE 4.8 Plot of ϕ_{CA} versus ϕ_{BA} for 20 $3/2^+$ resonances in ^{51}Mn in the channel spin representation. Data points indicated by a large circle correspond to the set of solutions with the smaller $\ell'=2$ admixture, and data points indicated by a small triangle correspond to the set of solutions with the larger $\ell'=2$ admixture. Note that for two resonances the solutions are degenerate.

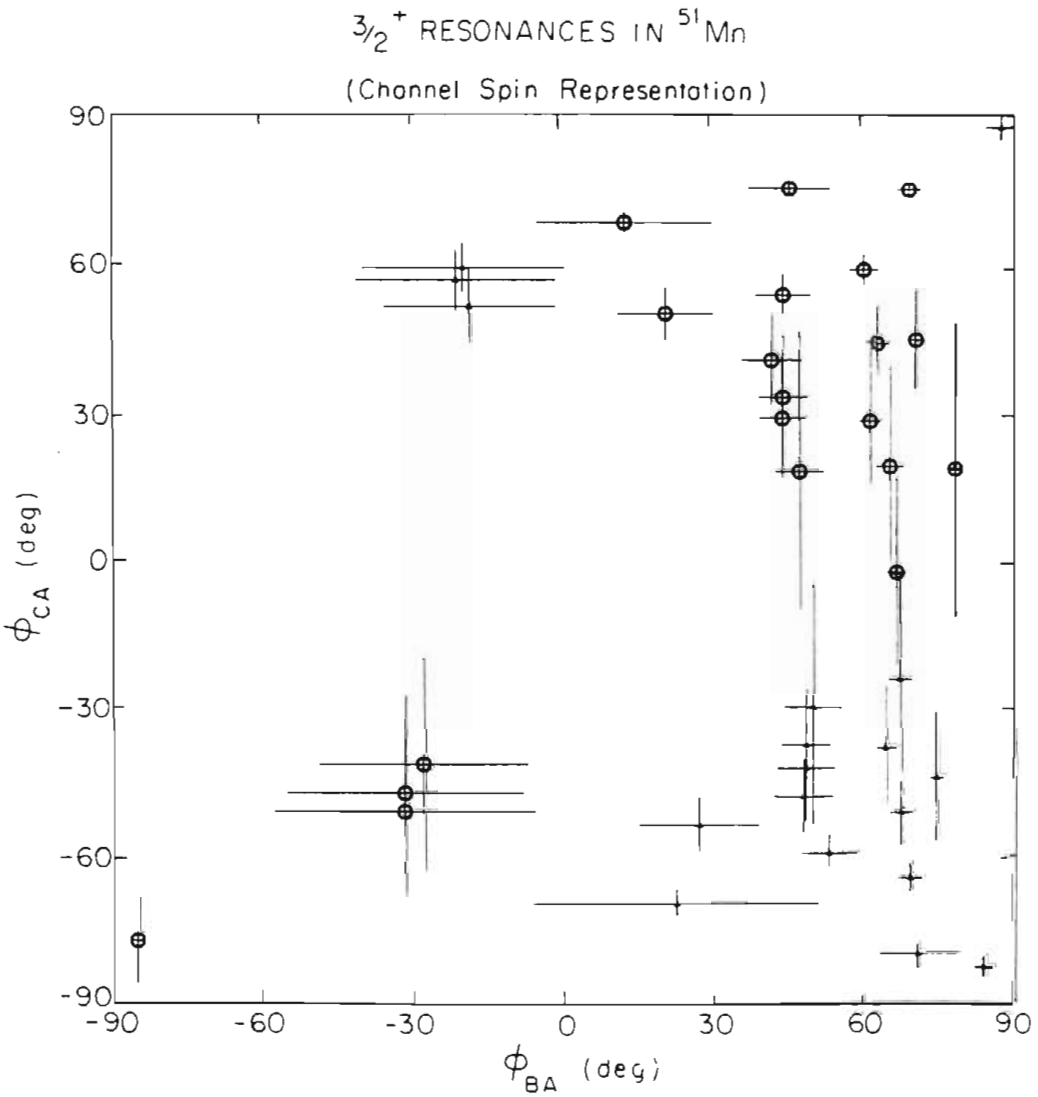
3/2+ RESONANCES IN 51Mn
(Channel Spin Representation)
90
60
30
0
-30
-60
-90
-90
-60
-30
0
30
60
90
φCA (deg)
φBA (deg)

figures, data points indicated by an open circle correspond to the set of solutions with the smaller $\ell'=2$ admixture, and data points indicated by a small triangle correspond to the set of solutions with the larger $\ell'=2$ admixture. For two resonances the solutions were degenerate. From figures 4.7 and 4.8 it is evident that the distribution of ϕ's (and therefore of δ's) is non-statistical. Particularly striking features of the plots are the clustering effect and the seemingly excluded region surrounding the origin.

Resonances with $J^{\pi}= 5/2^{+}$ also have three open channels, labeled as $\ell'=0$ $j'=1/2$, $\ell'=2$ $j'=3/2$, and $\ell'=2$ $j'=5/2$ in the total angular momentum representation, and as $\ell'=0$ $s'=5/2$, $\ell'=2$ $s'=3/2$, and $\ell'=2$ $s'=5/2$ in the channel spin representation. Again, $\ell'=4$ contributions are neglected. The two independent mixing ratios and one dependent mixing ratio are $\delta_{jBA}= \gamma_{j23}/\gamma_{j01}$, $\delta_{jCA}= \gamma_{j25}/\gamma_{j01}$, and $\delta_{jCB}= \gamma_{j25}/\gamma_{j23}$ for the total angular momentum representation, and $\delta_{sBA}= \gamma_{s23}/\gamma_{s05}$, $\delta_{sCA}= \gamma_{s25}/\gamma_{s05}$, and $\delta_{sCB}= \gamma_{s25}/\gamma_{s23}$ for the channel spin representation. The mixing angles are $\phi_{jBA}= \tan^{-1}\delta_{jBA}$, $\phi_{jCA}= \tan^{-1}\delta_{jCA}$, and $\phi_{jCB}= \tan^{-1}\delta_{jCB}$ for the total angular momentum representation, and $\phi_{sBA}= \tan^{-1}\delta_{sBA}$, $\phi_{sCA}= \tan^{-1}\delta_{sCA}$, and $\phi_{sCB}= \tan^{-1}\delta_{sCB}$ for the channel spin representation. The ε^2 parameter again represents the $\ell'=2$ admixture for each resonance. It is not an independent parameter, and the penetrability factors have been removed from its definition.

For $5/2^{+}$ resonances, the coefficients a_{4p} and $a_{4\gamma}$ may be non-zero, and thus a unique solution for the mixing ratios can be obtained. Tables 4.9 and 4.10 list values for $5/2^{+}$ resonances in the total angular momentum representation and the channel spin representation, respectively. The corresponding mixing angle plots are presented in figures 4.9 and 4.10. As in the plots for $3/2^{+}$ resonances, a strong clustering effect is observed in both

TABLE 4.9

MIXING RATIOS, MIXING ANGLES, AND ε^2 FOR $5/2^+$ RESONANCES IN ^{51}Mn

Total Angular Momentum Representation

Resonance Number	ϕ_{jBA} (degrees)	ϕ_{jCA} (degrees)	ϕ_{jCB} (degrees)	δ_{jBA}	δ_{jCA}	δ_{jCB}	ε^2
2	-14.0 ± 12.1	54.6 ± 3.4	-80.0 ± 5.6	$-0.25 +0.22 -0.24$	$1.41 +0.20 -0.17$	$-5.67 +2.09 -7.33$	0.67
6	-18.7 ± 8.7	59.4 ± 2.4	-78.7 ± 4.2	$-0.34 +0.16 -0.18$	$1.69 +0.17 -0.15$	$-4.99 +1.38 -2.94$	0.75
8	-7.1 ± 9.3	52.5 ± 3.3	-84.6 ± 3.3	$-0.12 +0.16 -0.17$	$1.30 +0.17 -0.15$	$-10.50 +3.97 -15.85$	0.63
22	-14.0 ± 11.2	54.9 ± 3.2	-80.0 ± 5.2	$-0.25 +0.20 -0.22$	$1.42 +0.18 -0.15$	$-5.68 +2.00 -6.32$	0.68
26	-23.0 ± 12.3	59.9 ± 2.7	-76.2 ± 6.4	$-0.42 +0.24 -0.28$	$1.72 +0.21 -0.17$	$-4.07 +1.35 -3.61$	0.76
27	-24.6 ± 9.6	54.2 ± 3.5	-71.7 ± 7.1	$-0.46 +0.19 -0.22$	$1.38 +0.20 -0.17$	$-3.02 +0.92 -2.03$	0.68
48	-66.6 ± 1.8	15.4 ± 14.7	-6.8 ± 6.8	$-2.31 +0.19 -0.22$	$0.27 +0.30 -0.26$	$-0.12 +0.12 -0.12$	0.84
49	-61.3 ± 2.2	8.4 ± 17.4	-4.7 ± 9.7	$-1.83 +0.16 -0.18$	$0.15 +0.34 -0.31$	$-0.08 +0.17 -0.17$	0.77

TABLE 4.9 (continued)

Resonance Number	ϕ_{jBA} (degrees)	ϕ_{jCA} (degrees)	ϕ_{jCB} (degrees)	δ_{jBA}	δ_{jCA}	δ_{jCB}	ε^2
59	-0.5 ± 19.3	49.8 ± 3.7	-89.1 ± 0.6	$-0.01 + 0.35 - 0.35$	$1.18 + 0.17 - 0.14$	$-63.10 + 24.79 -115.50$	0.58
62	-3.5 ± 22.6	61.5 ± 2.4	-88.1 ± 0.9	$-0.06 + 0.41 - 0.43$	$1.84 + 0.20 - 0.17$	$-29.53 + 9.29 - 24.98$	0.77
66	34.8 ± 11.3	48.3 ± 3.6	58.2 ± 14.1	$0.70 + 0.35 - 0.26$	$1.12 + 0.15 - 0.13$	$1.61 + 1.52 - 0.64$	0.64
68	63.0 ± 2.1	-1.1 ± 9.2	-0.6 ± 4.7	$1.96 + 0.19 - 0.17$	$-0.02 + 0.16 - 0.16$	$-0.01 + 0.08 - 0.08$	0.79
70	-9.4 ± 12.1	35.2 ± 7.5	-76.7 ± 8.2	$-0.17 + 0.21 - 0.23$	$0.70 + 0.22 - 0.18$	$-4.23 + 1.69 - 6.98$	0.34
71	59.8 ± 2.4	4.7 ± 9.6	2.7 ± 5.6	$1.72 + 0.18 - 0.16$	$0.08 + 0.17 - 0.17$	$0.05 + 0.10 - 0.10$	0.75
73	56.2 ± 4.7	58.9 ± 2.3	48.0 ± 5.8	$1.49 + 0.30 - 0.24$	$1.66 + 0.16 - 0.14$	$1.11 + 0.25 - 0.20$	0.83
78	-14.6 ± 13.5	62.4 ± 2.1	-82.2 ± 3.2	$-0.26 + 0.24 - 0.27$	$1.91 + 0.18 - 0.16$	$-7.32 + 2.15 - 5.06$	0.79
80	-19.2 ± 8.0	-64.4 ± 2.2	80.6 ± 7.7	$-0.35 + 0.15 - 0.16$	$-2.09 + 0.19 - 0.22$	$6.02 + 26.76 - 2.77$	0.82
81	-52.8 ± 4.0	-68.6 ± 2.1	62.7 ± 5.2	$-1.32 + 0.17 - 0.21$	$-2.55 + 0.26 - 0.31$	$1.93 + 0.52 - 0.37$	0.89

TABLE 4.9 (continued)

Resonance Number	ϕ_{jBA} (degrees)	ϕ_{jCA} (degrees)	ϕ_{jCB} (degrees)	δ_{jBA}	δ_{jCA}	δ_{jCB}	ε^2
96	−2.6 ± 8.6	−58.3 ± 2.8	88.4 ± 1.1	−0.05 + 0.15 − 0.15	−1.62 + 0.17 − 0.19	35.42 + 69.54 − 14.12	0.72
100	−41.3 ± 4.9	−70.2 ± 1.6	72.5 ± 3.6	−0.88 + 0.14 − 0.17	−2.78 + 0.23 − 0.27	3.17 + 0.86 − 0.58	0.89
101	−28.0 ± 9.7	62.7 ± 2.3	−74.7 ± 4.7	−0.53 + 0.20 − 0.24	1.94 + 0.20 − 0.18	−3.65 + 0.91 − 1.69	0.80
106	54.9 ± 3.4	40.2 ± 4.3	30.7 ± 5.1	1.42 + 0.20 − 0.17	0.85 + 0.14 − 0.12	0.59 + 0.13 − 0.11	0.73
107	−52.0 ± 4.3	69.8 ± 1.8	−64.7 ± 3.8	−1.28 + 0.18 − 0.22	2.71 + 0.29 − 0.25	−2.12 + 0.32 − 0.43	0.90
110	−41.2 ± 6.1	11.7 ± 19.5	−13.3 ± 23.1	−0.88 + 0.17 − 0.21	0.21 + 0.40 − 0.34	−0.24 + 0.41 − 0.50	0.45
114	−56.4 ± 2.8	−17.5 ± 12.2	11.8 ± 9.0	−1.50 + 0.15 − 0.17	−0.31 + 0.22 − 0.26	0.21 + 0.17 − 0.16	0.70
115	−33.6 ± 13.7	45.4 ± 8.7	−56.7 ± 17.2	−0.67 + 0.30 − 0.42	1.01 + 0.37 − 0.27	−1.52 + 0.70 − 1.94	0.60
118	−49.9 ± 4.9	55.3 ± 4.3	−50.6 ± 7.2	−1.19 + 0.19 − 0.23	1.44 + 0.26 − 0.21	−1.22 + 0.27 − 0.37	0.78
121	33.3 ± 6.3	−55.8 ± 3.8	−65.9 ± 6.3	0.66 + 0.17 − 0.15	−1.47 + 0.19 − 0.23	−2.24 + 0.53 − 0.88	0.72

TABLE 4.9 (continued)

Resonance Number	ϕ_{jBA} (degrees)	ϕ_{jCA} (degrees)	ϕ_{jCB} (degrees)	δ_{jBA}	δ_{jCA}	δ_{jCB}	ε^2
123	−36.4 ± 5.2	−17.9 ± 11.8	23.6 ± 15.1	−0.74 + 0.13 − 0.15	−0.32 + 0.22 − 0.25	0.44 + 0.37 − 0.29	0.39
134	−21.1 ± 10.0	70.8 ± 1.5	−82.4 ± 2.4	−0.39 + 0.19 − 0.22	2.88 + 0.26 − 0.22	−7.47 + 1.83 − 3.53	0.89
138	−14.1 ± 17.1	30.4 ± 11.3	−66.9 ± 30.0	−0.25 + 0.30 − 0.35	0.59 + 0.30 − 0.24	−2.34 + 1.59 −999.99	0.29
150	53.6 ± 3.5	−24.3 ± 12.9	−18.4 ± 11.5	1.36 + 0.19 − 0.16	−0.45 + 0.25 − 0.31	−0.33 + 0.21 − 0.24	0.67
152	−75.4 ± 1.3	−13.6 ± 10.5	3.6 ± 2.8	−3.84 + 0.33 − 0.39	−0.24 + 0.19 − 0.20	0.06 + 0.05 − 0.05	0.94
160	−26.1 ± 10.9	50.0 ± 4.3	−67.7 ± 8.8	−0.49 + 0.22 − 0.26	1.19 + 0.20 − 0.17	−2.43 + 0.78 − 1.73	0.63
161	−67.6 ± 1.7	−34.6 ± 7.8	15.9 ± 4.7	−2.43 + 0.19 − 0.22	−0.69 + 0.18 − 0.22	0.28 + 0.09 − 0.09	0.86
164	−56.5 ± 3.1	−52.8 ± 5.1	41.1 ± 7.8	−1.51 + 0.17 − 0.19	−1.31 + 0.22 − 0.28	0.87 + 0.27 − 0.21	0.80
165	36.2 ± 7.1	35.8 ± 4.9	44.5 ± 9.1	0.73 + 0.21 − 0.18	0.72 + 0.14 − 0.12	0.98 + 0.37 − 0.27	0.51
173	−17.3 ± 11.9	39.3 ± 6.0	−69.1 ± 11.8	−0.31 + 0.22 − 0.25	0.82 + 0.19 − 0.16	−2.62 + 1.06 − 3.62	0.43

TABLE 4.10

MIXING RATIOS, MIXING ANGLES, AND ε^2 FOR $5/2^+$ RESONANCES IN ^{51}Mn

Channel Spin Representation

Resonance Number	ϕ_{sBA} (degrees)	ϕ_{sCA} (degrees)	ϕ_{sCB} (degrees)	δ_{sBA}	δ_{sCA}	δ_{sCB}	ε^2
2	44.4 ± 6.0	46.2 ± 5.5	46.9 ± 9.1	0.98 + 0.23 − 0.19	1.04 + 0.22 − 0.18	1.07 + 0.41 − 0.29	0.67
6	49.0 ± 4.2	52.1 ± 3.5	48.2 ± 5.7	1.15 + 0.18 − 0.16	1.28 + 0.17 − 0.15	1.12 + 0.26 − 0.20	0.75
8	44.0 ± 5.3	41.3 ± 4.6	42.3 ± 7.4	0.97 + 0.20 − 0.17	0.88 + 0.15 − 0.13	0.91 + 0.27 − 0.21	0.63
22	44.6 ± 6.0	46.5 ± 4.6	46.8 ± 8.6	0.99 + 0.23 − 0.19	1.05 + 0.18 − 0.16	1.07 + 0.39 − 0.28	0.68
26	48.4 ± 5.2	54.0 ± 4.7	50.7 ± 8.1	1.13 + 0.23 − 0.19	1.37 + 0.27 − 0.21	1.22 + 0.43 − 0.30	0.76
27	39.8 ± 7.4	50.1 ± 3.8	55.2 ± 9.1	0.83 + 0.25 − 0.20	1.20 + 0.17 − 0.15	1.44 + 0.64 − 0.40	0.68
48	−49.3 ± 6.2	63.5 ± 2.5	−59.9 ± 6.4	−1.16 + 0.23 − 0.29	2.01 + 0.25 − 0.21	−1.73 + 0.37 − 0.55	0.84
49	−44.3 ± 8.1	57.2 ± 3.7	−57.8 ± 8.5	−0.98 + 0.24 − 0.32	1.55 + 0.24 − 0.20	−1.59 + 0.42 − 0.69	0.77

TABLE 4.10 (continued)

Resonance Number	ϕ_{sBA} (degrees)	ϕ_{sCA} (degrees)	ϕ_{sCB} (degrees)	δ_{sBA}	δ_{sCA}	δ_{sCB}	ε^2
96	-52.9 ± 3.2	-43.0 ± 5.3	35.3 ± 5.4	$-1.32 \begin{smallmatrix}+0.14\\-0.17\end{smallmatrix}$	$-0.93 \begin{smallmatrix}+0.16\\-0.19\end{smallmatrix}$	$0.71 \begin{smallmatrix}+0.15\\-0.13\end{smallmatrix}$	0.72
100	-70.0 ± 1.3	-44.0 ± 6.3	19.3 ± 3.5	$-2.75 \begin{smallmatrix}+0.18\\-0.21\end{smallmatrix}$	$-0.97 \begin{smallmatrix}+0.19\\-0.24\end{smallmatrix}$	$0.35 \begin{smallmatrix}+0.07\\-0.07\end{smallmatrix}$	0.89
101	50.9 ± 4.2	57.8 ± 3.6	52.2 ± 6.0	$1.23 \begin{smallmatrix}+0.21\\-0.17\end{smallmatrix}$	$1.59 \begin{smallmatrix}+0.24\\-0.20\end{smallmatrix}$	$1.29 \begin{smallmatrix}+0.33\\-0.25\end{smallmatrix}$	0.80
106	56.9 ± 2.5	-32.3 ± 6.9	-22.4 ± 5.2	$1.53 \begin{smallmatrix}+0.16\\-0.14\end{smallmatrix}$	$-0.63 \begin{smallmatrix}+0.16\\-0.18\end{smallmatrix}$	$-0.41 \begin{smallmatrix}+0.10\\-0.11\end{smallmatrix}$	0.73
107	54.5 ± 4.6	69.3 ± 1.7	62.2 ± 4.1	$1.40 \begin{smallmatrix}+0.27\\-0.22\end{smallmatrix}$	$2.65 \begin{smallmatrix}+0.25\\-0.22\end{smallmatrix}$	$1.89 \begin{smallmatrix}+0.38\\-0.29\end{smallmatrix}$	0.90
110	-19.8 ± 17.3	39.5 ± 6.9	-66.4 ± 13.4	$-0.36 \begin{smallmatrix}+0.32\\-0.40\end{smallmatrix}$	$0.82 \begin{smallmatrix}+0.23\\-0.18\end{smallmatrix}$	$-2.29 \begin{smallmatrix}+0.97\\-3.30\end{smallmatrix}$	0.45
114	-49.1 ± 4.6	45.4 ± 6.0	-41.3 ± 9.2	$-1.15 \begin{smallmatrix}+0.17\\-0.21\end{smallmatrix}$	$1.01 \begin{smallmatrix}+0.24\\-0.19\end{smallmatrix}$	$-0.88 \begin{smallmatrix}+0.25\\-0.33\end{smallmatrix}$	0.70
115	22.4 ± 20.8	48.8 ± 5.1	70.1 ± 18.0	$0.41 \begin{smallmatrix}+0.53\\-0.38\end{smallmatrix}$	$1.14 \begin{smallmatrix}+0.23\\-0.18\end{smallmatrix}$	$2.77 \begin{smallmatrix}+28.02\\-1.49\end{smallmatrix}$	0.60
118	23.9 ± 11.8	61.2 ± 2.6	76.3 ± 13.0	$0.44 \begin{smallmatrix}+0.27\\-0.23\end{smallmatrix}$	$1.82 \begin{smallmatrix}+0.21\\-0.18\end{smallmatrix}$	$4.10 \begin{smallmatrix}+82.28\\-2.12\end{smallmatrix}$	0.78
121	-38.0 ± 7.9	-54.6 ± 2.7	60.9 ± 7.8	$-0.78 \begin{smallmatrix}+0.20\\-0.25\end{smallmatrix}$	$-1.41 \begin{smallmatrix}+0.13\\-0.15\end{smallmatrix}$	$1.80 \begin{smallmatrix}+0.77\\-0.46\end{smallmatrix}$	0.72

TABLE 4.10 (continued)

Resonance Number	ϕ_{sBA} (degrees)	ϕ_{sCA} (degrees)	ϕ_{sCB} (degrees)	δ_{sBA}	δ_{sCA}	δ_{sCB}	ε^2
123	-35.0 ± 7.9	21.6 ± 8.4	-29.5 ± 15.5	-0.70 + 0.19 - 0.23	0.40 + 0.18 - 0.16	-0.57 + 0.32 - 0.43	0.39
134	64.2 ± 2.1	63.8 ± 2.7	44.5 ± 3.8	2.07 + 0.21 - 0.18	2.03 + 0.26 - 0.22	0.98 + 0.14 - 0.12	0.89
138	17.7 ± 19.6	28.9 ± 8.3	60.0 ± 29.2	0.32 + 0.44 - 0.35	0.55 + 0.21 - 0.18	1.73 + 72.79 - 1.14	0.29
150	24.3 ± 13.5	-53.6 ± 3.2	-71.5 ± 7.7	0.45 + 0.32 - 0.26	-1.36 + 0.15 - 0.17	-3.00 + 0.96 - 2.24	0.67
152	-68.2 ± 2.2	71.1 ± 1.7	-49.5 ± 2.8	-2.50 + 0.26 - 0.31	2.93 + 0.31 - 0.26	-1.17 + 0.11 - 0.12	0.94
160	33.5 ± 9.6	48.0 ± 4.5	59.2 ± 12.1	0.66 + 0.28 - 0.22	1.11 + 0.19 - 0.16	1.68 + 1.28 - 0.60	0.63
161	-63.5 ± 2.2	56.8 ± 3.8	-37.3 ± 4.7	-2.01 + 0.18 - 0.20	1.53 + 0.24 - 0.20	-0.76 + 0.12 - 0.14	0.86
164	-62.9 ± 2.0	22.7 ± 12.3	-12.1 ± 7.6	-1.96 + 0.16 - 0.18	0.42 + 0.28 - 0.23	-0.21 + 0.14 - 0.14	0.80
165	45.4 ± 4.1	-8.7 ± 10.0	-8.6 ± 9.5	1.02 + 0.16 - 0.14	-0.15 + 0.18 - 0.18	-0.15 + 0.17 - 0.18	0.51
173	25.0 ± 11.3	36.5 ± 6.0	57.8 ± 16.9	0.47 + 0.27 - 0.22	0.74 + 0.18 - 0.15	1.59 + 2.07 - 0.72	0.43

FIGURE 4.9 Plot of ϕ_{CA} versus φ_{BA} for 38 $5/2^+$ resonances in ^{51}Mn in the total angular momentum representation.

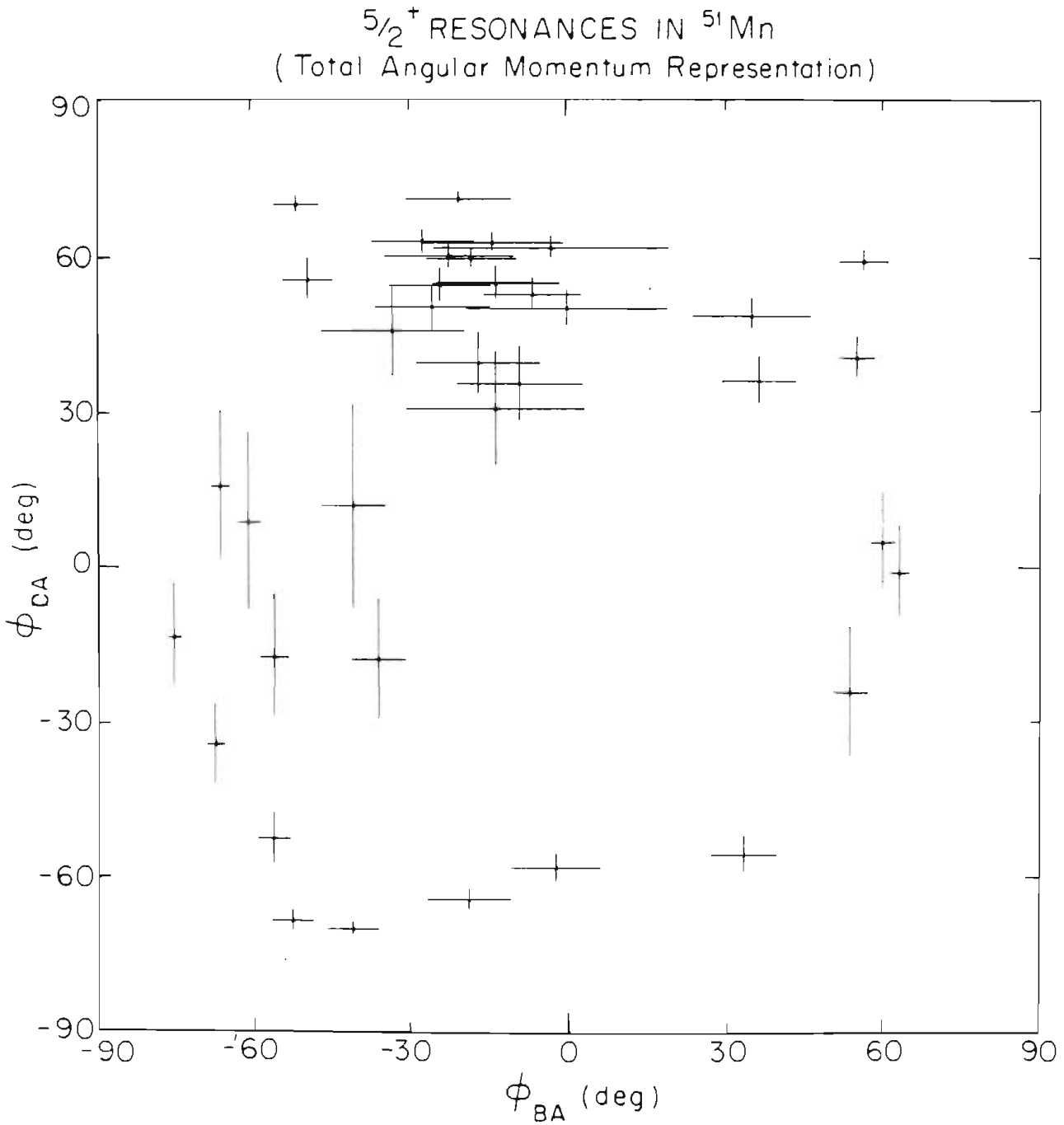
$5/2^+$ RESONANCES IN ^{51}Mn
(Total Angular Momentum Representation)
90
60
30
0
-30
-60
-90
ϕ_{CA} (deg)
-90
-60
-30
0
30
60
90
ϕ_{BA} (deg)

FIGURE 4.10 Plot of ϕ_{CA} versus ϕ_{BA} for 38 $5/2^+$ resonances in ^{51}Mn in the channel spin representation.

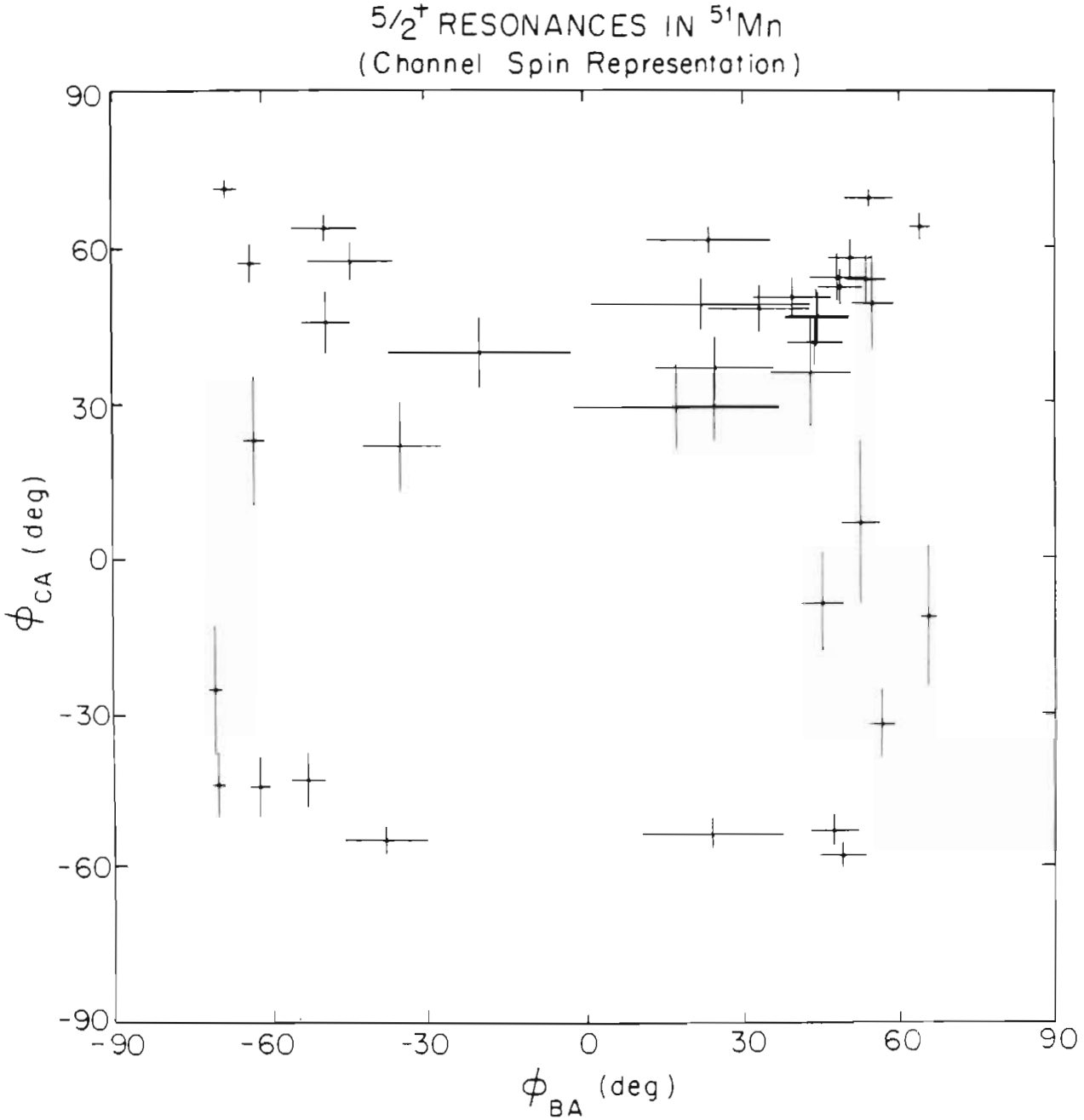
5/2+ RESONANCES IN 51Mn
(Channel Spin Representation)
90
60
30
0
-30
-60
-90
-90
-60
-30
0
30
60
90
φCA (deg)
φBA (deg)

representations, and the region surrounding the origin appears empty. When the correction for the differences in average reduced width for the two channels is included, the same qualitative effects are observed in both representations.

Values of the three channel reduced widths and of the products of the channel reduced width amplitudes are listed in table 4.11 for the total angular momentum representation and in table 4.12 for the channel spin representation. The total elastic and inelastic widths and reduced widths for each resonance are listed in table A.1. Differential and integral plots of the elastic and total inelastic reduced widths versus energy are shown in figure 4.11. No unusual structure is evident in these plots. Differential and integral plots of the channel reduced widths versus energy are presented in figures 4.12 and 4.13 for the total angular momentum representation and the channel spin representation. No unusual structure is evident in these plots, except for the large strength exhibited by the $5/2^+$ resonance at E_p = 3.6750 MeV in all channels except γ^2_{s25}. Figures 4.14 and 4.15 show the products of channel reduced widths in each representation. All three products in the channel spin representation and the $\gamma_{j01}\gamma_{j25}$ plot show non-statistical sign distributions: the integral plot is always positive in all four cases.

3. f-wave Resonances

a. Preliminary Analysis

If the proton incident on the ^{50}Cr target has $\ell = 3$, then $5/2^-$ or $7/2^-$ resonances are formed in ^{51}Mn. The angular distribution equations for decay from $7/2^-$ resonances are:

$$W_p(\theta) = a_{op}(1 + a_{2p}P_2 + a_{4p}P_4 + a_{6p}P_6) \qquad (4.7)$$

TABLE 4.11

INELASTIC REDUCED WIDTHS AND AMPLITUDE PRODUCTS FOR $5/2^+$ RESONANCES IN ^{51}Mn

Total Angular Momentum Representation

Resonance Number	γ^2_{j01} (keV)	γ^2_{j23} (keV)	γ^2_{j25} (keV)	$\gamma_{j01}\gamma_{j23}$ (keV)	$\gamma_{j01}\gamma_{j25}$ (keV)	$\gamma_{j23}\gamma_{j25}$ (keV)
2	0.257	0.016	0.511	−0.064	0.362	−0.090
6	0.584	0.067	1.667	−0.198	0.987	−0.334
8	1.575	0.024	2.667	−0.195	2.049	−0.254
22	2.390	0.149	4.829	−0.598	3.397	−0.850
26	1.034	0.186	3.076	−0.438	1.784	−0.755
27	1.814	0.381	3.477	−0.832	2.511	−1.152
48	0.258	1.371	0.019	−0.594	0.071	−0.163
49	0.131	0.437	0.003	−0.239	0.019	−0.036
59	0.328	0.000	0.458	−0.003	0.387	−0.003
62	0.377	0.001	1.278	−0.023	0.694	−0.043
66	3.573	1.733	4.517	2.488	4.017	2.798
68	0.123	0.475	0.000	0.242	−0.002	−0.005
70	1.211	0.034	0.602	−0.202	0.854	−0.142
71	0.613	1.808	0.004	1.053	0.050	0.086
73	0.119	0.265	0.326	0.177	0.197	0.294
78	0.770	0.052	2.818	−0.201	1.472	−0.384
80	0.022	0.003	0.095	−0.008	−0.045	0.016
81	0.002	0.003	0.012	−0.003	−0.005	0.006
96	1.369	0.003	3.578	−0.063	−2.213	0.101

TABLE 4.11 (continued)

Resonance Number	γ^2_{j01} (keV)	γ^2_{j23} (keV)	γ^2_{j25} (keV)	$\gamma_{j01}\gamma_{j23}$ (keV)	$\gamma_{j01}\gamma_{j25}$ (keV)	$\gamma_{j23}\gamma_{j25}$ (keV)
100	0.158	0.122	1.223	−0.139	−0.440	0.386
101	0.175	0.049	0.655	−0.093	0.338	−0.179
106	0.162	0.328	0.116	0.230	0.137	0.195
107	0.063	0.103	0.462	−0.080	0.170	−0.218
110	0.091	0.070	0.004	−0.080	0.019	−0.017
114	0.159	0.359	0.016	−0.239	−0.050	0.075
115	0.225	0.099	0.231	−0.150	0.228	−0.152
118	0.192	0.270	0.399	−0.227	0.276	−0.328
121	0.123	0.053	0.265	0.080	−0.180	−0.118
123	0.346	0.189	0.036	−0.256	−0.112	0.083
134	0.065	0.010	0.536	−0.025	0.186	−0.072
138	0.306	0.019	0.105	−0.077	0.179	−0.045
150	0.071	0.131	0.015	0.096	−0.032	−0.044
152	0.040	0.594	0.002	−0.155	−0.010	0.037
160	0.404	0.097	0.576	−0.198	0.483	−0.237
161	0.046	0.273	0.022	−0.113	−0.032	0.078
164	0.058	0.133	0.101	−0.088	−0.077	0.116
165	0.201	0.108	0.104	0.147	0.145	0.106
173	0.083	0.008	0.055	−0.026	0.068	−0.021

TABLE 4.12

INELASTIC REDUCED WIDTHS AND AMPLITUDE PRODUCTS FOR $5/2^+$ RESONANCES IN ^{51}Mn

Channel Spin Representation

Resonance Number	γ^2_{s05} (keV)	γ^2_{s23} (keV)	γ^2_{s25} (keV)	$\gamma_{s05}\gamma_{s23}$ (keV)	$\gamma_{s05}\gamma_{s25}$ (keV)	$\gamma_{s23}\gamma_{s25}$ (keV)
2	0.257	0.246	0.280	0.252	0.269	0.263
6	0.584	0.771	0.964	0.671	0.751	0.862
8	1.575	1.473	1.219	1.523	1.386	1.340
22	2.390	2.329	2.650	2.359	2.517	2.484
26	1.034	1.310	1.952	1.164	1.421	1.599
27	1.814	1.257	2.601	1.510	2.172	1.808
48	0.258	0.349	1.041	-0.300	0.518	-0.603
49	0.131	0.125	0.315	-0.128	0.203	-0.198
59	0.328	0.290	0.168	0.308	0.235	0.221
62	0.377	0.776	0.501	0.541	0.435	0.624
66	3.573	6.200	0.049	4.706	0.420	0.553
68	0.123	0.167	0.309	0.143	-0.195	-0.227
70	1.211	0.261	0.374	0.562	0.673	0.312
71	0.613	0.736	1.076	0.672	-0.812	-0.890
73	0.119	0.586	0.005	0.264	-0.024	-0.053
78	0.770	1.453	1.417	1.057	1.044	1.435
80	0.022	0.077	0.021	-0.041	-0.021	0.040
81	0.002	0.015	0.000	-0.005	-0.001	0.003
96	1.369	2.388	1.193	-1.808	-1.278	1.688

TABLE 4.12 (continued)

Resonance Number	γ^2_{s05} (keV)	γ^2_{s23} (keV)	γ^2_{s25} (keV)	$\gamma_{s05}\gamma_{s23}$ (keV)	$\gamma_{s05}\gamma_{s25}$ (keV)	$\gamma_{s23}\gamma_{s25}$ (keV)
100	0.158	1.197	0.148	-0.435	-0.153	0.420
101	0.175	0.264	0.439	0.215	0.277	0.341
106	0.162	0.379	0.065	0.248	-0.102	-0.157
107	0.063	0.123	0.442	0.088	0.167	0.233
110	0.091	0.012	0.062	-0.033	0.075	-0.027
114	0.159	0.211	0.163	-0.183	0.161	-0.186
115	0.225	0.038	0.293	0.093	0.256	0.106
118	0.192	0.038	0.631	0.085	0.348	0.154
121	0.123	0.075	0.243	-0.096	-0.173	0.135
123	0.346	0.170	0.055	-0.243	0.137	-0.096
134	0.065	0.277	0.268	0.134	0.132	0.273
138	0.306	0.031	0.093	0.098	0.169	0.054
150	0.071	0.015	0.131	0.032	-0.096	-0.044
152	0.040	0.251	0.345	-0.101	0.118	-0.294
160	0.404	0.177	0.497	0.267	0.448	0.296
161	0.046	0.187	0.108	-0.093	0.071	-0.142
164	0.058	0.223	0.010	-0.114	0.024	-0.048
165	0.201	0.208	0.005	0.204	-0.031	-0.031
173	0.083	0.018	0.045	0.039	0.061	0.029

FIGURE 4.11 Plots of reduced widths and the cumulative sums of reduced widths for the elastic and total inelastic decay channels for $5/2^+$ resonances in ^{51}Mn.

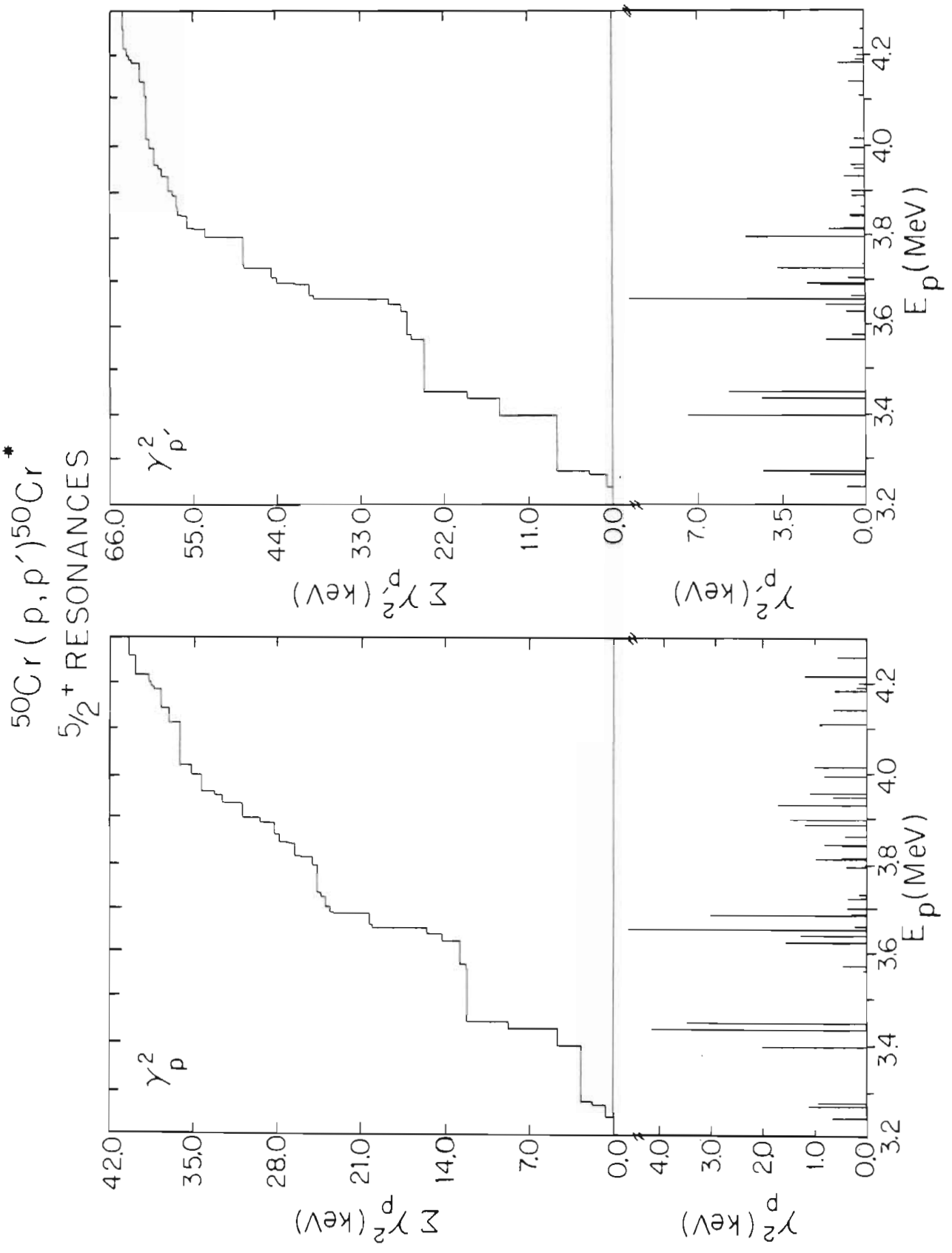
$^{50}Cr(p,p')^{50}Cr^{*}$
$5/2^{+}$ RESONANCES
γ_p^2
$\Sigma\gamma_p^2$ (keV)
γ_p^2 (keV)
E_p(MeV)
$\gamma_{p'}^2$
$\Sigma\gamma_{p'}^2$ (keV)
$\gamma_{p'}^2$ (keV)
E_p(MeV)

FIGURE 4.12 Plots of reduced widths and the cumulative sums of reduced widths for the three inelastic decay channels for $5/2^+$ resonances in ^{51}Mn in the total angular momentum representation.

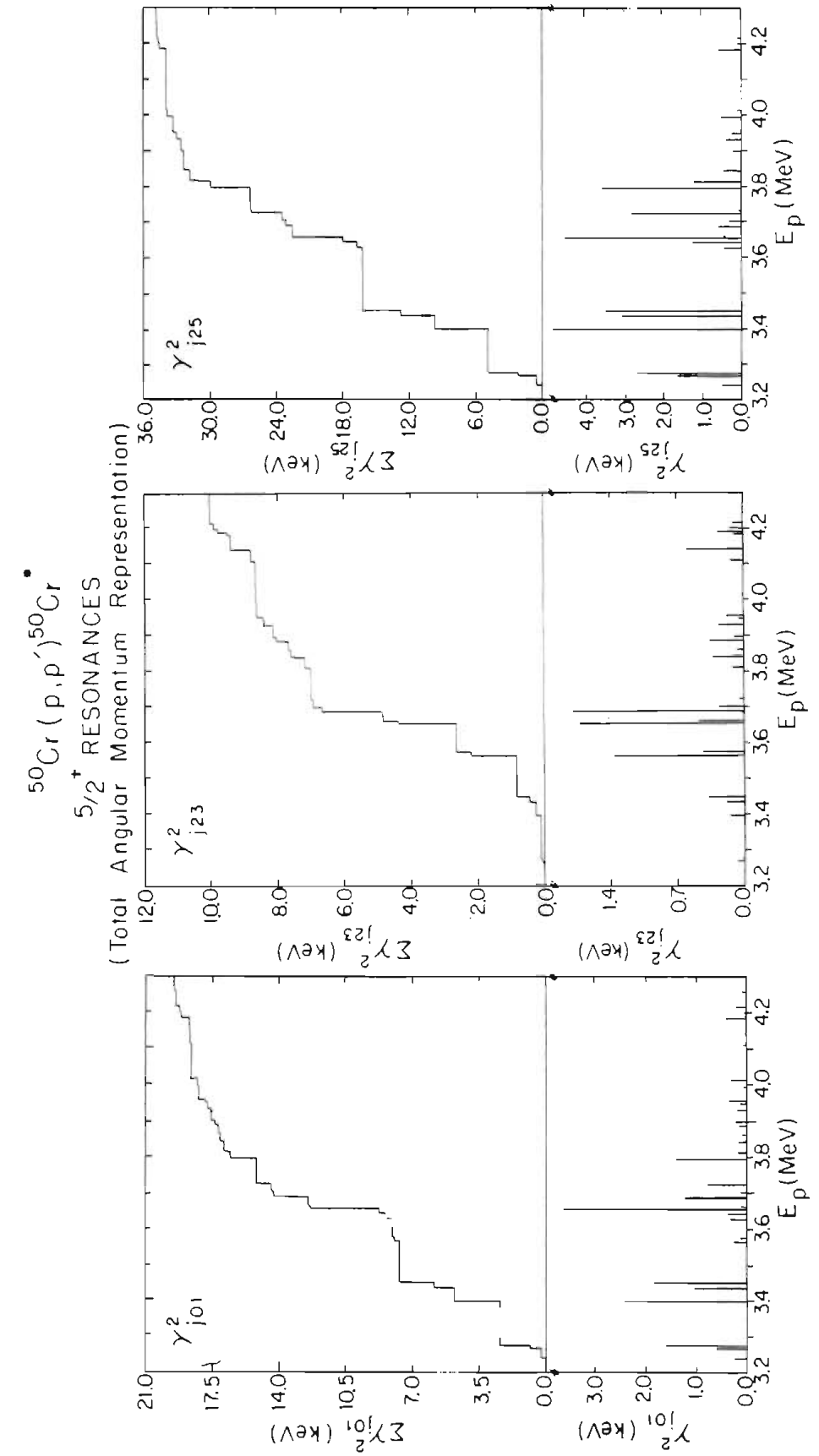
$^{50}Cr(p,p')^{50}Cr^*$
$5/2^+$ RESONANCES
(Total Angular Momentum Representation)
γ^2_{j01}
$\Sigma\gamma^2_{j01}$ (keV)
γ^2_{j01} (keV)
γ^2_{j23}
$\Sigma\gamma^2_{j23}$ (keV)
γ^2_{j23} (keV)
γ^2_{j25}
$\Sigma\gamma^2_{j25}$ (keV)
γ^2_{j25} (keV)
E_p(MeV)

FIGURE 4.13 Plots of reduced widths and the cumulative sums of reduced widths for the three inelastic decay channels for $5/2^+$ resonances in ^{51}Mn in the channel spin representation.

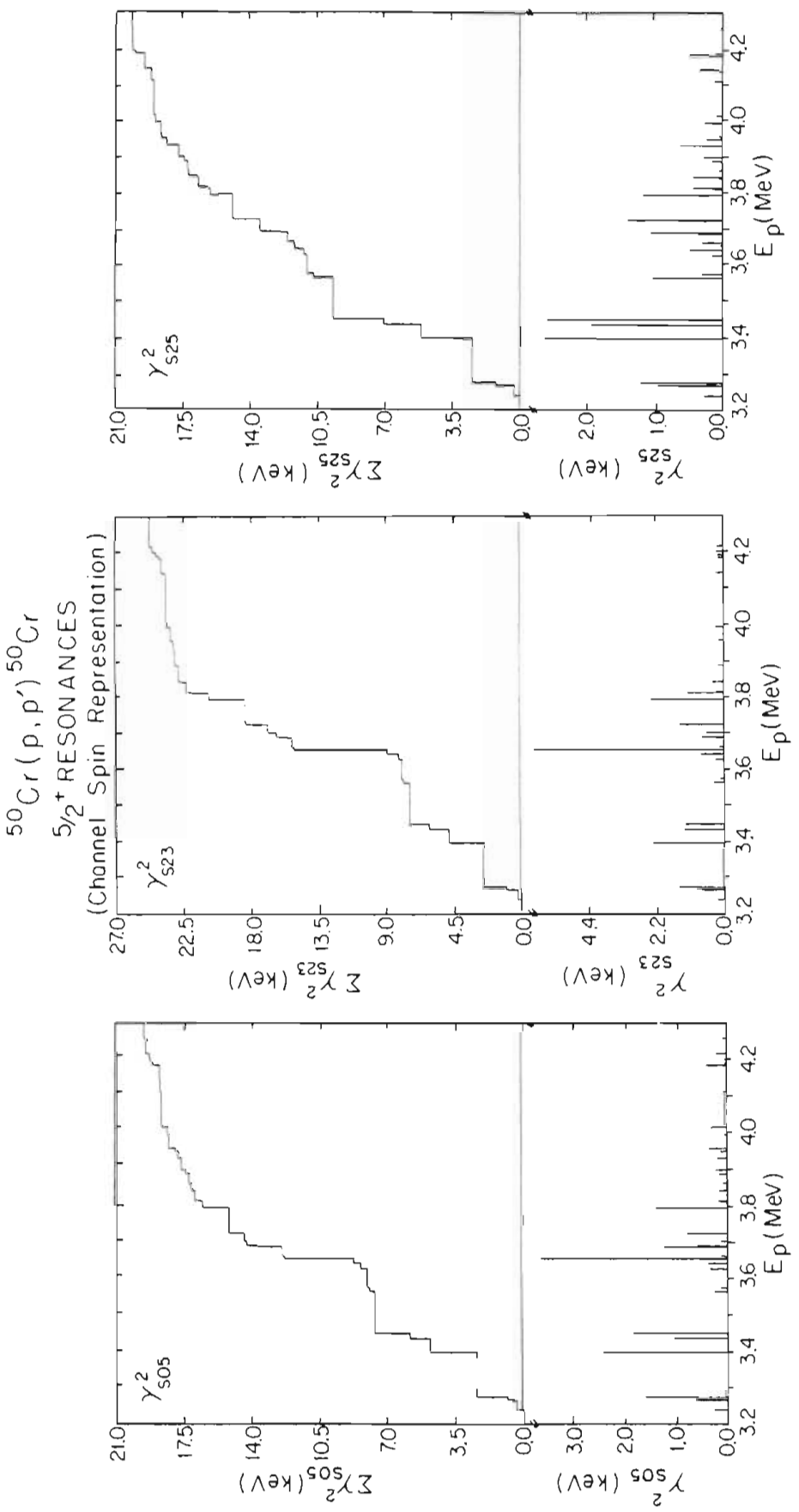
$^{50}Cr(p,p')^{50}Cr$
$5/2^+$ RESONANCES
(Channel Spin Representation)
γ^2_{s05}
$\Sigma\gamma^2_{s05}$ (keV)
γ^2_{s05} (keV)
γ^2_{s23}
$\Sigma\gamma^2_{s23}$ (keV)
γ^2_{s23} (keV)
γ^2_{s25}
$\Sigma\gamma^2_{s25}$ (keV)
γ^2_{s25} (keV)
Ep(MeV)

FIGURE 4.14 Products of inelastic decay amplitudes and cumulative sums of the products versus energy for the three inelastic decay channels for $5/2^+$ resonances in ^{51}Mn in the total angular momentum representation.

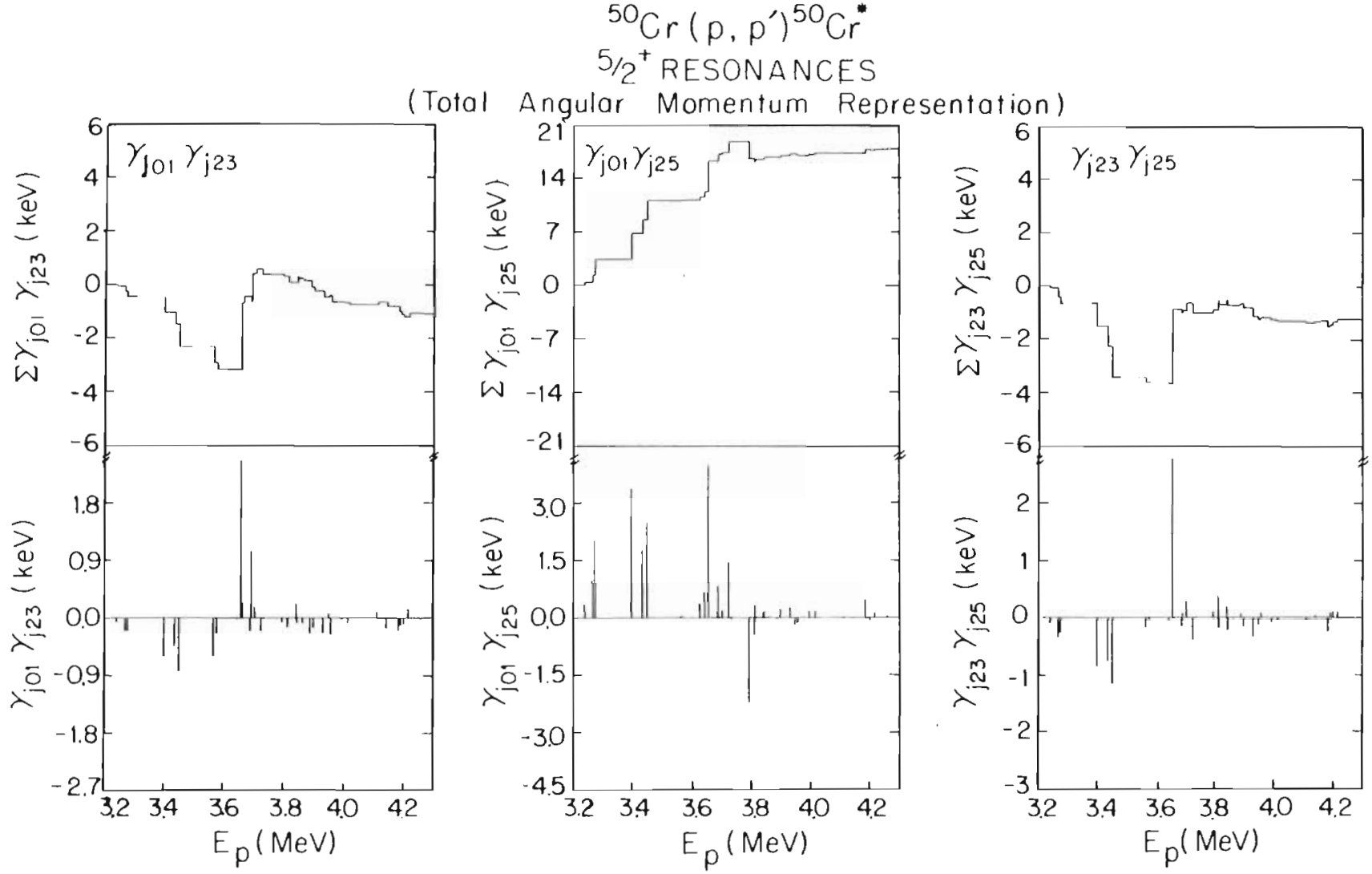
$^{50}Cr(p,p')^{50}Cr^*$
$5/2^+$ RESONANCES
(Total Angular Momentum Representation)
$\gamma_{j01}\gamma_{j23}$
$\Sigma\gamma_{j01}\gamma_{j23}$ (keV)
$\gamma_{j01}\gamma_{j23}$ (keV)
$\gamma_{j01}\gamma_{j25}$
$\Sigma\gamma_{j01}\gamma_{j25}$ (keV)
$\gamma_{j01}\gamma_{j25}$ (keV)
$\gamma_{j23}\gamma_{j25}$
$\Sigma\gamma_{j23}\gamma_{j25}$ (keV)
$\gamma_{j23}\gamma_{j25}$ (keV)
E_p (MeV)

FIGURE 4.15 Products of inelastic decay amplitudes and cumulative sums of the products versus energy for the three inelastic decay channels for $5/2^+$ resonances in ^{51}Mn in the channel spin representation.

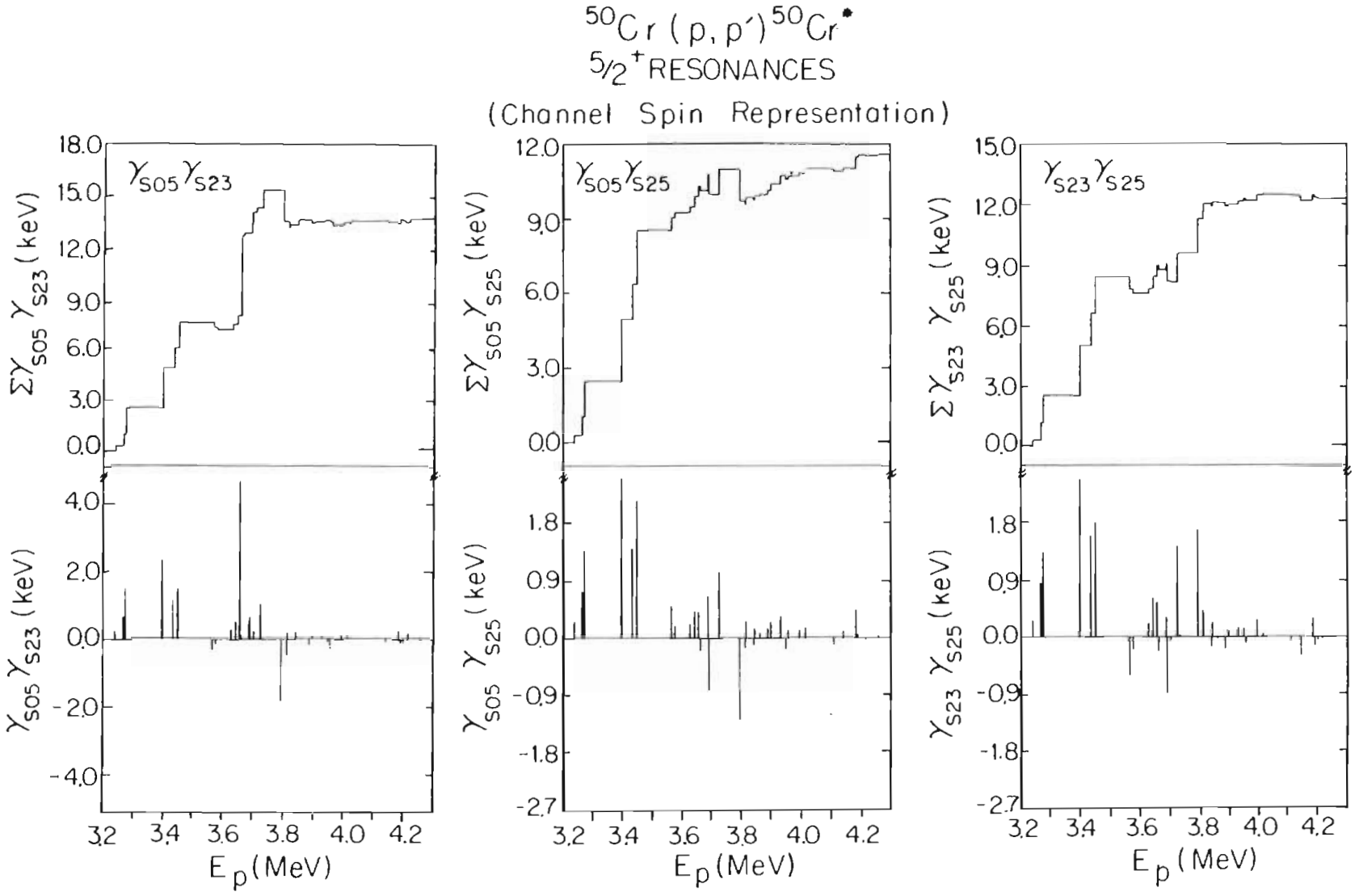
$^{50}Cr(p,p')^{50}Cr^*$
$5/2^+$ RESONANCES
(Channel Spin Representation)
$\gamma_{S05}\gamma_{S23}$
$\gamma_{S05}\gamma_{S25}$
$\gamma_{S23}\gamma_{S25}$
$\Sigma\gamma_{S05}\gamma_{S23}$ (keV)
$\gamma_{S05}\gamma_{S23}$ (keV)
$\Sigma\gamma_{S05}\gamma_{S25}$ (keV)
$\gamma_{S05}\gamma_{S25}$ (keV)
$\Sigma\gamma_{S23}\gamma_{S25}$ (keV)
$\gamma_{S23}\gamma_{S25}$ (keV)
E_p (MeV)

$$W_\gamma(\Theta) = a_{o\gamma}(1 + a_{2\gamma}P_2 + a_{4\gamma}P_4). \qquad (4.8)$$

For $5/2^-$ resonances, $a_{6p} = 0$. Sample angular distribution plots for a $5/2^-$ resonance are shown in figure 4.16. The solid line is the best fit to the data. All 7 f-wave resonances studied were assigned $J^\pi = 5/2^-$. A list of $\ell = 3$ resonances, with J^π assignments and measured Legendre polynomial coefficients, is presented in table 4.13.

Resonances with $J^\pi = 5/2^-$ have four open exit channels, labeled as $\ell'=1$ $j'=1/2$, $\ell'=1$ $j'=3/2$, $\ell'=3$ $j'=5/2$, and $\ell'=3$ $j'=7/2$ in the total angular momentum representation, and as $\ell'=1$ $s'=3/2$, $\ell'=1$ $s'=5/2$, $\ell'=3$ $s'=3/2$, and $\ell'=3$ $s'=5/2$ in the channel spin representation. All $\ell'=5$ contributions are neglected because the Coulomb penetrability is extremely low relative to the $\ell'=1$ and $\ell'=3$ contributions. Two independent mixing ratios are defined: $\delta_{jL} = \gamma_{j13}/\gamma_{j11}$ and $\delta_{jU} = \gamma_{j37}/\gamma_{j35}$ in the total angular momentum representation, and $\delta_{sL} = \gamma_{s15}/\gamma_{s13}$ and $\delta_{sU} = \gamma_{s35}/\gamma_{s33}$ in the channel spin representation. The mixing angles are $\phi_{jL} = \tan^{-1}\delta_{jL}$ and $\phi_{jU} = \tan^{-1}\delta_{jU}$ in the total angular momentum representation, and $\phi_{sL} = \tan^{-1}\delta_{sL}$ and $\phi_{sU} = \tan^{-1}\delta_{sU}$ in the channel spin representation. The ε^2 parameter now represents the $\ell'=3$ admixture for each resonance: $\varepsilon^2 = (\Gamma_{j35} + \Gamma_{j37})/\Gamma_p$, in the total angular momentum representation. Note that for f-wave and g-wave resonances the range of ϕ_L is $-90^\circ \leq \phi_L \leq 90^\circ$, the range of ϕ_U is $-180^\circ \leq \phi_U \leq 180^\circ$, and ε^2 is an independent parameter.

Unique solutions for the mixing ratios for $5/2^-$ resonances were obtained. Tables 4.14 and 4.15 list these solutions in the total angular momentum representation and the channel spin representation, respectively. Plots of the mixing angles versus energy are shown in figure 4.17. Due to the small sample size, no definite conclusions can be drawn from these plots, but

FIGURE 4.16 Sample angular distributions for a $5/2^-$ resonance. The top figure is the inelastically scattered proton distribution, and the bottom figure is the γ-ray distribution.

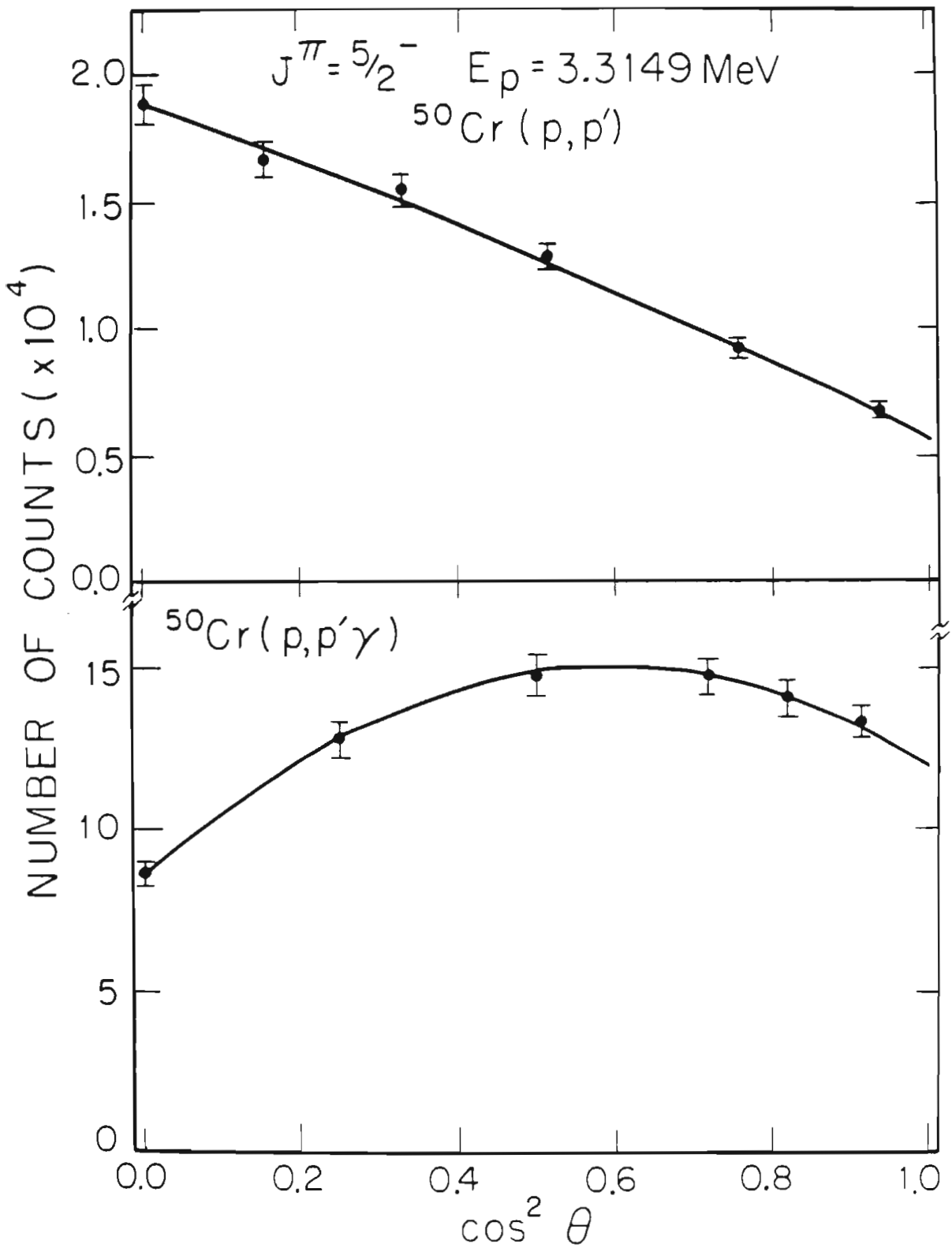
$J^{\pi} = 5/2^-$ $E_p = 3.3149$ MeV
$^{50}Cr(p,p')$
$^{50}Cr(p,p'\gamma)$
NUMBER OF COUNTS ($\times 10^4$)
$\cos^2\theta$
2.0
1.5
1.0
0.5
0.0
15
10
5
0
0.0
0.2
0.4
0.6
0.8
1.0

TABLE 4.13

LEGENDRE POLYNOMIAL COEFFICIENTS FOR ℓ=3 RESONANCES IN ^{51}Mn

Resonance Number	J^{π}	Experiment	a_2	a_4
10	5/2-	p	−0.568 ± 0.030	−0.043 ± 0.037
		γ	0.340 ± 0.033	−0.355 ± 0.051
12	5/2-	p	0.338 ± 0.036	−0.043 ± 0.046
		γ	0.451 ± 0.030	−0.624 ± 0.048
40	5/2-	p	−0.213 ± 0.061	−0.011 ± 0.076
		γ	0.234 ± 0.041	0.026 ± 0.063
86	5/2-	p	−0.104 ± 0.224	−0.051 ± 0.183
		γ	0.419 ± 0.037	−0.646 ± 0.061
98	5/2-	p	0.483 ± 0.050	−0.095 ± 0.055
		γ	0.365 ± 0.041	−0.219 ± 0.064
109	5/2-	p	−0.523 ± 0.050	0.103 ± 0.061
		γ	0.452 ± 0.038	−0.557 ± 0.062
144	5/2-	p	0.320 ± 0.044	−0.158 ± 0.056
		γ	0.321 ± 0.038	−0.410 ± 0.062

TABLE 4.14

MIXING RATIOS, MIXING ANGLES, AND ε^2 FOR $5/2^-$ RESONANCES IN ^{51}Mn

Total Angular Momentum Representation

Res. No.	ϕ_{jL} (degrees)	ϕ_{jU} (degrees)	δ_{jL}	δ_{jU}	ε^2
10	-24.5 ± 1.27	-28.0 ± 32.1	$-0.46 \begin{smallmatrix} +0.03 \\ -0.03 \end{smallmatrix}$	$-0.53 \begin{smallmatrix} +0.60 \\ -1.21 \end{smallmatrix}$	0.206 ± 0.038
12	11.1 ± 1.89	-167.4 ± 23.3	$0.20 \begin{smallmatrix} +0.03 \\ -0.03 \end{smallmatrix}$	$0.22 \begin{smallmatrix} +0.50 \\ -0.22 \end{smallmatrix}$	0.120 ± 0.034
40	-35.0 ± 5.22	-110.8 ± 16.6	$-0.70 \begin{smallmatrix} +0.13 \\ -0.15 \end{smallmatrix}$	$2.63 \begin{smallmatrix} +10.95 \\ -1.32 \end{smallmatrix}$	0.358 ± 0.027
86	-2.7 ± 3.07	-3.8 ± 26.9	$-0.05 \begin{smallmatrix} +0.05 \\ -0.05 \end{smallmatrix}$	$-0.07 \begin{smallmatrix} +0.49 \\ -0.53 \end{smallmatrix}$	0.150 ± 0.038
98	27.8 ± 3.22	-32.3 ± 24.7	$0.53 \begin{smallmatrix} +0.07 \\ -0.07 \end{smallmatrix}$	$-0.63 \begin{smallmatrix} +0.50 \\ -0.91 \end{smallmatrix}$	0.216 ± 0.038
109	-15.5 ± 1.62	-34.9 ± 37.1	$-0.28 \begin{smallmatrix} +0.03 \\ -0.03 \end{smallmatrix}$	$-0.70 \begin{smallmatrix} +0.74 \\ -2.39 \end{smallmatrix}$	0.066 ± 0.042
144	14.4 ± 2.63	146.8 ± 29.5	$0.26 \begin{smallmatrix} +0.05 \\ -0.05 \end{smallmatrix}$	$-0.66 \begin{smallmatrix} +0.59 \\ -1.28 \end{smallmatrix}$	0.288 ± 0.060

TABLE 4.15

MIXING RATIOS, MIXING ANGLES, AND ε^2 FOR $5/2^-$ RESONANCES IN ^{51}Mn

Channel Spin Representation

Res. No.	ϕ_{sL} (degrees)	ϕ_{sU} (degrees)	δ_{sL}	δ_{sU}	ε^2
10	-67.6 ± 1.3	-89.4 ± 32.0	$-2.43 \begin{smallmatrix}+0.14\\-0.16\end{smallmatrix}$	$-97.44 \begin{smallmatrix}+95.88\\-99.08\end{smallmatrix}$	0.206 ± 0.038
12	-32.0 ± 1.9	131.1 ± 23.3	$-0.63 \begin{smallmatrix}+0.04\\-0.05\end{smallmatrix}$	$-1.14 \begin{smallmatrix}+0.67\\-1.96\end{smallmatrix}$	0.120 ± 0.034
40	-78.1 ± 5.2	-172.2 ± 16.6	$-4.73 \begin{smallmatrix}+1.49\\-3.75\end{smallmatrix}$	$0.14 \begin{smallmatrix}+0.32\\-0.14\end{smallmatrix}$	0.358 ± 0.027
86	-45.8 ± 3.1	-65.2 ± 26.9	$-1.03 \begin{smallmatrix}+0.10\\-0.12\end{smallmatrix}$	$-2.17 \begin{smallmatrix}+1.38\\-29.40\end{smallmatrix}$	0.150 ± 0.038
98	-15.3 ± 3.2	-93.8 ± 24.7	$-0.27 \begin{smallmatrix}+0.06\\-0.06\end{smallmatrix}$	$15.26 \begin{smallmatrix}+17.87\\-13.41\end{smallmatrix}$	0.216 ± 0.038
109	-58.6 ± 1.6	-96.4 ± 37.0	$-1.64 \begin{smallmatrix}+0.10\\-0.11\end{smallmatrix}$	$8.96 \begin{smallmatrix}+10.65\\-7.90\end{smallmatrix}$	0.066 ± 0.042
144	-28.7 ± 2.6	85.3 ± 29.5	$-0.55 \begin{smallmatrix}+0.06\\-0.06\end{smallmatrix}$	$12.21 \begin{smallmatrix}+14.37\\-10.73\end{smallmatrix}$	0.288 ± 0.060

FIGURE 4.17 Mixing angles versus incident proton energy for $5/2^-$ resonances. The top figure is φ_L versus energy in both representations. The bottom figure is φ_U versus energy in both representations.

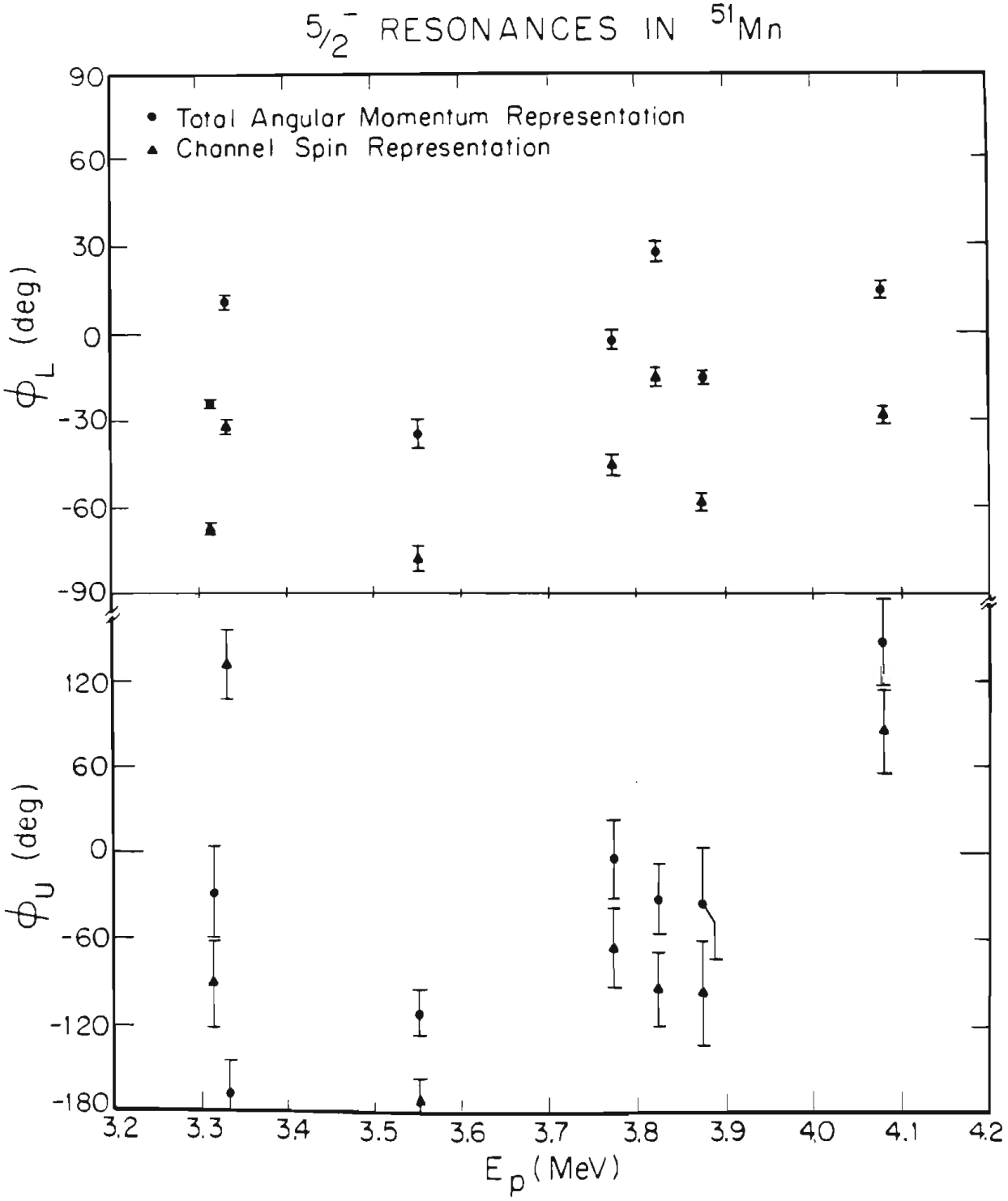
$5/2^-$ RESONANCES IN ^{51}Mn
• Total Angular Momentum Representation
▲ Channel Spin Representation
ϕ_L (deg)
ϕ_U (deg)
E_p (MeV)
90
60
30
0
-30
-60
-90
120
60
0
-60
-120
-180
3.2
3.3
3.4
3.5
3.6
3.7
3.8
3.9
4.0
4.1
4.2

the mixing angles do not seem to be uniformly distributed.

Values of the four channel reduced widths and three reduced width amplitude products are listed in table 4.16 for the total angular momentum representation and in table 4.17 for the channel spin representation. The elastic and total inelastic widths and reduced widths for each resonance are listed in table A.1. Differential and integral plots of the elastic and total inelastic reduced widths versus energy are shown in figure 4.18.

b. Analog States

Interesting relations exist between nuclear states which are members of isobaric spin (or isospin) multiplets. These states have identical values of T, the isospin quantum number, but different values of T_z. T is strictly conserved only in the absence of Coulomb interactions and is approximately conserved when the Coulomb effects are small compared to nuclear interactions. Experimentally one normally observes only the two members of the multiplet which contain the greatest number of neutrons. The member of the multiplet with the most neutrons, the $T_z = T$ member, is called the 'parent' state, and is typically a low energy state. The $T_z = T - 1$ member of the multiplet is the isobaric analog resonance (IAR). Of the seven $5/2^-$ resonances studied in ^{51}Mn, two are fragments of an analog state.

There is a $5/2^-$ state in ^{51}Cr at 4.002 MeV. Corresponding to this parent state, a state of the same J^π is expected in ^{51}Mn at $E_p = \Delta E_c - B_n + E_{exc}$ in the center of mass frame, where B_n is the binding energy of the last neutron in the parent system, ΔE_c is the Coulomb energy difference between the parent state and the analog state, and E_{exc} is the excitation energy of the parent state in the parent nucleus. A semi-empirical formula for ΔE_c is given by Jänecke (1969): $\Delta E_c = (1389\ Z_t - 2041) / A^{1/3}$ keV,

TABLE 4.16

INELASTIC REDUCED WIDTHS AND AMPLITUDE PRODUCTS FOR $5/2^-$ RESONANCES IN ^{51}Mn

Total Angular Momentum Representation

Res. No.	γ^2_{j11} (keV)	γ^2_{j13} (keV)	γ^2_{j35} (keV)	γ^2_{j37} (keV)	$\gamma_{j11}\gamma_{j13}$ (keV)	$\gamma_{j11}\gamma_{j35}$ (keV)	$\gamma_{j11}\gamma_{j37}$ (keV)
10	0.19	0.04	1.83	0.52	-0.09	0.59	-0.31
12	0.16	0.01	0.86	0.04	0.03	-0.37	-0.08
40	0.06	0.03	0.22	1.55	-0.04	-0.12	-0.31
86	0.20	0.00	1.04	0.00	-0.01	0.45	-0.03
98	0.06	0.02	0.47	0.19	0.03	0.18	-0.11
109	0.10	0.01	0.14	0.07	-0.03	0.12	-0.08
144	0.32	0.02	2.41	1.04	0.08	-0.88	0.58

TABLE 4.17

INELASTIC REDUCED WIDTHS AND AMPLITUDE PRODUCTS FOR $5/2^-$ RESONANCES IN ^{51}Mn

Channel Spin Representation

Res. No.	γ^2_{s13} (keV)	γ^2_{s15} (keV)	γ^2_{s33} (keV)	γ^2_{s35} (keV)	$\gamma_{s13}\gamma_{s15}$ (keV)	$\gamma_{s13}\gamma_{s33}$ (keV)	$\gamma_{s13}\gamma_{s35}$ (keV)
10	0.03	0.19	0.00	2.35	-0.08	0.00	-0.28
12	0.12	0.05	0.39	0.51	-0.08	-0.22	0.25
40	0.00	0.09	1.75	0.03	-0.02	-0.08	-0.01
86	0.10	0.10	0.18	0.86	-0.10	0.13	-0.29
98	0.08	0.01	0.00	0.66	-0.02	-0.01	-0.23
109	0.03	0.08	0.00	0.21	-0.05	-0.01	-0.08
144	0.26	0.08	0.02	3.42	-0.15	0.08	0.95

FIGURE 4.18 Plots of reduced widths and the cumulative sums of reduced widths for the elastic and total inelastic decay channels for $5/2^-$ resonances in ^{51}Mn.

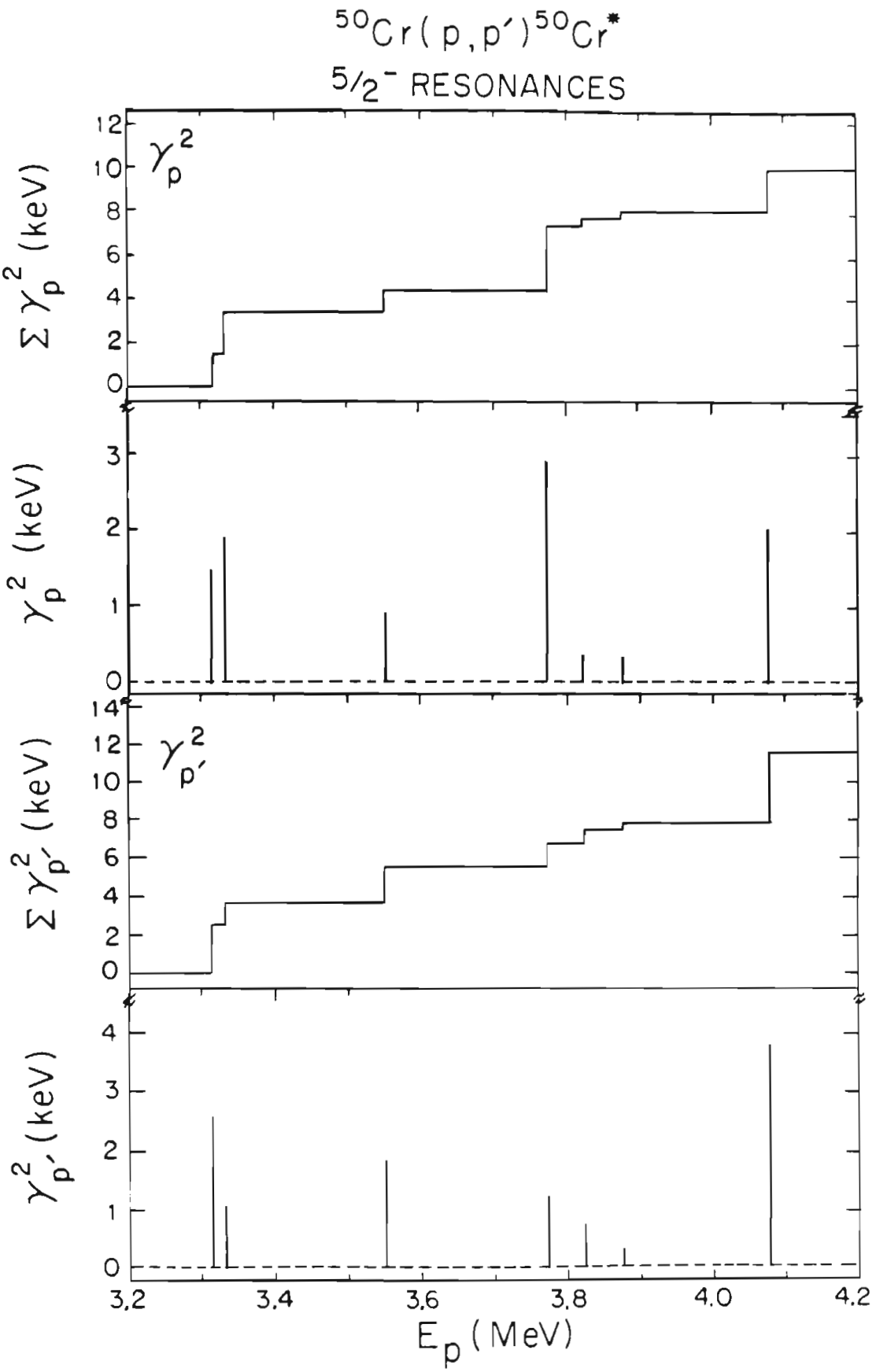
$^{50}Cr(p,p')^{50}Cr^*$
$5/2^-$ RESONANCES
$\Sigma\gamma_p^2$ (keV)
γ_p^2
γ_p^2 (keV)
$\Sigma\gamma_{p'}^2$ (keV)
$\gamma_{p'}^2$
$\gamma_{p'}^2$ (keV)
E_p (MeV)

where Z_t is the proton number of the target and A is the mass of the parent (or analog) system. For the 4.002 MeV state in ^{50}Cr, this approximation yields ΔE_c = 8.44 MeV and E_p = 3.24 MeV in the laboratory frame. Two $5/2^-$ resonances were observed near this energy, one at E_p = 3.3149 MeV and the other at E_p = 3.3323 MeV. The centroid of these two resonances falls at E_p = 3.32 MeV, which is within 80 keV of the expected value. The two $5/2^-$ resonances are therefore considered to be fragments of the analog state whose parent is the E_p = 4.002 MeV level in ^{51}Cr.

Another way to verify that the two $5/2^-$ resonances are analog states is to consider the strengths of the parent and resonance states. The spectroscopic factor for elastic scattering is defined as Γ_{pp}/Γ_{sp}, where Γ_{pp} is the laboratory elastic width and Γ_{sp} is the single particle width. The elastic width was determined directly from the data obtained in the present experiment. The analog strength is expected to be only a fraction $1/(2T_o + 1)$ of the parent strength. For convenience the analog spectroscopic factor is usually defined as $S_{pp} = (2T_o + 1)\Gamma_{pp}/\Gamma_{sp}$. The single particle width was determined with the computer code "HANS" which is based on the theory by Harney and Weidenmüller (1969). This method is described in detail in the review article by Bilpuch et al. (1976). The parameters used in "HANS" are as follows: the binding energy of the last neutron in the parent nucleus B_n = −9.264 MeV, the incident proton laboratory energy E_p = 3.3248 MeV, the excitation energy in the parent nucleus E_x =4.002 MeV, and the excitation energy of the final target nucleus E_{gam} = 0.7833 MeV. A value of 1.246 keV was obtained for $\Gamma_{sp}/(2\ T_o + 1)$, and a value of 0.035 keV for $\Gamma_{pp} = \Gamma_{pp1} + \Gamma_{pp2}$. With these two values, S_{pp} was found to be 0.028. This value is slightly less than the value for S_{dp} (0.04) given by Robertshaw et al. (1968). This is consistent with previous results: values for S_{pp} are

generally lower than those for S_{dp}. The value quoted by Salzmann et al. is 0.05; however, Salzmann postulated the existence of a third $5/2^-$ resonance at E_p = 3.3629 MeV. When fit with "MULTI" in the present experiment, this resonance was assigned $J^\pi = 3/2^-$.

One can also use Γ'_{pp}, and Γ'_{sp}, the inelastic laboratory width and the single particle width, to obtain the $S_{pp'}$, the spectroscopic factors for each of the four exit channels for the $5/2^-$ analog states. These values are listed in table 4.18. Γ'_{pp}, is the sum of the channel inelastic widths for both resonances. Spectroscopic factors for the inelastic decays provide unique information, the equivalent of a (d,p) experiment on the excited state of the target. The experimental values of the inelastic spectroscopic factors are comparable to the elastic spectroscopic factors. This result is consistent with previous observations in the same mass-energy region. However, the small values of the spectroscopic factors prevent any detailed conclusions.

4. g-wave Resonances

If the incident proton has $\ell = 4$, then $7/2^+$ or $9/2^+$ resonances are formed. Angular distribution equations for decay from $9/2^+$ resonances are:

$$W_p(\theta) = a_{op}(1 + a_{2p}P_2 + a_{4p}P_4 + a_{6p}P_6 + a_{8p}P_8) \qquad (4.9)$$

$$W_\gamma(\theta) = a_{o\gamma}(1 + a_{2\gamma}P_2 + a_{4\gamma}P_4). \qquad (4.10)$$

For $7/2^+$ resonances, $a_{8p} = 0$. Only two g-wave resonances were studied. Resonance 1 was assigned $J^\pi = 7/2^+$. Results for resonance 1A were ambiguous and it was tentatively assigned $J^\pi = 9/2^+$. Salzmann classified both resonances as parts of several $9/2^+$ analog states. Since one resonance had $J^\pi = 7/2^+$ and the assignment for the other is uncertain, no analysis of the analog state was performed. The Legendre polynomial coefficients and spin assignments for the

TABLE 4.18

SPECTROSCOPIC FACTORS FOR $5/2^-$ ANALOG STATES

J^π	Configuration	$\Gamma_{sp}/(2T_o+1)$ (keV)	$\Gamma_{pp}(\Gamma_{pp}')$ (keV)	$S_{pp}(S_{pp}')$
$5/2^-$	$1f\frac{5}{2} \otimes 0^+$	1.2	0.035	0.028
	$2p\frac{1}{2} \otimes 2^+$	9.6	0.018	0.0019
	$2p\frac{3}{2} \otimes 2^+$	9.7	0.002	0.0002
	$1f\frac{5}{2} \otimes 2^+$	0.15	0.003	0.023
	$1f\frac{7}{2} \otimes 2^+$	0.16	0.0007	0.0043

two g-wave resonances are given in table 4.19. A portion of the analysis of the g-wave resonances was performed by P. Ramakrishnan with a program written by J. F. Shriner, Jr.

The $7/2^+$ resonance had four open exit channels: in the total angular momentum representation, $\ell'=2$ $j'=3/2$, $\ell'=2$ $j'=5/2$, $\ell'=4$ $j'=7/2$, and $\ell'=4$ $j'=9/2$, and in the channel spin representation $\ell'=2$ $s'=3/2$, $\ell'=2$ $s'=5/2$, $\ell'=4$ $s'=3/2$, and $\ell'=4$ $s'=5/2$. Any $\ell'=6$ contributions are neglected because the Coulomb penetrability is extremely low relative to the $\ell'=2$ and $\ell'=4$ contributions. The mixing ratios are $\delta_{jL}= \gamma_{j25}/\gamma_{j23}$ and $\delta_{jU}= \gamma_{j49}/\gamma_{j47}$ in the total angular momentum representation, and $\delta_{sL}= \gamma_{s25}/\gamma_{s23}$ and $\delta_{sU}= \gamma_{s45}/\gamma_{s43}$ in the channel spin representation. The mixing angles are $\phi_{jL}= \tan^{-1}\delta_{jL}$ and $\phi_{jU}= \tan^{-1}\delta_{jU}$ in the total angular momentum representation, and $\phi_{sL}= \tan^{-1}\delta_{sL}$ and $\phi_{sL}= \tan^{-1}\delta_{sL}$ in the channel spin representation. The ε^2 parameter is a measure of the $\ell'=4$ admixture for each resonance.

A $9/2^+$ resonance has three open exit channels: in the total angular momentum representation, $\ell'=2$ $j'=5/2$, $\ell'=4$ $j'=7/2$, and $\ell'=4$ $j'=9/2$, and in the channel spin representation $\ell'=2$ $s'=5/2$, $\ell'=4$ $s'=3/2$, and $\ell'=4$ $s'=5/2$. Again, $\ell'=6$ contributions are neglected. Only one mixing ratio is defined: $\delta_{jU}= \gamma_{j49}/\gamma_{j47}$ in the total angular momentum representation and $\delta_{sU}= \gamma_{s45}/\gamma_{s43}$ in the channel spin representation. The mixing angle in the total angular momentum representation is $\phi_{jU}= \tan^{-1}\delta_{jU}$, and in the channel spin representation $\phi_{sU}= \tan^{-1}\delta_{sU}$. The ε^2 parameter is a measure of the $\ell'=4$ admixture for each resonance, and is defined as $\varepsilon^2= (\Gamma_{j47}+ \Gamma_{j49})/\Gamma_p$, in the total angular momentum representation. Table 4.20 lists values of the mixing ratios, mixing angles, and ε^2 for both resonances in both representations. Values of the channel reduced widths are listed in table 4.21 for both resonances in both representations.

TABLE 4.19

LEGENDRE POLYNOMIAL COEFFICIENTS FOR ℓ=4 RESONANCES IN ^{51}Mn

Res. No.	J^{π}	Exp.	a_2	a_4	a_6	a_8
1A	9/2+	P	1.063 ± 0.077	0.522 ± 0.084	0.030 ± 0.111	0.104 ± 0.154
		γ	0.372 ± 0.051	−0.335 ± 0.053	−0.009 ± 0.064	0.036 ± 0.098
1	7/2+	P	0.847 ± 0.039	0.169 ± 0.052	−0.059 ± 0.061	
		γ	0.339 ± 0.036	−0.269 ± 0.053	−0.004 ± 0.064	

TABLE 4.20

MIXING RATIOS, MIXING ANGLES, AND ε^2 FOR ℓ=4 RESONANCES IN ^{51}Mn

Total Angular Momentum Representation

Res. No.	ϕ_{jL} (degrees)	ϕ_{jU} (degrees)	δ_{jL}	δ_{jU}	ε^2
1A		-167.1 ± 20.8		$0.23 \begin{smallmatrix}+0.44\\-0.23\end{smallmatrix}$	0.144 ± 0.045
1	20.7 ± 2.7	-13.2 ± 11.4	$0.38 \begin{smallmatrix}+0.05\\-0.05\end{smallmatrix}$	$-0.23 \begin{smallmatrix}+0.20\\-0.22\end{smallmatrix}$	0.163 ± 0.033

Channel Spin Representation

Res. No.	ϕ_{sL} (degrees)	ϕ_{sU} (degrees)	δ_{sL}	δ_{sU}	ε^2
1A		-60.3 ± 24.6		$-1.75 \begin{smallmatrix}+1.04\\-9.57\end{smallmatrix}$	0.059 ± 0.034
1	-16.1 ± 2.7	-72.1 ± 11.4	$-0.29 \begin{smallmatrix}+0.05\\-0.05\end{smallmatrix}$	$-3.09 \begin{smallmatrix}+1.31\\-5.70\end{smallmatrix}$	0.163 ± 0.033

TABLE 4.21

INELASTIC REDUCED WIDTHS AND AMPLITUDE PRODUCTS FOR ℓ=4 RESONANCES IN ^{51}Mn

Total Angular Momentum Representation

Res. No.	γ^2_{j23} (keV)	γ^2_{j25} (keV)	γ^2_{j47} (keV)	γ^2_{j49} (keV)	$\gamma_{j23}\gamma_{j25}$ (keV)	$\gamma_{j23}\gamma_{j47}$ (keV)	$\gamma_{j23}\gamma_{j49}$ (keV)
1	15.12	2.17	423.6	23.15	5.73	80.04	-18.71
1A	6.79	0.91	164.2	8.63	2.48	-33.38	-7.65

Channel Spin Representation

Res. No.	γ^2_{s23} (keV)	γ^2_{s25} (keV)	γ^2_{s43} (keV)	γ^2_{s45} (keV)	$\gamma_{s23}\gamma_{s25}$ (keV)	$\gamma_{s23}\gamma_{s43}$ (keV)	$\gamma_{s23}\gamma_{s45}$ (keV)
1	16.00	1.34	42.35	404.4	-4.62	26.00	-80.32
1A	8.11	0.35	17.24	53.11	-1.68	11.83	-20.76

CHAPTER V

STATISTICAL PROPERTIES

A. Introduction

Due to the large number of states present at the excitation energies involved in these experiments (about 11 MeV), a theoretical consideration of individual states is inappropriate. Instead, a statistical approach is employed in the description of properties of levels such as the energy distribution and the widths and reduced widths of states. The theoretical background of the statistical approach will be summarized briefly.

B. Level Spacings and Proton Strength Functions

A quantum state of a system is specified by a set of observables and their corresponding operators. In simple systems, all interactions are specified through the Hamiltonian H, and the Schrödinger equation is solved: $H\Psi_i = E_i\Psi_i$, where the Ψ_i are the wave functions and the E_i are the energy eigenvalues. The system Hamiltonian H defined for the study of the statistical properties of compound nuclear states is required to be invariant under time reversal and rotations: H is therefore real and symmetric ($H = H^* = \tilde{H}$). The canonical transformation group which preserves the properties of a real symmetric Hamiltonian is the orthogonal group.

A simple level sequence is one in which all levels have the same

conserved quantities, such as spin and parity (Mehta 1967). Wigner (1967) suggested that eigenfunctions Ψ could be chosen as functions of the conserved quantities. The Hamiltonian can be reduced to a matrix containing diagonal blocks (Mehta 1967), each of which has the same conserved quantities as a simple level sequence. The statistical behavior of the simple level sequence is represented by the eigenvalues of the corresponding block. Interactions between levels in the same sequence (and therefore in the same block) are sufficiently strong that other interactions are negligible: therefore no further diagonalization of the matrix is considered, and levels corresponding to different blocks are considered statistically uncorrelated. Each of the blocks can be considered separately as an NxN orthogonal matrix whose elements are random variables with the maximum statistical independence allowed under the symmetry requirements, where N is a large fixed positive number. The analytic form of the probability distribution function was derived by Porter and Rosenzweig (1960). Detailed descriptions of the derivation can be found in Chou (1980) and Watson (1980). From the general distribution the corresponding eigenvalue distribution, the Wishart distribution, can be obtained. The single eigenvalue distribution is derived by integrating over all but one eigenvalue; this procedure is very complicated. For the nearest neighbor distributions the result is essentially the same as that proposed by Wigner. Detailed comparison of spacing data with random matrix theory is given in the comprehensive review by Brody et al. (1981). The present data are not sufficiently complete (too few levels and too many missing levels) for such detailed comparison. However, the same limitation does not apply to measurements of the width and amplitude correlations. Such measurements are so new that even fragmentary results are important, since qualitative properties and trends have not yet been established.

Average properties also can be obtained. One useful combination of two average properties is the proton strength function, defined as $S = \overline{\gamma_c^2}/D$, where $\overline{\gamma_c^2}$ is the average reduced width in channel c, as previously defined, and D is the observed average level spacing. Table 5.1 presents the proton strength functions for $3/2^-$ resonances, and table 5.2 presents the proton strength functions for $5/2^+$ resonances in ^{51}Mn.

C. Reduced Width Amplitudes

The probability distribution function for reduced width amplitudes γ_λ in the case of m channels is the Krieger-Porter distribution:

$$P_{cc'c''\ldots} = \prod_\lambda \frac{|M|^{1/2}}{(2\pi)^{m/2}} \exp\left(-\frac{1}{2}(\gamma_\lambda, M\gamma_\lambda)\right) , \tag{5.1}$$

where M is an mxm real symmetric positive definite matrix defined as $M = \overline{(\gamma_\lambda \times \gamma_\lambda)}^{-1}$ and $|M|$ is the determinant of matrix M. The bar indicates an average over levels. M is equal to the inverse of the covariance matrix Σ, where $\Sigma = \overline{(\gamma_\lambda \times \gamma_\lambda)}$. The channel correlation coefficient for the reduced width amplitudes is:

$$C(\gamma_c, \gamma_{c'}) = \frac{\overline{\gamma_{\lambda c}\gamma_{\lambda c'}}}{(\overline{\gamma_c^2}\,\overline{\gamma_{c'}^2})^{1/2}} , \tag{5.2}$$

assuming the random phase approximation ($\overline{\gamma_{\lambda c}} = 0$). The reduced width correlation coefficient is:

$$C(\gamma_c^2, \gamma_{c'}^2) = \frac{\overline{\gamma_{\lambda c}^2\gamma_{\lambda c'}^2} - \overline{\gamma_{\lambda c}^2}\,\overline{\gamma_{\lambda c'}^2}}{[(\overline{\gamma_{\lambda c}^4} - (\overline{\gamma_{\lambda c}^2})^2)(\overline{\gamma_{\lambda c'}^4} - (\overline{\gamma_{\lambda c'}^2})^2)]^{1/2}} \tag{5.3}$$

$$= (C(\gamma_c, \gamma_{c'}))^2 \tag{5.4}$$

These equations are from Krieger and Porter (1963).

TABLE 5.1

PROTON STRENGTH FUNCTIONS FOR 30 $3/2^-$ RESONANCES IN ^{51}Mn

Channel	$\Sigma\gamma^2$ (keV)	$\overline{\gamma^2}$ (keV)	S
γ^2_p	34.54	1.151	0.028
$\gamma^2_{p'}$	25.07	0.836	0.020
γ^2_{j11}	11.13	0.371	0.009
γ^2_{j13}	13.94	0.465	0.011
γ^2_{s13}	11.88	0.396	0.010
γ^2_{s15}	13.19	0.440	0.011

D = 41.2 keV

TABLE 5.2

PROTON STRENGTH FUNCTIONS FOR 38 $5/2^+$ RESONANCES IN ^{51}Mn

Channel	$\Sigma\gamma^2$ (keV)	$\overline{\gamma^2}$ (keV)	S
γ_p^2	40.48	1.065	0.040
$\gamma_{p'}^2$	64.40	1.695	0.063
γ_{j01}^2	19.52	0.514	0.019
γ_{j23}^2	10.02	0.264	0.010
γ_{j25}^2	34.84	0.917	0.034
γ_{s05}^2	19.52	0.514	0.019
γ_{s23}^2	24.69	0.650	0.024
γ_{s25}^2	20.18	0.531	0.020

D = 26.9 keV

1. p-wave Resonances

There are no $3/2^-$ analog states in the energy range considered. Therefore, a statistical approach is appropriate for analysis of the set of $3/2^-$ resonances. If the reduced width amplitude distribution is assumed to be a Gaussian distribution with zero mean (the Krieger-Porter distribution in the one channel limit):

$$P(x) = \frac{1}{(2\pi)^{1/2}} \exp(-x^2/2), \text{ where } x = (\gamma^2/\overline{\gamma^2})^{1/2} , \qquad (5.5)$$

then the reduced width distribution is expected to follow the Porter-Thomas distribution:

$$P(y) = \frac{1}{(2\pi y)^{1/2}} \exp(-y/2), \text{ where } y = x^2 = \gamma^2/\overline{\gamma^2} . \qquad (5.6)$$

Note that this is a singlet distribution and is independent of channel correlations. The experimental reduced width histograms are shown in figure 5.1 for the elastic and total inelastic channels, in figure 5.2 for the inelastic channels in the total angular momentum representation, and in figure 5.3 for the inelastic channels in the channel spin representation. The solid curve in each plot is the Porter-Thomas distribution for N levels. A log-log scale was used to accentuate the effect of missing small levels. The data agree quite well with the Porter-Thomas distribution, although it is clear from the $\overline{\gamma_p^2}$ and $\overline{\gamma_p^2}$, plots that many small levels were not seen. Approximately 11% of the levels were missed.

2. d-wave Resonances

Since there are no analog states in the energy range considered, the reduced width distribution for the d-wave resonances is also expected to follow the Porter-Thomas distribution. The experimental reduced width

FIGURE 5.1 The distribution of reduced widths for the elastic and total inelastic decay channels for $3/2^-$ resonances in ^{51}Mn. The solid line in both cases is the normalized Porter-Thomas distribution.

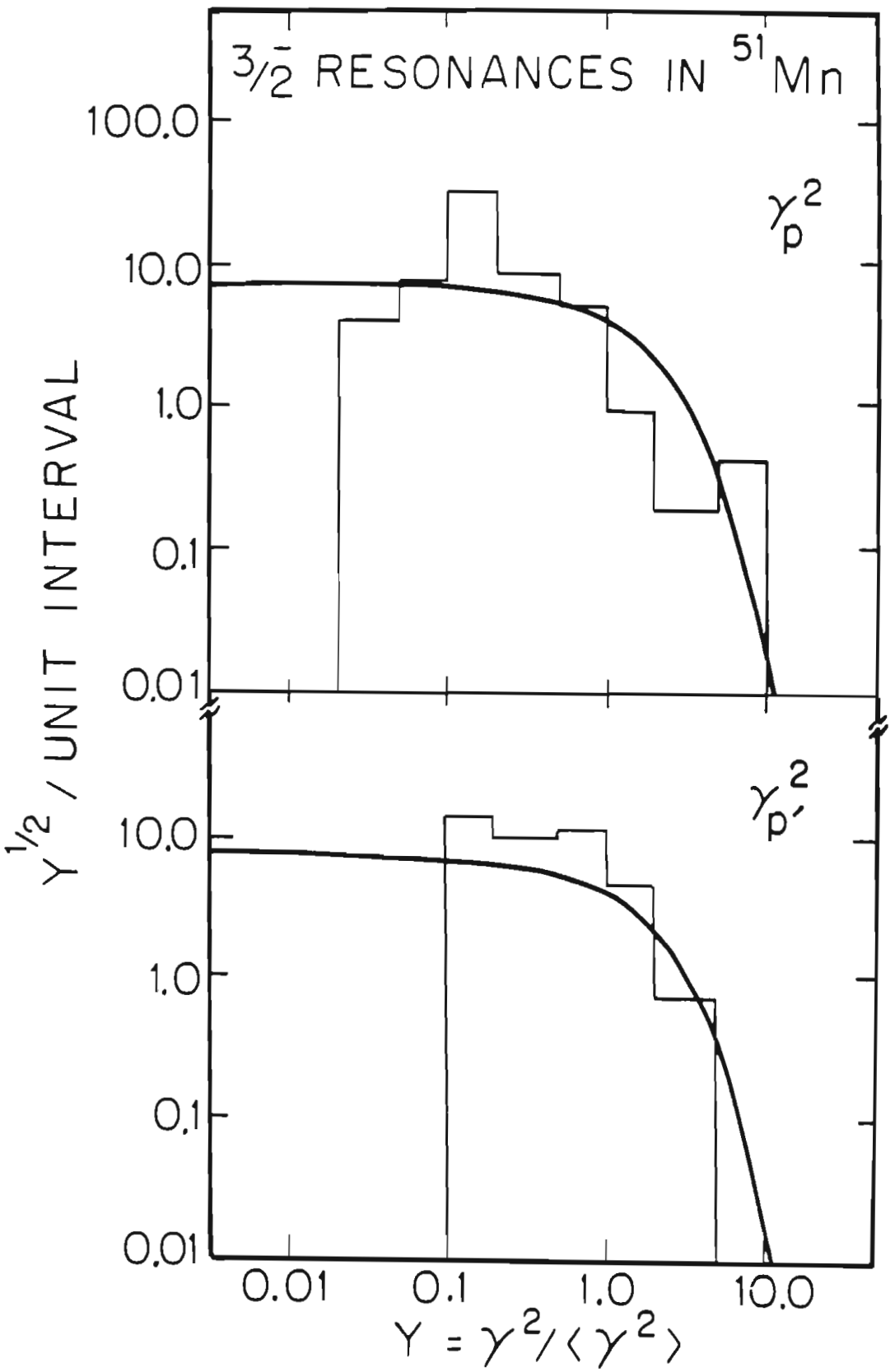
3/2⁻ RESONANCES IN 51Mn
100.0
10.0
1.0
0.1
0.01
γ_p^2
$\gamma_{p'}^2$
$Y^{1/2}$ / UNIT INTERVAL
10.0
1.0
0.1
0.01
0.01
0.1
1.0
10.0
$Y = \gamma^2/\langle\gamma^2\rangle$

FIGURE 5.2 The distribution of reduced widths for the inelastic decay channels for $3/2^-$ resonances in ^{51}Mn in the total angular momentum representation. The solid line in both cases is the normalized Porter-Thomas distribution.

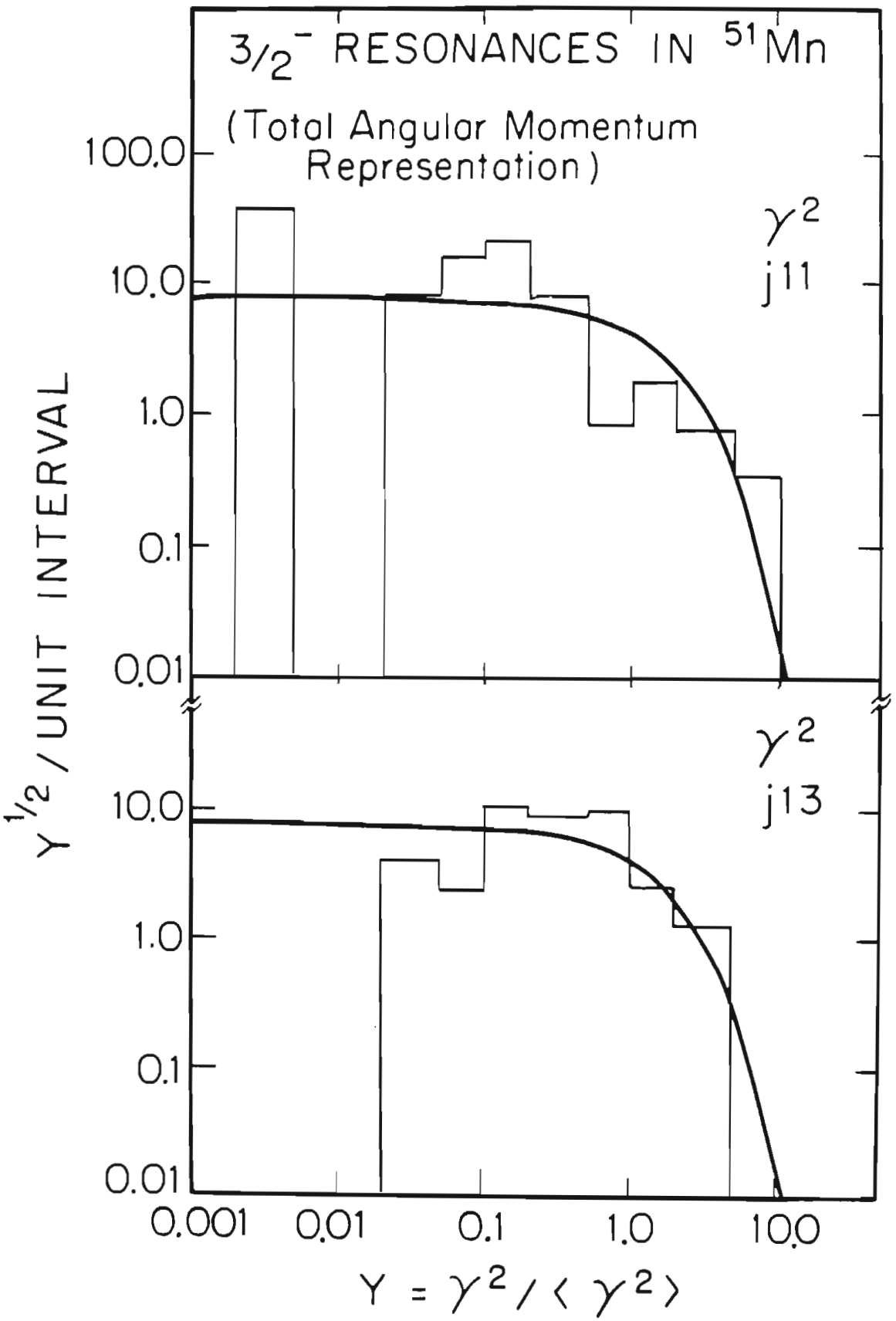
3/2⁻ RESONANCES IN 51Mn
(Total Angular Momentum Representation)
γ²
j11
γ²
j13
100.0
10.0
1.0
0.1
0.01
0.001
0.01
0.1
1.0
10.0
γ^1/2 / UNIT INTERVAL
Y = γ² / ⟨γ²⟩

FIGURE 5.3 The distribution of reduced widths for the inelastic decay channels for $3/2^-$ resonances in ^{51}Mn in the channel spin representation. The solid line in both cases is the normalized Porter-Thomas distribution.

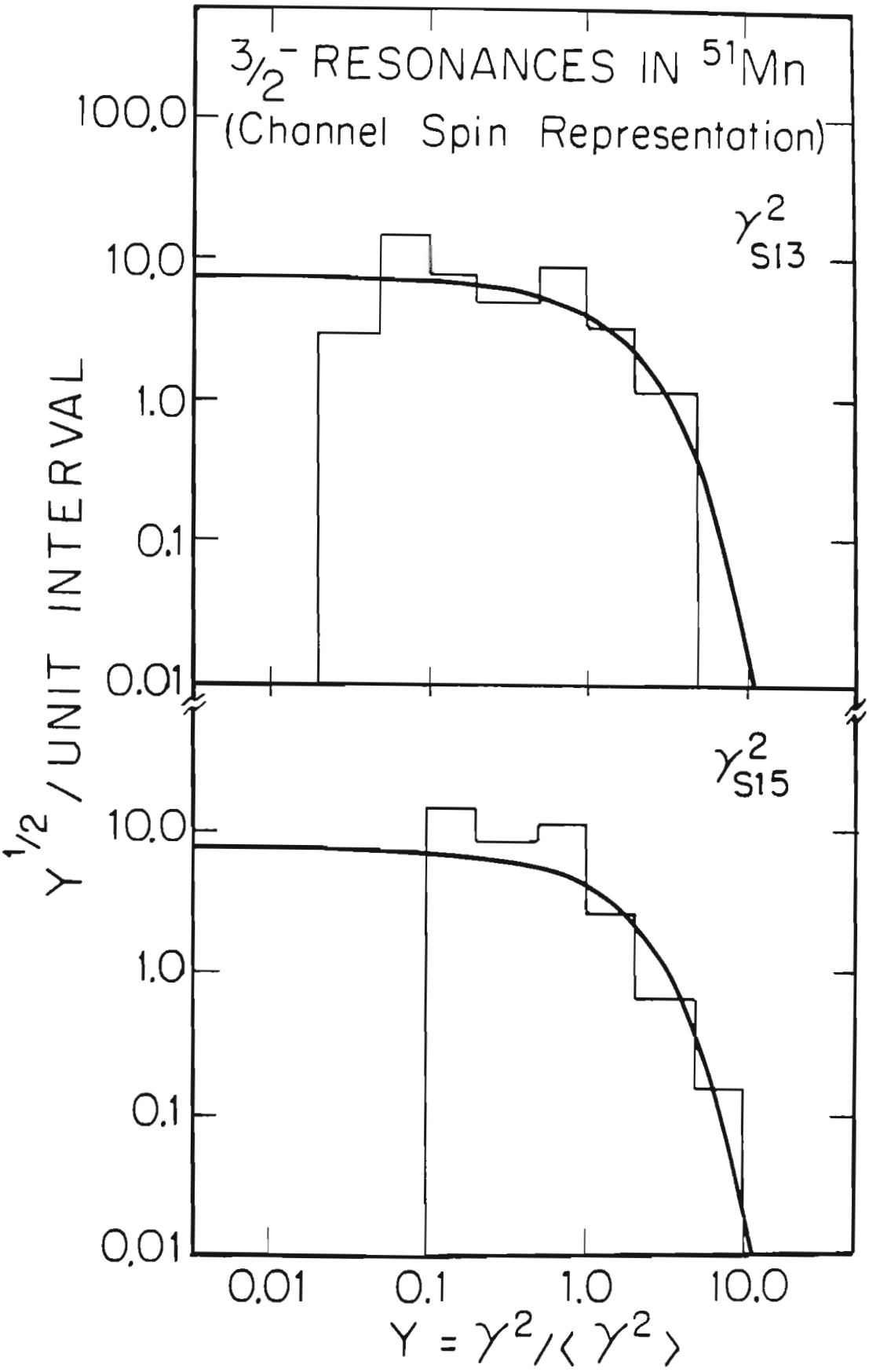
3/2⁻ RESONANCES IN 51Mn
(Channel Spin Representation)
γ^2_{S13}
γ^2_{S15}
100.0
10.0
1.0
0.1
0.01
$Y^{1/2}$ / UNIT INTERVAL
0.01
0.1
1.0
10.0
$Y = \gamma^2 / \langle \gamma^2 \rangle$

histograms for the elastic and total inelastic channels are shown in figure 5.4, for the inelastic channels in the total angular momentum representation in figure 5.5, and for the inelastic channels in the channel spin representation in figure 5.6. The solid curve is the theoretical prediction of the Porter-Thomas distribution. As in the case of the p-waves, the data agree well with the theory, but it is clear that many small levels were not seen. Approximately 19% of the levels were missed.

D. Mixing Ratios

In quantum mechanical systems, absolute phase is unmeasurable; only the relative phase between wave functions can be determined. Previously, only the magnitudes of the amplitudes were measured. The present method determines the relative signs between reduced width amplitudes corresponding to different decay channels. That is, both the sign and magnitude of the mixing ratio of two reduced width amplitudes are obtained.

1. p-wave Resonances

As derived by Chou (1980), the probability distribution function for mixing ratios in the two channel case is:

$$P(\delta) = \frac{|M|^{1/2}}{\pi(M_{11} + M_{22}\delta^2 + 2M_{12}\delta)} \text{ , where:} \qquad (5.7)$$

$$|M| = \frac{1}{\overline{\gamma_1^2}\,\overline{\gamma_2^2} - (\overline{\gamma_1\gamma_2})^2} \text{ ,} \qquad M_{11} = \overline{\gamma_2^2}\,|M| \text{ ,}$$

$$M_{22} = \overline{\gamma_1^2}\,|M| \text{ ,} \qquad M_{12} = -\,\overline{\gamma_1\gamma_2}\,|M| \text{ .}$$

In terms of the mixing angle ϕ, the probability distribution function is:

$$P(\phi) = \frac{|M|^{1/2}}{\pi(M_{11}\cos^2\phi + M_{22}\sin^2\phi + M_{12}\sin 2\phi)} \text{ .} \qquad (5.8)$$

FIGURE 5.4 The distribution of reduced widths for the elastic and total inelastic decay channels for $5/2^+$ resonances in ^{51}Mn. The solid line in both cases is the normalized Porter-Thomas distribution.

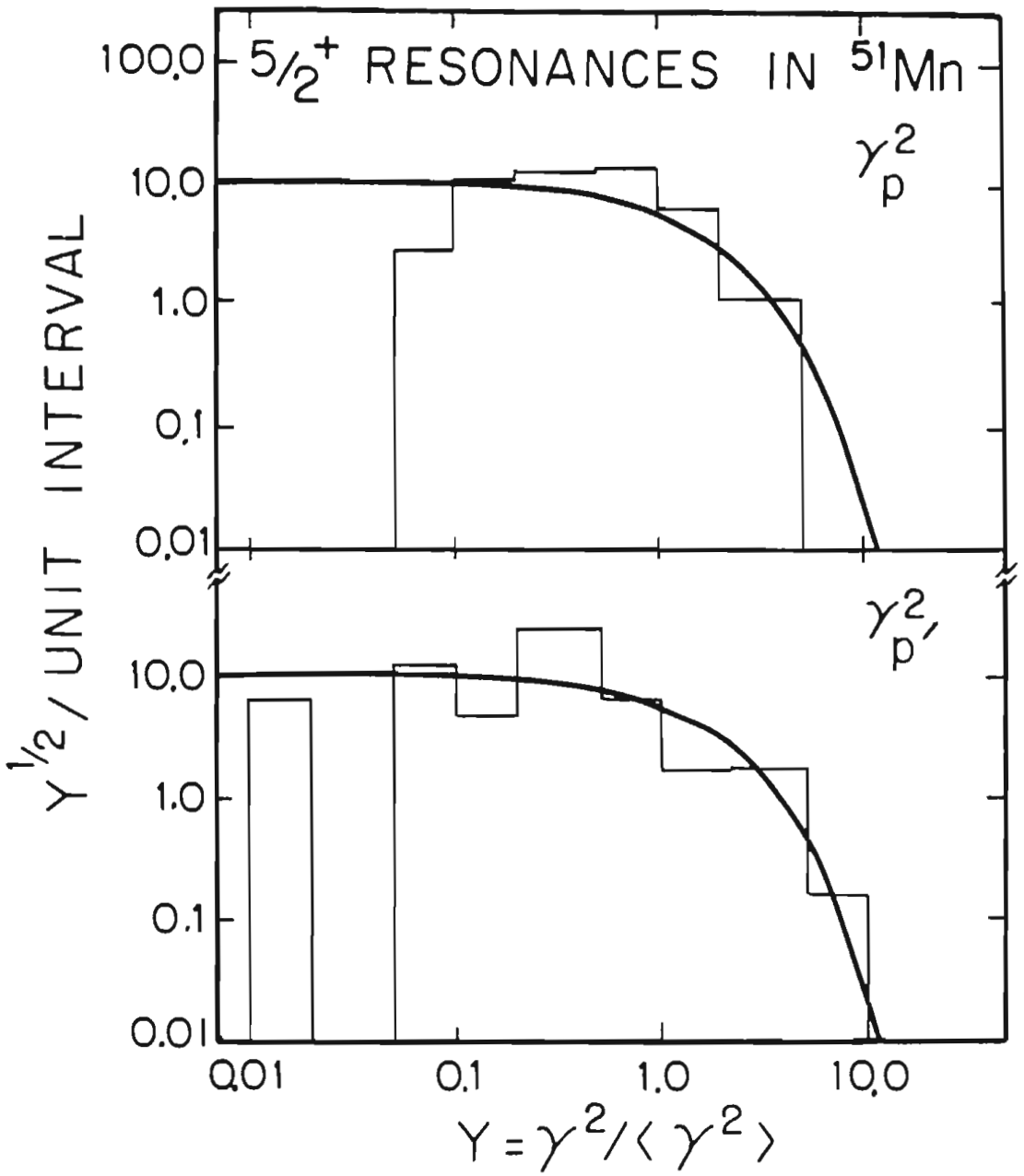
$5/2^+$ RESONANCES IN ^{51}Mn
γ_p^2
$\gamma_{p'}^2$
100.0
10.0
1.0
0.1
0.01
$Y^{1/2}$ / UNIT INTERVAL
0.01
0.1
1.0
10.0
$Y = \gamma^2/\langle\gamma^2\rangle$

FIGURE 5.5 The distribution of reduced widths for the inelastic decay channels for $5/2^+$ resonances in ^{51}Mn in the total angular momentum representation. The solid line in all three cases is the normalized Porter-Thomas distribution.

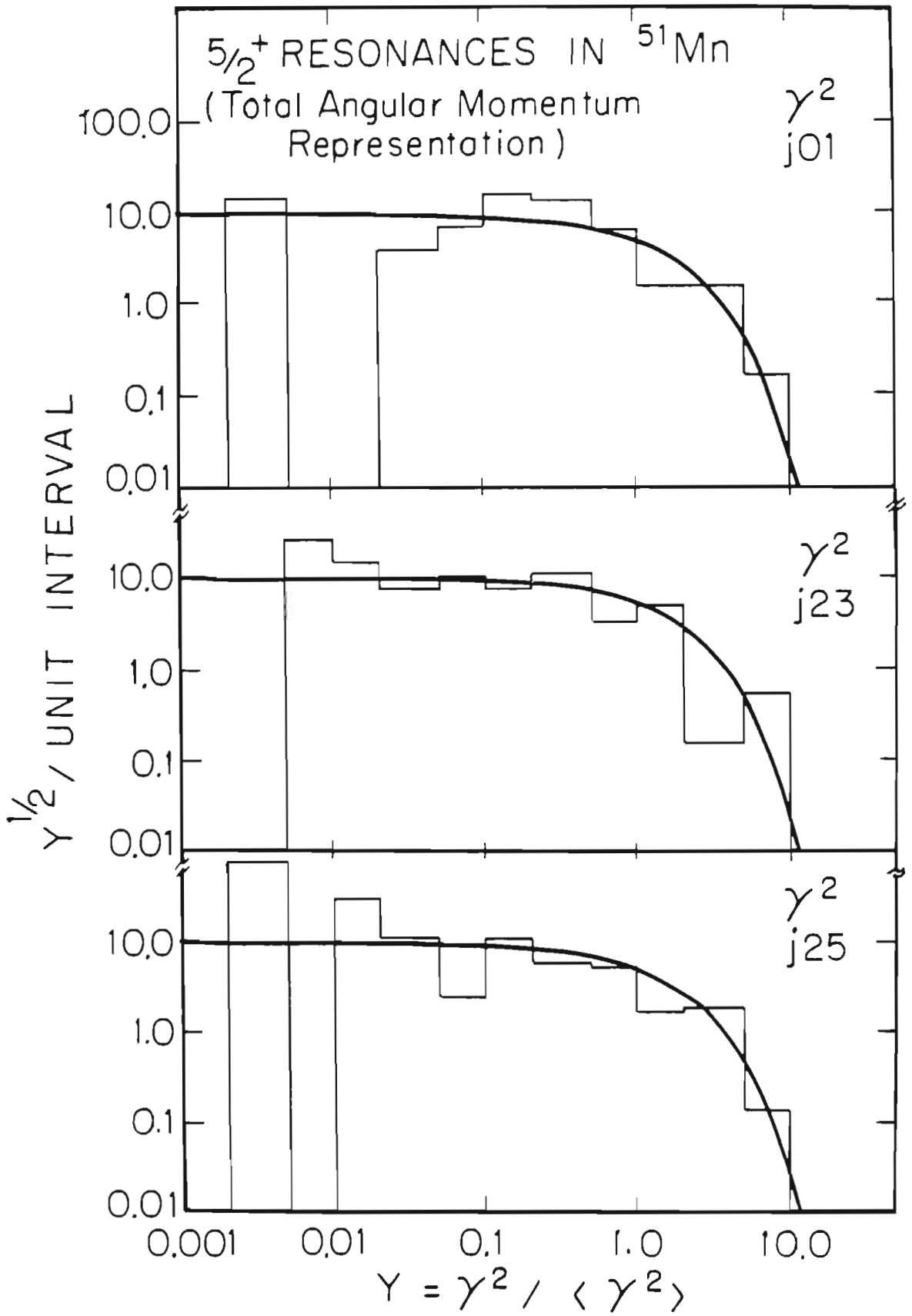
5/2+ RESONANCES IN 51Mn
(Total Angular Momentum Representation)
γ2 j01
γ2 j23
γ2 j25
100.0
10.0
1.0
0.1
0.01
0.001
0.01
0.1
1.0
10.0
γ1/2 / UNIT INTERVAL
Y = γ2 / ⟨γ2⟩

FIGURE 5.6 The distribution of reduced widths for the inelastic decay channels for $5/2^+$ resonances in ^{51}Mn in the channel spin representation. The solid line in all three cases is the normalized Porter–Thomas distribution.

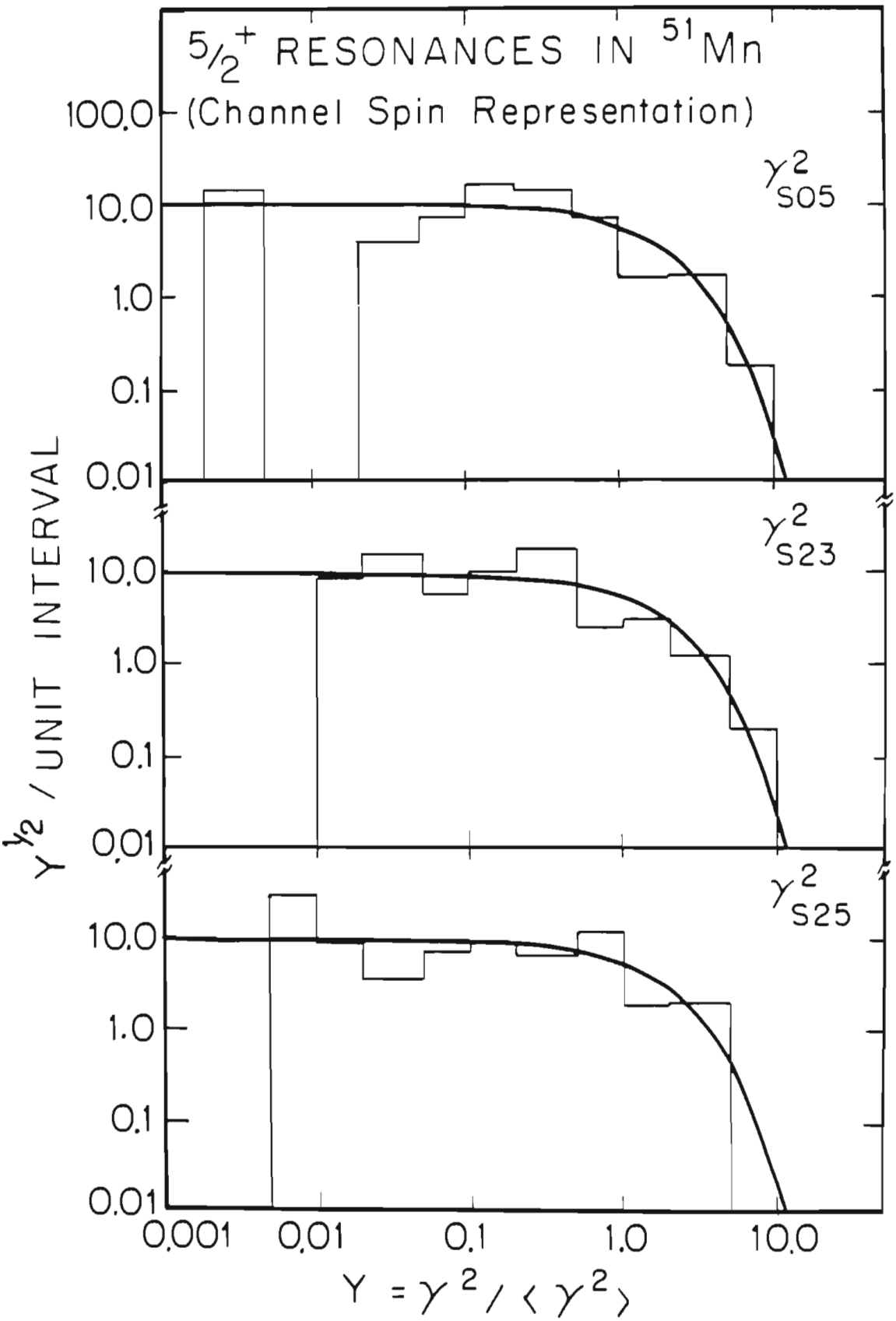
5/2+ RESONANCES IN 51Mn
(Channel Spin Representation)
γ^2_{S05}
γ^2_{S23}
γ^2_{S25}
100.0
10.0
1.0
0.1
0.01
0.001
$Y^{1/2}$ / UNIT INTERVAL
$Y = \gamma^2 / \langle \gamma^2 \rangle$

If the average reduced widths in the two channel case are equal, then $P(\delta)$ and $P(\phi)$ reduce to:

$$P(\delta) = \frac{C}{1 + \delta^2 + 2M'\delta} \quad \text{and} \quad P(\phi) = \frac{C}{1 + M' \sin 2\phi} \quad , \text{where} \tag{5.9}$$

$$M' = \frac{M_{12}}{M_{11}} = \frac{-\overline{\gamma_1\gamma_2}}{(\overline{\gamma_1^2}\ \overline{\gamma_2^2})^{1/2}} \quad , \text{and}$$

$$C = \frac{|M|^{1/2}}{\pi M_{11}} = \frac{(\overline{\gamma_1^2}\ \overline{\gamma_2^2} - (\overline{\gamma_1\gamma_2})^2)^{1/2}}{\pi(\overline{\gamma_1^2}\ \overline{\gamma_2^2})^{1/2}} \ .$$

If $\overline{\gamma_1\gamma_2} = 0$, that is, there is no channel correlation, then $P(\delta)$ reduces to a Cauchy distribution and $P(\phi)$ reduces to a uniform distribution. Figure 5.7 shows a comparison between the data histogram and the theoretical prediction from eqn. 5.9 for both representations. The theoretical values have been normalized to the data by multiplying by a factor of $N\pi/I$, where N is the total number of resonances and I is the number of bins in the histogram. The theoretical prediction follows the general trends of the data, but does not agree well.

The extreme statistical model predicts that there should be no correlations between decay channels and that the average value of each channel amplitude should be zero. If the experimental mixing ratios are normalized for equal average reduced widths and plotted as histograms, the extreme statistical model then predicts a uniform distribution. Figure 5.8 presents the data histogram for $3/2^-$ resonances in both representations. The dashed lines are the predicted distributions. Strong non-statistical effects are obvious in both representations. In the total angular momentum representation, only 8 resonances out of 30 have positive signs, and in the channel spin representation only 6 resonances out of 30 have negative signs.

FIGURE 5.7 Histograms of the number of resonances with a given mixing angle for $3/2^-$ resonances in ^{51}Mn in both representations. The solid curves are the Krieger–Porter predictions for each case. The experimental parameters used in these predictions (in keV) are $\langle\gamma^2_{j11}\rangle = 0.371$, $\langle\gamma^2_{j13}\rangle = 0.465$, $\langle\gamma_{j11}\gamma_{j13}\rangle = -0.062$, $\langle\gamma^2_{s13}\rangle = 0.396$, $\langle\gamma^2_{s15}\rangle = 0.440$, $\langle\gamma_{s13}\gamma_{s15}\rangle = 0.075$.

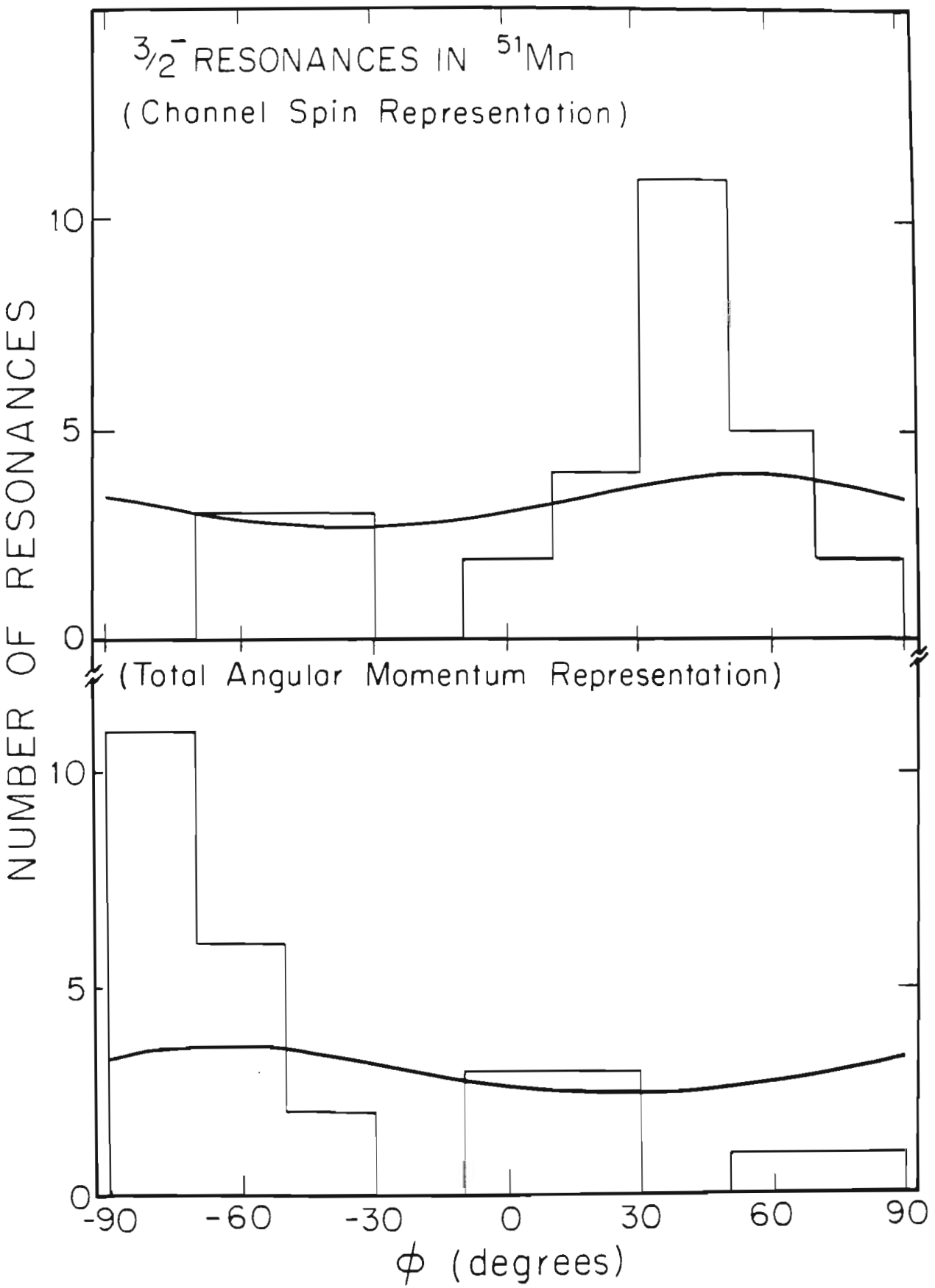
$3/2^-$ RESONANCES IN ^{51}Mn
(Channel Spin Representation)
(Total Angular Momentum Representation)
NUMBER OF RESONANCES
0
5
10
-90
-60
-30
0
30
60
90
ϕ (degrees)

FIGURE 5.8 Histograms of the number of resonances with a given mixing angle, normalized for equal average reduced widths, for $3/2^-$ resonances in ^{51}Mn in both representations. The dashed lines are the uniform distributions predicted assuming no channel-channel correlations.

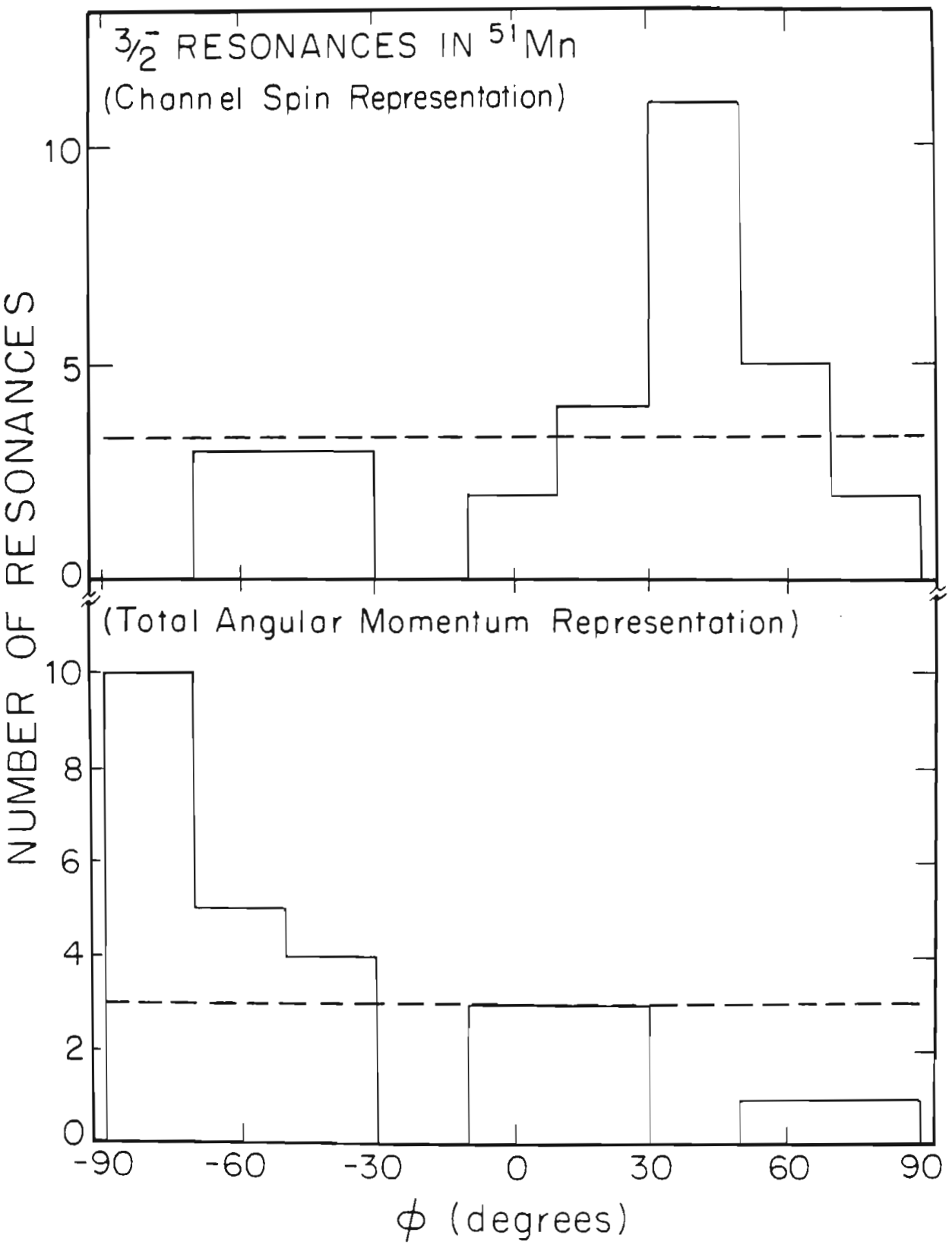
3/2⁻ RESONANCES IN 51Mn
(Channel Spin Representation)
(Total Angular Momentum Representation)
NUMBER OF RESONANCES
0
5
10
0
2
4
6
8
10
-90
-60
-30
0
30
60
90
φ (degrees)

In both representations the mixing ratios tend to cluster. Plots of the mixing angles versus energy, shown in figure 5.9 for both representations, demonstrate that the effect is not localized in energy.

As one test of the significance of the clustering effect, the Z-statistic of Wells (1978) is used. In this technique the data histogram and the extreme statistical model are compared through a statistic Z^2, defined as:

$$Z^2 = \sum_{i=1}^{N} (N_i - N_R/N_B)^2 \ , \qquad (5.10)$$

where N_i = the number of resonances for which the value of the mixing angle falls in the ith bin (bins are of equal width), N_R = the total number of resonances, and N_B = the number of bins. The procedure is as follows: a random number generator generates N_R random numbers ranging from -90^o to 90^o, then sorts these values into bins of a set size, and the corresponding Z^2 value is calculated. This procedure is repeated 100,000 times. The values of Z^2 obtained for each repetition are sorted into bins of width 1.0. The calculated values of Z from the data are Z= 9.00 in the total angular momentum representation, and Z= 9.38 in the channel spin representation. In the calculated distribution of Z for 30 $3/2^-$ resonances with 9 bins (each of width 20^o), there are 246 cases out of 100,000 in which $Z \geq 9.0$. Therefore, the probability for the observed data to be sampled from a uniform distribution is about 0.2%, and the level of significance of the deviation of the data from a uniform distribution is 99.8%.

2. d-wave Resonances

In the three channel case, there are two independent mixing ratios and two independent mixing angles. Chou (1980) derives the following equations

FIGURE 5.9 Plots of the mixing angle ϕ versus the energy of the incident proton for $3/2^-$ resonances in ^{51}Mn in both representations.

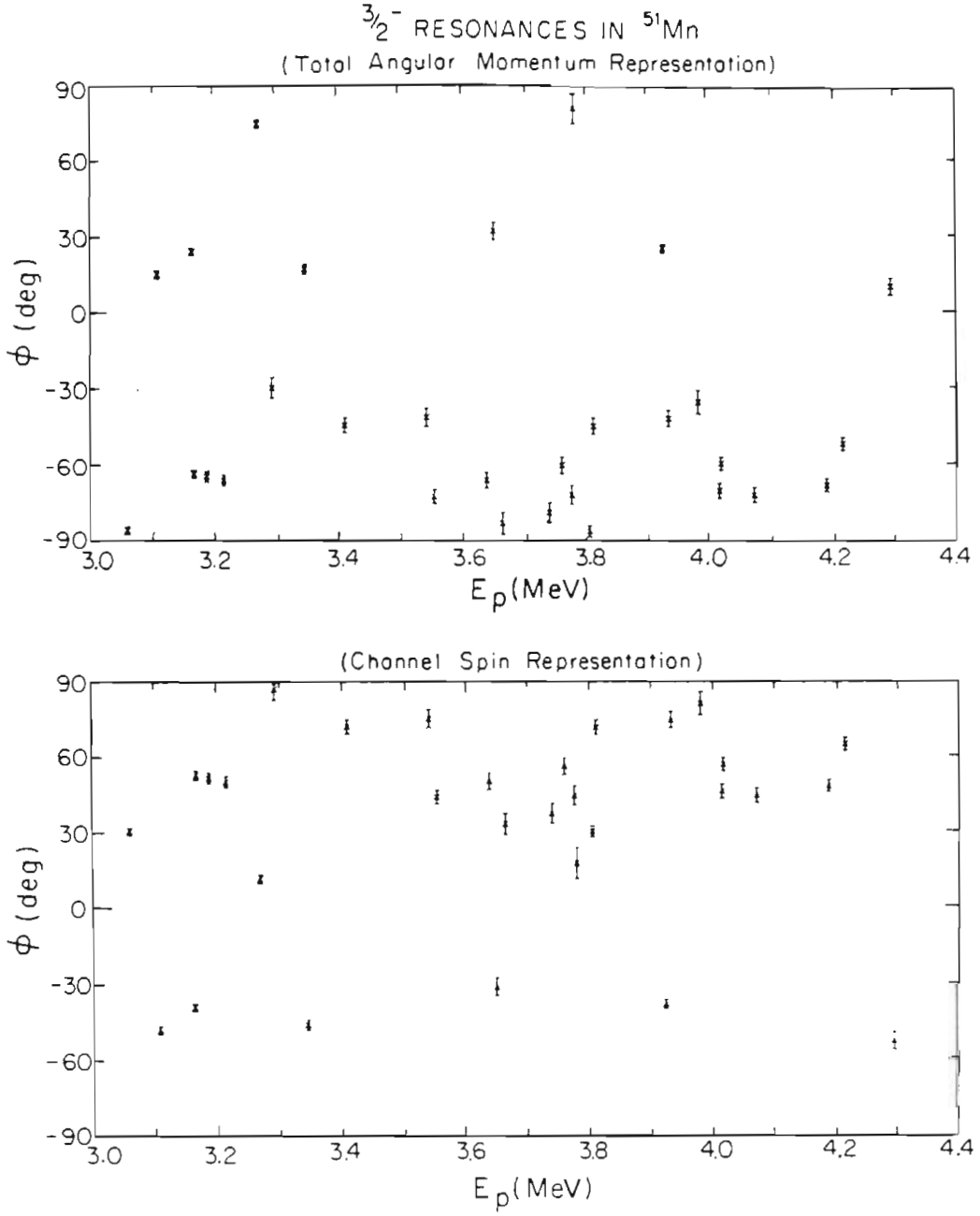
3/2⁻ RESONANCES IN 51Mn
(Total Angular Momentum Representation)
90
60
30
0
-30
-60
-90
φ (deg)
3.0
3.2
3.4
3.6
3.8
4.0
4.2
4.4
Ep (MeV)
(Channel Spin Representation)
90
60
30
0
-30
-60
-90
φ (deg)
3.0
3.2
3.4
3.6
3.8
4.0
4.2
4.4
Ep (MeV)

for the probability distribution functions:

$$P(\delta_1,\delta_2) = \frac{|M|^{1/2}}{2\pi} \frac{1}{(M_{11}\delta_1^2 + M_{22}\delta_2^2 + M_{33} + 2M_{12}\delta_1\delta_2 + 2M_{23}\delta_2 + 2M_{13}\delta_1)^{3/2}}, \tag{5.11}$$

$$P(\phi_1,\phi_2) = \frac{|M|^{1/2}}{2\pi} \cdot \frac{\sec^2\phi_1 \sec^2\phi_2}{(M_{11}\tan^2\phi_1 + M_{22}\tan^2\phi_2 + M_{33} + 2M_{12}\tan\phi_1\tan\phi_2 + 2M_{23}\tan\phi_2 + 2M_{13}\tan\phi_1)^{3/2}}, \tag{5.12}$$

where:

$$|M| = [\overline{\gamma_1^2}\,\overline{\gamma_2^2}\,\overline{\gamma_3^2} + 2\overline{\gamma_1\gamma_2}\,\overline{\gamma_2\gamma_3}\,\overline{\gamma_1\gamma_3} - \overline{\gamma_2^2}(\overline{\gamma_1\gamma_3})^2 - \overline{\gamma_3^2}(\overline{\gamma_1\gamma_2})^2 - \overline{\gamma_1^2}(\overline{\gamma_2\gamma_3})^2]^{-1},$$

$$M_{11} = |M|(\overline{\gamma_2^2}\,\overline{\gamma_3^2} - (\overline{\gamma_2\gamma_3})^2), \qquad M_{22} = |M|(\overline{\gamma_1^2}\,\overline{\gamma_3^2} - (\overline{\gamma_1\gamma_3})^2),$$

$$M_{33} = |M|(\overline{\gamma_1^2}\,\overline{\gamma_2^2} - (\overline{\gamma_1\gamma_2})^2), \qquad M_{12} = |M|(\overline{\gamma_1\gamma_3}\,\overline{\gamma_2\gamma_3} - \overline{\gamma_1\gamma_2}\,\overline{\gamma_3^2}),$$

$$M_{23} = |M|(\overline{\gamma_1\gamma_2}\,\overline{\gamma_1\gamma_3} - \overline{\gamma_2\gamma_3}\,\overline{\gamma_1^2}), \qquad M_{13} = |M|(\overline{\gamma_1\gamma_2}\,\overline{\gamma_2\gamma_3} - \overline{\gamma_1\gamma_3}\,\overline{\gamma_2^2}).$$

The distribution function for either mixing ratio or mixing angle can be found by integrating out the other. The single mixing ratio probability distribution functions reduce to the two channel case. Chou (1980) also points out that for the special case where $\overline{\gamma_1^2} = \overline{\gamma_2^2} = \overline{\gamma_3^2}$, and if $M_{12} = M_{23} = M_{13} = 0$ (no channel correlations), then eqns. 5.11 and 5.12 reduce to:

$$P(\delta_1,\delta_2) = \frac{|M|^{1/2}}{2\pi} \frac{1}{(1 + \delta_1^2 + \delta_2^2)^{3/2}(M_{11})^{3/2}}, \text{ and} \tag{5.13}$$

$$P(\phi_1,\phi_2) = \frac{|M|^{1/2}}{2\pi} \frac{\sec^2\phi_1 \sec^2\phi_2}{(1 + \tan^2\phi_1 + \tan^2\phi_2)^{3/2}(M_{11})^{3/2}}. \tag{5.14}$$

Figures 5.10 and 5.11 present plots of the data histogram and the theoretical predictions (two channel case) for the total angular momentum representation and the channel spin representation, respectively. Again, the theoretical values have been normalized to the data. For the highly correlated channels ϕ_{jCB}, ϕ_{sBA}, ϕ_{sCA}, and ϕ_{sCB} the theory and data agree quite well. Even in the other two channels the general trends of the data are reproduced by the theory. The mixing ratio distributions seem to follow the Krieger-Porter reduced width amplitude distribution.

Histograms of the measured mixing angles for $5/2^+$ resonances normalized to correct for unequal average reduced widths are shown in figure 5.12 for the total angular momentum representation and in figure 5.13 for the channel spin representation. The dashed lines are the predicted uniform distributions. Strong non-statistical effects are observed in the plots of ϕ_{jBA}, ϕ_{jCB}, and all three mixing angles in the channel spin representation. The clustering effect is also obvious. In plots of the mixing angles versus energy, shown in figure 5.14 for the total angular momentum representation and in figure 5.15 for the channel spin representation, it is clear that the clustering effect is not localized in energy.

The Z-statistic was also calculated for $5/2^+$ resonances. In the total angular momentum representation, $Z= 10.75$ for ϕ_{jBA}, $Z= 11.30$ for ϕ_{jCA}, and $Z= 8.81$ for ϕ_{jCB}. In the channel spin representation, $Z= 9.47$ for ϕ_{sBA}, $Z= 9.57$ for ϕ_{sCA}, and $Z= 7.05$ for ϕ_{sCB}. In the generated distribution of Z for 38 $5/2^+$ resonances with 12 bins (each of width 15°), there are 15,945 cases out of 100,000 with $Z \geq 7$, 3921 cases with $Z \geq 8$, 887 cases with $Z \geq 9$, 124 cases with $Z \geq 10$, and 19 cases with $Z \geq 11$. Therefore, the probability for the observed data to be sampled from a uniform distribution is about 16% for ϕ_{sCB}, 4% for ϕ_{jCB}, 0.9% for ϕ_{sBA} and ϕ_{sCA}, and less than 0.2% for ϕ_{jBA} and ϕ_{jCA}.

FIGURE 5.10 Histograms of the number of resonances with a given mixing angle for $5/2^+$ resonances in ^{51}Mn in the total angular momentum representation. $\phi_{BA} = \tan^{-1}(\gamma_{j23}/\gamma_{j01})$, $\phi_{CA} = \tan^{-1}(\gamma_{j25}/\gamma_{j01})$, $\phi_{CB} = \tan^{-1}(\gamma_{j25}/\gamma_{j23})$. Only two of these three variables are independent. The solid curves are the Krieger-Porter predictions for each case. The experimental parameters used in these predictions (in keV) are $\langle\gamma^2_{j01}\rangle = 0.513$, $\langle\gamma^2_{j23}\rangle = 0.264$, $\langle\gamma^2_{j25}\rangle = 0.917$, $\langle\gamma_{j01}\gamma_{j23}\rangle = -0.029$, $\langle\gamma_{j01}\gamma_{j25}\rangle = 0.470$, $\langle\gamma_{j23}\gamma_{j25}\rangle = -0.033$.

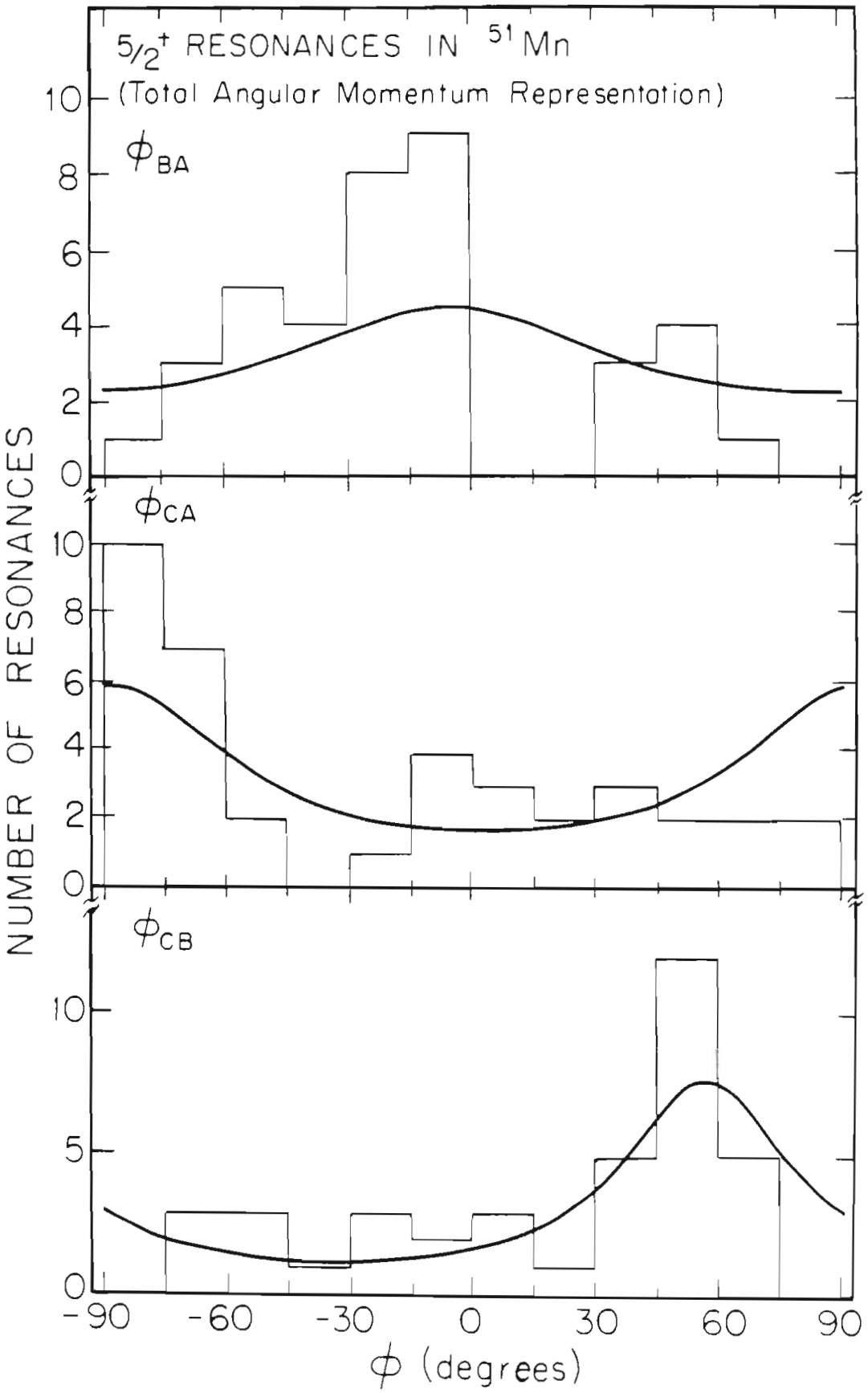
5/2+ RESONANCES IN 51Mn
(Total Angular Momentum Representation)
φBA
φCA
φCB
NUMBER OF RESONANCES
φ (degrees)
-90
-60
-30
0
30
60
90

FIGURE 5.11 Histograms of the number of resonances with a given mixing angle for $5/2^+$ resonances in ^{51}Mn in the channel spin representation. $\phi_{BA} = \tan^{-1}(\gamma_{s23}/\gamma_{s05})$, $\phi_{CA} = \tan^{-1}(\gamma_{s25}/\gamma_{s05})$, $\phi_{CB} = \tan^{-1}(\gamma_{s25}/\gamma_{s23})$. Only two of these three variables are independent. The solid curves are the Krieger-Porter predictions for each case. The experimental parameters used in these predictions (in keV) are $\langle\gamma^2_{s05}\rangle = 0.513$, $\langle\gamma^2_{s23}\rangle = 0.650$, $\langle\gamma^2_{s25}\rangle = 0.513$, $\langle\gamma_{s05}\gamma_{s23}\rangle = 0.359$, $\langle\gamma_{s05}\gamma_{s25}\rangle = 0.305$, $\langle\gamma_{s23}\gamma_{s25}\rangle = 0.323$.

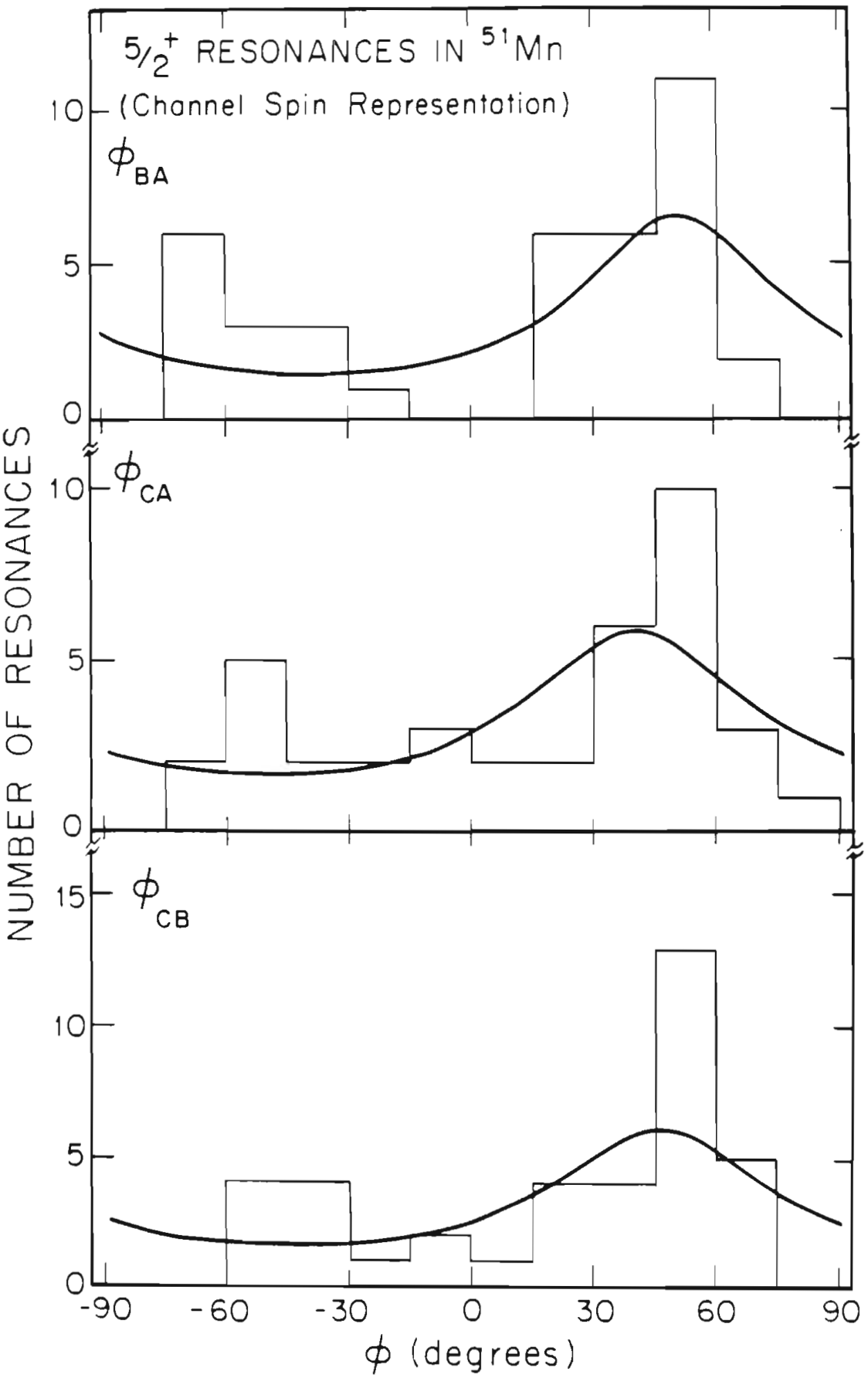
5/2+ RESONANCES IN 51Mn
(Channel Spin Representation)
φBA
φCA
φCB
NUMBER OF RESONANCES
0
5
10
15
-90
-60
-30
0
30
60
90
φ (degrees)

FIGURE 5.12 Histograms of the number of resonances with a given mixing angle, normalized for equal average reduced widths, for $5/2^+$ resonances in ^{51}Mn in the channel spin representation. The dashed lines are the uniform distributions predicted assuming no channel-channel correlations.

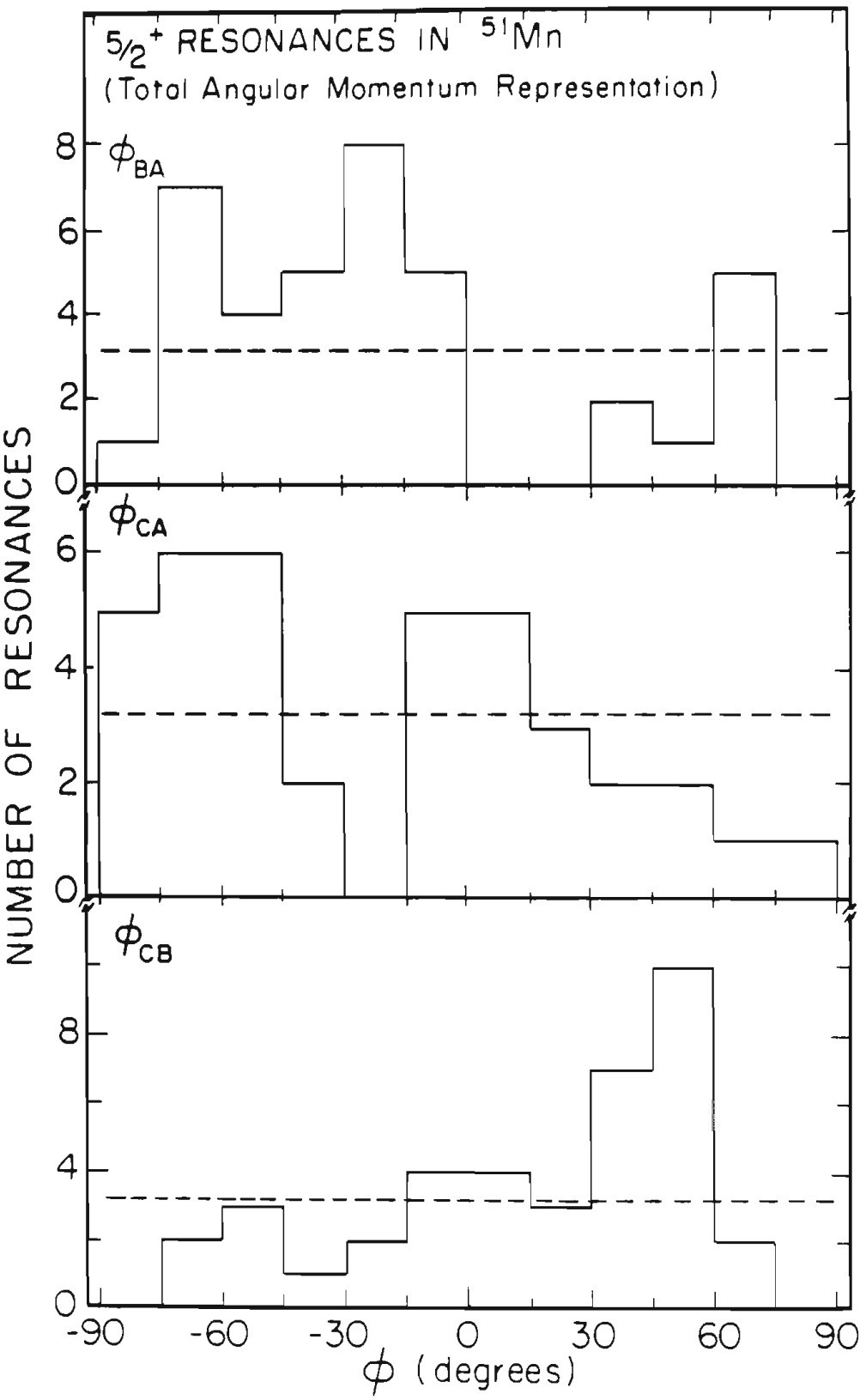
5/2+ RESONANCES IN 51Mn
(Total Angular Momentum Representation)
φBA
φCA
φCB
NUMBER OF RESONANCES
0
2
4
6
8
-90
-60
-30
0
30
60
90
φ (degrees)

FIGURE 5.13 Histograms of the number of resonances with a given mixing angle, normalized for equal average reduced widths, for $5/2^+$ resonances in ^{51}Mn in the total angular momentum representation. The dashed lines are the uniform distributions predicted assuming no channel-channel correlations.

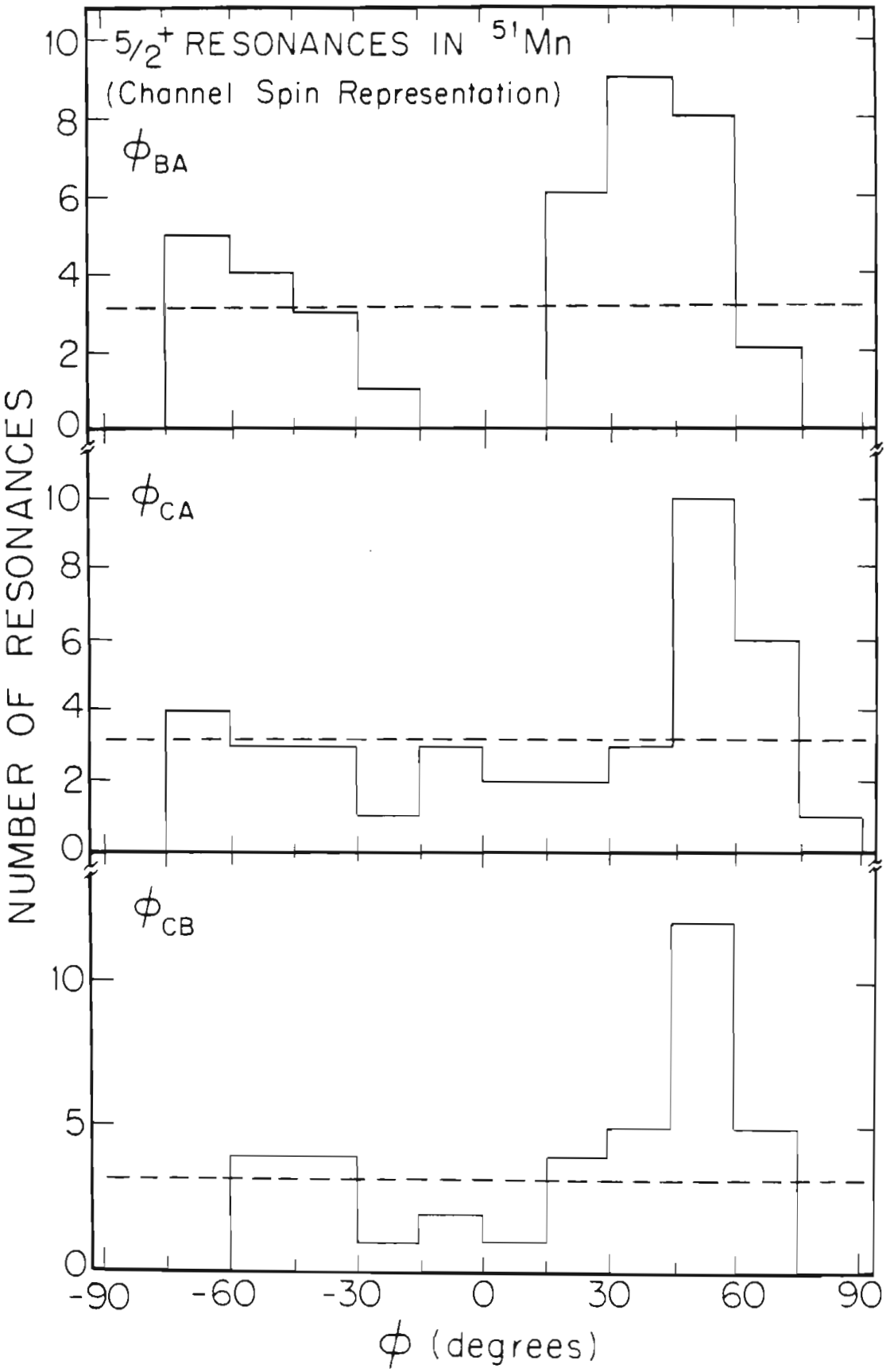
5/2+ RESONANCES IN 51Mn
(Channel Spin Representation)
φBA
φCA
φCB
NUMBER OF RESONANCES
φ (degrees)
-90
-60
-30
0
30
60
90

FIGURE 5.14 Plots of the mixing angles versus the energy of the incident proton for $5/2^+$ resonances in ^{51}Mn in the total angular momentum representation.

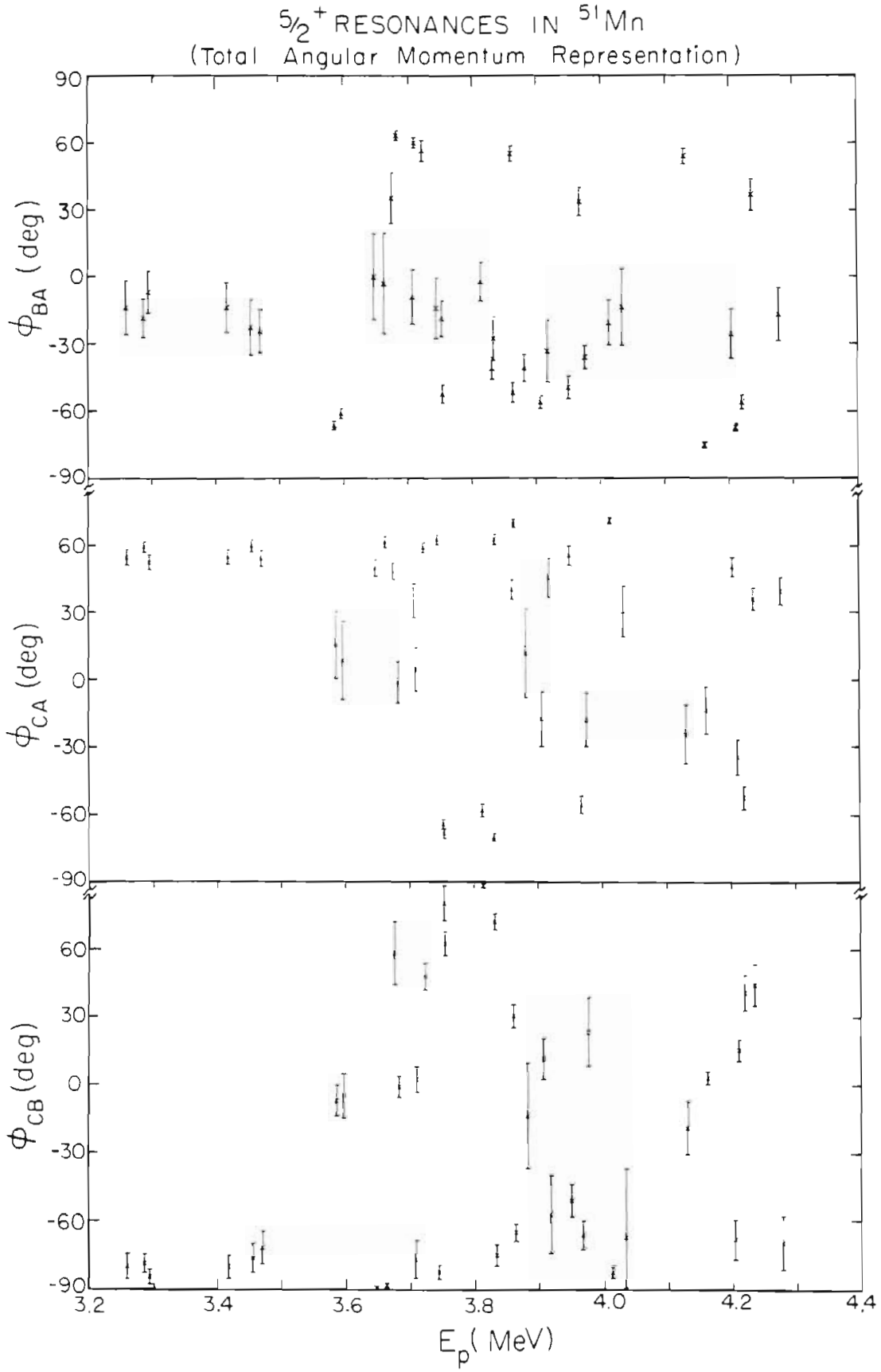
5/2+ RESONANCES IN 51Mn
(Total Angular Momentum Representation)
φBA (deg)
φCA (deg)
φCB (deg)
90
60
30
0
-30
-60
-90
3.2
3.4
3.6
3.8
4.0
4.2
4.4
Ep (MeV)

FIGURE 5.15 Plots of the mixing angles versus the energy of the incident proton for $5/2^+$ resonances in ^{51}Mn in the channel spin representation.

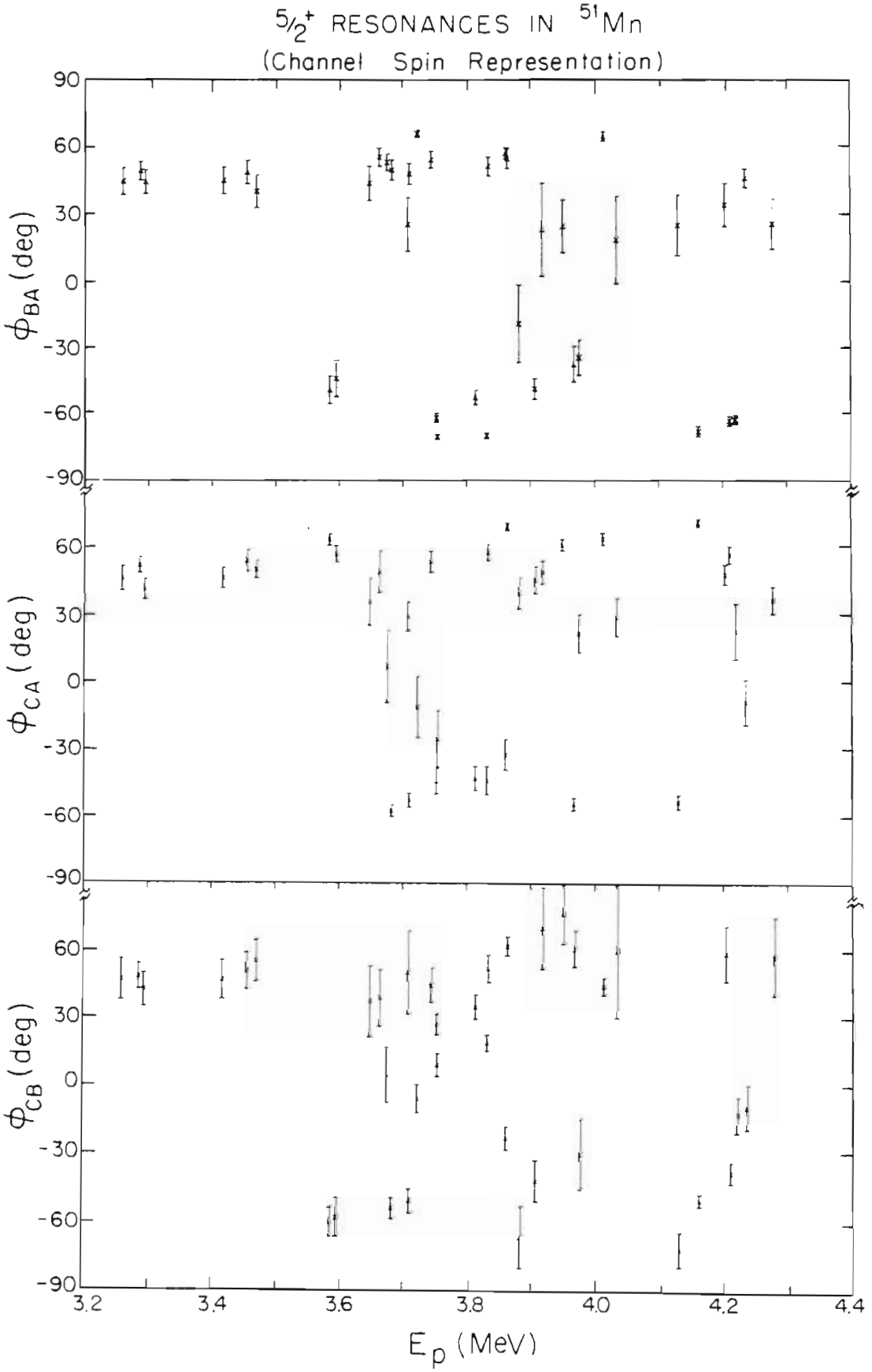
5/2+ RESONANCES IN 51Mn
(Channel Spin Representation)
φBA (deg)
φCA (deg)
φCB (deg)
90
60
30
0
-30
-60
-90
3.2
3.4
3.6
3.8
4.0
4.2
4.4
Ep (MeV)

The level of significance of the deviation of the data from a uniform distribution is about 84% for ϕ_{sCB}, 96% for ϕ_{jCB}, 99.1% for ϕ_{sBA} and ϕ_{sCA}, and greater than 99.8% for ϕ_{jBA} and ϕ_{jCA}.

E. Linear Correlation Coefficients

The linear correlation coefficient is a convenient measure of the relationship between two sets of variables x_i and y_i. If r is equal to $\pm$ 1, then x and y are completely correlated, and y = ax + b. If x and y are independent, then r is equal to 0. The linear correlation coefficient is defined as:

$$r(x,y) = \frac{\sum_{i=1}^{N} (x_i-\overline{x_i})\ (y_i-\overline{y_i})}{[\sum_{i=1}^{N} (x_i-\overline{x_i})^2 \sum_{i=1}^{N} (y_i-\overline{y_i})^2]^{1/2}} \quad . \tag{5.15}$$

The significance of the correlation between x and y is dependent upon N and upon the parent distributions. Baudinet-Robinet (1974) developed a distribution free test on the significance of the correlation indicated by r which is closely approximated by a Student's t distribution with N-2 degrees of freedom. The independence of x and y is therefore rejected on a significance level α, where

$$P(|t| > t_o) = \alpha \quad \text{and} \quad t_o = \left[\frac{(N-2)r^2}{1-r^2}\right]^{1/2} \quad . \tag{5.16}$$

The confidence interval for r is given by $P \simeq 1 - 2\alpha$.

1. p-wave Resonances

Values of the linear correlation coefficients calculated from the data for $3/2^-$ resonances for all channels with eqns. 5.2 and 5.3 are listed as the superdiagonal terms in table 5.3 for the total angular momentum representation

TABLE 5.3

LINEAR CORRELATION COEFFICIENTS BETWEEN REDUCED WIDTHS

FOR $3/2^-$ RESONANCES IN ^{51}Mn

Total Angular Momentum Representation

	γ_p^2	$\gamma_{p'}^2$	γ_{j11}^2	γ_{j13}^2
γ_p^2	1	−0.127	−0.143	−0.024
$\gamma_{p'}^2$	50%	1	0.815	0.620
γ_{j11}^2	55%	>99.9%	1	0.051
γ_{j13}^2	10%	>99.9%	21%	1

The amplitude correlation is $\rho(\gamma_{j11},\gamma_{j13}) = -0.150$. The significance level of the amplitude correlation is 57%.

and in table 5.4 for the channel spin representation. The subdiagonal terms in each table are the corresponding significance levels. Non-statistical effects are indicated by significant correlations between channels. For the $3/2^-$ resonances, the linear correlation coefficients are small, and the significance levels are low. The data indicate that there are no strong correlations for $3/2^-$ resonances, despite the non-statistical behavior observed in figures 5.7 and 5.8. In agreement with eqn. 5.4, the reduced width correlation coefficient is approximately equal to the square of the reduced width amplitude correlation coefficient.

2. d-wave Resonances

Values of the linear correlation coefficients calculated from the data for $5/2^+$ resonances with eqns. 5.2 and 5.3 are listed as the superdiagonal terms in table 5.5 for the total angular momentum representation in table 5.6 for the channel spin representation. The subdiagonal terms in each table are the corresponding significance levels. The occurrence of non-statistical effects is indicated by the significant correlations between channels. For the $5/2^+$ resonances, the linear correlation coefficients are large and the significance levels are quite high, especially in the channel spin representation. The reduced width correlation coefficients are not equal to the squares of the reduced width amplitude correlation coefficients for $5/2^+$ resonances, as is evident from tables 5.5 and 5.6.

TABLE 5.4

LINEAR CORRELATION COEFFICIENTS BETWEEN REDUCED WIDTHS FOR $3/2^-$ RESONANCES IN ^{51}Mn

Channel Spin Representation

	γ_p^2	$\gamma_{p'}^2$	γ_{s13}^2	γ_{s15}^2
γ_p^2	1	-0.127	-0.068	-0.122
$\gamma_{p'}^2$	50%	1	0.722	0.805
γ_{j11}^2	28%	>99.9%	1	0.171
γ_{j13}^2	48%	>99.9%	63%	1

The amplitude correlation is $\rho(\gamma_{s13},\gamma_{s15}) = 0.179$. The significance level of the amplitude correlation is 66%.

TABLE 5.5

LINEAR CORRELATION COEFFICIENTS BETWEEN REDUCED WIDTHS FOR $5/2^+$ RESONANCES IN ^{51}Mn

Total Angular Momentum Representation

	γ_p^2	$\gamma_{p'}^2$	γ_{j01}^2	γ_{j23}^2	γ_{j25}^2
γ_p^2	1	0.671	0.724	0.195	0.617
$\gamma_{p'}^2$	>99.9%	1	0.968	0.388	0.948
γ_{j01}^2	>99.9%	>99.9%	1	0.367	0.886
γ_{j23}^2	76%	98.3%	97.5%	1	0.102
γ_{j25}^2	>99.9%	>99.9%	>99.9%	46%	1

The amplitude correlations are $\rho(\gamma_{j01},\gamma_{j23}) = -0.078$, (significance level = 36%), $\rho(\gamma_{j01},\gamma_{j25}) = 0.686$, (significance level = >99.9%), and $\rho(\gamma_{j23},\gamma_{j25}) = -0.068$, (significance level = 31%).

TABLE 5.6

LINEAR CORRELATION COEFFICIENTS BETWEEN REDUCED WIDTHS FOR $5/2^+$ RESONANCES IN ^{51}Mn

Channel Spin Representation

	γ_p^2	$\gamma_{p'}^2$	γ_{s05}^2	γ_{s23}^2	γ_{s25}^2
γ_p^2	1	0.671	0.724	0.595	0.399
$\gamma_{p'}^2$	>99.9%	1	0.968	0.915	0.667
γ_{s05}^2	>99.9%	>99.9%	1	0.899	0.556
γ_{s23}^2	>99.9%	>99.9%	>99.9%	1	0.330
γ_{s25}^2	98.6%	>99.9%	>99.9%	98.2%	1

The amplitude correlations are $\rho(\gamma_{s05},\gamma_{s23}) = 0.622$, (significance level = >99.9%), $\rho(\gamma_{s05},\gamma_{s25}) = 0.585$, (significance level = >99.9%), and $\rho(\gamma_{s23},\gamma_{s25}) = 0.550$, (significance level = >99.9%).

CHAPTER VI

CONCLUSIONS

Detailed angular distribution measurements on the inelastically scattered proton and de-excitation γ-ray in the $^{50}Cr(p,p'\gamma)$ reaction were performed for 107 resonances in ^{51}Mn with a variety of J^{π} values, ranging from $1/2^-$ to $9/2^+$. The f-wave analog state fragments at $E_p = 3.3149$ MeV and $E_p = 3.3323$ MeV were analyzed and discussed.

Mixing ratios for the inelastic decay amplitudes were uniquely determined for all resonances except those assigned $1/2^-$ and $3/2^+$. For $1/2^-$ resonances, there is only one open decay channel. For $3/2^+$ resonances, two solutions for the mixing ratio were found for each resonance.

General angular distribution theory was briefly discussed. The angular distribution equations needed for $\ell = 1$, 2, 3, and 4 resonances were presented in both the total angular momentum representation and in the channel spin representation. Transformations between these two representations were given for the mixing angles.

The general statistical theory of fluctuations and the random matrix hypothesis as applied to reduced width distributions were outlined. Mixing ratio distributions including channel-channel correlations were stated. Statistical studies were performed on the set of $3/2^-$ resonances and on the set of $5/2^+$ resonances.

The data show that the reduced width distributions follow a Porter-Thomas distribution, consistent with the expected reduced width amplitude distribution -- Gaussian with zero mean. Since $\overline{\gamma\gamma'} \neq 0$ for the $5/2^+$ resonances, large correlations between channels exist. Such correlations violate the extreme statistical model. Channel-channel correlations are included in the Krieger-Porter formulation: the experimental mixing ratio distributions are consistent with the Krieger-Porter amplitude distribution. The physical origin of the correlations has not yet been explained. To date, correlations have been observed in every case measured by the high resolution group at the Triangle Universities Nuclear Laboratory. However, all of these measurements have been performed in the A = 40-56 mass region and with protons of energies between 1 and 4.5 MeV. More experimental information is essential to determine whether these correlation effects are of a general nature or an anomaly confined to a narrow mass-energy region.

APPENDIX

FIGURE A.1 Differential cross section of proton elastic and inelastic scattering on ^{50}Cr from E_p = 3.240 MeV to E_p = 3.440 MeV. These data are reproduced from Salzmann (1975) and Salzmann et al. (1977).

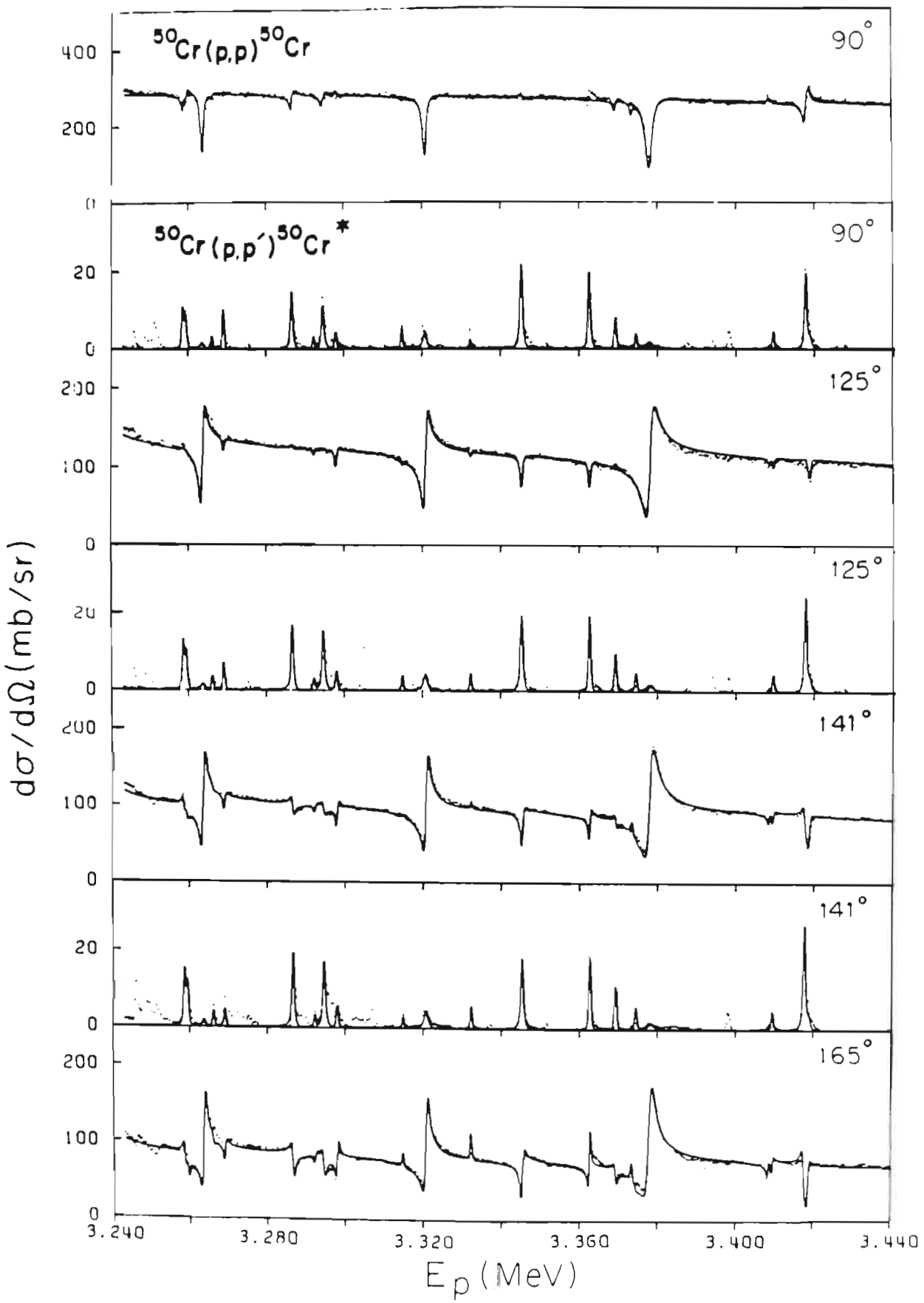
$^{50}Cr(p,p)^{50}Cr$
90°
$^{50}Cr(p,p')^{50}Cr^*$
90°
125°
125°
141°
141°
165°
400
200
0
20
200
100
0
20
0
200
100
0
20
0
200
100
0
3.240
3.280
3.320
3.360
3.400
3.440
E_p (MeV)
$d\sigma/d\Omega$ (mb/sr)

FIGURE A.2 Differential cross section of proton elastic and inelastic scattering on ^{50}Cr from E_p = 3.440 MeV to E_p = 3.640 MeV. These data are reproduced from Salzmann (1975) and Salzmann et al. (1977).

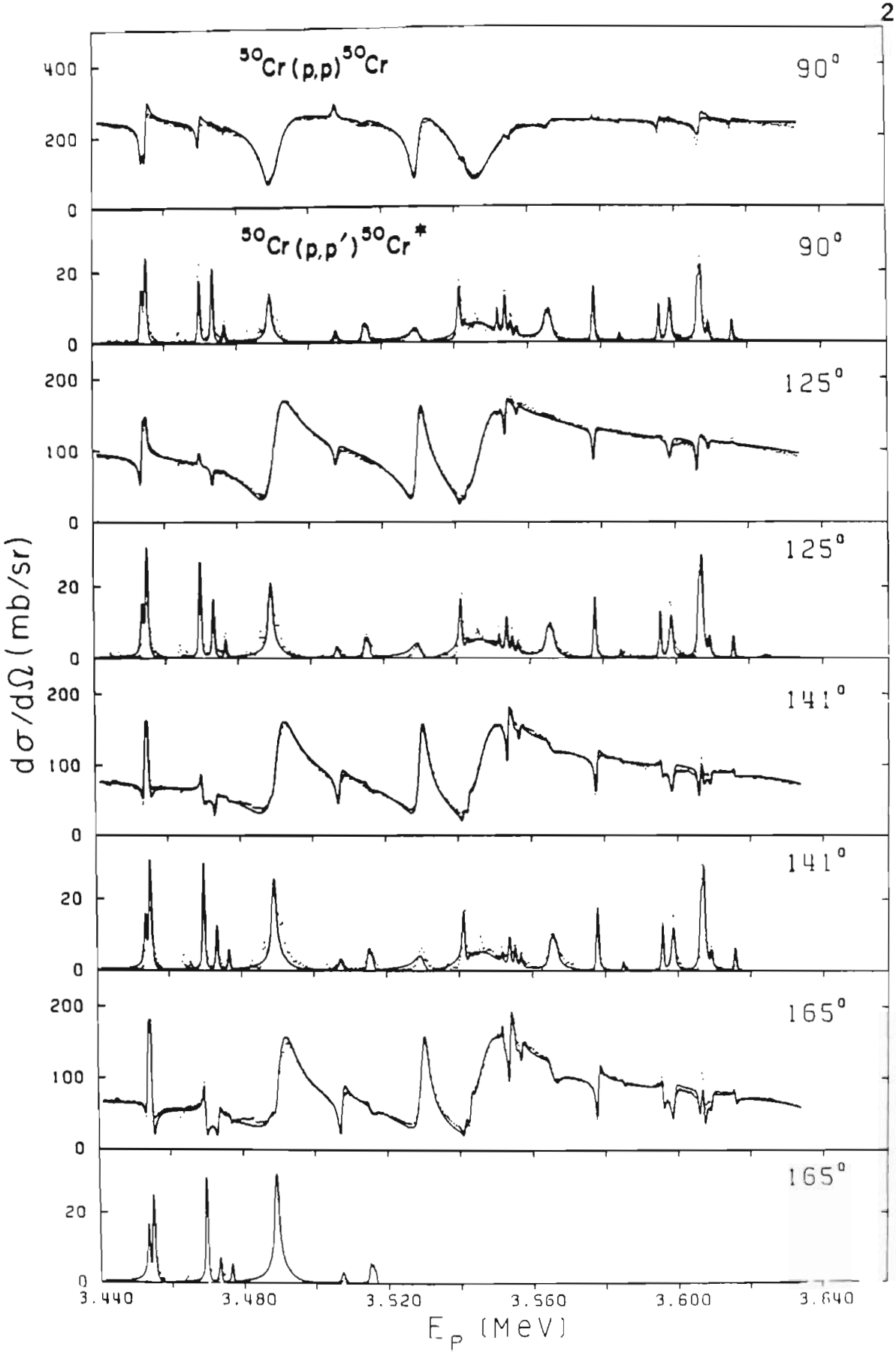
$^{50}Cr(p,p)^{50}Cr$
90°
$^{50}Cr(p,p')^{50}Cr^*$
90°
125°
125°
141°
141°
165°
165°
400
200
0
20
100
3.440
3.480
3.520
3.560
3.600
3.640
$d\sigma/d\Omega$ (mb/sr)
E_p (MeV)

FIGURE A.3 Differential cross section of proton elastic and inelastic scattering on ^{50}Cr from E_p = 3.620 MeV to E_p = 3.820 MeV. These data are reproduced from Salzmann (1975) and Salzmann et al. (1977).

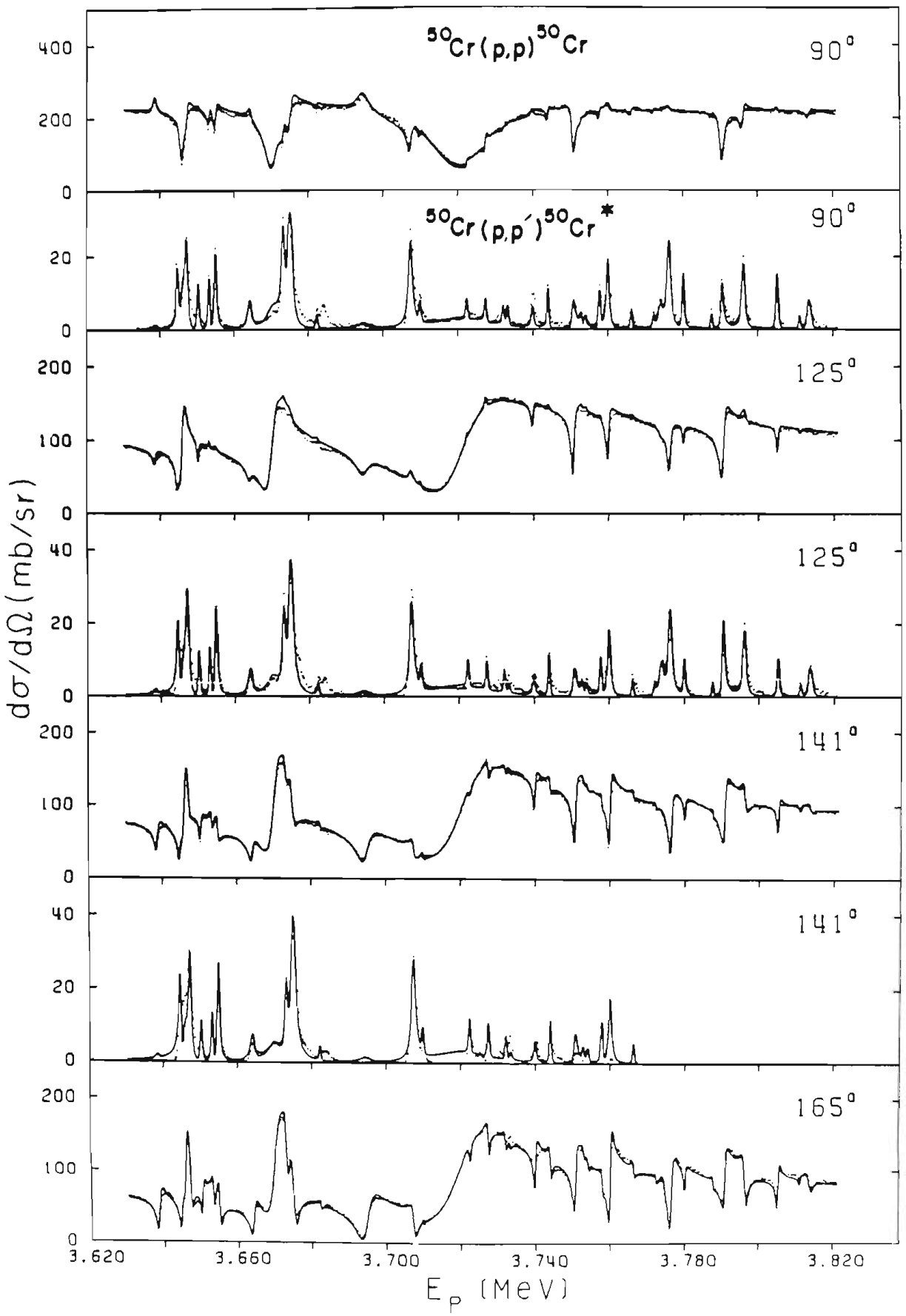
$^{50}Cr(p,p)^{50}Cr$
90°
$^{50}Cr(p,p')^{50}Cr^*$
90°
125°
125°
141°
141°
165°
400
200
0
20
0
200
100
0
40
20
0
200
100
0
40
20
0
200
100
0
dσ/dΩ (mb/sr)
3.620
3.660
3.700
3.740
3.780
3.820
E_p (MeV)

FIGURE A.4 Differential cross section of proton elastic and inelastic scattering on ^{50}Cr from E_p = 3.820 MeV to E_p = 4.040 MeV. These data are reproduced from Salzmann (1975) and Salzmann et al. (1977).

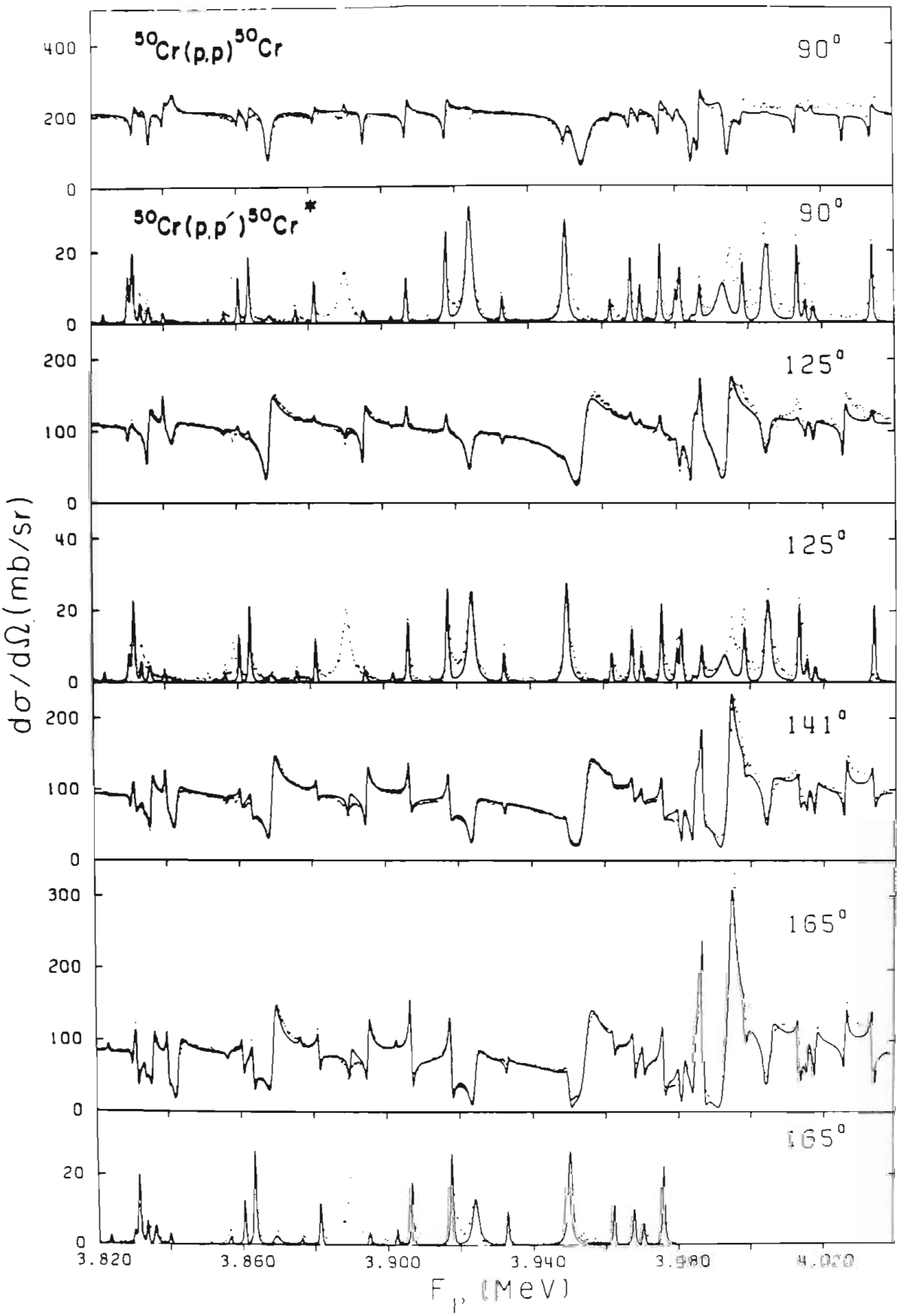
$^{50}Cr(p,p)^{50}Cr$
90°
$^{50}Cr(p,p')^{50}Cr^{*}$
90°
125°
125°
141°
165°
165°
400
200
0
20
0
200
100
0
40
20
0
200
100
0
300
200
100
0
20
0
3.820
3.860
3.900
3.940
3.980
4.020
E_p (MeV)
$d\sigma/d\Omega$ (mb/sr)

FIGURE A.5 Differential cross section of proton elastic and inelastic scattering on ^{50}Cr from E_p = 4.040 MeV to E_p = 4.400 MeV. These data are reproduced from Salzmann (1975) and Salzmann et al. (1977).

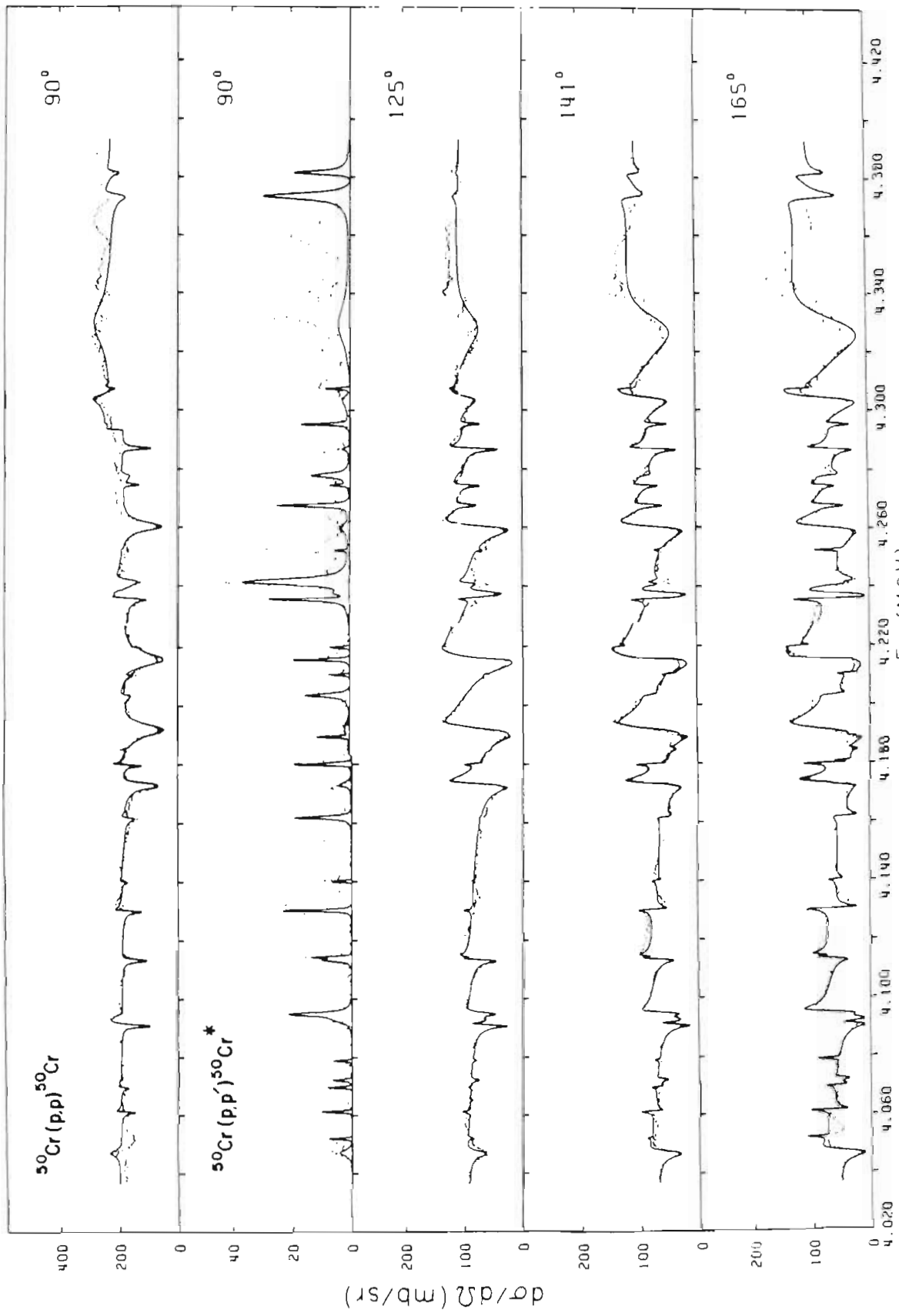
90°
90°
125°
141°
165°
$^{50}Cr(p,p)^{50}Cr$
$^{50}Cr(p,p')^{50}Cr^{*}$
dσ/dΩ (mb/sr)
E_p (MeV)

TABLE A.1

RESONANCES PARAMETERS FOR RESONANCES IN ^{51}Mn

Res. No.	E_p (MeV)	J^π	Γ_p (eV)	γ_p^2 (keV)	$\Gamma_{p'}$ (eV)	$\gamma_{p'}^2$ (keV)
M1	3.0594	$3/2^{-*}$	1700*	10.66*	10*	0.39*
M2	3.0689	$(3/2^-)$	200	1.24		
M3	3.1075	$3/2^{-*}$	25*	0.14*	35*	1.23*
M4	3.1125	$1/2^-$	75	0.43	37*	1.31*
M5	3.1634	$3/2^{-*}$	25*	0.13*	90*	2.72*
M6	3.1668	$3/2^{-*}$	700*	3.65*	27*	0.81*
M7	3.1872	$3/2^{-*}$	1625*	8.20*	9*	0.26*
M8	3.2148	$3/2^{-*}$	125*	0.60*	17*	0.44*
1A	3.2461	$9/2^+$	12*	16.15*	80*	78.82*
1	3.2587	$7/2^{+*}$	33*	43.04*	191*	464.01*
2	3.2594	$5/2^+$	40	0.66	29*	0.78*
3	3.2637	$1/2^+$	650	1.54	25	2.66
4	3.2662	$(5/2^+)$	10	0.16	40	
4A	3.2664	$(9/2^+)$	this resonance was not observed			
5	3.2691	$3/2^-$	50	0.22	53*	1.20*
6	3.2867	$5/2^+$	70	1.10	77*	2.32*
7	3.2923	$3/2^{-*}$	25*	0.11*	5*	0.10*
8	3.2946	$5/2^+$	60	0.93	191*	4.27*
9	3.2980	$1/2^{-*}$	200*	0.84*	16*	0.33*
10	3.3149	$5/2^-$	15	1.50	14*	2.58*
11	3.3208	$1/2^+$	800	1.76	80	7.20

TABLE A.1 (continued)

Res. No.	E_p (MeV)	J^π	Γ_p (eV)	γ_p^2 (keV)	$\Gamma_{p'}$ (eV)	$\gamma_{p'}^2$ (keV)
12	3.3323	$5/2^-$	20	1.93	10	1.07*
13	3.3454	$3/2^-$	200	0.79	42*	0.77*
14	3.3626	$(5/2^+)$*	35*	0.47*	70*	
15	3.3629	$(3/2^-)$*	180*	0.69*	15*	
16	3.3693	$3/2^+$	60	0.81	50*	1.36*
17	3.3735	$(5/2^+)$	20	0.27	5	0.04
18	3.3745	$3/2^+$*	23*	0.30*	5*	0.14*
19	3.3780	$1/2^+$	1800	3.67	60	4.60
20	3.4085	$(1/2^-)$	90	0.32	10	0.16
21	3.4095	$3/2^-$*	45*	0.16*	7*	0.11*
22	3.4177	$5/2^+$	160*	1.99*	402*	7.37*
23	3.4189	$(1/2^-)$	300	1.06	30	0.47
24	3.4535	$(3/2^-)$	this resonance was not observed			
25	3.4537	$1/2^+$	300	0.56	100	6.25
26	3.4549	$5/2^+$	350	4.09	207*	4.30*
27	3.4697	$5/2^+$	300*	3.42*	344*	5.67*
28	3.4733	$(3/2^-)$	150	0.49	150	
29	3.4767	$3/2^+$*	30*	0.34*	17*	0.22*
30	3.4892	$(3/2^+)$*	225*	2.48*	1575*	
31	3.4899	$1/2^+$	6000	10.68	300	17.07
32	3.5074	$1/2^-$	750	2.35	8*	0.10*
33	3.5150	$3/2^+$*	23*	0.24*	37*	0.43*

TABLE A.1 (continued)

Res. No.	E_p (MeV)	J^π	Γ_p (eV)	γ_p^2 (keV)	$\Gamma_{p'}$ (eV)	$\gamma_{p'}^2$ (keV)
34	3.5156	$(5/2^+)$	this resonance was not observed			
35	3.5162	$(5/2^+)$	this resonance was not observed			
36	3.5294	$1/2^+$	2500	4.25	200	10.23
37	3.5413	$3/2^-$	80	0.24	28*	0.33*
38	3.5430	$(1/2^-)$	120	0.36	10	0.12
39	3.5461	$1/2^+$	10000	16.68	1100	54.23
40	3.5518	$5/2^-$	15	0.94	12*	1.87*
41	3.5538	$3/2^-$	150	0.44	58*	0.66*
42	3.5554	$3/2^{+*}$	80*	0.79*	102*	4.73*
43	3.5570	$(1/2^-)$	80	0.24	30	0.34
44	3.5652	$(5/2^+)$	this resonance was not observed			
45	3.5657	$3/2^{+*}$	200*	1.95*	1224*	18.67*
46	3.5662	$(5/2^+)$	this resonance was not observed			
47	3.5779	$1/2^{-*}$	400*	1.14*	192*	2.07*
48	3.5850	$5/2^+$	8*	0.08*	81*	1.65*
49	3.5958	$5/2^+$	50	0.47	36*	0.57*
50	3.5987	$(3/2^-)^*$	200*	0.56*	200*	2.07*
51	3.6061	$(3/2^-)$	300	0.83		
52	3.6065	$(5/2^+)$	100	0.91	200	
53	3.6071	$(5/2^+)$	170	1.55	280	
54	3.6092	$(1/2^-)$	90	0.25	70	0.71
55	3.6157	$3/2^{+*}$	65*	0.59*	70*	0.74*

TABLE A.1 (continued)

Res. No.	E_p (MeV)	J^π	Γ_p (eV)	γ_p^2 (keV)	$\Gamma_{p'}$ (eV)	$\gamma_{p'}^2$ (keV)
56	3.6385	$3/2^{-*}$	375*	0.99*	15*	0.14*
57	3.6447	$(3/2^-)$	190	0.50	190	1.79
58	3.6459	$1/2^+$	800	1.20	200	7.76
59	3.6472	$5/2^+$	180	1.55	84*	0.79*
60	3.6503	$3/2^-$	150	0.39	53*	0.49*
61	3.6532	$3/2^{+*}$	105*	0.89*	149*	2.82*
62	3.6549	$5/2^+$	150	1.26	117*	1.63*
63	3.6642	$3/2^{-*}$	400*	1.03*	92*	0.83*
64	3.6701	$1/2^+$	3500	5.11	400	14.67
65	3.6732	$3/2^+$	250	2.07	382*	3.95*
66	3.6750	$5/2^+$	550*	4.54*	994*	9.82*
67	3.6753	$(5/2^+)$	this resonance was not observed			
68	3.6823	$5/2^{+*}$	30*	0.24*	42*	0.60*
69	3.6947	$1/2^-$	3500	8.66	41*	0.35*
70	3.7074	$5/2^{+*}$	380*	2.99*	314*	1.85*
71	3.7099	$5/2^+$	40	0.31	204*	2.42*
72	3.7208	$1/2^+$	17500	24.24	1000	32.68
73	3.7224	$5/2^+$	50	0.38	48*	0.71*
74	3.7274	$(3/2^+)^*$	105*	0.80*	45*	0.18*
75	3.7321	$3/2^{+*}$	30*	0.23*	178*	4.42*
76	3.7333	$(5/2^+)$	10	0.08	100	
77	3.7399	$3/2^{-*}$	150*	0.35*	104*	0.81*

TABLE A.1 (continued)

Res. No.	E_p (MeV)	J^π	Γ_p (eV)	γ_p^2 (keV)	$\Gamma_{p'}$ (eV)	$\gamma_{p'}^2$ (keV)
78	3.7440	$5/2^+$	50	0.37	292*	3.64*
79	3.7509	$1/2^+$	850	1.14	200	6.11
80	3.7528	$5/2^+$	20	0.15	9*	0.12*
81	3.7540	$5/2^+$	20	0.15	1*	0.02*
82	3.7578	$3/2^{+*}$	60*	0.44*	23*	0.52*
83	3.7600	$3/2^-$	450	1.03	209*	1.57*
84	3.7662	$3/2^{+*}$	60*	0.43*	388*	3.03*
85	3.7722	$(5/2^+)$	15	0.11	15	0.06
86	3.7740	$5/2^-$	70	2.92	32*	1.24*
87	3.7763	$3/2^-$	550	1.24	211*	1.53*
88	3.7801	$3/2^-$	100*	0.22*	220*	1.59*
89	3.7876	$3/2^{+*}$	30*	0.21*	23*	0.46*
90	3.7905	$(5/2^+)$	100	0.69	105	0.21
91	3.7908	$1/2^+$	1000	1.29	200	5.60
92	3.7960	$3/2^+$	300*	2.07*	635*	4.75*
93	3.7963	$(3/2^+)$	this resonance was not observed			
94	3.8051	$3/2^-$	160	0.35	45*	0.31*
95	3.8111	$3/2^{-*}$	25*	0.05*	39*	0.26*
96	3.8135	$5/2^{+*}$	60*	0.40*	533*	4.95*
97	3.8140	$(3/2^+)$	this resonance was not observed			
98	3.8233	$5/2^-$	10	0.38	16*	0.74*
99	3.8302	$(3/2^-)$	70	0.15	150	0.99

TABLE A.1 (continued)

Res. No.	E_p (MeV)	J^π	Γ_p (eV)	γ_p^2 (keV)	$\Gamma_{p'}$ (eV)	$\gamma_{p'}^2$ (keV)
100	3.8314	$5/2^+$	150	0.99	100*	1.50*
101	3.8336	$5/2^+$	75*	0.49*	80*	0.88*
102	3.8358	$1/2^+$	400	0.50	75	1.91
103	3.8399	$3/2^+$	150	0.98	17*	0.21*
104	3.8425	$(1/2^-)$	this resonance was not observed			
105	3.8566	$(3/2^-)^*$	20*	0.04*	20*	0.13*
106	3.8606	$5/2^+$	75	0.47	69*	0.61*
107	3.8635	$5/2^+$	130	0.82	43*	0.63*
108	3.8690	$1/2^+$	1500	1.80	70	1.66
109	3.8764	$5/2^-$	10	0.35	19*	0.32*
110	3.8815	$5/2^+$	70	0.43	33*	0.16*
111	3.8900	$(3/2^-)^*$	125*	0.25*		
112	3.8950	$1/2^+$	400	0.47	50	1.13
113	3.9025	$(5/2^-)$	10	0.33	20	0.11
114	3.9067	$5/2^+$	200	1.19	71*	0.53*
115	3.9176	$5/2^+$	250	1.46	93*	0.56*
116	3.9240	$3/2^-$	850	1.63	415*	2.32*
117	3.9329	$3/2^-$	100*	0.19*	514*	2.83*
118	3.9500	$5/2^+$	300	1.68	102*	0.86*
119	3.9547	$1/2^+$	4000	4.40		
120	3.9622	$3/2^+$	75*	0.41*	242*	2.40*
121	3.9677	$5/2^{+*}$	120*	0.66*	62*	0.44*

TABLE A.1 (continued)

Res. No.	E_p (MeV)	J^π	Γ_p (eV)	γ_p^2 (keV)	$\Gamma_{p'}$ (eV)	$\gamma_{p'}^2$ (keV)
122	3.9703	$3/2^+$	90	0.49	54*	0.26*
123	3.9758	$5/2^+$	200	1.08	141*	0.57*
124	3.9800	$(5/2^+)$	40	0.21	40	0.10
125	3.9812	$3/2^-$	300	0.54	252*	1.28*
126	3.9845	$1/2^+$	900	0.97	30	0.55
127	3.9867	$(5/2^+)$	400	2.09	50	0.13
128	3.9930	$(3/2^-)$	3000	5.27	260	1.27
129	3.9945	$1/2^+$	1500	1.59		
130	3.9984	$3/2^{+*}$	150*	0.79*	61*	0.55*
131	4.0042	$(3/2^-)$	100	0.17	100	
132	4.0047	$(3/2^-)$	450	0.78	450	
133	4.0054	$(3/2^-)$	150	0.26	120	0.57
134	4.0133	$5/2^+$	160	0.83	56*	0.61*
135	4.0156	$3/2^{-*}$	100*	0.17*	102*	0.49*
136	4.0177	$3/2^{-*}$	200*	0.35*	19*	0.09*
137	4.0260	$1/2^+$	300	0.31		
138	4.0338	$5/2^+$	200	1.01	132*	0.43*
139	4.0471	$(1/2^-)$	this resonance was not observed			
140	4.0520	$(5/2^-)$	30	0.77	30	0.13
141	4.0613	$3/2^{+*}$	150*	0.73*	89*	0.91*
142	4.0697	$(5/2^+)$	50	0.24	50	0.12
143	4.0722	$3/2^{-*}$	75*	0.12*	36*	0.16*

TABLE A.1 (continued)

Res. No.	E_p (MeV)	J^π	Γ_p (eV)	γ_p^2 (keV)	$\Gamma_{p'}$ (eV)	$\gamma_{p'}^2$ (keV)
144	4.0788	$5/2^-$	80*	2.04*	111*	3.79*
145	4.0910	$1/2^+$	600	0.59		
146	4.0928	$(1/2^-)$	1800	2.87	200	0.84
147	4.0948	$1/2^{-*}$	1200*	1.90*	302*	1.28*
148	4.1133	$1/2^+$	500	0.48	300	4.36
149	4.1143	$(3/2^-)$	80	0.13	80	0.32
150	4.1302	$5/2^+$	200	0.89	43*	0.22*
151	4.1401	$3/2^{+*}$	150*	0.66*	428*	1.70*
152	4.1619	$5/2^+$	150	0.65	63*	0.64*
153	4.1727	$(5/2^+)$	80	0.33	10	0.02
154	4.1733	$1/2^+$	1800	1.66	150	1.96
155	4.1800	$(5/2^+)$	200	0.83	120	0.24
156	4.1807	$(5/2^-)$	50	1.06	50	0.18
157	4.1851	$(3/2^-)^*$	75*	0.11*		
158	4.1893	$3/2^-$	75	0.11	101*	0.37*
159	4.1920	$1/2^+$	4500	4.09	200	2.53
160	4.2036	$5/2^+$	150	0.62	258*	1.08*
161	4.2105	$5/2^+$	50	0.20	47*	0.34*
162	4.2158	$3/2^-$	150	0.22	103*	0.36*
163	4.2162	$1/2^+$	5000	4.46		
164	4.2200	$5/2^+$	40	0.16	49*	0.29*
165	4.2355	$5/2^+$	300	1.19	124*	0.41*

TABLE A.1 (continued)

Res. No.	E_p (MeV)	J^π	Γ_p (eV)	γ_p^2 (keV)	$\Gamma_{p'}$ (eV)	$\gamma_{p'}^2$ (keV)
166	4.2375	$(3/2^-)$	1500	2.09	100	0.34
167	4.2408	$(1/2^-)$	600	0.84	300	1.01
168	4.2415	$(5/2^+)$	700	2.69	1500	2.77
169	4.2521	$(5/2^-)$	50	0.96	50	0.17
170	4.2603	$1/2^+$	3200	2.77	200	2.25
171	4.2675	$(3/2^-)$	250	0.34	450	1.46
172	4.2744	$1/2^+$	200	0.17	150	1.65
173	4.2779	$5/2^+$	150	0.56	52*	0.15*
174	4.2869	$1/2^+$	600	0.51	50	0.54
175	4.2953	$3/2^-$	150	0.20	185*	0.59*

() indicates uncertain spin assignment

* indicates new spin assignment or width

BIBLIOGRAPHY

Baudinet-Robinet, V. 1974. Nucl. Phys. A222, 525.

Bevington, P. R. 1969. Data Reduction and Error Analysis for the Physical Sciences. New York: McGraw-Hill.

Biedenharn, L. C. 1960. "V. C. Angular Correlations in Nuclear Spectroscopy". In Nuclear Spectroscopy. Part B, p. 732. Edited by F. Ajzenberg-Selove, New York: Academic Press.

Biedenharn, L. C., and Rose, M. E. 1953. Rev. Mod. Phys. 25, 729.

Bilpuch, E. G., Lane, A. M., Mitchell, G. E., and Moses, J. D. 1976. Phys. Rep. 28C, 147.

Blatt, J. M., and Biedenharn, L. C. 1952. Rev. Mod. Phys. 24, 258.

Bleck, M. E. 1978. unpublished Ph.D. dissertation, Duke University.

Brody, T. A., Flores, J., French, J. B., Mello, P. A., Pandey, A., and Wong, S. S. M. 1981. Rev. Mod. Phys. 53, 385.

Chou, B. H. 1980. unpublished Ph.D. dissertation, North Carolina State University.

Coester, F., and Jauch, J. M. 1953. Helv. Phys. Acta. 26, 3.

Dittrich, T. R. 1976. unpublished Ph.D. dissertation, North Carolina State University.

Dyson, F. J. 1962. J. Math. Phys. 3, 1199.

Endt, P. M. and Demeur, M., eds. 1959. Nuclear Reactions. Vol. 1. Amsterdam: North-Holland.

Fano, U. 1953. Phys. Rev. 90, 577.

Fano, U. 1957. Rev. Mod. Phys. 29, 74.

Ferguson, A. J. 1965. Angular Correlation Methods in Gamma Ray Spectroscopy. New York: John Wiley and Sons.

Fisher, R. A., and Yates, F. 1963. Statistical Tables for Biological, Agricultural, and Medical Research. 6th ed. p. 46. New York: Hafner.

Gere, E. A., Lie, H. P., and Miller, G. L. 1967. IEEE Trans. on Nucl. Sci. NS-14, 161.

Goldfarb, L. J. B. 1959. "Angular Correlations and Polarization". In Nuclear Reactions. Vol. 1, p. 159. Edited by P. M. Endt and M. Demeur. Amsterdam: North- Holland.

Gove, H. E. 1959. "Resonance Reactions, Experimental". In Nuclear Reactions. Vol. 1, p. 259. Edited by P. M. Endt and M. Demeur. Amsterdam: North-Holland.

Harney, H. L., and Weidenmüller, H. A. 1969. Nucl. Phys. A139, 241.

Heisenberg, W. 1943. Z. Phys. 120, 673.

Huby, R. 1954. Proc. Phys. Soc. A67, 1103.

Jänecke, J. 1969. In Isospin in Nuclear Physics. p.297. Edited by D. H. Wilkinson, Amsterdam: North-Holland.

Krieger, T. J., and Porter, C. E. 1963. J. Math. Phys. 4, 1272.

Lane, A. M. 1971. Ann. Phys. 63, 171.

Marion, J. B. 1960. Nuclear Data Tables. Washington: National Acadamy of Science.

Marion, J. B., and Young, F. C. 1968. Nuclear Reaction Analysis. Amsterdam: North-Holland.

Mehta, M. L. 1967. Random Matrices and the Statistical Theory of Energy Levels. New York: Academic Press.

Moses, J. D. 1970. unpublished Ph.D. dissertation, Duke University.

Peters, W. C. 1972. unpublished Ph.D. dissertation, Duke University.

Porter, C. E., ed. 1965. Statistical Theories of Spectra: Fluctuations. New York: Academic Press

Porter, C. E., and Rosenzweig, N. 1960. Ann. Acad. Sci. Fennicae AVI 44, 5.

Porter, C. E., and Thomas, R. G. 1956. Phys. Rev. 104, 483.

Robertshaw, J. E., Mecca, S., Sperduto, A., and Buechner, W. W. 1968. Phys. Rev. 170, 1013.

Salzmann, M. 1975. unpublished Ph.D. dissertation, University of Zurich.

Salzmann, M., Meyer, V., and Bründle, H. 1977. Nucl. Phys. A282, 317.

Satchler, G. R. 1955. unpublished Ph.D. dissertation, Oxford University.

Sellin, D. L. 1969. unpublished Ph.D. dissertation, Duke University.

Shriner, J. F., Jr., Bilpuch, E. G., Westerfeldt, C. R., and Mitchell, G. E. 1982. Z. Phys. A305, 307.

Taylor, J. R. 1972. Scattering Theory: the Quantum Theory of Nonrelativistic Collisions. New York: John Wiley and Sons.

Watson, W. A., III. 1980. unpublished Ph.D. dissertation, Duke University.

Watson, W. A., III, Bilpuch, E. G., and Mitchell, G. E. 1980. Z. Phys. A294, 153.

Wells, W. K. 1978. unpublished Ph.D. dissertation, Duke University.

Wigner, E. P. 1967. In Oak Ridge National Laboratory Report, ORNL-2309, 59.

Wigner, E. P., and Eisenbud, L. 1947. Phys. Rev. 72, 29.

Wilkinson, D. H., ed. 1969. Isospin in Nuclear Physics. Amsterdam: North-Holland.

Wilson, W. M. 1973. unpublished Ph.D. dissertation, Duke University.

Wimpey, J. F. 1974. unpublished Ph.D. dissertation, Duke University.

BIOGRAPHY

KATHERINE MEIBURG WHATLEY

Personal:	Born December 29, 1954, Louisville, Kentucky Married August 12, 1978, to Michael Jac Whatley
Education:	B.S. in Physics, Wake Forest University, 1977 M.A. in Physics, Duke University, 1980
Abstract:	Whatley, K. M., Westerfeldt, C. R., Bilpuch, E. G., and Mitchell, G. E. "High Resolution Proton Inelastic Scattering from Resonances in ^{51}Mn." Bull. Am. Phys. Soc. 27, 497.
Positions:	Teaching Assistant, Duke University, 1977-1978 Research Assistant, Duke University, 1978-present Visiting Assistant Professor, Wake Forest University, July-August, 1981
Fellowships and Memberships:	Shell Teaching Fellow, 1977-1978 American Physical Society Sigma Xi